Poly (ethylene glycol)-interpenetrated genipin-crosslinked chitosan hydrogels for controlled drug delivery

by

Nga Thi Ngoc Vo

A thesis presented for the degree of

Doctor of Philosophy

School of Engineering

Newcastle University, United Kingdom

April 2021

Abstract

Smart hydrogels are of increasing interest for controlled drug delivery as they can be used as drug carriers to deliver cargo biomolecules in response to specific physiological signals at tailored rhythm. In this project, pH-responsive hydrogels containing chitosan, genipin, and poly (ethylene glycol) (PEG) are investigated. Owing to good biocompatibility and pH-sensitivity, chitosan was used as the main polymeric backbone, while genipin was employed as a low-toxic crosslinker to bridge chitosan molecules. To enhance the level of control in hydrogel microarchitecture and achieve reproducible properties, PEG was added to form semi-interpenetrating networks. The aim of this project was to develop and evaluate injectable and degradable chitosan-genipin-PEG hydrogels and the feasibility of using them to control drug delivery.

The chitosan-genipin hydrogels, with and without PEG, were synthesised under mild conditions (37^{o}C, 24 h) and in a range of shapes (disc, bead, and film). The hydrogels had dark blue colour and intrinsic fluorescence (580 nm excitation and 630 nm emission), due to oxygen radical-induced polymerisation of genipin, as well as the reaction with amino groups of chitosan. The bead-shaped hydrogels were discrete and spherical with diameters ranging from 1 to 30 μm. The disc-shaped hydrogels (13 mm in diameter and 8 mm in height) had microporous structures with pore diameters ranging from 11 to 57 μm and average cross-sectional porous areas of 40% to 64%. Compared to disc-shaped chitosan-genipin hydrogels, presence of PEG up to 1.9 mM generated the same effect as increasing the genipin content, yielding structures with a smaller pore diameter, a lower swelling degree in pH 2 buffer and a higher elastic modulus. Considering cost effectiveness and scale-up production, reducing genipin content by the addition of PEG is favourable. Importantly, hydrogels containing higher concentration of PEG (2.9 mM and above) showed a sudden increase in the swelling degree accompanied with a decrease in the elastic modulus. The release profiles of two drug molecules (perindopril erbumine and 1-methyl D-tryptophan) with different solubility from disc-shaped hydrogels revealed their swelling-controlled kinetic, which fitted well to the Korsmeyer-Peppas model, indicating a non-Fickian transport mechanism.

Cytotoxicity assays of hydrogel films towards 3T3 fibroblasts showed that the cells retained normal adhesive properties and high viability on gels with 3.1 mM and 4.4 mM genipin but not on gels with 1.7 mM genipin, suggesting a strong correlation between hydrogels' stiffness and cell attachment/growth. Adding PEG enhanced the viability of 3T3 cells cultured on hydrogel films. To facilitate comparison, the inflammatory responses of DC 2.4 dendritic cells, RAW 264.7

macrophage cells, and bone marrow-derived macrophages to uncrosslinked chitosan and crosslinked chitosan-genipin hydrogel films/beads were investigated. Despite induced mRNA expression of some cytokines in all treated cell types (especially up to 2435-fold increase in interferon-β gene expression found in hydrogel film-exposed DC 2.4), no increased levels of five inflammatory cytokines were detected, suggesting the hypo-inflammatory properties of chitosan-genipin hydrogels. The biodegradation of hydrogel films upon exposure to lysozyme and the biodegradation of macrogels after subcutaneous injection in mice were monitored efficiently using the intrinsic fluorescence of hydrogels. Results suggest that the *in vivo* degradation rate depends critically on where the hydrogel is deposited in tissues. The subcutaneous injection of hydrogel beads induced interferon-β gene transcription significantly and no local skin lesion was observed, suggesting a good biocompatibility *in vivo*. Collectively, the findings presented in this study provide valuable guidance to further develop these biocompatible, biodegradable, and injectable chitosan-genipin hydrogels as autonomous drug delivery systems.

Acknowledgements

This PhD has been the toughest journey I have experienced so far, and I would not have finished it without the support and guidance from many people. Firstly, I would like to express my deepest gratitude to my supervisor, Dr. Katarina Novakovic for giving me this PhD studentship, and for her immeasurable support and encouragement throughout my study. Her outstanding contribution to my PhD completion is undeniable. My sincere thanks also go to Prof. Andrew Mellor for his valuable inputs as a co-supervisor. I am extremely grateful to Dr. Lei Huang, who has helped me shape my career and professional life and showed me how to transform mistakes into skills. I would like to thank Dr. Henrique Lemos for his help in animal experiments and valuable discussions. I gratefully acknowledge the Research Excellence Academy and CEAM for financial support. Many thanks to my colleagues, the technicians, and research staffs in School of Engineering, Institute of Cellular Medicine, and Electron Microscopy Research Services for their considerable contributions to this project.

No matter how challenging it has been during these four years, this PhD journey also taught me the power of friendship. I have met many friends who are always there for me with heartfelt caring and support. Thanks to all my adorable friends for all the joy and tears we have had together. Deeply thanks to Hang Xiang, who always understands me, encourages me, and gives me advice on how to pull through the difficult time I was passing.

Lastly, I am deeply grateful to my parents, who have guided and strengthened me, given me wings and let me fly on my own, given me confidence to push forward and love that surrounds me. I know I could not say it enough, for the things that they have done to support me throughout my study. I also thanks to the rest of my family, whose faithful support and encouragement are highly appreciated.

Table of Contents

List of Publications and Conferences

Publications

1. **N.T.N. Vo**, L. Huang, H. Lemos, A. Mellor, and K. Novakovic, *Poly (ethylene glycol)-interpenetrated genipin-crosslinked chitosan hydrogels: structure, pH-responsiveness, gelation kinetics, and rheology*. Journal of Applied Polymer Science, 2020. **137**: p. 49259.
2. **N.T.N. Vo**, L. Huang, H. Lemos, A. Mellor, K. Novakovic. *Genipin-crosslinked chitosan hydrogels: preliminary evaluation of the in vitro biocompatibility and biodegradation*. Journal of Applied Polymer Science. 2021 (accepted for publication).
3. Z. Wang, X. Zang, B. Qin, M. Wang, J. Feng, C. Zhang, D. Zhou, C. Zhu, S. He, H. Liu, M. Huang, Y. Wang, P. Wang, S. Lu, Z. Cheng, J. Miao, W. Zhou, W. Liu, Y. Mao, L. Yao, S. Wu, **N.T.N. Vo**, L. Huang, W. Liu. *Engineering environmentally-responsive nanoparticles to overcome biological barriers in delivering siRNA for anti-tumour therapy*. Theranostics. 2021 (under revision).

Selected conference presentations

1. **N.T.N. Vo**, L. Huang, H. Lemos, A. Mellor, and K. Novakovic. *Smart chitosan-based hydrogels for targeted drug delivery applications*. In: Chem Eng Day UK. 2019, Edinburgh, UK.
2. **N.T.N. Vo**, L. Huang, H. Lemos, A. Mellor, and K. Novakovic. *Smart chitosan-based hydrogels for targeted drug delivery applications*. In: NEPIC Technology Showcase Event. 2019, Middlesbrough, UK.
3. **N.T.N. Vo**, L. Huang, H. Lemos, A. Mellor, and K. Novakovic. *Smart chitosan-based hydrogels for targeted drug delivery applications*. In: 4th International Conference on Biomedical Polymers and Polymeric Biomaterials (ISBPPB 2018). 2018, Krakow, Poland.

List of Figures

List of Tables

List of Abbreviations

AFM	Atomic force microscopy
ATP	Adenosine triphosphate
BSA	Bovine serum albumin
cGAS	Cytoplasmic DNA sensor
CLSM	Confocal laser scanning microscopy
CND	Carbon nanodots
CS-GEN	Chitosan-genipin
D-1MT	1-methyl D-tryptophan
DAPI	4’,6-diamidino-2-phenylindole
DDA	Degree of deacetylation
DI	Deionised
DMEM	Dulbecco’s modified Eagle medium
DSC	Differential scanning calorimetry
ESEM	Environmental scanning electron microscopy
FITC	Fluorescein isothiocyanate
FTIR	Fourier-transform Infrared Spectroscopy
GFR	Green Fluorescent Protein
GP	β-glycerophosphate
hADSCs	Human adipose-derived stem cells
H&E	Haematoxylin and eosin
HMDS	Hexamethyldisilazana
HPLC	High Performance Liquid Chromatography
IFN-β	Interferon-β
IL-1ra	Interleukin-1 receptor antagonist

IL-1β	Interleukin-1β
IL-6	Interleukin-6
IP-10	Interferon gamma-induced protein 10
IPNs	Interpenetrating networks
ISO	International Organisation for Standardisation
IVIS	*In Vivo* Imaging System
LDH	Lactate dehydrogenase
LVR	Linear viscoelastic regime
M-CSF	Macrophage colony-stimulating factor
MP/NPs	Microparticles/nanoparticles
MTT	3-(4,5-dimethylthiazol-2-yl)-2,5-diphenyl tetrazolium bromide
MW	Molecular weight
NLRP3	Nucleotide-binding and oligomerization domain-like receptor protein 3
PBS	Phosphate buffered saline
PCPOC	Palladium-catalysed phenylacetylene oxidative carbonylation
PECs	Polyelectrolyte complexes
PEG	Poly (ethylene glycol)
PER	Perindopril erbumine
PSD	Particle size distribution
PTFE	Polytetrafluoroethylene
PVA	Poly vinyl alcohol
PVP	Poly vinyl pyrrolidone
RFP	Red Fluorescent Protein
RFU	Relative fluorescent unit
RPMI	Roswell Park Memorial Institute

RT-PCR	Reverse transcription polymerase chain reaction
SAOS	Small-amplitude oscillatory shear rheology
SEM	Scanning electron microscopy
Semi-IPN	Semi-interpenetrating network
SD	Standard deviation
STING	Stimulator of interferon genes
TNF-α	Tumour necrosis factor- α
TPP	Sodium tripolyphosphate
W/O	Water-in-oil

Chapter 1 Introduction

1.1 Overview of smart hydrogels

Hydrogels are three-dimensional crosslinked networks that have the ability to absorb a significant amount of water while maintaining their distinct structures [1]. Hydrogels can be classified into physical gels or chemical gels based on the preparation method. Physically crosslinked hydrogels are reversible and unstable networks in which the polymeric chains are connected by molecular entanglement and/or physical interactions including ionic crosslinks, hydrogen bonds, and hydrophobic interactions [2]. In contrast, chemically crosslinked hydrogels are irreversible and stable due to the covalent connection between chemical crosslinkers and functional groups in polymers [3]. The hydrophilicity and the swelling ability in biological conditions endow hydrogels with excellent biocompatibility, presenting a soft and rubbery consistency common to living tissues, higher permeability to small molecules, and the release of entrapped molecules in a controlled manner [4]. The hydrogels can be fabricated in different physical forms (such as disc, membrane, sheet, micro-/nano-particles (MP/NPs), and coating layer) with various dimensions (from nanometre to centimetre) [5].

Their applications have been broadened extensively with the concept of "Smart" hydrogels. Smart hydrogels contain responsive functional groups which can sense the surrounding environment and adjust themselves accordingly to different external or internal stimuli such as pH, temperature, light, or specific molecules. Smart hydrogels have been utilised in a wide range of biomedical applications, including wound dressing, contact lenses, scaffold, cell growth, agriculture, and regenerative medicine [6]. Among different biomedical applications, smart hydrogels have emerged as potent chronotherapeutic carriers to control drug delivery in pulse or self-regulated mechanisms. Owing to stimuli-responsive behaviours, the tunable physico-chemical properties, controllable degradability, and the ability to protect labile drugs from degradation, the designated smart hydrogels show capability to sense the physiological signals and respond accordingly to deliver the entrapped biomolecules when and where required [7].

1.2 Chitosan: versatile polymer for formulation of pH-responsive hydrogels

The use of polysaccharides for development of smart hydrogels has strongly grown in the last decade due to their intriguing properties of low toxicity, good biocompatibility, easy degradation, rich sources, and low cost [8]. Alginate, starch, carrageenan, cellulose, and chitosan are common

polysaccharides which have been utilised for hydrogel fabrication. Among them, chitosan, a linear cationic polysaccharide, has attracted a great deal of interest.

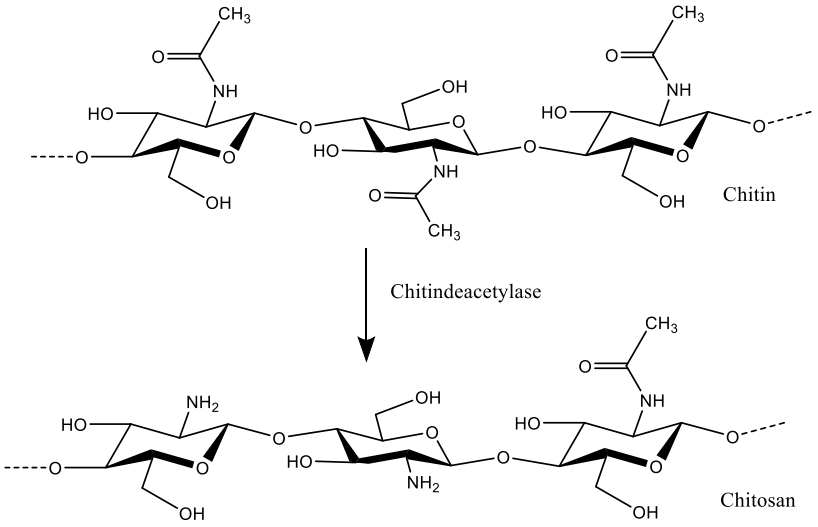

Figure 1.1 Structures of chitin and chitosan.

Chitosan is a semi-synthetic biopolymer obtained from chitin, which is the second most abundant polysaccharide (after cellulose) [4]. Chitin consists of a sugar backbone with β-1,4-linked glucosamine units with high degree of acetylation while chitosan is the alkaline deacetylated product of chitin, composed of randomly located N-acetyl glucosamine and D-glucosamine units, with high degree of deacetylation and varying molecular weight (MW) (**Figure 1.1**) [9]. The degree of deacetylation (DDA) is calculated as the ratio of D-glucosamine to the sum of D-glucosamine and N-acetyl glucosamine, indicating the number of amino groups along the chains, and it should be at least 60% for the material to be called chitosan [10]. As the deacetylated product of chitin, chitosan has plentiful free amino groups ($-NH_2$), making them a weak polybase (pKa of around 6.5) with charge density in the pH range of 6 - 6.5 [9]. At pH below 6.5 (towards acidic environments), free amino groups on chitosan chains can be protonated (converted to $-NH_3^+$) and make chitosan a polycationic polymer with high density of positive charge. Therefore, diluted solutions of acetic acid (1 - 3%, v/v) or citric acid (3 - 4%, v/v) are commonly used to prepare chitosan solutions. Alternatively, at pH above 6.5 (towards neutral/basic environments), chitosan is insoluble with low charge density. This pH-sensitivity of chitosan occurs at pH range of 6 - 6.5, which is a convenient range for biological applications. It is evident that DDA and MW might affect the cationic charge density of chitosan and hence its solubility as well as chemical properties [11]. Today, pH-responsive hydrogels based on chitosan have been widely explored in various fields, including tissue engineering, enzyme immobilisation, wound dressing, water purification,

and controlled drug delivery [12-14]. Favourable advantages of chitosan in the development of smart hydrogels for medical purposes are listed below.

- Chitosan has a **wide spectrum of DDA and MW** to meet end-use applications. On market, chitosan is available in range of MWs, for examples, low MW (50 - 190 kDa), medium MW (190 - 310 kDa), and high MW (310 - 375 kDa). Chitosan can also be prepared in a variety of dimensions (from nanometre to centimetre) and forms (such as disc, membrane, sheet, particles, and coating layer) [15].
- Chitosan can be **functionalised** into different derivatives according to the designated applications, such as carboxylmethyl chitosan for delivery of hydrophobic molecules [16]. The simplicity of chemical modification is one of the great strengths of chitosan [17].
- Chitosan and its derivatives can be **combined** with other polymers/compounds with different properties. For instance, chitosan might have electrostatic interaction with anionic polysaccharides (such as alginate, gum xanthan, hyaluronic acid, pectin, heparin, and dextran sulphate), proteins (such as gelatin, albumin, and collagen), and anionic synthetic proteins (such as polyacrylic acid) to form polyelectrolyte complexes. These complexations are much stronger than other secondary binding forces and could be employed to improve the properties of chitosan microparticles [18].
- Chitosan is recognised for its **low toxicity, biocompatibility, and biodegradability**. Chitosan is found to be a biologically compatible polymer with minimal toxicity [19]. No significant pyrogenic and toxic effects of chitosan were reported in mice, rabbits, and guinea pigs [20]. The modification could produce chitosan derivatives with more or less toxicity and the removal of residual reactants needs to be considered. Chitosan can be degraded *in vivo* by several enzymes, mainly by lysozyme [21]. Furthermore, the products from degradation are non-toxic oligosaccharides which can be then excreted or incorporated to glycosaminoglycans and glycoproteins [6, 22].
- Chitosan offers **mucoadhesion**. Its mucoadhesive property stems from the electrostatic interaction between positively charged amino groups on chitosan and negatively charged mucin and the contribution of hydrogen bonding and hydrophobic effect [23]. Chitosan may also enhance drug penetration by opening the tight junctions between epithelial cells [24, 25].
- Chitosan offers strong **immune stimulatory capability** and low **off-target immunogenicity** [26]**.** The concomitant use of chitosan as a vaccine delivery and as an

immune adjuvant has been reported [27]. As a potential adjuvant, chitosan was demonstrated to be equipotent to incomplete Freund's adjuvant and superior to aluminium hydroxide [28].

In summary, these striking properties make chitosan an ideal component for the development of pH-responsive hydrogels. Thus, chitosan was chosen as the core material in this project, seeking to develop injectable and degradable hydrogel formulations, capable of controlled drug delivery.

1.3 Remaining challenges for development of chitosan-based hydrogels

Although successful and fruitful results have been obtained, only a limited number of chitosan-based hydrogels are currently used in clinical applications. There are still many challenges in the development of chitosan-based hydrogels in the following aspects.

- Due to the hydrophilic nature, low solubility, and low mechanical resistance [17], long chitosan molecules need to be crosslinked to form stable hydrogels. In physical gels, it is difficult to obtain consistent performance *in vivo*, as these networks are unstable and reversible, posing a challenge to precisely control the physico-chemical properties, degradation, and dissolution [4]. In chemical gels, free unreacted crosslinkers and other auxiliary molecules cannot be completely excluded, leading to potential toxic effects even if purification step is applied [29]. Thus, there is an imperative need to utilise a non-toxic, biocompatible crosslinker for the preparation of chitosan hydrogels. In this project, genipin, a naturally occurring substance, was chosen as the crosslinker to bridge chitosan molecules, due to its well-reported biocompatibility and minimal toxicity [30].
- Batch-to-batch variations in the MW distribution of chitosan pose a challenge in consistently achieving hydrogels with reproducible properties (such as porosity, swelling, and rheological properties) [31]. It is also difficult to precisely predict the release profiles of entrapped molecules due to high structure variability of chitosan (such as crystallinity, DDA, and distribution of deacetylated groups). Moreover, during hydrogel swelling, a rapid burst drug release is often observed, which is probably due to desorption of entrapped drug on gel surface [32], poor drug distribution within gel network [33], and heterogeneous nature of polymeric network [34]. Hydrogels are often deemed weak with low mechanical strength, due to the intrinsic heterogeneity of the network structure and/or lack of efficient energy-dissipation mechanisms [35]. To enhance reproducibility and consistency, overcome rapid dissolution and fast drug release, as well as further improve mechanical

robustness, it is necessary to introduce a hybrid network and combine the characteristics of physical and chemical hydrogels. One simple solution may lie in the use of a linear polymeric chain, such as poly (ethylene glycol) (PEG). Addition of a linear PEG polymer appears promising due to the potential to improve the mechanical strength of hydrogels, enhance water adsorption capacity and add extra level of control in physical properties without extra complicated processing steps [36].

- The delivery of multiple drugs from a single system or the development of multi-stimuli-responsive hydrogels (such as pH and temperature, or pH and light) based on chitosan remains challenging. On-demand release of therapeutic molecules with high level of control and the ability to maintain this smart response throughout the lifetime are currently unmet in most hydrogel systems [7, 37]. Moreover, in these systems, there is a need of appropriate external stimuli to trigger the conformation changes, implying that intervention is required on a high frequency basis. Thus, the concept of self-regulating hydrogels able to expand and collapse autonomously (without the need of external stimuli) is of growing interest [38]. Idea behind this concept is to chemically couple smart biomaterials with an oscillatory chemical reaction (producing oscillations in pH) and enable oscillations of stimulus (pH) inside the smart gels, causing the network to swell or collapse promptly and release the loaded moieties periodically. Most recently, a pulsatile release system employing chitosan macrogels and the palladium-catalysed oxidative carbonylation reaction has been reported [39], expanding the horizons of chitosan-based hydrogels towards pulsatile drug delivery. However, to fully materialise the concept, in parallel to developing oscillatory chemical processes, more work is needed on chitosan-based hydrogels to achieve a high level of control in release kinetics and a long-lasting response.
- To reach clinical applications, a biomedical system must be minimally cytotoxic and biodegradable enzymatically or hydrolytically. In case of genipin-crosslinked hydrogels, the biocompatibility of individual components does not guarantee the bio-safety of resulting hydrogels. Only limited studies have been done to evaluate the efficiency and cytotoxicity of genipin as well as the biocompatibility profiles of chitosan-genipin hydrogels. Thus, there is an urgent need to deeply understand the *in vitro* and *in vivo* biocompatibility of these systems, bringing them one step closer to clinical trials. Furthermore, during translation process, there are several factors that researchers need to consider, such as scale-up production, the optimal storage conditions, regulatory requirements, and cost [7]. A hydrogel encapsulated drug is regulated as a combination product, requiring a longer

approval time (than a single system without any payload), adding extra hurdles towards commercialisation [40].

Although there are still many remaining challenges that researchers need to tackle, it is undoubted that further research on chitosan-based hydrogels and the search for new directions in its use with other polymers will reveal greater prospects and properties of this unique polymer, expanding the existing arsenal of material systems and enhancing the impact on human healthcare.

1.4 Aims and objectives of this thesis

The aim of this project is to develop injectable and degradable chitosan-based hydrogels crosslinked by genipin and modified by other polymers for controlled drug delivery applications. To achieve the aim, several objectives are set:

- Synthesise and optimise the fabrication process of genipin-crosslinked chitosan hydrogels produced in different physical forms (disc, bead, and film shapes).
- Evaluate the physical and chemical properties of the developed hydrogels as a function of their composition and gelation conditions.
- Investigate the *in vitro* and *in vivo* biocompatibility of the developed hydrogels in different physical forms and in comparison with uncrosslinked chitosan.
- Determine the release kinetics of model entrapped molecules.

1.5 Thesis structure

The thesis is divided into six chapters. **Chapter 1** is the introduction, providing an overview of smart chitosan-based hydrogels, their advantages in drug delivery applications, and the remaining challenges together with aims and objectives. **Chapter 2** provides an extensive literature review on the hydrogel synthesis and gelation mechanism, key characteristic of chitosan-based hydrogels and their applications in drug delivery. **Chapter 3** details the preparation methods for producing disc-shaped and bead-shaped hydrogels, experimental set-ups, and analytical techniques to evaluate the physico-chemical properties as well as *in vitro* and *in vivo* biocompatibility of the developed hydrogels. Results and discussions are presented in Chapters 4 and 5. **Chapter 4** covers the physico-chemical characterisations of the hydrogels using a wide range of analytical techniques as well as release profiles of the encapsulated biomolecules. **Chapter 5** focuses on the biocompatibility profiles of the hydrogels produced in different forms towards a range of *in vitro* cultured cells and primary cells. The *in vivo* biocompatibility and biodegradation upon

subcutaneous injection is also evaluated in Chapter 5. Finally, conclusions are drawn and recommendations for future work are offered in **Chapter 6**.

Chapter 2 Literature review

This Chapter presents the state-of-the-art literature in the field of chitosan-based hydrogels from synthesis and characterisation to biomedical applications. Drug loading and drug release mechanisms from hydrogel matrices are also discussed. Applications of smart chitosan hydrogels in vaccine delivery are included.

2.1 Synthesis of chitosan-based hydrogels

Many hydrogels' properties, such as porosity, swelling capacity, mechanical strength, and biodegradability are intrinsically affected by crosslinking methods [6]. Thus, the choice of preparation methods might ultimately govern the biological functions of resulting hydrogels. Based on the main interactions forming the network, hydrogels can be classified as physical or chemical gels. Physically crosslinked hydrogels are formed by secondary interactions, including electrostatic attraction, hydrogen bonding, and hydrophobic interaction [18]. Alternatively, chemically crosslinked hydrogels are formed by covalent bonds between functional groups of crosslinkers and chitosan. Certainly, in both types of hydrogels, physical interactions (such as hydrogen bridges and hydrophobic interaction) are always present in the networks, but the standard of this classification is whether physical interaction or covalent crosslinking is the dominant interaction producing the networks [4].

2.1.1 Physically crosslinked hydrogels

In physical hydrogels, polymeric chains are connected by molecular entanglement or physical interactions such as ionic attraction, hydrogen bonding, and hydrophobic interaction.

2.1.1.1 Electrostatic interactions

As a cationic polysaccharide, chitosan can induce electrostatic interactions with negatively charged molecules (low MW ions such as sulphates [41], citrates [42], and phosphates [43]) to form physical hydrogels in a simple and mild setting (**Figure 2.1a**). These ionic interactions are found to depend on the DDA, MW, and concentration of chitosan, as well as the size and ionic charge density of anionic moieties [44]. MP/NPs formed by ionic crosslinking between chitosan and sodium tripolyphosphate (TPP) have been utilised for targeted delivery of various biomolecules (such as ofloxacin [45], progesterone [46], and gentamycin [47]). Another promising approach is introducing inorganic nanoparticles (such as Ag NPs [48] , ZnO NPs [49], and CuO NPs [50]) into physically crosslinked hydrogels (formed by chitosan and TPP), as the resulting nanocomposite

hydrogels show remarkable improved mechanical properties compare to the non-modified chitosan hydrogels.

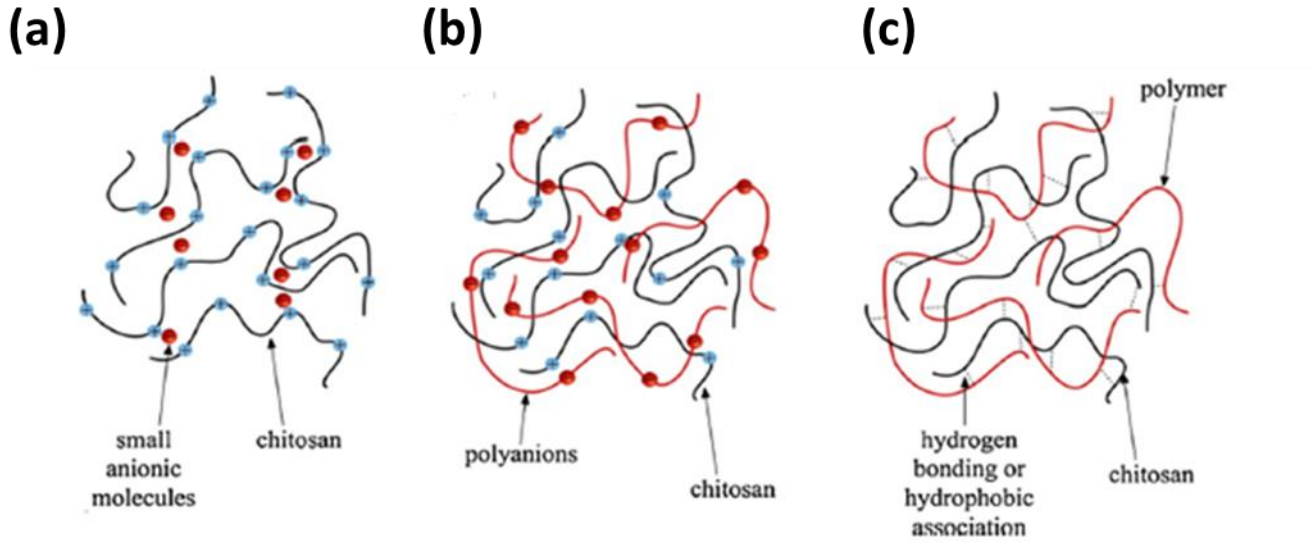

Figure 2.1 Schematic representation of physically crosslinked hydrogels, obtained by association with (a) small anions; (b) polyanion; (c) by hydrogen bonding/hydrophobic association [6].

Anionic polymers can form polyelectrolyte complexes (PECs) with chitosan (**Figure 2.1b**). These PECs are formed due to electrostatic interactions between oppositely charge polyions [51]. The subtle difference between PECs and the ionically crosslinked hydrogels (mentioned above) is the broad MW range of molecules that forms PECs. Most anionic polysaccharides (such as alginate, pectin, dextran, and gellan gum), proteins (such as silk fibroin protein and collagen), and synthetic polymers (such as poly (acrylic acid), poly (L-lactide), and polyphosphate) can form PECs with chitosan [4]. The main advantages of PECs are: i) the interactions present in PECs are much stronger than secondary binding forces (such as hydrogen bonding and Van der Walls interaction) [18]; ii) no auxiliary molecules (such as catalyst, organic precursor, chemical crosslinker, and surfactant) are required [52]; and iii) biocompatibility of individual polymers is preserved [53]. However, several limitations need to be addressed by future research, such as unpredictable production yield (due to non-uniformity of the surface charge, decoupling of surface potential and density) [53], high variability of polymer chains (length and MW) [54], and small pH range of the complexation (as it needs to be in the vicinity of the pKa interval of the two polymers) [55].

2.1.1.2 Hydrogen bonding and hydrophobic interactions

Thermo-responsive hydrogels can undergo a phase separation corresponding to a particular change in the solution temperature [56]. These hydrogels are generally formed by hydrophobic interactions

and other secondary binding forces (**Figure 2.1c**). The most well-known thermo-sensitive chitosan hydrogel is made of chitosan and β-glycerophosphate (GP), which has sol-gel transition occurring when temperature increases. Gelation mechanism involves multiple interactions between chitosan, GP, and water. Major steps during the gelation include: i) at lower temperature, due to the basic action of the salt, electrostatic repulsion within chitosan chains is reduced while hydrogen bonding between multi-hydroxyls on chitosan chains and water is increased, preventing the aggregation of chitosan chains (so that chitosan remains in liquid form even at neutral pH of 6.8 - 7.2); ii) at higher temperature (37^{o}C), the water molecules are removed by the glycerol moieties, breaking the hydrogen bonding and promoting hydrophobic interactions among chitosan chains [57, 58]. Consequently, a gel is formed. The systems have been utilised for injectable *in situ* forming hydrogels, where the formulations are injected in liquid form and transformation into hydrogels occurs inside the body at physiological temperature. Many other *in situ* forming thermo-responsive chitosan-based systems have been developed, presenting a promising approach for future research. For instance, a thermo-responsive chitosan-graft-poly (N-isopropylacrylamide) injectable hydrogel has been developed for cultivation of chondrocytes and meniscus cells, showing sol-gel transition at around 30^{o}C [59]. Bhattarai et al. reported a thermosensitive hydrogel based on PEG-grafted chitosan encapsulating bovine serum albumin (BSA) as a model protein [60]. The reversible insoluble-soluble transition occurred at body temperature and a steady linear release of protein was achieved for a period of 70 h after an initial burst release in the first 5 h. A physically crosslinked chitosan-glycerol hydrogel carrying disulfiram has been developed for cancer therapy, which showed sol-gel transition at body temperature and released 95% of disulfiram *in vitro* (37^{o}C, pH 7.4) [61].

2.1.1.3 Multiple physical interactions

Some physical hydrogel networks are formed with multiple interactions rather than a single dominant interaction. For instance, chitosan/poly vinyl alcohol (PVA) hydrogels, formed by autoclaving, utilise hydrogen bonding (between hydroxyl groups of PVA and hydroxyl/amino groups of chitosan) as the main interaction, while chitosan/PVA hydrogels prepared by freeze-thawing method involve both hydrogen bonding and crystallisation (presence of crystallite junction zones between polymeric chains and inter-polymer complexation) [4].

Some physical hydrogels present self-assembly ability, which is a result of a balance between competing forces that favour assembly (such as hydrophobic interaction, hydrogen bonding, and electrostatic attraction) and forces that act against assembly (such as electrostatic repulsion and

solvation) [62]. Self-assembly is the main route of crosslinking to produce shear-thinning hydrogels. Due to the weak nature of these physical interactions, the pre-formed networks can be dissociated under applied shear and the resulting hydrogels, exhibiting viscous flow, can be delivered *in vivo* by injection (shear-thinning behaviour). Upon relaxation (when the shear is removed), the networks then reassemble into hydrogels (self-healing behaviour) [63]. The hydrogels are pre-formed *ex vivo*, allowing homogenous encapsulation of payload while the effect of local environment on crosslinking is deemed negligible [63]. Shear-thinning property allows the injection through needle without clogging, precludes the need of surgical implantation, and enhances therapeutic efficacy at the action sites by taking the shape of local area and maximising interfacial contact [64, 65]. Self-healing response in shear-thinning hydrogels is much faster than other chemically crosslinked hydrogels, preventing the leakage of precursor solution [66]. To date, several chitosan-based hydrogels have been explored towards this approach, such as chitosan grafted copolymers (made of acrylic acid and acrylamide) hydrogels for cancer therapy [67], quaternised chitosan-Pluronic F127 hydrogels for wound healing [68], and carboxylmethyl chitosan-xanthan hydrogels for local drug delivery [69]. However, more strategies must be developed to meet practical requirements and circumvent some challenges, such as insufficient mechanical strength, a balance between self-healing ability and mechanical robustness, and scale-up production.

In summary, physically crosslinked chitosan hydrogels have been explored extensively in drug delivery applications, owing to their well-known advantages including the absence of harsh chemical crosslinker, no chemical modification required, ease of fabrication process, minimal toxicity, and good biocompatibility [2, 70]. However, several drawbacks have restrained their development, including the nature of reversible and unstable networks being formed, low mechanical strength, and uncontrolled dissolution/degradation/matrix porosity [71, 72].

2.1.2 Chemically crosslinked hydrogels

In chemically crosslinked hydrogels, the dominant interactions forming the network are covalent crosslinks between multiple active amino and hydroxyl groups of chitosan and functional groups of crosslinker. In this section, chemically crosslinked chitosan hydrogels are reviewed from the perspective of chemical bonds which originate from chitosan chains directly rather than from chemically modified chitosan derivatives.

2.1.2.1 Imine bonds (Schiff base)

Imine bonds (-N=CH-, or so-called Schiff bases) are the most common bonds for producing covalently crosslinked chitosan hydrogels. Aldehyde groups (-CHO) can form covalent imine bonds with -NH_2 groups of chitosan. Dialdehydes (particularly glutaraldehyde [73]) are commonly used due to the ease of fabrication process, high speed of reaction, and mild gelation conditions (**Figure 2.2**). However, the biocompatibility of the resulting hydrogels is deemed insufficient for biomedical purposes, and the need to remove the excess neurotoxic glutaraldehyde remains a challenge. Monoaldehydes (such as formaldehyde [74] and salicylaldehyde [75]) can also be used, and the resulting hydrogels exhibit typical pH and temperature responsive behaviours, with self-healing ability and good mechanical strength.

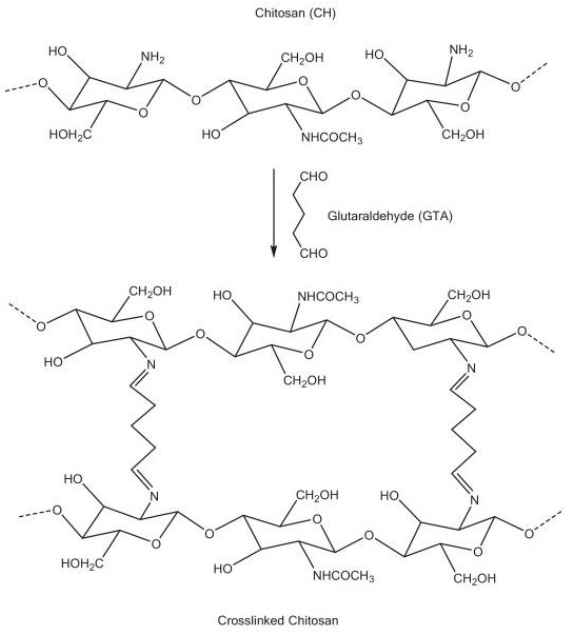

Figure 2.2 Crosslinking reaction between chitosan and glutaraldehyde [76].

Imine bonds are generated from not only the aldehyde with intrinsic functions but also introduced aldehydes via oxidation reactions [4]. The vicinal glycols in many saccharides and polysaccharides can be oxidised by periodate to form dialdehyde derivatives, which serve as crosslinkers to bridge chitosan chains via imine bonds [77]. A wide range of polyols (such as glucose [78], dextran [79], alginate [80], hyaluronic acid [81], and methylcellulose [82]) has been used to obtain dialdehyde structures and react with -NH_2 groups of chitosan to form hydrogels.

Another approach to obtain aldehyde structures is to graft small molecule aldehydes at the end of a polymer to form covalent bonds with chitosan. For instance, PEG was modified to form

dibenzaldehyde-terminated telechelic PEG which can form Schiff base linkages with chitosan [83]. The developed hydrogels exhibited multiple responsive behaviours (sensitive to pH, amino acids, and vitamin B6 derivatives), self-healing ability, and enzymatic degradability.

2.1.2.2 Amide bonds

Amide bonds (-N-C(=O)-) are formed between carboxyl groups (-COOH) of esterifying agents (such as carboxylic acids and carboxylic acid derivatives) and -NH_2 groups of chitosan. Amide bonds have been utilised as hydrogels' backbone in several systems, such as chitosan-gallic acid for antioxidant activity of hydrogel lens [84], methoxy-grafted-PEG and chitosan [85], and nanocomposite hydrogels of hexamethylene-1,6-di-(aminocarboxysulfonate) and chitosan [86]. Poly (L-glutamic acid) possesses carboxyl groups which can form amide bonds with -NH_2 groups of chitosan, resulting in porous, biocompatible, and biodegradable hydrogels for cartilage tissue engineering [87].

2.1.2.3 Heterocyclic amine and secondary amine bonds

Opposed to other covalent crosslinkers, genipin, a natural derived product extracted from *Gardenia jasminoides* Ellis is a desirable crosslinker for use in biomedical applications due to its well-reported low toxicity and good biocompatibility [88, 89]. The network formed by genipin and chitosan is found to correlate with the development of secondary amide and heterocyclic amine ring-stretching. The crosslinking mechanism will be discussed further in Section 2.2.

Additionally, secondary amine bonds (R-NH-R') can also be formed between ether groups (-R-O-R') of etherifying agents (such as organochlorine and epoxide compounds) and amino radicals on chitosan chains. Several studies have employed secondary amine bonds to produce stable chitosan hydrogels, such as chitosan hydrogels crosslinked by diglycidyl ether-terminated PEG [90], trimethylolpropane triglycidyl ether [91], and 1,4-butanediol diglycidyl ether [92].

In summary, chemically crosslinked hydrogels present a stable and irreversible network with enhanced mechanical strength, high level of control in chemical functionalisation, degradation, and dissolution. The release kinetic of entrapped molecules can be modulated with the crosslinking density, which is influenced by crosslinkers' type and concentration, the number of active crosslinking sites, and crosslinking method [4]. However, the residual of initiators and crosslinkers remains a challenge, which might compromise the biocompatibility and the requirement of purification process should be considered.

2.1.3 Interpenetrating hydrogels

To overcome those shortcomings of physical and chemical hydrogels which have been discussed previously, as well as to provide extra layer of control in the diffusion of payload from hydrogels, multi-component networks have been developed. Interpenetrating networks (IPNs) have attracted more attention due to their unique features in drug delivery applications. IPN-based hydrogels are conventionally defined as crosslinked polymers in which two or more separate crosslinked networks are not covalently bound to each other, but partially interlocking such that chemical bonds have to be broken to segregate the components (**Figure 2.3a**) [93]. IPN-based hydrogels are reported to have higher stiffness and improved mechanical properties with preserved stability of microstructural morphology [94]. Alternatively, if one of the components has a linear structure entrenched within the network, it will be called semi-IPN [95]. Basically, the crosslinked network and the linear polymer can be separated from one another while preserving the chemical bonds (**Figure 2.3b**). Therefore, semi-IPNs' responses to changes in pH and temperature are at higher rate compared to IPNs which have immensely interpenetrating elastic structure. Semi-IPNs also enhance the miscibility between polymeric segments. Additionally, semi-IPNs have advantages of tunable pore size, controlled drug release, and enhanced mechanical resistance which are similar to IPNs [96]. Thus, semi-IPNs are deemed as an intuitively appealing approach to surmount the problems arisen from polysaccharide-based hydrogels such as their heterogeneous structures and unstable mechanical properties which can lead to quick erosion and burst release effect. Recently, many IPNs and semi-IPNs based on chitosan have been developed, in which chitosan can combine with either synthetic (such as poly(vinylpyrrolidone) [97], polyvinyl alcohol [98], and (hydroxylethyl)methacrylate [99]) or natural polymers (such as gelatin [100], alginate [101], and dextran [102]).

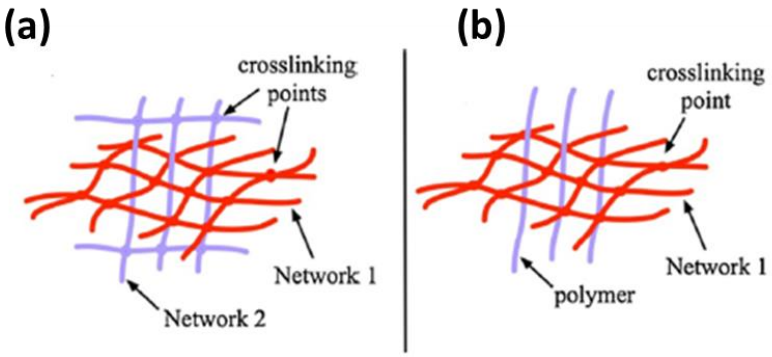

Figure 2.3 Schematic representation of (a) IPNs and (b) semi-IPNs [103].

2.2 Genipin-crosslinked chitosan networks

Pushing towards biocompatible materials fit for purpose, attention is now shifting to bio-safe crosslinkers such as genipin. Genipin is obtained from geniposide (extract from gardenia fruits) via enzymatic hydrolysis with β-glucosidase [104]. In Chinese traditional medicine, genipin is used to treat various diseases, such as pyrogenic infection, febrile disease, sprain, and swelling [105, 106]. As a biologically derived substance, genipin is deemed biocompatible and low toxic based on several studies on its biological functions. Using *in vitro* cultured 3T3 fibroblasts, the cytotoxicity of genipin is found to be 10000 times lower than that of glutaraldehyde [89]. In mice model, a median lethal dose of genipin is 382 mg/kg, which is 1000 times less toxic than glutaraldehyde [107]. Thus, genipin is deemed well-suited for biomedical applications. Genipin contains two active sites, namely C10 primary alcohol and C1 hemiacetal, showing high selectivity towards chitosan as it reacts with only primary amino groups ($-NH_2$) [108] . Based on selective reactivity and good biocompatibility, genipin was chosen as the crosslinker in this project.

2.2.1 Reaction mechanism

The crosslinking mechanism between chitosan and genipin is pH dependent. Under acidic and neutral conditions (pH 5.0 - 7.4), the amino groups at C2 of chitosan molecules initiate nucleophilic attack on the olefinic carbon atom at C3 of genipin, causing the opening of dihydropyran rings, which are subsequently attacked on the newly formed aldehyde groups by the secondary amine formed in the first step of the reaction [109]. Thereby heterocyclic compounds of genipin linked to the glucosamine units of chitosan are formed (**Figure 2.4a**) [15]. These intermediate compounds could further associate to form dimmers, trimers, and tetramers of linked bridges [110], leading to a polymeric network structure (**Figure 2.4b**). In acidic conditions, the presence of acid also improves the nucleophilic substitution of the ester groups on genipin to form a secondary amide with chitosan (**Figure 2.4c**) [111]. However, it is evident that the ring-opening reaction is predominant over nucleophilic substitution on the ester groups of genipin at acidic conditions (pH 5.0) [110].

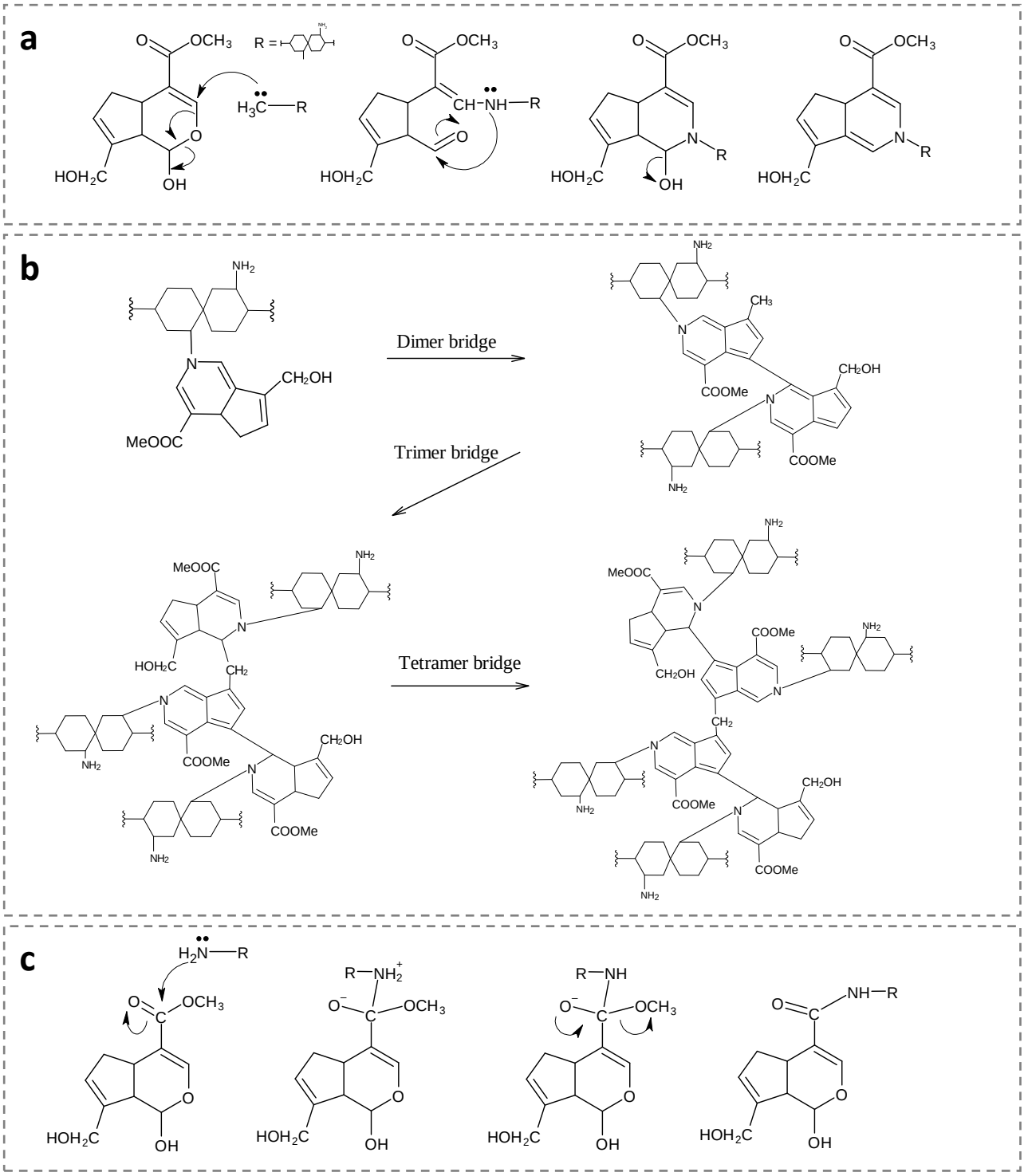

Figure 2.4 Presumed crosslinking mechanism of chitosan and genipin in acidic and neutral conditions: (a) formation of heterocyclic compounds of genipin linked to the glucosamine units of chitosan; (b) formation of linked bridges between these heterocyclic intermediate compounds; (c) the nucleophilic substitution of the ester groups on genipin to form a secondary amide with chitosan [110].

Under strong basic conditions (pH 13.6), the nucleophile -OH^- groups in the aqueous solution attack genipin molecules and open the dihydropyran rings to form aldehyde groups. These ring-opened intermediate can subsequently undergo aldol condensation and polymerise to form macromers (which have MW of 1600 - 20000 and consist of approximately 7 - 88 monomer units) [110]. These polymerised macromers possess terminal aldehyde groups, which can undergo a Schiff-base reaction to form imine bonds with -NH_2 groups of chitosan (**Figure 2.5**).

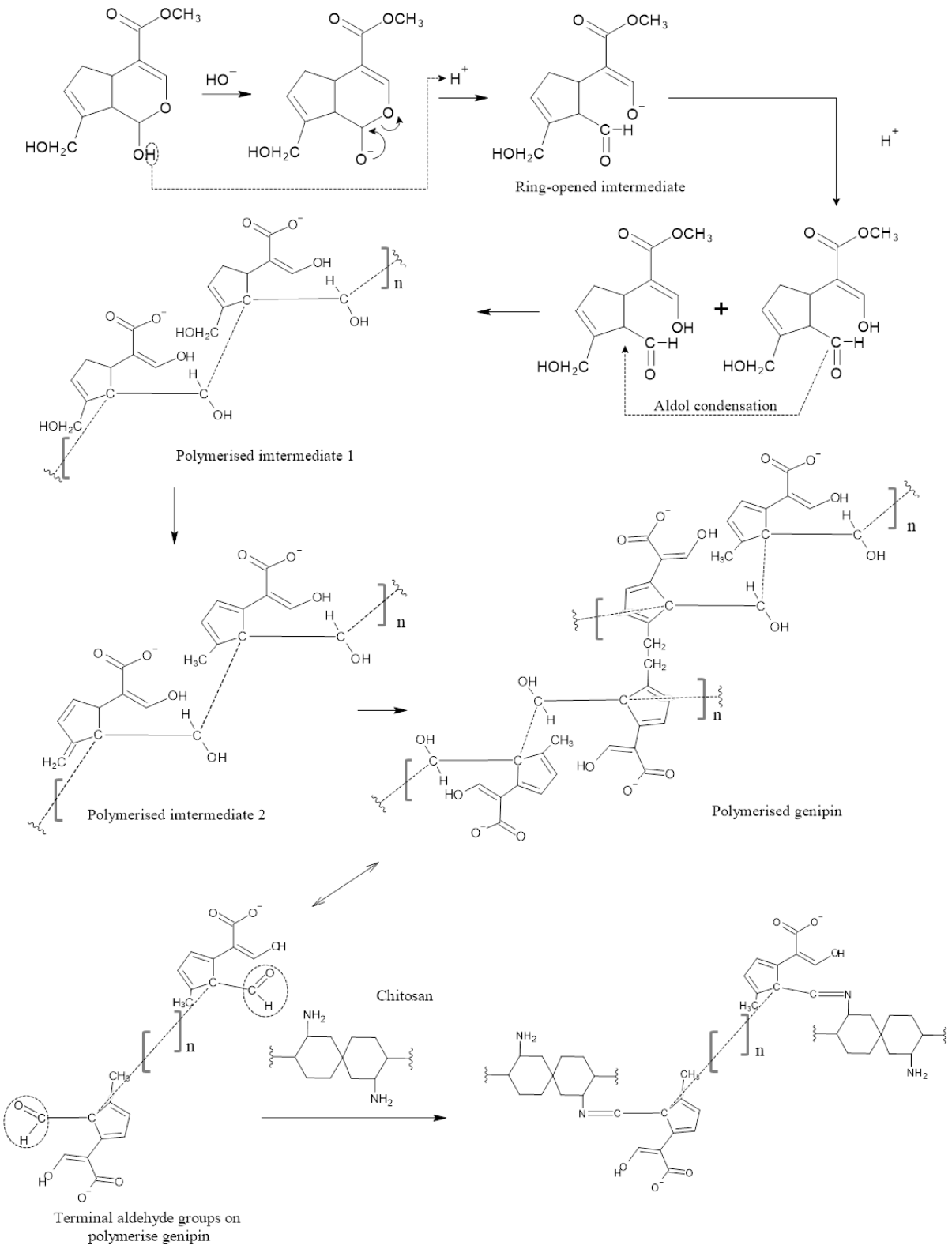

Figure 2.5 Presumed mechanism of polymerisation of genipin molecules and crosslinking mechanism of chitosan and genipin at strong basic conditions [110].

In summary, chitosan hydrogels crosslinked by genipin under acidic and neutral conditions (pH 5.0 - 7.4) consist of only short crosslinked bridges of associated heterocyclic amine (1 - 4 units) while the hydrogel networks prepared under strong basic conditions (pH 13.6) consist of only long crosslinked bridges of polymerised genipin (7 - 88 units). When crosslinking occurs at pH 9.0, the network segments contain both short crosslinked units of cyclic bridges and long crosslinked units of polymerised genipin.

The crosslinking reaction between chitosan and genipin is found to generate a blue-coloured and fluorescent product with pH-responsive behaviours. Genipin can also form blue pigments with primary amine-containing compounds such as glucosamine, bovine serum albumin, and gelatin [111]. It is evident that once the heterocyclic compounds linked to polymeric units have formed, the oxygen radical-induced polymerisation of genipin and dehydrogenation of intermediate compounds occur and cause the gel to assume a blue colour in the presence of air [108, 112]. The fluorescence behaviour of the crosslinked gels is a result of the π-π^* conjugation present in large conjugated system formed by chitosan-genipin reaction (as shown in **Figure 2.4**) [109]. The smart pH-responsive feature of chitosan-genipin hydrogels stems from the presence of free amino groups on chitosan chains, which can sense the environment and respond accordingly causing the network to swell or collapse. Detailed swelling/de-swelling mechanisms of chitosan-genipin hydrogels are discussed further in Section 2.3.1.

2.2.2 Chitosan-genipin hydrogels in the form of monolithic bulk network

The development of stable chitosan-based hydrogels with good biocompatibility and tuneable properties has been expanded with the use of genipin. To overcome those aforementioned shortcomings of physical and chemical hydrogels, as well as to add extra layer of control in the diffusion of payload from hydrogels, multi-component networks have been developed. By utilising chitosan-genipin crosslinked network as a polymeric backbone, hybrid systems can be achieved by addition of another synthetic/natural polymers or particulate systems. While not in a vast number, notable studies have reported several pH-responsive hydrogels based on chitosan-genipin crosslinking with promising properties in drug delivery applications (**Table 2.1**).

Table 2.1 Reported studies of hydrogels based on chitosan-genipin (CS-GEN) crosslinked network and their specific properties.

Types of hydrogels	Hydrogel formulations (including CS-GEN)	Functional properties	Ref.
CS-GEN only	-	Wound dressing materials with aqueous solution uptake capacity of 230%, hindering *E.coli* growth by 70%, *in vitro* biocompatible to fibroblasts and keratinocyte cells.	[113]
	-	Controlled and sustained release of tetracycline.	[114]
CS-GEN + another crosslinker	β-glycerol phosphate	Simultaneous *in situ* physical and covalent crosslinking with pH- and temperature-responsive behaviours. Controlled delivery of diclofenac.	[115]
CS-GEN + natural polymer	gelatin	pH-sensitive semi-IPNs, uniform distribution of metformin in hydrogel matrix with a controlled release in pH 1.2.	[116]
	gelatin + β-glycerol phosphate	Double crosslinking *in situ* with pH- and temperature-responsive behaviours. Topical eye drop formulation for sustained release of timolol maleate.	[117]
	silk fibroin	Promoting adhesion, proliferation, and matrix production of chondrocyte-like cells.	[118]
	bacterial cellulose	pH-sensitive semi-IPNs. Controlled release of quetiapine fumarate.	[119]
	collagen + tannic acid	Simultaneous physical and covalent crosslinking using two naturally derived crosslinkers, with potential applications in ophthalmology as an implant for temporary injured cornea.	[120]
CS-GEN + synthetic polymer	Poly vinyl alcohol	Optimal genipin concentration was determined as 0.25 mM. Controlled release of ibuprofen, suitable for use as pain suppressing wound dressing materials.	[121]
	Poly vinyl pyrrolidone (PVP)	pH-sensitive semi-IPNs, post-synthesis treatment (freeze-thawing) is found to affect on stability.	[122]

CS-GEN + particulate system	cellulose nanocrystals	Cellulose nanocrystals provided higher stiffness to hydrogels structure while decreasing the swelling degree.	[123]
	Silver sulfadiazine nanocrystals	Encapsulation of nanocrystals reduced their cytotoxicity, sustained the release, and remained high antibacterial activity.	[124]
	Upper layer: CS-GEN + Silver nanoparticles Lower layer: CS-GEN + partially oxidised Bletilla striata polysaccharide	Bilayer systems for wound dressing. The lower layer reduced gelling time, showed more uniform aperture distribution, higher water retention and mechanical strength.	[125]
Modified CS-GEN	Carboxylmethyl-hexanoyl CS-GEN	Amphipathic hydrogels with excellent water-absorption and water-retention ability under neutral conditions. Controlled release of ibuprofen, suitable for delivery of amphipathic agents.	[126]
	Lactose-modified CS-GEN	The developed hydrogels displayed hydrophobic domains.	
Modified CS-GEN + natural/ synthetic polymers	N,O-carboxylmethyl CS-GEN + alginate	Site-specific delivery of BSA into the intestine (the release of BSA was low at pH 1.2 but significantly increased at pH 7.4).	[13]
	N,O-carboxylmethyl CS-GEN + Poloxamer 407	A hybrid dual-sensitive hydrogel (pH and temperature) carrying baicalin (an ophthalmic anti-inflammatory drug) loaded in nanosized lipid carrier.	[127]

In those studies listed in **Table 2.1**, the hydrogels are found to respond to changes in pH of surrounding environments and subsequently release the entrapped biomolecules. Thus, there is a need of appropriate external stimuli to trigger the conformation changes in those hydrogels, implying that intervention is required on a high frequency basis to maintain this smart response throughout the lifetime of the systems. The concept of self-oscillating hydrogels is of growing interest, as pH-responsive hydrogels can be chemically coupled with an oscillatory chemical reaction which can produce oscillations in pH inside the smart gels and work as an internal driving force to trigger the smart response [39]. With several coupled architectures exist [128-130], the development of pH-controlled pulsed drug release based on chemical oscillators is still at its early stage. Acknowledging the potential of self-oscillating hydrogels for optimal drug delivery, the group led by Dr. Katarina Novakovic at Newcastle University has studied extensively this concept based on chitosan hydrogels and palladium-catalysed phenylacetylene oxidative carbonylation (PCPOC) reaction [131-133]. The PCPOC reaction is found to exhibit redox potential and pH oscillations in a simple conversion of an alkyne (phenylacetylene) into several products under constant supply of carbon monoxide gas [134]. Recently, Novakovic et al. showed, for the first time, the use of a polymeric substrate (monoalkyne-terminated PEG) in place of phenylacetylene to produce oscillations in pH while employing one hundred time less substrate and catalyst compared to the oscillations employing phenylacetylene [135]. This striking finding indicates the feasibility of an 'all-polymeric' system where all the components (substrate, catalyst, and smart gels) are combined within a single macromolecule. In parallel to developing and optimising oscillatory chemical processes, it is crucial to enhance understanding of the hydrogel formulation and its related properties for a smooth transition to an autonomous rhythmic system. Therefore, addition of a linear PEG polymer to chitosan-genipin networks to form semi-IPN hydrogels is the first step towards self-oscillating hydrogels based on PCPOC reaction.

2.2.3 Chitosan-genipin hydrogels in the form of microparticles

As a biocompatible and biodegradable polymer, chitosan has been widely explored in the formulation of particulate drug delivery systems, particularly in the form of microparticles (MPs). Microparticle network can provide controlled release of entrapped molecules, improve the bioavailability of fragile substances, and improve the uptake of hydrophilic substances across the epithelial layers [136]. Owing to its cationic nature, chitosan-based MPs can induce a strong interaction with anionic glycosaminoglycan receptors and prolong their retention at the target site of capillary region [137]. Different methods have been utilised to prepare chitosan-based MPs,

including emulsion crosslinking, precipitation, complex-coacervation, and spray-drying. The hydrogel network can be formed via physical (interaction with anions) or chemical crosslinking as discussed above.

In the case of chemical crosslinking using genipin, emulsification is the most commonly used method to produce stable MPs [27]. Generally, in the emulsion crosslinking method, chitosan solution is first prepared in acidic solution. This solution is then added dropwise to an oil phase (such as liquid paraffin, mineral oil, ethyl acetate, or olive oil) containing a suitable surfactant (to stabilise the chitosan droplets). A crosslinker is then added to the stable water-in-oil emulsion to solidify the polymeric droplets. The established MPs are then filtered, washed thoroughly with organic solvents (n-hexane and ethanol) to remove the excess oil, and then dried. The desirable particle size range can be obtained by tuning the concentration of the crosslinker and the extent of stirring (time and speed). The fabrication process occurs in a simple and mild setting, suitable for developing proof-of-concept materials in laboratory. However, the process poses several challenges that require further optimisation, including the complete removal of auxiliary compounds (such as oil, surfactant, and organic solvents) and unreacted crosslinkers, unwanted interaction between crosslinker and entrapped drugs/stabilisers, and potential leakage of payload during emulsification [136]. To date, several drug delivery systems based on chitosan-genipin MPs have been developed (**Table 2.2**), showing great potential for various biomedical applications.

Table 2.2 Reported studies of drug delivery systems based on chitosan-genipin (CS-GEN) microparticles.

Hydrogel formulations	Preparation methods	Loaded biomolecules	Ref.
CS-GEN	Emulsion crosslinking	Indomethacin	[138]
CS-GEN	Emulsion crosslinking	Flurbiprofen	[139]
CS-GEN	Emulsion crosslinking	BSA	[140]
CS-GEN	Emulsion crosslinking	Clarithromycin, Tramadol and Heparin	[141]
CS-GEN	Emulsion crosslinking	Mesalamine	[142]
CS-GEN	Spray drying	Levofloxacin	[143]
CS-GEN-TPP	Reverse emulsion and ionic gelation	Sonic Hedgehog	[144]
CS-GEN-alginate	Emulsion crosslinking	Fluorescein	[145]
CS-GEN-gelatin	Emulsion crosslinking	Methylene blue	[146]
CS-GEN-carboxylmethyl cellulose	Emulsion crosslinking	Probiotic	[147]
CS-GEN-ethyl cellulose	Spray drying	Rifabutin	[148]
CS-GEN-silk fibroin	Emulsion crosslinking	BSA	[149]
Quaternised CS-GEN	Reverse emulsion	Heparin	[150]
Stearic acid-grafted CS-GEN	Ion precipitation	BSA	[151]
β-cyclodextrin-grafted CS-GEN	Spray drying	BSA	[152]

2.3 Key characteristics of chitosan-based hydrogels

2.3.1 Swelling/de-swelling properties

One of the most favourable characteristics of chitosan hydrogels is the ability to change their conformation (swell/shrink) once in contact with solvent. Swelling is considered as a process in which, un-solvated glassy or partially rubbery state is transformed to a relaxed rubbery state [153]. When a hydrogel is in initial contact with a bio-fluid, the solvent molecules attack the hydrogel surface and diffuse into the polymeric network. The polymeric chains start relaxing to allow more solvent molecules penetrating into the network, which induces the unswollen-swollen boundary between the un-solvated glassy phase and the relaxed rubbery phase [154]. Against the favourable osmotic force which induces swelling, there is an opposite elasticity force which balances the stretching of the network and prevents its deformation. When these two forces are balanced, the

equilibrium swelling state is achieved (no changes in swelling ratio are further recorded) [154]. The mechanisms of solute transport within the network can be classified based on the two main processes (the solvent diffusion and polymeric chain relaxation) which govern the phase transition from unswollen to swollen state [153]. In Fickian (or Case I) transport, the polymeric chains have high mobility, and the water penetrates easily in the hydrated network. The solvent diffusion rate is obviously slower than the polymer relaxation rate, and thus the glassy-rubbery transition is diffusion-controlled. In a polymer slab, Fickian transport is characterised by a linear relationship between the increase in hydrogels' mass and the square root of experimental time. It asymptotically approaches a fixed equilibrium swelling value [154]. In non-Fickian transport, the polymer chains have restricted mobility which does not allow fast diffusion of solvent into the network. Depending on the relative rates of chain relaxation and diffusion, non-Fickian transport is further sub-classified into Case II transport and anomalous transport. In Case II transport, the transition mechanism is a relaxation-controlled process in which the diffusion rate is very fast and unobservable while the chain relaxation occurs slowly at an observable rate. Hence, the rate of increase in mass is directly proportional to time. In anomalous transport, the solvent diffusion and chain relaxation rates are comparable. The ability of changing its swelling degree in response to changes in environmental pH is the most important feature of pH-sensitive hydrogels, which derives this type of smart hydrogels into 2 groups, cationic hydrogels and anionic hydrogels.

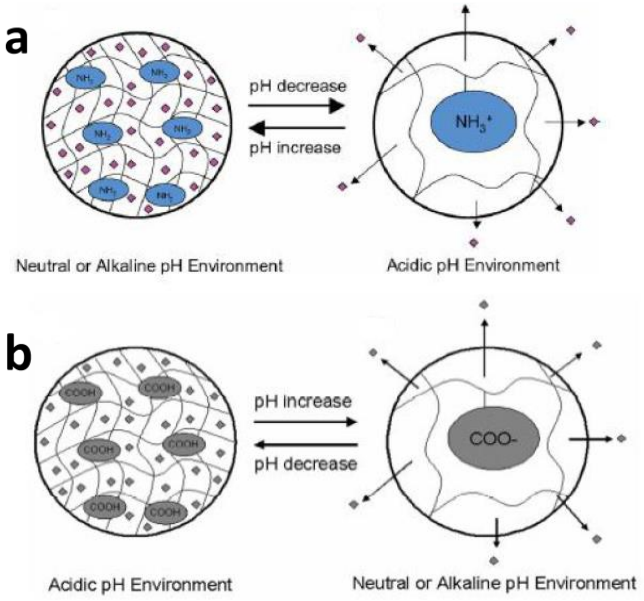

Figure 2.6 Schematic representation of (a) cationic hydrogels and (b) anionic hydrogels [155].

The polymers with functional basic groups (such as chitosan with -NH_2 groups) are known as polybases or polycations (**Figure 2.6a**). At pH lower than their associated pKa, these amino groups receive protons (so-called protonation) and carry positive charge leading to the increased electrostatic repulsion within the network. As a result, the polymer chain relaxation occurs and the network starts expanding in its volume until reaching the equilibrium state. Alternatively, at high pH, the hydrogel contraction occurs due to the decreased electrostatic repulsion. The polymers with functional acid groups (such as poly (acrylic acid) with -COOH groups) are known as polyacids or polyanions (**Figure 2.6b**). The swelling of hydrogels made up with these polymer increases at pH > pKa and decreases at pH < pKa. The pH-sensitive swelling of smart hydrogels can be explored to achieve targeted delivery of biomolecules by modulating their swelling behaviours according to the pH range at intended target sites. Generally, the swelling of hydrogels is mainly influenced by hydrogel composition (such as polymer MW, presence of hydrophobic monomers, and amount of crosslinkers), preparation conditions (such as heating time, radiation dose, and applied electric field), type of solvents, and addition of electrolyte/surfactant in the solvent [154].

The swelling ratio can be determined by various techniques ranging from macroscale to microscale. In macroscale, the degree of swelling can be evaluated by observing the variation in mass (weight) or volume (surface area and height) over time. A simple and commonly used formula (**Equation 2.1**) can be applied to calculate swelling degree.

$$Swelling\ (\%) = \frac{m_t - m_o}{m_o} \times 100 \quad \textbf{(Equation 2.1)}$$

where m_t is the weight of swollen hydrogel and m_o is the weight of un-solvated hydrogel.

In microscale, the degree of swelling can be determined by the extent of porosity. As the hydrogels swell, the mesh size starts expanding as a result of solvent diffusion and chain relaxation. The expanding or collapsing of these porous structures can be measured through a range of experimental techniques or calculated by application of network deformation theories [156]. Micro-eletromechanical systems can also be used to evaluate the swelling degree. For instance, by observing the deflection length of a microcantilever, information about mechanical amplification of a signal due to change in the surface properties can be achieved [157]. It is of high importance to investigate more aspects of swelling behaviours of hydrogels as it is crucial for designing controlled drug delivery where drug is released in the desired amount and for the desired time at intended sites in human body.

2.3.2 Network structure

Generally, there are three important parameters defining the hydrogel structure including the polymer volume fraction in the swollen state, $\nu_{2,s}$, the effective MW of the polymer chain between crosslinking point, $\overline{M_c}$, and the correlation distance between two adjacent crosslinks (mesh size), ξ (**Figure 2.7a**) [153]

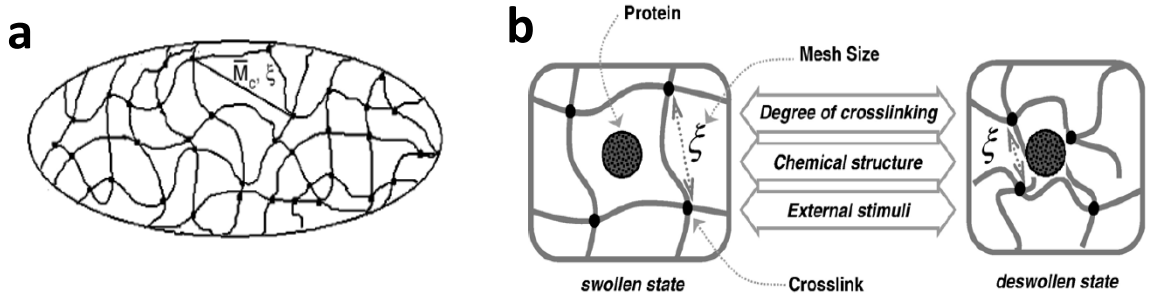

Figure 2.7 Schematic representation of (a) crosslinked structure of hydrogels and (b) mesh size of hydrogels in swollen and de-swollen states [153, 158].

The polymer volume fraction in the swollen state, $\nu_{2,s}$, is an important parameter to describe the water-sorption capability. It represents the amount of liquid that can be imbibed in hydrogels and is expressed as a ratio of the polymer volume (V_p) to the swollen gel volume (V_g) or as a reciprocal of the volumetric swollen ratio (Q) (**Equation 2.2**).

$$\nu_{2,s} = \frac{V_p}{V_g} = \frac{1}{Q} = \frac{\frac{1}{\rho_2}}{\frac{Qm}{\rho_1}+\frac{1}{\rho_2}} \qquad \textbf{(Equation 2.2)}$$

where ρ_1 is the density of solvent, ρ_2 is the density of polymer, and Q_m is the mass swollen ratio.

The effective MW of polymer chain between crosslinking point, $\overline{M_c}$ is related to the degree of crosslinking of the hydrogel network, which can be expressed by Flory-Rehner equation [158]. The correlation distance between sequential crosslinking points, ξ, also known as mesh (pore) size, represents an estimate of accessible spaces between polymeric chains for biomolecules diffusion. It can be calculated from **Equation 2.3**.

$$\xi = {\nu_{2,s}}^{-1/3} \times l \times \left(\frac{C_n.2\,\overline{M_c}}{M_r}\right)^{1/2} \textbf{(Equation 2.3)}$$

where C_n is a constant Flory characteristic ratio for a given polymer-solvent system, l is the carbon-carbon bond length, and M_r is the weight of repeating units from which the polymer chain is composed [153, 159]. The pore size is mainly influenced by the degree of crosslinking, chemical

structure of polymeric network, and external stimuli (such as pH, temperature, or ionic strength) (**Figure 2.7b**) [158]. The porosity is an important indicative parameter as it is highly related to swelling ability, drug loading ability, and mechanical attributes of hydrogels. For instance, a gel with high porosity will exhibit higher responsiveness to changes in surrounding environments but it is more likely to have low mechanical strength and that may limit its future applications. Understanding the microstructure of hydrogel network is the first step towards designing controlled release system where the rate and extent of gel swelling can be tailored to deliver biomolecules efficiently.

Several imaging techniques have been employed to elucidate the hydrogel structure. Scanning electron microscopy (SEM) is a well-known technique to study the morphology of hydrogels in their dry states [160]. The outer surface and cross section of the hydrogel can provide the information about the number and size of pores as well as the channels and pore arrangements within the network. SEM provides the images by scanning the structure with a focused beam of electrons. The electron interacts with the surface of samples in a raster scan pattern and the reflection beam is combined with the secondary signal from samples that can be converted and amplified to voltages [161]. By using a special detector, the brightness from signal intensity is determined and an image displaying the topography is created. Alternatively, environmental scanning electron microscopy (ESEM) can be used to observe the structure porosity in solvated states. Therefore, wet, oily, non-conductive, and unclean samples can be analysed in their native states without any further modification required as the contaminants do not affect the quality of images [162]. However, the hydrogels cannot be placed in liquid during the analysis and the details are more difficult to elucidate in their solvated state. Confocal laser scanning microscopy (CLSM) has emerged as a promising technique to investigate the morphological properties of hydrogels while the gels are immersed in the solvent. In CLSM, a specialised light microscope is used in which a laser beam is scanned across the samples and the images are collected via computer control [163]. The main advantage of CLSM over conventional light microscope is that it focuses into a small area of the sample or in other words, it works on a narrow depth of field which is as small as 0.4 mm. The ability to control depth of field, elimination or reduction of background effects, and the capability to collect serial optical sections from thick specimens are the superior properties of CLSM that make it an invaluable tool for advanced biomedical sciences [164]. Other advantages of CLSM that are worth noticing are the fine details resolved from its images (100 nm), the fast image collection, the preview option before saving, and the reduced chemical waste. The atomic

force microscopy (AFM) is a helpful probe microscope which can reveal the surface topography of hydrogel either in contact mode or in tapping mode. AFM is operated by scanning the probe over small areas of samples and the forces between probe and samples are recorded [165]. AFM can provide the three-dimensional (3D) images of specimens without any specific modification before the analysis. While SEM is operated in an expensive vacuum environment, AFM is mostly operated in ambient atmosphere or even a liquid environment. Basically, images from AFM can show higher resolution and contrast than those obtained from SEM.

2.3.3 Molecule loading and release mechanisms

2.3.3.1 Drug loading methods

As reviewed previously (Section 2.2), number of studies have employed the superior advantages of chitosan-based hydrogels for drug delivery applications. The diversity in chemical and physical properties of entrapped molecules results in different methods of loading drugs. Owing to their hydrophilic nature, hydrogels are a great platform to incorporate highly water-soluble drugs. The way drugs are loaded into hydrogel matrix will directly affect the availability of drugs for the release from the formulation. The simplest method to directly incorporate drugs into hydrogel matrix is by immersing the fully formed hydrogel into the medium containing therapeutic agents (**Figure 2.8a**) [166]. Drug uptake occurs slowly under the driving force of diffusion depending on the porosity of hydrogel, physical and chemical properties of drugs and hydrogel [34]. This way is particularly effective for hydrophilic drugs and less likely to cause drug deactivation. Larger molecules (such as peptides and proteins) are not able to diffuse freely through the small pores [167]. Drug release duration lasts for hours to days and is determined by diffusion and/or swelling mechanisms. The loading process may take a long time to complete and the exact amount of drugs loading into the hydrogel is difficult to elucidate the details [95].

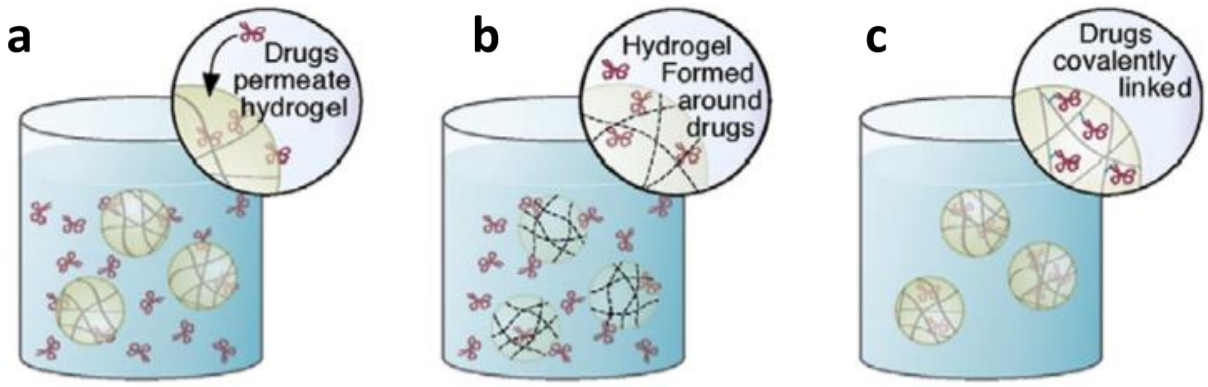

Figure 2.8 Schematic representation of three different loading methods which can be applied for chitosan-based hydrogels: (a) permeation; (b) entrapment; (c) covalent bonding [34].

Another approach is allowing the encapsulation and gelation to occur at the same time (**Figure 2.8b**). Drugs are mixed with polymeric precursors and suitable crosslinker/s, initiators are added to form drug-loaded hydrogel [158]. The entrapment process allows the incorporation of heavier payload into hydrogel network (such as peptides and proteins) and release duration may last for days to weeks. While the diffusion is not applicable in the case of *in situ* gelling process, the entrapment is effective to deliver drugs *in situ* by mixing drugs with one of the polymeric precursors prior to administration and once administered, gelation occurs at the same time with encapsulation process [65]. However, it is required to carefully take into account the chemical properties of entrapped drugs to avoid drug deactivation and undesirable crosslinking between drugs and polymers and/or crosslinkers. Both entrapment and diffusion, allowing the free movement of loaded drugs out of the network, may lead to the initial burst release *in vivo* [168].

To limit the loss of therapeutic agents via burst release and reduce the risk of toxic exposure, tethering method can be applied in which drugs can be covalently bonded to the polymer chains via physical or chemical crosslinking prior to gelation. Physical attachment is achieved by charge interaction between ionic polymers and charged drugs or anionic and cationic functional groups in carbohydrate-based polymers (**Figure 2.8c**) [103]. The chemically attached drugs will be released either due to the network degradation or due to the chemical cleaving of the polymer-drug bonding. If the bond is susceptible to environmental enzyme, a smart hydrogel-based drug delivery is favourable as its drug release is more specific to the target site [169]. The release duration may be extended from weeks to months. One challenge when using this method is the high chance of drug deactivation during the covalent bonding with polymer.

Owing to their hydrophilic nature, formulations of hydrogel-based system for delivery of hydrophobic drug remain a challenge. This challenge has two-fold including how to load drug into the hydrogel matrix and how to release the drug into aqueous solution. With the advances in engineering and technology, several effective solutions have been developed to expand the range of drug amenable for hydrogel-based delivery. The most frequently used approach is co-formulating particulate systems (such as microsphere, liposome, microparticles, microemulsion droplets, surfactant-micelles, and polymeric micelles) into the hydrogel matrix to form composite hydrogels [103]. The hydrophilic nature of hydrogel provides the composite with excellent biocompatibility while the hydrogel matrix acts as a membrane to protect the particles from premature degradation and clearance effect at target sites *in vivo*. By incorporating drug-loaded particles into the polymeric mesh, a prolonged drug delivery may be achieved. The loaded particles may be slowly released from hydrogel matrix followed by the release of entrapped drug from the particles. In other way, the drug will be released from particles and subsequently diffused through the hydrogel pores. In some cases, drug dissolution is a combination of both mechanisms [71]. Another common approach is presenting more hydrophobic domains within the polymeric backbone. This can be done by copolymerising with hydrophobic monomers or grafting techniques to introduce constitutional or configurational features that differ from those in the main chains [170]. For instance, chitosan-based micelles bearing a small amount of highly hydrophobic groups were obtained by N-acylation of chitosan with hydrophobic fatty acid chains (stearoyl, octanoyl, and palmitoyl), showing the ability of self-aggregation in water to form nanoparticles and carry hydrophobic molecules [171]. N-alkylation of chitosan (such as N-lauryl-N-methylene phosphonic chitosan) also presents both hydrophobic and hydrophilic branches in its structure [172]. The simplicity and versatility of chitosan in functionalising into different derivatives offer feasible ways to expand the range of drugs amenable for hydrogel-based delivery.

2.3.3.2 Drug release mechanisms

The physical and chemical properties of hydrogels and the chosen loading method will affect the mechanism by which the encapsulated drug is released from the polymeric network. Researchers have focused to manipulate key factors that govern the drug delivery to accurately predict the entire release patterns. There are three different modes by which the release of loaded drug is facilitated including diffusion-controlled release, swelling-controlled release, and chemically-controlled release. In diffusion-controlled release, the release rate is mainly affected by the solvent diffusion into the network, which leads to the dissociation of drug and subsequently diffusion of the dissolved

drug from the region of high concentration (inside the hydrogel) to a region of low concentration (outside the hydrogel) [173]. The drug can be uniformly dispersed in a hydrogel network (matrix device) or can be placed in a core entrapped within a hydrogel membrane (reservoir device). In swelling-controlled release, drug is dispersed within a polymeric network which starts swelling once in contact with solvents. The relaxation of polymer chains allows the system to expand beyond its boundary leading to the diffusion of drugs. The concentration gradient between the hydrogel and surrounding solutions permits the movement of the loaded drug. Chemically-controlled release can be further categorised as kinetic-controlled release where the system is degraded to release drug and the diffusion term can be negligible, and reaction-diffusion-controlled release where the diffusion term and the interaction between polymer and drug must be covered to accurately predict the drug release [158].

To describe the release profiles of drug from polymeric networks, there are several kinetic models that can be applied, such as zero-order model, first-order model, Higuchi model, and Korsmeyer-Peppas (**Table 2.3**). By fitting the experimental data into various kinetic models, the release pattern of drug from a dosage form could be better understood, enabling the design of an effective formulation.

Table 2.3 Kinetic models of drug release from controlled drug delivery systems.

Kinetic models	Equations	Release patterns
Zero order [174]	$Q_t = Q_0 + K_0 t$	- Release rate is constant (concentration-independent) over time - Data plot: cumulative drug release versus time (the slope gives the value of K)
First order [175]	$Log\ C_t = Log\ C_0 - Kt/2.303$	- Release rate is concentration-dependent - Data plot: log cumulative of % drug remaining versus time (the slope gives the value of -K/2.303)
Higuchi [176]	$Q = A\ [D\ (2C - C_s)C_s t]^2$ Simplified as: $Q = K_H t^{1/2}$	- The simplified model describes Fickian transport. - Data plot: cumulative of % drug release versus square root of time (the slope gives the value of K_H)
Korsmeyer-Peppas [177]	$M_t/M_\infty = k \times t^n$	- Use only first 60% of drug release data - For a cylindrical polymeric network: n = 0.45 → Fickian transport (diffusion-controlled release) n = 0.89 → Case II transport (swelling-controlled release) 0.45 < n < 0.89 → Anomalous transport - Data plot: log cumulative of % drug release versus log time (the slope gives the value of n while the intercept gives the value of log k)

where: Q_t = amount of drug released at time t
Q_0 = initial amount of drug in solution
K_0 = the zero-order release constant (unit: concentration/time)
C_t = concentration of drug in solution at time t
C_0 = initial drug concentration
K = the first order rate constant (unit: time^{-1})
Q = amount of drug released in time t per unit area A
C = initial drug concentration
C_s = drug solubility in the medium
D = diffusion coefficient of drug in the matrix
K_H = Higuchi dissolution constant (unit: time^{-1})
M_t = the amount of drug released up to any time t
M_∞ = the total amount of drug release
k = a structural/geometric release rate constant for a particular system (unit: time^{-1})
n = release exponent representing the release mechanism

2.3.4 Gelation kinetics and mechanical properties

To elucidate the mechanical properties of a material, deformation behaviours should be studied. When a specimen is subjected to an external force (such as tensile force, compressive force, or shear force), an internal force is created across the specimen which is called stress [178]. The intensity of stress, σ (N/m^2 or Pa), is calculated by **Equation 2.4**, where F is the external force (N) applied on a deformation area (A_0, m^2). The stress value (or intensity of stress) gives information about how strong the material is, i.e. how much force is required to cause the sample's deformation.

$$\sigma = \frac{F}{A_0} \qquad \textbf{(Equation 2.4)}$$

Under an applied stress, the deformation/displacement of the material occurs, which is represented by a strain value. Strain, ε, is defined as the deformation per unit length. For example, in tensile test, strain is also known as elongation as the sample becomes longer under applied tensile force. It shows how much changes in length the sample can withstand before it breaks. The strain can be calculated by **Equation 2.5**, where L_o is the original length of the sample and L is the length of the sample after being subjected to stretch. Stress and strain can be plotted to produce information about material modulus which reflects to what extent a material can resist the deformation [179].

$$\varepsilon = \frac{L - L_0}{L_0} \qquad \textbf{(Equation 2.5)}$$

Owing to the substantial amount of water in hydrogel matrix, hydrogels are considered as weak materials with poor mechanical properties limiting the widespread adoption of hydrogels for biomedical purpose [180]. Hydrogels exhibit the behaviours of both liquid and solid at the same time (viscoelastic behaviours), presenting significant challenges to measure and interpret mechanical data. Among common techniques used for mechanical characterisation (such as tensile test, compression test, local indentation, and dynamic mechanical analysis), small-amplitude oscillatory shear rheology (SAOS) is an emerging technique for characterising the mechanical properties of hydrogels as it allows to monitor the phase transition at 'rest' condition without disrupting the structures [181, 182]. It is also quick, sensitive, requires small amount of samples, and effectively provides information about gelation kinetics, crosslinking degree, structural distribution, and mechanical integrity of hydrogels. In the linear oscillatory rheology, a small oscillatory stress is applied to the material and the resulting deformation is measured in the form of strain (**Equation 2.6**).

$$\gamma = A\sin(\omega t) \qquad \textbf{(Equation 2.6)}$$

where γ is the strain, A is the oscillation amplitude, and ω is the oscillation frequency [183]. For a purely elastic material, the stress wave is exactly in phase with the strain wave. For a purely viscous material, the stress wave is exactly 90^0 out-of-phase with the imposed deformation [184]. Elastic behaviour is the ability of materials to restore their original shape once the applied force is removed while viscous (or plastic) materials do not have reversible rearrangement once the applied force is removed. Hydrogels act as a viscoelastic solid, behaving somewhere between these two extremes. Thus, the stress wave will have a phase difference δ ($0 < \delta < 90^0$). The modulus which is in phase with the deformation is called the shear elastic (or storage) modulus G' whereas the modulus which is out-of-phase with the deformation is called the shear viscous (or loss) modulus G''. The complex modulus G^* is then defined by **Equation 2.7**:

$$G^* = (G'^2 + G''^2)^{1/2} \qquad \textbf{(Equation 2.7)}$$

The loss tangent, or tan(δ), which is the ratio G''/G' at a frequency ω, can be used as an indicator for the overall viscoelasticity [181]. As the gelation is a gradual transition from a viscoelastic liquid to a viscoelastic solid, the dynamic rheological measurement can be used to characterise the gelation kinetics. The sol-gel transition point can be determined as a sudden loss of flow when the viscoelastic properties change abruptly from a liquid-like state to a solid-like state [185]. The correct profiles of G', G'', and dynamic viscosity are obtained only in the small strain limit. In other words, the frequency-dependent dynamic shear moduli (G' and G'') must be measured in the linear viscoelastic regime (LVR), where the moduli are independent of the amplitude of the deformation [182]. Oscillatory rheometry can be operated in time, stress/strain, and frequency sweep modes to monitor the viscoelastic properties during crosslinking process and characterise the mechanical properties of resulting hydrogels.

2.3.5 Biocompatibility and biodegradation

2.3.5.1 Biocompatibility

Biocompatibility is the ability of a material to perform with an appropriate host response in a specific application [186]. Biocompatibility is the major determinant for a successful functioning hydrogel, as non-biocompatible systems can induce inflammatory response *in vivo* and limit their uses in living systems. *In vitro* methods are encouraged as preliminary experiments to screen the safety prior to animal testing. *In vitro* studies provide a simple and convenient way to evaluate the cytotoxic effects/inflammation responses on various cell lines before conducting animal experiments. For both qualitative and quantitative assessment of cytotoxicity, the direct contact or

extraction methods can be used [187]. In direct contact, the hydrogel contacts with live host cells for at least 24 h and hence the cytotoxicity is determined. In extraction method, the hydrogel is placed in a suitable solution (such as culture medium with/without serum, physiological saline solution, or dimethyl sulfoxide) for a defined period to allow any leaching of unreacted monomer, oligomers, and crosslinkers. The extract (or its dilution series) is then added to cell culture and incubated for at least 24 h before determining cytotoxicity according to the selected assays. Qualitative evaluation is deemed appropriate for screening purposes as the cells are examined microscopically with/without cytochemical staining. Any changes in general morphology, vacuolization, detachment, cell lysis, and membrane integrity may be graded, indicating levels of reactivity: 0 (none), 1 (slight), 2 (mild), 3 (moderate), and 4 (severe). A grade of higher than 2 is considered as a cytotoxic effect (International Organisation for Standardisation (ISO), 10993-2018). For quantitative evaluation, percentages of cell viability/death can be quantified based on various cell functions such as enzyme activity (such as the reduction of 3-(4,5-dimethylthiazol-2-yl)-2,5-diphenyl tetrazolium bromide (MTT) by enzymes produced from viable cells, **Figure 2.9**), adenosine tri phosphate (ATP)-production, and nucleotide uptake activity (Tritium-labelled thymidine). Generally, reduction of cell viability by more than 30% is considered a cytotoxic effect (ISO, 10993-2018). Another recommended assessment is genotoxic effect, as genotoxicity might eventually lead to abnormal and reduced cell growth, even if the cells initially appear cytocompatible [14]. DNA damage caused by genotoxic effect can be assessed by a number of techniques, such as single-cell gel electrophoresis [188], mutations [189], and chromosome aberration assays [190]. The *in vitro* biocompatibility assessment would be incomplete without testing for an elevated expression of cytokines, which are low molecule weight glycoproteins regulating immunologic responses to inflammatory stimuli. The inflammatory cytokines induced by cell-gel contact can be quantified at both protein level (using enzyme-linked immunosorbent assay (ELISA)) and mRNA level (using reverse transcription polymerase chain reaction (RT-PCR)). There are several factors that need to be considered when planning *in vitro* experiments, such as negative/positive controls, sterilisation, extraction vehicle (polar/non-polar), cell line, and end-point assays.

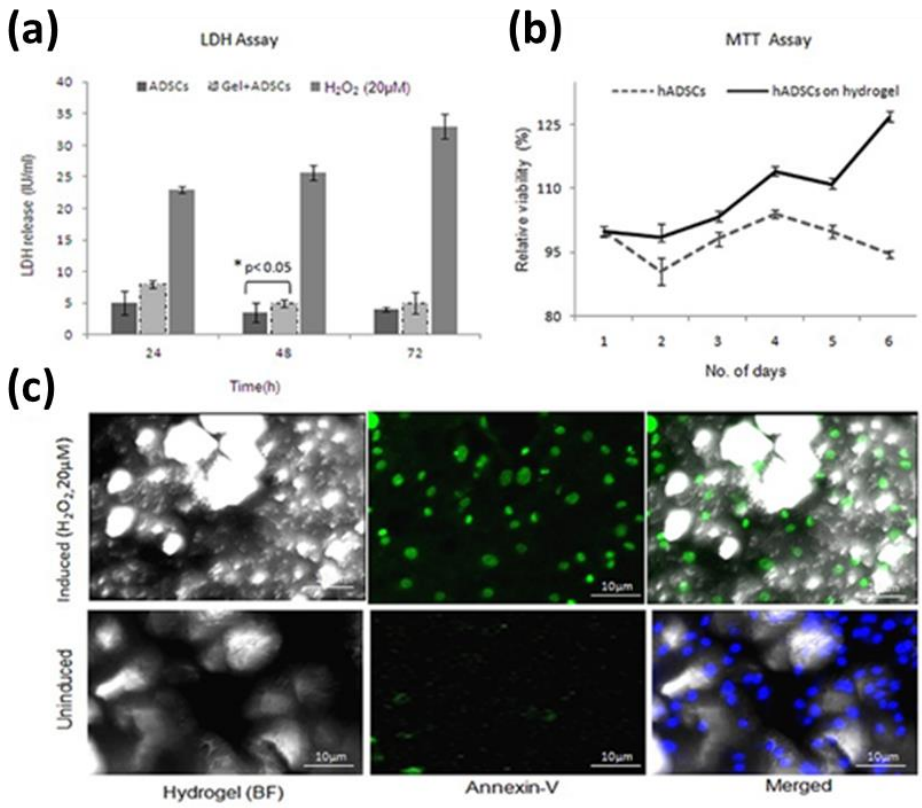

Figure 2.9 Biocompatibility profiles of human adipose-derived stem cells (hADSCs) cultured on glutaraldehyde-crosslinked chitosan-poly (acrylic acid) hydrogels. (a) Lactate dehydrogenase (LDH) was used as an indicator for cytotoxic effect as LDH level released in the supernatant is proportional to the number of lysed cells. (b) Cell viability of hADSCs was evaluated using MTT assay (mean ± standard deviation, n = 3). (c) Apoptosis assays demonstrated that the cells did not undergo apoptosis when cultured on hydrogels. In contrast, cells induced with H_20_2 underwent apoptosis (n = 3) [191].

Owing to the hydrophilicity and soft nature resembling extracellular matrix, hydrogels are deemed biocompatible. Hydrogels composed of chitosan backbone are expected to be biocompatible and biodegradable due to the wide-reported biocompatibility of chitosan. However, chemically crosslinked chitosan hydrogels require the use of crosslinkers, which might bring cytotoxic effect, such as neurotoxicity reported when using glutaraldehyde as a crosslinker for chitosan hydrogels. The biocompatibility profiles of chitosan-genipin hydrogels with or without additional polymer have been reported, showing good cytocompatibility towards various cell lines (**Table 2.4**). Even though the use of a naturally occurring crosslinker, genipin, may ensure good biocompatibility,

there is a need for deeper understanding of the biological performance of genipin crosslinked chitosan hydrogels, especially the inflammatory response.

Table 2.4 Reported *in vitro* biocompatibility studies of hydrogels based on chitosan-genipin (CS-GEN) crosslinked network.

Hydrogel formulations	Testing cells	Main findings	Ref.
CS-GEN film	3T3 fibroblast cells	Gel-exposed cells were 2.29 times more numerous compared to fibroblasts seeded on non-crosslinked chitosan films.	[192]
CS-GEN membrane	Human fibroblast cells	Cell morphology and density on crosslinked membrane were the same as control cells after 3 days incubation.	[193]
CS-GEN membrane	MG63 Human osteoblast-like cells and human mesenchymal stem cells (MSCs)	Gel-exposed cells showed no significant effects on metabolic activity and cell proliferation with respect to control cells within 7 days of incubation.	[194]
CS-GEN film	Retinal pigment epithelial cells	Chitosan-genipin films showed a less level of cytotoxicity and interleukin-6 concentration compared to chitosan-glutaraldehyde films.	[195]
CS-GEN-alginate disc	3T3 fibroblast cells	After 32h incubation, the well was filled with fibroblasts in the vicinity of chitosan disk. The residues (chitosan, alginate, genipin) released from the disc had no toxic effect on the seeded cells.	[196]
CS-GEN-silk sponge	ATDC5 chondrocyte-like cells	Cell viability was around 100% in all sponges.	[118]
CS-GEN-PVP hydrogel	Adult MSCs	The hydrogels were benign to studied cells. Cell proliferation propagated beneath the gel surface via interconnected pores within the hydrogels.	[197]
CS-GEN-collagen film	Rabbit chondrocytes	Gel-exposed cells showed a continuous increase in viability values while the control cells remained unchanged.	[198]

Though *in vitro* tests are being preferred by researchers to provide initial information about biocompatibility of the materials, *in vivo* tests are required as the next step towards getting regulatory approval. *In vivo* studies can be used to evaluate the systemic toxicity of a material upon being administered in animal species. For acute oral, intravenous, dermal, and inhalation studies, mouse or rat is preferable while for implantation, the use of rabbit is encouraged [199]. As the

precision of systemic evaluation depends heavily on the extent of the number of animals used per dose level, the size and number of animal groups can be decided based on the purpose of the study. For example, a minimum of 5 rodent species is required for acute toxicity evaluation while a minimum of 40 rodent species is needed for chronic response (ISO, 10993-2018). The administration route can be chosen based on the most clinically relevant to the use of the device, where possible. Most frequently, hydrogels are subcutaneously implanted [200-202] or injected [203-205] to study the *in vivo* host responses. Maximum dosage volumes vary amongst animal species and testing routes. For example via subcutaneous route, maximum doses in mouse and rabbit are 50 mL/kg and 10 mL/kg, respectively [206]. Upon administration, to detect and measure any adverse systemic effects, regular observations are required, such as piloerection, mobility, abnormal posture, and body weight change. Clinical/gross pathology, organ weights, and histopathology should be performed to investigate toxic effects in tissues, organs, and other systems. As shown in **Table 2.5**, although a limited number of *in vivo* studies have been reported, hydrogels based on chitosan-genipin crosslinking have shown good biocompatibility upon administration, particularly *in situ* forming hydrogels for ocular drug delivery. In addition to synthesis and proof-of-concept *in vitro* studies, it is necessary to provide in-depth *in vivo* characterisation and promote the clinical transitions of these chitosan-genipin hydrogels.

Table 2.5 Reported *in vivo* biocompatibility studies of hydrogels based on chitosan-genipin (CS-GEN) crosslinked network.

Hydrogel formulations	Animal models	Route of administrations	Main findings	Ref.
CS-GEN membrane	Rabbit	Implantation (ocular anterior chamber)	No signs of ocular inflammation were evident. The implants improved the preservation of corneal endothelial cell density and had better anti-inflammatory activities.	[207]
CS-GEN disc	Mice	Subcutaneous implantation	Histologically no visible difference was observed compared to the control.	[114]
CS-GEN microsphere	Rat	Intra-articular injection	No inflammatory infiltrates were observed. Intra-articular delivery of flurbiprofen.	[139]
CS-GEN-gelatin film	Rabbit	Oral	The gels carrying metformin were biocompatible, without signs of haemorrhage, lesion, and changes in tissue structure within the organs. Complete blood analysis showed normal values.	[208]
CS-GEN- β-glycerol phosphate *in situ* forming hydrogel	Mice	Subcutaneous injection of gel solution (dorsal region)	Tissue reaction was favourable with minimal inflammation after 30 days. No foreign body reaction was evident.	[203]
CS-GEN-gelatin- β-glycerol phosphate *in situ* forming hydrogel	Rabbit	Injection of gel solution (subconjunctival space of rabbit eyes)	The gels carrying timolol maleate showed a long-lasting efficacy of intraocular pressure lowering.	[117]
CS-GEN-hyaluronic acid- β-glycerol phosphate *in situ* forming hydrogel	Rats	Subcutaneous injection of gel solution	The gels were formed *in vivo* within a short time and remained localised for over 1 week while the rats remained healthy and active without apparent discomfort.	[209]
CS-GEN-silver sulfadiazine nanocrystals film	Mice	Implantation (burn wound models)	The wounds treated by hydrogels containing nanocrystals showed better healing process compared to the blank hydrogels.	[124]

Catechol-functionalised CS-GEN	Rabbit	Buccal implantation	The gels were compatible without any tissue inflammation. Buccal delivery of lidocaine.	[210]
Glutamate CS- GEN disc	Mice	Subcutaneous injection	No inflammatory reaction was observed.	[211]
N,O-carboxylmethyl CS-GEN *in situ* forming hydrogel	Mice	Injection of gel solution (subconjunctival space of rabbit eyes)	The gels carrying 5-fluorouracil or bevacizumab were non-toxic to the cornea and gradually degraded in the eyes.	[212]
N,O-carboxylmethyl CS-GEN-poloxamer 407 *in situ* forming hydrogel	Rabbit	Ocular administration (drops of gel solution into rabbit eyes)	The gels carrying quercetin increased the precorneal resident time of quercetin (drug concentration was 4.4-fold higher than control group).	[213]

2.3.5.2 Biodegradation

To reach clinical applications, a biomedical system should be non- or low-cytotoxic and enzymatically or hydrolytically degradable [94]. The ability to be degraded inside living bodies eliminates the need of surgical removal of implanted/injected hydrogels and the degradation kinetic is also highly relevant to the release kinetic of entrapped cargo *in vivo*. Previous studies have commonly used the mass loss to monitor the degradation of hydrogels *in vitro* via gravimetric/volume measurements. The initial mass/volume and their changes over incubation time with testing solutions are recorded. As it is an invasive method with loads of intermittent steps, attention is now shifting to fluorescence-related approach, which allows tracking and monitoring degradation in real time and in minimally invasive manner. Fluorescent probes are normally required to label hydrogels, such as fluorescein and Texas Red [214], fluorescein isothiocyanate [215], carbon nanodots [216] (**Figure 2.10**), and tetramethyl rhodamine isothiocyanate [217]. One should consider the potential toxicity of fluorescent markers, photoleaching during incubation and the potential interference with crosslinking reaction.

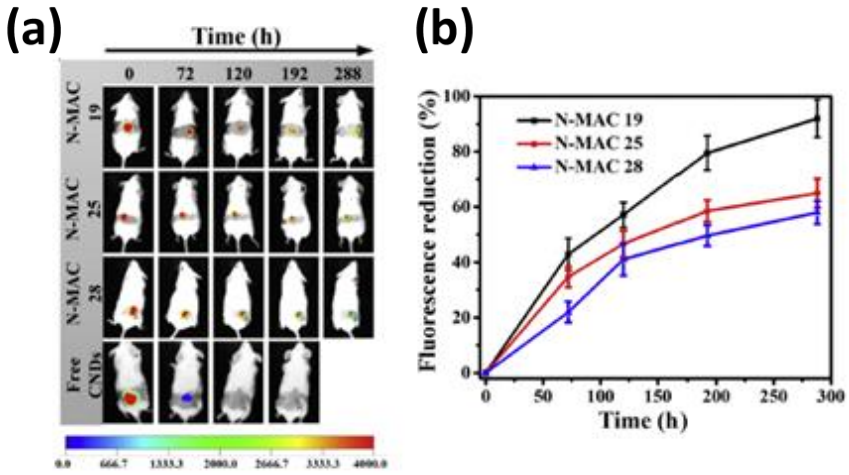

Figure 2.10 Visual *in vivo* degradation of hybrid hydrogels composed of carbon nanodots (CNDs) and N-methacryloyl chitosan by real-time and non-invasive fluorescence tracking. (a) Pseudo-coloured images of the hydrogels upon subcutaneous injection over 288 h, showing a gradual decrease in fluorescence signal in all samples with different rates. (b) Quantitative *in vivo* degradation of CNDs hybrid hydrogels by monitoring fluorescence reduction as a function of time [216].

It is evident that chitosan is degraded in vertebrates mainly by lysozyme and by bacterial enzymes in the colon. The rate and extent of biodegradability are influenced mainly by the DDA of chitosan.

Furthermore, the degradation products are non-toxic oligosaccharides which can be then excreted or incorporated to glycosaminoglycans and glycoproteins [6, 22]. Given appropriate time and conditions, chitosan would degrade eventually and sufficiently in most cases to be excreted [19]. Owing to the biodegradability of chitosan, hydrogels made up of chitosan chains are deemed biodegradable. However, the degradation rate might be affected by crosslinking density and the biocompatibility profiles of degradation products are unclear. As shown in **Table 2.6**, *in vitro* biodegradation of chitosan-based hydrogels has often evaluated upon exposure to lysozyme solution and changes in hydrogels' weight or amount of free amino groups released in the incubation solution are measured.

Table 2.6 Reported *in vitro* biodegradation studies of hydrogels based on chitosan-genipin (CS-GEN) crosslinked network (lysozyme was the enzyme used in all listed studies).

Hydrogel formulations	Measurements	Main findings	Ref.
CS-GEN	Mass loss	Total degradation did not exceed 50%.	[115]
CS-GEN	Free amino groups (released into the solution) determined by ninhydrin assay	The gels crosslinked by genipin had a slower degradation than glutaraldehyde-crosslinked chitosan hydrogels.	[193]
CS-GEN-TPP	Free amino groups (released into the solution) determined by ninhydrin assay	The crosslinked beads showed a significant slower degradation than uncrosslinked beads.	[218]
CS-GEN-β-glycerol phosphate	Mass loss	The gels retained their structural integrity after four weeks.	[203]
CS-GEN-gelatin- β-glycerol phosphate	Mass loss	After incubation for 30 days, the weight loss was ~43% (gels with 10 µg/mL genipin) and ~25% (gels with 100 µg/mL genipin).	[117]
CS-GEN-collagen-hyaluronic acid	Mass loss	After incubation of 4 h, the weight loss was 30 - 70% (gels with 10 mM genipin) and 20 - 40% (gels with 20 mM genipin)	[219]
CS-GEN-alginate-Ca^{2+}	Mass loss	The triple network structure offered a dense microstructure and delayed the degradation.	[220]
CS-GEN-silk protein sericin	Mass loss	The gels showed degradation between 38% and 50%.	[221]

2.4 Chitosan-based hydrogels for vaccine delivery

The immune-regulatory mechanisms of chitosan have been studied over years. The DDA, MW, polydispersity, purity, form, and dose, all of which can influence the innate immune response to chitosan. Chitosan with high DDA induces a weak leukocyte infiltration response while chitosan with low DDA attracts polymorphonuclear cells and triggers neutrophils to release inflammatory mediators which later amplify the recruitment of neutrophils and macrophages [222]. The immune response induced by chitosan is antigen-dependent [223]. In the absence of antigen, the subcutaneous injection of chitosan is found to be ineffective. In the presence of antigen, chitosan enhances both humoral and cell-mediated immune responses [28, 224]. As a potential adjuvant, chitosan is demonstrated to be equipotent to incomplete Freund's adjuvant and superior to aluminium hydroxide [28]. The intracellular signalling pathway of chitosan can be described via cytoplasmic DNA sensor (cGAS) and stimulator of interferon genes (STING) and via nucleotide-binding and oligomerization domain (NOD)-like receptor protein 3 (NLRP3) [26]. These pathways are triggered as macrophages expose to chitosan with 80 - 90% DDA and 3 - 4 kDa in MW.

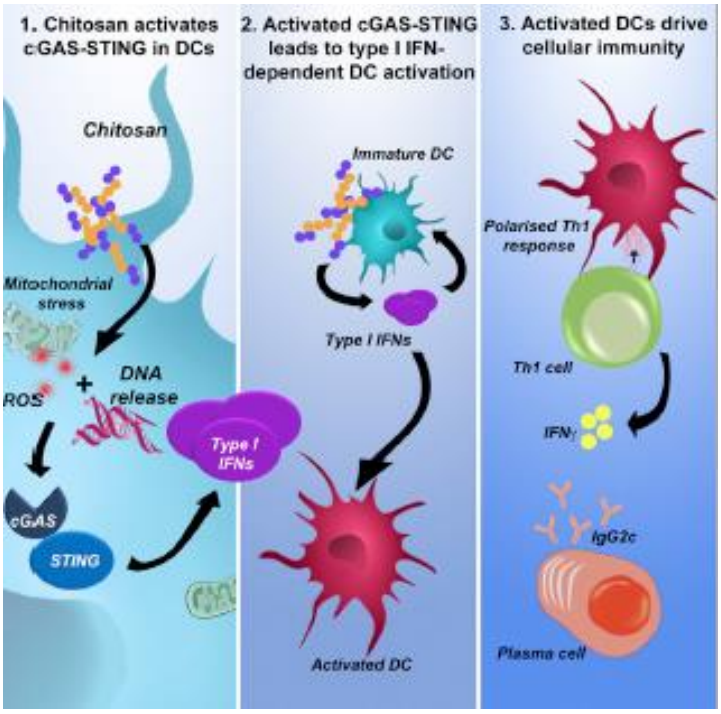

Figure 2.11 Schematic representation of immune stimulating properties of chitosan which engage DNA sensor cGAS-STING pathway [225].

Via cGAS-STING, chitosan induces type 1 interferon (IFN) and enhances antigen-specific T helper 1 (Th1) response, resulting in dendritic cells maturation (**Figure 2.11**) [225]. Type 1 IFN response

induces the release of therapeutically related anti-inflammatory factor, interleukin-1 receptor antagonist (IL-1ra), and interferon gamma-induced protein 10 (IP-10) [26]. Via NLRP3, chitosan induces a robust interleukin-1β (IL-1β) response in primed mouse bone-marrow derived macrophages (BMDM) and leads to the release of pro-inflammatory factors, IL-1β, and prostaglandin E_2 [226]. In unprimed BMDM, chitosan does not stimulate significant release of any of 22 cytokines (including tumour necrosis factor- α (TNF-α) and interleukin-6 (IL-6)) and chemokines assayed. Whether chitosan is a pro-inflammatory or anti-inflammatory material depends on the macrophages that it is exposed to. When macrophages are polarised towards an M1 state, chitosan stimulates the release of pro-inflammatory cytokines via NLRP3 pathway. When macrophages are polarised towards an M2 state, chitosan triggers the release of anti-inflammatory cytokines via cGAS-STING pathway [26, 222].

Owing to the well-defined properties including biocompatibility, biodegradability, and mucoadhesiveness, chitosan has been studied as a promising carrier for mucosal vaccination, particularly via the oral and nasal routes to enhance immune responses (**Table 2.7**). Chitosan is found to be able to loosen up the tight junction between epithelial cells, reduce the transepithelial electrical resistance, and enhance paracellular uptake. Thus, chitosan-based systems can act as an antigen depot (protecting the antigens from premature proteolytic degradation and prolonging the release of antigen at target sites) and as an adjuvant itself (driving potent cell-mediated immunity).

Table 2.7 Reported studies of chitosan-based particulate systems for vaccine delivery.

Types of particles	Main constituents	Model antigens	Delivery routes	Ref
Microparticles	Chitosan and sodium sulphate	Ovalbumin	Oral	[227]

Microparticles	Chitosan, alginate	Fowl typhoid	Oral	[228]
Microparticles	Mannosylated chitosan	Bordetella bronchiseptica dermonecrotoxin	Nasal	[229]
Microparticles	Chitosan, Pluronic F127	Tetanus toxoid	Nasal	[230]
Nanoparticles	Mannosylated chitosan	Recombinant hepatitis B surface antigen	Intraperitoneal injection	[231]
Nanoparticles	Chitosan	Plasmid pCMVArah2 encoding peanut allergen gene	Oral	[232]
Nanoparticles	Trimethyl chitosan, dextran	Lipopeptide-based antigen against group A Streptococcus	Nasal	[233]

Within this literature review, the potential of chitosan-based hydrogels in drug delivery applications has been discussed. Based on the gaps identified in this review, the research objectives were formulated and detailed below.

- As there is a need to utilise a bio-safe crosslinker for production of chitosan-based hydrogels, genipin was selected on the basic of its selective reactivity and good biocompatibility. To enhance the level of control in hydrogels' microstructure and to serve as a part of strategic development towards pulsatile drug delivery devices, addition of a linear PEG polymer to chitosan-genipin network was evaluated. Acknowledging the versatility of chitosan to form hydrogels in different sizes and shapes, aim was set to fabricate chitosan hydrogels with different geometries to be applicable for various administrative routes, such as oral, implantation, and nasal delivery.
- To tailor the hydrogels' microstructure efficiently for anticipated applications, it was decided to evaluate their properties as a function of hydrogel composition and gelation conditions. Therefore, different analytical techniques were selected to characterise the physico-chemical properties of hydrogels.
- As there are only a few studies reporting the *in vitro* and *in vivo* biocompatibility and biodegradation of chitosan-genipin hydrogels, it was decided to explore the bioactivity of the hydrogels towards inflammatory cells with a broader range of cytokines involved. The reported intrinsic fluorescence of hydrogels upon chitosan-genipin crosslinking was deemed of interest to exploit as a versatile approach to evaluate the bioactivity of the hydrogels *in vitro* and *in vivo* without using a fluorescent marker.

- Ultimately, to verify the potential to serve as chronotherapeutic carriers for controlled drug delivery, it was decided to evaluate the release kinetics of entrapped biomolecules from the hydrogels.

Study presented in this thesis combines efforts in hydrogel synthesis, characterisation, and evaluation, all required to eventually achieve a versatile polymeric system with tunable physico-chemical properties, good biocompatibility, controllable biodegradability, fit for controlled drug delivery and further developments in the area of pulsatile, autonomous, drug delivery devices.

Chapter 3 Methodology

As discussed in Chapter 2, cationic pH-responsive chitosan-genipin hydrogels, interpenetrated by PEG, are considered as a prospective controlled drug delivery system, with a great potential for medical applications. This Chapter details the materials, equipment, and methods used to perform the synthesis, characterisation, and evaluation of pH-responsive hydrogels composed of chitosan, genipin, and PEG.

3.1 Materials

Chitosan (medium MW, 82% deacetylation, viscosity 420 centipoise, product number 448877, lot number STBG5137V), PEG (MW 6000 g/mol), genipin (MW 226 g/mol, ≥ 98%), glacial acetic acid, ethanol, hexamethyldisilazane (HMDS), and perindopril erbumine (PER) were supplied from Sigma Aldrich (United Kingdom). Glycine (pH 2), phthalate (pH 4), phosphate (pH 7), and borate (pH 10) buffer solutions, phosphate buffered saline (PBS), trypsin 0.05% - EDTA 1X solution, and Trypan Blue 0.4% solution were obtained from Fisher Scientific (United Kingdom). 1-methyl D-tryptophan (D-1MT) was a kind gift from NewLink Genetics. 3T3 mouse fibroblast cells, RAW 264.7 macrophage cells, and DC 2.4 dendritic cells were from Huang and Mellor's lab (Translational and Clinical Research Institute, Newcastle University, UK). The complete culture medium used was Dulbecco's modified Eagle medium (DMEM) or Roswell Park Memorial Institute (RPMI) - 1640 medium, supplemented with 10% foetal calf serum, 2 mM L-glutamine, 100 U/mL penicillin, and 100 U/mL streptomycin. ELISA kits for TNF-α, IL-6, and IL-1β were supplied from Biolegend while ELISA kits for IP-10 and IFN-β were supplied from R&D System. Complementary DNA reverse transcription kit was supplied from Clontech (United States).

3.2 Preparation of chitosan-genipin hydrogels, with and without PEG

To facilitate diverse measurements and evaluate the hydrogels' properties thoroughly, chitosan-genipin hydrogels, with and without PEG, were prepared in various geometries (as summarised in **Figure 3.1**). In general, firstly individual aqueous solutions of chitosan, genipin, and PEG were made. Following, these solutions were combined in desirable amounts in vials, multi-well plates, syringes, or in oil phase, and then the gelation took place.

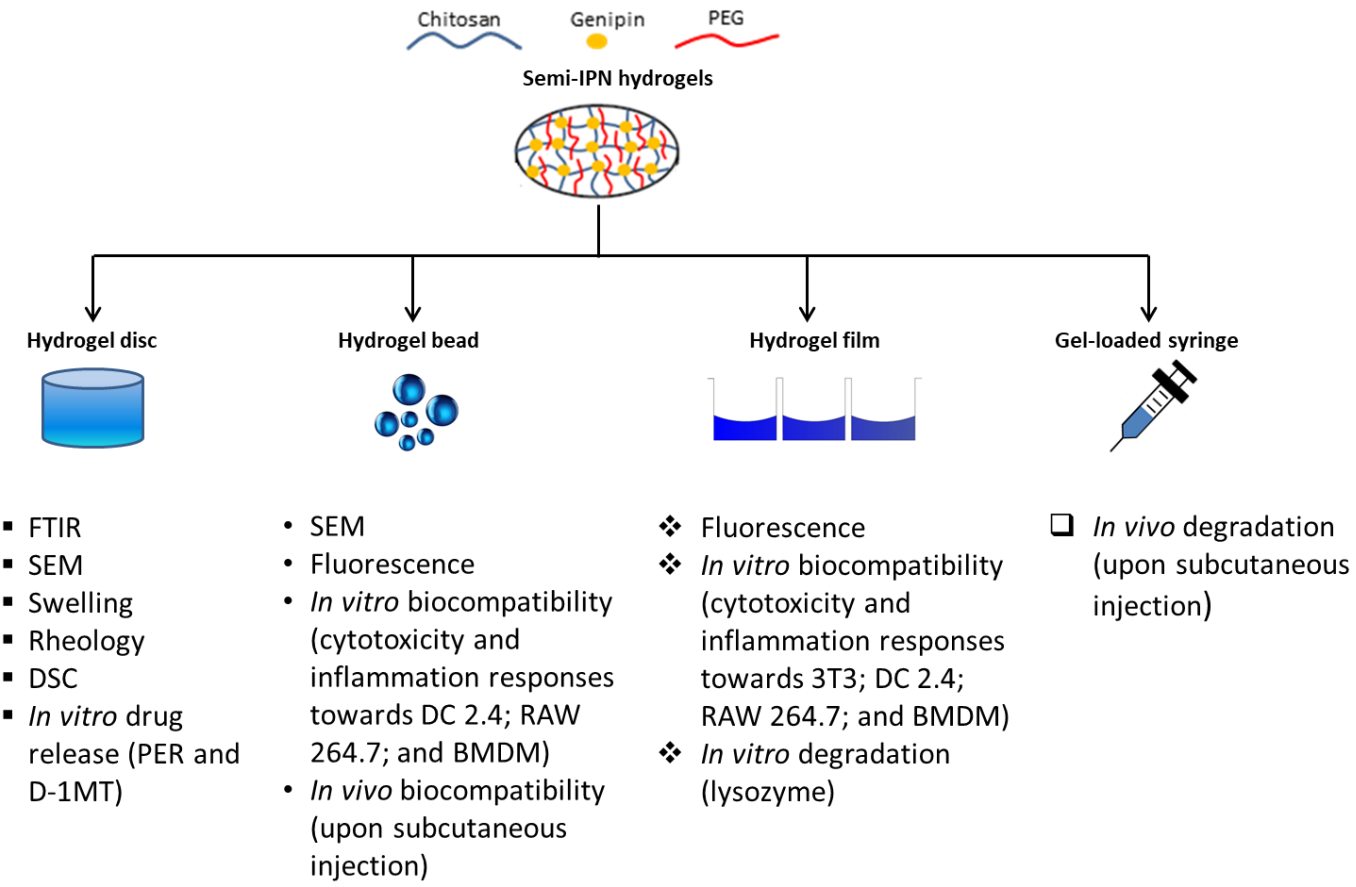

Figure 3.1 Preparation of chitosan-genipin hydrogels, with and without PEG, in various containers to form various shapes and facilitate diverse analysis.

3.2.1 Preparation of disc-shaped crosslinked hydrogels

Chitosan was dissolved in a 1% (v/v) acetic acid solution at room temperature for 24 h to obtain a pale yellow, viscous solution with a concentration of 1.5% (w/v). Genipin was dissolved in deionised (DI) water using a sonication bath at room temperature to form a 0.5% (w/v) or 1% (w/v) solution. PEG was dissolved in DI water to form transparent solutions with different concentrations. Hydrogels were then prepared using defined quantities of chitosan, genipin, and PEG solutions (**Table 3.1**). Defined amounts of chitosan, genipin, and PEG solutions were pipetted into a cylindrical polyethylene vial (internal diameter: 13 mm, capacity: 5 mL) and continuously stirred at room temperature for 15 min. Following, the stirrer bar was removed, and the vial was sealed with parafilm before being placed in an oven at 37^{o}C for 24 h to form a gel. Once removed from the oven, the vial was stored in a fridge at 5^{o}C. Prior to use, the vial base was removed with a sharp knife and a cork borer was used to gently push the disc-shaped gel out of the vial.

Table 3.1 The composition of disc-shaped chitosan-genipin hydrogels, with and without PEG, prepared in cylindrical polyethylene vials.

Sample name	Initial feed solution (%, w/v)			$[C]_{PEG}$/hydrogel (mM)	$[C]_{genipin}$/hydrogel (mM)
	Chitosan (1 mL)	PEG (0.2 mL)	Genipin (0.2 mL)		
CP0G5	1.0	-*	0.5	0.0	3.1
CP0G10		-*	1.0	0.0	6.3
CP5G5		5.0	0.5	1.2	3.1
CP5G10		5.0	1.0	1.2	6.3
CP15G5		15.0	0.5	3.6	3.1
CP15G10		15.0	1.0	3.6	6.3

(*) 0.2 mL of DI water was added instead of PEG solution to preserve desirable concentrations of genipin and enable direct comparison of samples.

To investigate further the effect of PEG content on swelling behaviour, another series of disc-shaped chitosan-genipin hydrogels, with varied PEG content, was synthesised (**Table 3.2**).

Table 3.2 The composition of disc-shaped chitosan-genipin hydrogels with varied PEG content, used for swelling measurements.

Sample name	Initial feed solution (%, w/v)			$[C]_{PEG}$/hydrogel (mM)	$[C]_{genipin}$/hydrogel (mM)
	Chitosan (1 mL)	PEG (0.2 mL)	Genipin (0.2 mL)		
CP0G5	1.5	-*	0.5	0.0	3.1
CP2G5		2.0		0.5	
CP3.5G5		3.5		0.8	
CP5G5		5.0		1.2	
CP8G5		8.0		1.9	
CP12G5		12.0		2.9	
CP15G5		15.0		3.6	

(*) 0.2 mL of DI water was added instead of PEG solution to preserve desirable concentrations of genipin and enable direct comparison of samples.

3.2.2 Preparation of bead-shaped crosslinked hydrogels

Bead-shaped chitosan-genipin hydrogels were prepared by water-in-oil (W/O) emulsion crosslinking (**Figure 3.2**). The oil phase contained 40 mL of mineral oil and 0.8 mL of Span 80. The water dispersed phase contained 3 mL of chitosan solution (1.5% w/v in acetic acid). The water phase was then dispersed, drop by drop, into the oil phase and continuously stirred (250 - 500 - 750 rpm) using a magnetic stirrer for 10 min. Genipin solution (0.5% w/v in ethanol 70% v/v) was then

added dropwise into the W/O emulsion to crosslink the particles. The emulsion was maintained at fixed temperature (20 - 37 - 50°C) for 24 h with continuous stirring. At the endpoint, the particles were separated out using centrifugation, and then washed three times with hexane followed by ethanol.

To produce bead-shaped chitosan-genipin hydrogels interpenetrated by PEG, 0.6 mL of PEG solution (5% w/v in DI water) was added to the chitosan water phase prior to dispersing into the oil phase (**Figure 3.2**). To produce bead-shaped PEG-coated hydrogels, the newly formed chitosan-genipin particles were placed in PEG solution (5% w/v in DI water) for 6 h.

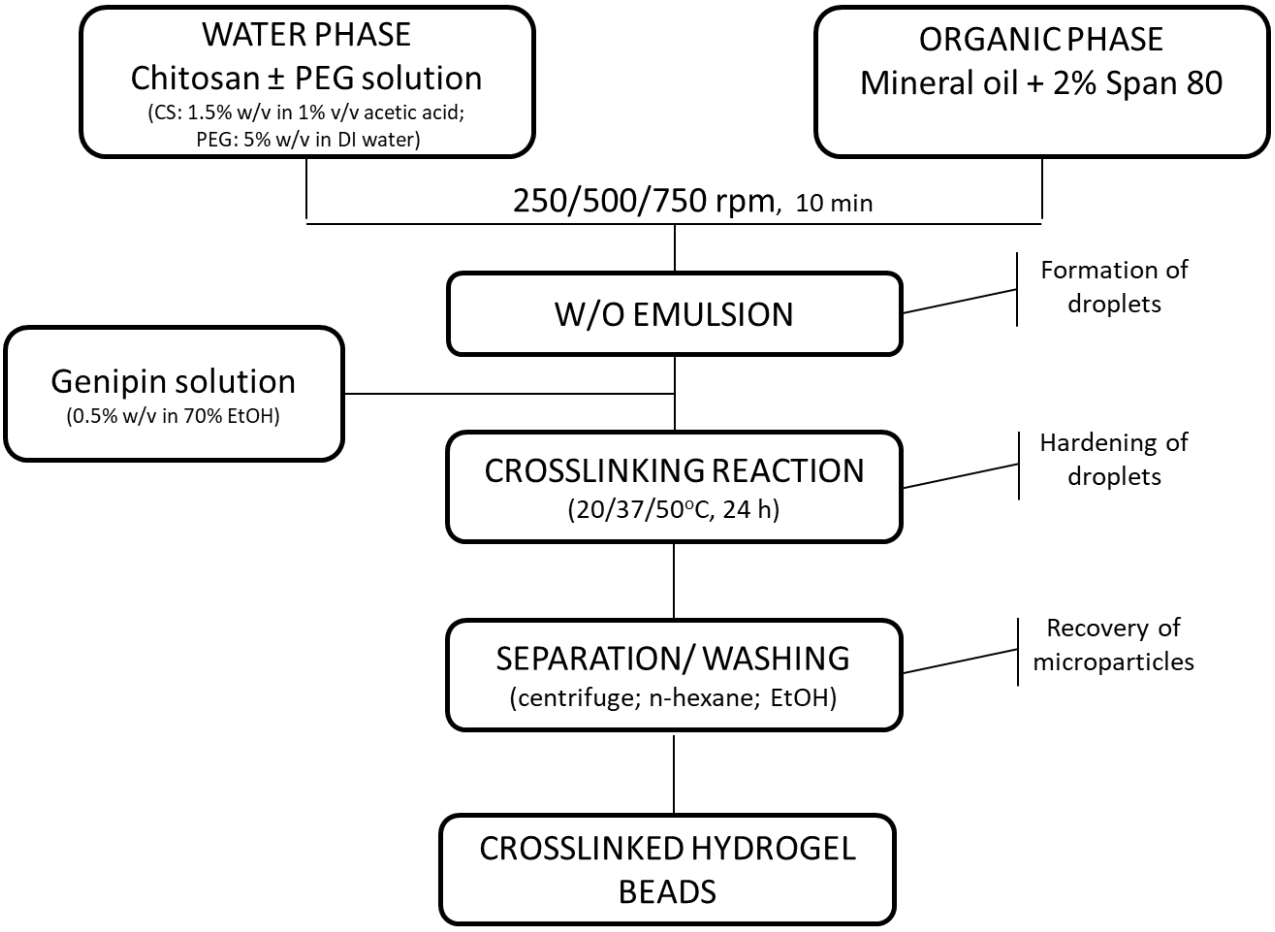

Figure 3.2 Preparation process of bead-shaped chitosan-genipin hydrogels, with and without PEG, using emulsion crosslinking method.

The particles' yield was calculated as percentage of weight of dried beads obtained compared to the total amount of dry solids in the initial feed solution (**Equation 3.1**).

$$Yield\ (\%) = \frac{Weight\ of\ dried\ hydrogel\ beads}{Total\ weight\ of\ dry\ solids\ in\ feed\ solution} \times 100 \quad \textbf{(Equation 3.1)}$$

3.2.3 Preparation of film-shaped crosslinked hydrogels

The hydrogel films were prepared in multi-well plates and used for *in vitro* studies of cytotoxicity, inflammatory response, and biodegradation. Chitosan (1.5% w/v) was prepared in acetic acid solution (1% v/v) and sterilised in autoclave (136ºC, 90 min). Genipin (0.5% w/v in DI water) and PEG (5% w/v in DI water) were sterilised using 0.22 µm syringe filters. Defined quantities of chitosan, genipin, and PEG solutions were pipetted into a cylindrical polyethylene vial and continuously stirred at room temperature for 15 min (**Table 3.3**). A specified volume of each feed solution was pipetted into multi-well plates (300 µL in 24-well plates and 100 µL in 96-well plates). The plates were incubated at 37ºC for 24 h to facilitate the gelation. Once finished, the hydrogel films were washed with PBS for 2 h and incubated with culture medium for 24 h at 37ºC (for *in vitro* toxicity and cytokine analysis). For testing *in vitro* degradation, once removed from oven, the hydrogel films were directly exposed to lysozyme solution.

Table 3.3 The composition of feed solutions of chitosan, genipin, and PEG in polyethylene vials.

Sample name	**Initial feed solution***			**$[C]_{PEG}$/hydrogel (mM)**	**$[C]_{genipin}$/hydrogel (mM)**
	$V_{chitosan}$ (mL)	V_{PEG} (mL)	$V_{genipin}$ (mL)		
F1	1.0	- **	0.1	- **	1.7
F2			0.2		3.1
F3			0.3		4.4
F1P		0.2	0.1	1.3	1.7
F2P			0.2	1.2	3.1
F3P			0.3	1.1	4.4

(*) Chitosan 1.5% (w/v), genipin 0.5% (w/v), and PEG 5% (w/v).

(**) 0.2 mL of DI water was added instead of PEG solution to preserve desirable concentrations of genipin and enable direct comparison of samples.

To confirm the biocompatibility of uncrosslinked chitosan and allow a direct comparison between uncrosslinked and crosslinked matrices, chitosan films (without crosslinking) were prepared by casting chitosan solution (1.5% w/v) in multi-well plates (300 µL in 24-well plates and 100 µL in 96-well plates) and air-drying them for 24 h. A thin film of uncrosslinked chitosan was formed in each well. The chitosan-coated plates were washed with PBS for 2 h and incubated with culture medium for 24 h at 37ºC prior to seeding cells.

3.2.4 Preparation of disc-shaped crosslinked hydrogels for in vitro drug release

To investigate the controlled release patterns of therapeutic agents loaded in the hydrogels, two drug compounds were chosen, perindopril erbumine (PER), a water-soluble substance, and 1-methyl D-tryptophan (D-1MT), sparingly soluble in aqueous solution. Drug-loaded hydrogels were prepared by weighing a defined amount of PER or D-1MT and adding it to a cylindrical polyethylene vial containing defined amounts of chitosan and PEG solution (Table 3.3). The mixture was continuously stirred at room temperature for 10 min. Genipin solution was then added to the vial and stirred for further 10 min. The vial was placed in oven at 37^{o}C for 24 h to allow gelation.

3.2.5 Preparation of crosslinked hydrogels loaded in syringes for subcutaneous injection

To investigate the *in vivo* biocompatibility, the hydrogels were prepared directly in a syringe and subcutaneously injected into mice. Chitosan (1.5% w/v), genipin (0.5% w/v), and PEG (5% w/v) sterilised solutions were prepared as described in Section 3.2.3. Chitosan (1 mL), genipin (0.05 mL), and PEG (0.2 mL) solutions were pipetted into a vial and continuously stirred at room temperature for 15 min. This homogeneous mixture was then transferred to a 2 mL sterile polypropylene syringe and allowed to polymerise at 37^{o}C for 48 h. At the endpoint, the macrogel-loaded syringe was removed from oven and allowed to rest at room temperature for 30 min before injection.

3.3 Fourier-transform Infrared spectroscopy

To investigate the structural changes induced by crosslinking reaction between chitosan and genipin, Fourier-transform Infrared spectroscopy (FTIR) was performed using an Agilent Cary 630 FTIR spectrometer equipped with diamond attenuated total reflection. FTIR was performed on dried samples to minimise the overlapped peaks derived from water molecules [234]. The disc-shaped chitosan-genipin hydrogels, with and without PEG, were synthesised (Table 3.1, Section 3.2.1), rapidly frozen in liquid nitrogen, and then dried for 48 h in a freeze-dryer (Edwards, Labconco) with the condenser set at -55^{o}C.

To investigate propagation of chemical changes induced by crosslinking reaction, disc-shaped chitosan-genipin-PEG hydrogels (sample CP5G5, Table 3.1) were synthesised at different gelation times (3 - 6 - 12 - 24 h), freeze-dried, and scanned using FTIR.

3.4 Fluorescence measurements

To evaluate the ability of hydrogels to fluoresce upon chitosan-genipin crosslinking, a fluorescence spectroscope (Tecan Spark 20M Fluorescence Reader) was used. Chitosan-genipin hydrogels, with and without PEG, were prepared in 24-well black plates with clear bottom (PerkinElmer), as detailed in Section 3.2.3. Black plates were required to reduce fluorescent signal crosstalk and background. 3D fluorescence scans with excitation range of 350 - 600 nm and emission range of 450 - 700 nm were performed to determine the optimal excitation and emission wavelengths. Fluorescence was scanned bottom-up with multipoint reading. To investigate propagation of fluorescence intensity induced by crosslinking reaction, chitosan-genipin-PEG hydrogels (samples F1P and F3P, Table 3.3) were prepared in 24-well clear-bottomed black plates. Once the feed solution was loaded into the plates, the hydrogels' fluorescence was recorded dynamically every 2 h for 24 h at 37^{o}C, using the excitation and emission wavelengths obtained from the 3D scanning. All experiments were performed in duplicate.

To confirm the fluorescence of hydrogels produced in bead shape, chitosan-genipin particles synthesised using the method detailed in Section 3.2.2, were dispersed in ethanol and placed on a microscope slide. A cover slip was placed on top and the beads were observed under a fluorescence microscope (EVOS FL, Life Technologies), with transmitted light and three fluorescence lights designed for 4',6-diamidino-2-phenylindole (DAPI; 360 nm excitation - 447 nm emission), Green Fluorescent Protein (GFP; 470 nm excitation - 525 nm emission), and Red Fluorescent Protein (RFP; 530 nm excitation - 593 nm emission).

3.5 Scanning electron microscopy

To characterise the hydrogels' morphology in disc shape, SEM was performed using an ultra-fast scanning Tescan VEGA3 microscope. SEM was performed on dried samples as it is operated under vacuum [235]. The disc-shaped chitosan-genipin hydrogels, with and without PEG, were synthesised (Table 3.1, Section 3.2.1) and freeze-dried (as detailed in Section 3.3). The dried gels were attached to a holder using conductive carbon tape and coated with a 15 nm layer of gold to enhance the conductivity. The hydrogel surface and internal microstructure were investigated at 8 kV with a spot size of 10 dp and working distance of 8 - 12 mm at different magnifications. From SEM images, the porosity analysis and particle size determination were performed using ImageJ software in which dimensions (area and diameter) are converted to a binary format.

To characterise the hydrogels' morphology in bead shape, SEM and light microscope were performed. The bead-shaped chitosan-genipin hydrogels, with and without PEG, were synthesised using emulsion crosslinking (as detailed in Section 3.2.2). For light microscope, the hydrogel beads were dispersed in ethanol and wet-mounted on a microscope slide. For SEM, the hydrogel beads were dehydrated using ethanol, HMDS gradient, and air-dried at room temperature. The dried beads were observed under SEM to visualise their morphology and several images per sample were used to determine mean particle size and its distribution using ImageJ software.

3.6 Swelling measurements

3.6.1 Gravimetric swelling measurements

To evaluate the pH-responsiveness of crosslinked hydrogels, gravimetric swelling measurements were conducted. Disc-shaped chitosan-genipin-PEG hydrogels (sample CP5G5, Table 3.1) were synthesised (as detailed in Section 3.2.1) and pre-weighed (m_o, g). The gels were then placed in different buffer solutions (pH 2 glycine, pH 4 phthalate, pH 7 phosphate, and pH 10 borate buffers) at 20^{o}C (**Table 3.4**). A polytetrafluoroethylene (PTFE) cage was used to facilitate the transfer of hydrogels from the medium to the balance. The swollen gels were weighed (m_t, g) at fixed time intervals after decanting excess solution from the cage and removing remaining solution from the gel surface using filter papers. Each experiment ended when no significant changes in weight were measured over three adjacent time intervals at which point it was assumed that the gels achieved equilibrium swelling state. The swelling ratio, S (%), was calculated using **Equation 3.2**.

$$S\ (\%) = \frac{m_t - m_o}{m_o} \times 100 \quad \textbf{(Equation 3.2)}$$

To evaluate the effect of hydrogel composition (genipin and PEG content) on swelling, two sets of disc-shaped chitosan-genipin hydrogels, with and without PEG (denoted in Table 3.1 and Table 3.2, Section 3.2.1) were synthesised and placed in pH 2 buffer solutions at 20^{o}C (**Table 3.4**). Their swelling ratios at the equilibrium state were recorded.

To evaluate the effect of gelation time and temperature on swelling, disc-shaped chitosan-genipin-PEG hydrogels (sample CP2G5, Table 3.2) were synthesised (as detailed in Section 3.2.1) at different gelation times and temperatures and placed in pH 2 buffer solutions at 20^{o}C (**Table 3.4**).

Their swelling ratios at the equilibrium state were recorded. All experiments were performed in triplicate.

Table 3.4 Disc-shaped chitosan-genipin hydrogels, with and without PEG, used for gravimetric swelling measurements.

Samples	Gelation time (h)	Gelation temperature (ºC)	pH of buffer solutions
CP5G5 (Table 3.1)	24	37	2 (glycine) 4 (phthalate) 7 (phosphate) 10 (borate)
All gels listed in Table 3.1 and Table 3.2	24	37	2 (glycine)
CP2G5 (Table 3.2)	8 - 12 - 24 - 48 - 72 - 96	37	2 (glycine)
CP2G5 (Table 3.2)	24	20 - 37 - 45 - 60	2 (glycine)

3.6.2 Oscillatory swelling measurements

To evaluate the feasibility of hydrogels to be coupled with oscillatory reaction, disc-shaped chitosan-genipin-PEG hydrogels (sample CP2G5, Table 3.2) were synthesised (as detailed in Section 3.2.1). The hydrogels enclosed in a PTFE cage were pre-weighed and immersed in a pH 2 glycine buffer solution at 20ºC. After 15 min, the cage and gel were removed. After decanting excess solution from the cage and removing remaining solution from the gel surface using filter papers, the swollen gels were weighed. The cage and gel were then placed in another buffer solution (pH 4 phthalate buffer or pH 7 borate buffer) for a further 15 min. The mass was determined again after 15 min as described above. This process was continued in an alternating fashion for 6 h. All experiments were performed in duplicate.

3.7 Rheological measurements

Rheological measurement was performed on a Malvern Kinexus Pro+ rheometer, equipped with standard steel parallel-plate geometry of 20 mm diameter and a circulating environmental controller. The measurements were carried out in the linear viscoelastic region (LVR) of the material to ensure that the measured rheological parameters were independent of the magnitude of imposed strain or stress [236]. The samples were subjected to tests in which the rheological parameters were monitored as a function of time, strain, and frequency.

3.7.1 Oscillatory time sweep

To determine the gel point, oscillatory time sweeps were performed to track the temporal evolution of dynamic shear moduli over time [237]. A sample (initial feed solution of chitosan, genipin, and PEG; as defined in Table 3.1) was loaded onto a preheated plate (37°C) as a liquid. The test geometry was then lowered to a gap height of 1 mm and excess solution was discarded. The tests were conducted at 37ºC to resemble physiological conditions. The gel point was determined by two different approaches, the cross-over point and the Winter-Chambon criterion [181, 182, 238]. In the cross-over point approach, a constant frequency of 10 Hz and a shear strain of 1% were arbitrarily chosen to ensure the time sweep was performed in the LVR. The shear elastic modulus (G') and shear viscous modulus (G'') were automatically calculated by the software. The gel point was determined as the cross-over point at which G' intersects G''. In the Winter-Chambon approach, the samples were subjected to oscillatory time sweeps with a range of frequencies (2.5, 5, 7.5, and 10 Hz) and a constant strain of 1%. The loss factor, which is known as tan(δ), is the ratio of G'' and G'. The gel point was defined as the point at which tan(δ) is independent of the applied frequency.

3.7.2 Oscillatory strain sweep

To determine the LVR within which G' and G'' were independent of shear strain, oscillatory strain sweeps were performed. The strain sweeps were performed on crosslinked hydrogels with the curing time of 6 h. A sample (initial feed solution of chitosan, genipin, and PEG; as defined in Table 3.1) was loaded onto a preheated plate (37°C) as a liquid and allowed to cure for 6 h without any rheological monitoring. Then, a strain sweep from 0.1% to 100% was conducted at a constant frequency (10 Hz) to monitor the modulus versus strain.

3.7.3 Oscillatory frequency sweep

To measure the mechanical strength of the crosslinked hydrogels, oscillatory frequency sweeps were performed. The frequency sweeps were performed on the crosslinked hydrogels with the curing time of 6 h. Similar to oscillatory strain sweep, chitosan-genipin hydrogels, with and without PEG, were allowed to form at 37°C for 6 h without monitoring rheological response. After 6 h of curing, samples were swept from 0.01 Hz to 100 Hz with a constant strain value that was determined in the strain sweep previously. All oscillatory sweeps were performed in duplicate.

3.8 Differential scanning calorimetry

To evaluate the thermal properties of hydrogels, differential scanning calorimetry (DSC) was performed using a DSC Q20 (TA instrument) equipped with the Universal Analysis 2000 software. Disc-shaped chitosan-genipin hydrogels, with and without PEG (samples CP0G5, CP5G5, and CP5G10; Table 3.1) were synthesised (as detailed in Section 3.2.1) and freeze-dried (as detailed in Section 3.3). Freeze-dried hydrogels weighing approximately 5 mg were placed in aluminium pans and sealed with pierced lids. An empty pan was used as reference. The samples were subjected to three heating - cooling cycles (**Table 3.5**). In the first cycle, the samples were heated from 25^{o}C to 200^{o}C at a constant rate of 10^{o}C/min under constant purging of dry nitrogen at 50 ml/min. The samples were then held at 200^{o}C for 5 min and cooled to -90^{o}C at a cooling rate of 20^{o}C/min. In the second and third cycles, the gels were heated up from -90^{o}C to 500^{o}C and then hold at 500^{o}C for 5 min before being cooled down to -90^{o}C at a cooling rate of 20^{o}C/min. All experiments were performed in triplicate. The onset temperature, peak temperature, and enthalpy of any transition events occurred during heating and cooling modes, were integrated.

Table 3.5 Three heating - cooling cycles applied for freeze-dried disc-shaped chitosan-genipin hydrogels, with and without PEG.

Cycles	**Running segment description**
1st	- Equilibrate at 25^{o}C - Ramp 10^{o}C/min to 200^{o}C - Isothermal at 200^{o}C for 5 min - Ramp 20^{o}C/min to -90^{o}C
2nd	- Ramp 10^{o}C/min to 500^{o}C - Isothermal at 500^{o}C for 5 min - Ramp 20^{o}C/min to -90^{o}C
3rd	- Ramp 10^{o}C/min to 500^{o}C - Isothermal at 500^{o}C for 5 min - Ramp 20^{o}C/min to -90^{o}C

3.9 *In vitro* drug release measurements from disc-shaped hydrogels

To evaluate the release kinetics of loaded biomolecules from the hydrogels, two drug models (PER and D-1MT) were used. PER-loaded or D-1MT loaded disc-shaped hydrogels were synthesised as

detailed in Section 3.2.4. To quantify the amount of PER or D-1MT released from the hydrogel matrices, High Performance Liquid Chromatography (HPLC) methods were developed and validated (**Table 3.6**). The drug-loaded disc-shaped hydrogels were placed in 20 mL of pH 2 glycine buffer solutions. At fixed time points, 2 mL of medium was taken out and assayed. An equal volume of fresh buffer was added immediately to maintain volume of the medium approximately constant. All experiments were performed in triplicate.

Table 3.6 Parameters of HPLC methods used to quantify the amount of therapeutic agents released from hydrogels.

Parameters	PER quantification	D-1MT quantification
System	Varian Pro-star (Agilent)	Nexera XR LC-20 AD (Shimadzu)
Column	Microsorb-MV 5 µm C18 (150 x 4.6 mm)	Hyperclone 5 µm BDS C18 130 Å (250 x 4.6 mm)
Injection volume	20 µL	25 µL
Detector	UV/Vis set at 209 nm	Fluorescence set at 285 nm excitation and 365 nm emission
Mobile phase	Acetonitrile – phosphate buffer pH 2 (65 : 35 v/v)	Phase A: 2.5% acetonitrile + 15 nM sodium acetate Phase B: 100% acetonitrile
Flow rate	1 mL/min	1 mL/min
Oven temperature	30°C	40°C
Standard solutions	From 0.5 to 100 µg/mL	From 0.5 to 20 µg/mL

3.10 *In vitro* assays to investigate inflammatory property of chitosan-based hydrogels

3.10.1 Preparing cell suspension

Various *in vitro* cultured cells (3T3, DC 2.4, and RAW 264.7) were used to investigate the biocompatibility. The cells were cultured in the complete culture medium (DMEM for 3T3, RPMI-1640 for RAW 264.7 and DC 2.4) at 37°C in a humidified atmosphere containing 5% CO_2. The cells growing in a logarithmic phase were collected for passage or seeding. The cell suspension was centrifuged (1200 rpm, 5 min) and the cells were re-suspended in culture medium. The total number of live cells was counted using a trypan blue 0.4% solution and a haemocytometer. For all *in vitro* tests, the control cells and treated cells were incubated at 37°C/5% CO_2.

As primary macrophages exhibit more physiological features (such as phagocytic activity, cytokine production, and regulation of oxidative burst) than macrophage cell lines [239], inflammatory responses to hydrogels were investigated using mouse bone marrow-derived macrophages. Bone marrow cells were collected from mice's femurs and tibia. The cells were then grown in culture dishes with RPMI-1640 medium in the presence of macrophage colony-stimulating factor (M-CSF) and gentamicin at 37°C/5% CO_2. Under these conditions, the bone marrow monocyte/macrophage progenitors proliferated and differentiated into a homogenous population of mature macrophages (so-called bone marrow derived macrophages - BMDM). On day 4, 10 mL of medium was removed and 10 mL of fresh medium with M-CSF was added. On day 7, BMDM were harvested for experimental uses.

3.10.2 Cell viability assays

To evaluate the cytotoxicity of uncrosslinked chitosan and crosslinked hydrogels, direct-contact method was used, in which the cells were directly exposed to the test samples.

In 96-well opaque plates, three types of test samples (uncrosslinked chitosan films, crosslinked hydrogel films, and crosslinked hydrogel beads) were prepared. Uncrosslinked chitosan films and crosslinked chitosan-genipin hydrogel films with and without PEG (Table 3.3) were synthesised using the method detailed in Section 3.2.3. Crosslinked chitosan-genipin hydrogel beads were synthesised using emulsion crosslinking (as detailed in Section 3.2.2). After the last wash with ethanol, the particles were re-suspended in PBS and counted by haemocytometer. In 96-well opaque plates, 100 µL of particle suspension was added to each well (number of particles per well: 15×10^4).

The cell suspensions of 3T3, DC 2.4, RAW 264.7, and BMDM were prepared (as detailed in Section 3.10.1) and seeded directly in 96-well opaque plates containing test samples. 100 µL of cell suspension was added to each well with gently rotating to distribute the cells evenly (**Table 3.7**). For reference purpose, cells were seeded in wells containing fresh culture medium only (negative control cells) and processed in same manners as the treated cells. Cell viability upon direct contact with the test samples was quantified using an ATP-based assay, which measures the amount of ATP produced by viable cells in the supernatant. At scheduled times, 100 µL of CellTiter-Glo® 2.0 reagent was added. The plates were placed on an orbital shaker for 2 min and allowed to equilibrate at room temperature in dark place for 10 min. The luminescence signals were recorded using a plate reader. All experiments were performed in triplicate.

Table 3.7 Test for cytotoxicity by direct-contact method using various *in vitro* cultured cells and primary mouse cells.

Test samples	**Type of cells**	**Number of cells per well***
Chitosan films	DC 2.4	5×10^4
	RAW 264.7	5×10^4
	BMDM	1×10^4
Hydrogel films	3T3	5×10^3
	3T3**	5×10^4 (24-well plate)
	DC 2.4	5×10^4
	RAW 264.7	5×10^4
	BMDM	1×10^4
Hydrogel beads	DC 2.4	5×10^4
	RAW 264.7	5×10^4
	BMDM	1×10^4

(*) Cells were seeded in 96-well opaque plates (Corning) containing test samples. Volume of cell suspension in each well: 100 µL

(**) The morphology of 3T3 fibroblasts grown on crosslinked hydrogel films was investigated in 24-well plates by means of inverted light microscope and SEM. Volume of cell suspension in each well: 500 µL

3.10.3 Inflammatory cytokine analysis

To evaluate the inflammatory response to uncrosslinked chitosan and crosslinked hydrogels, the inflammatory cytokines induced by direct contact between cells and test samples were measured.

In multi-well plates, three types of test samples (uncrosslinked chitosan films, crosslinked hydrogel films, and crosslinked hydrogel beads) were prepared. Uncrosslinked chitosan films and crosslinked chitosan-genipin hydrogel films with and without PEG (Table 3.3) were synthesised using the method detailed in Section 3.2.3. Crosslinked chitosan-genipin hydrogel beads were synthesised using emulsion crosslinking (as detailed in Section 3.2.2). After the last wash with ethanol, the particles were re-suspended in PBS and counted by haemocytometer (bead density: 15×10^4 / 100 µL).

The cell suspensions of DC 2.4, RAW 264.7, and BMDM were prepared (as detailed in Section 3.10.1) and seeded directly in multi-well plates containing test samples (**Table 3.8**). For reference

purpose, cells were seeded in wells containing fresh culture medium only (negative control cells) and processed in same manners as the treated cells. At scheduled times, supernatant was collected to measure cytokine production by ELISA while the cells were lysed to measure cytokine gene expression by RT-PCR. The production of five inflammatory cytokines (TNF-α, IL-6, IP-10, IL-1β, and IFN-β) was measured by ELISA according to manufacturer protocols. The total RNA was isolated from the lysed cells by trizol and the extracted RNA was reverse-transcribed using a random hexamer cDNA RT kit (Clontech). Quantitative RT-PCR was performed on AriaMx RT-PCR system (Agilent) with iQ^{TM} SYBR^{TM} Green Supermix (Bio-rad). A house keeping gene, glyceraldehyde-3-phosphate dehydrogenase (GAPDH) was used as the endogenous RNA control. All experiments were performed in triplicate.

Table 3.8 Test for inflammatory response by inflammatory cells cultured on chitosan samples.

Test samples	**Type of plates**	**Type of cells**	**Volume of cell suspension per well**	**Cell number per well**
Chitosan films Hydrogel films	24-well transparent plate (NUNC ThermoFisher)	DC 2.4	500 µL	5×10^5
		RAW 264.7		5×10^5
		BMDM		1×10^5
Hydrogel beads	96-well F-bottom transparent plate (Costar)	DC 2.4	100 µL	5×10^4
		RAW 264.7		5×10^4
		BMDM		1×10^4

3.11 *In vitro* degradation test under lysozyme activity

To evaluate the biodegradation of hydrogels, their intrinsic fluorescence was monitored in the presence of lysozyme. Chitosan-genipin hydrogels, with and without PEG (Table 3.3), were prepared in 24-well black plates with clear bottom (PerkinElmer), as detailed in Section 3.2.3. Lysozyme with an activity of 100000 U/mg was dissolved in PBS (0.5 mg/mL) and then added to the gel samples (1 mL per well). The samples were then incubated at 37^{o}C. At scheduled times, the solutions were aspirated, and the plates were read for fluorescent signals. After each reading, the same amount of treatment solution was added to each well. For reference purpose, the control samples were tested under the same condition as described above using PBS solution without adding lysozyme. All experiments were performed in duplicate.

3.12 *In vivo* biocompatibility test of crosslinked hydrogels

All experiments were performed on C57BL/6 mice under approval from the Newcastle Ethical Review Committee and a UK Home Office license. All research work was carried out in compliance with the Animal (Scientific Procedure) Act 1986 and its associated Code of Practice.

3.12.1 Subcutaneous injection with macrogels and monitoring biodegradation

To evaluate the *in vivo* biodegradation of hydrogels upon subcutaneous injection, their intrinsic fluorescence was monitored non-invasively using *In Vivo* Imaging System (IVIS). Chitosan-genipin-PEG hydrogels loaded in syringes were prepared as detailed in Section 3.2.5. Mice were subcutaneously injected with 200 µL of sterile hydrogels using a 20 G needle. The needle was inserted into the lower right quadrant of abdomen avoiding the abdominal midline and the hydrogel was injected. The mice were examined everyday (body weight, any signs of local skin lesion, and inflammation). At scheduled times, mice were anesthetised under isoflurane and IVIS imaged (with an excitation filter of 605 nm and an emission filter of 660 nm, Caliper Life Science). The images were analysed using Living Image 4.4 software. The regions of interest (ROI) were drawn and the average radiant efficiency [p/s/cm^2/sr]/[µW/cm^2] was calculated after subtracting the background signal (from the lower left quadrant area). After the last IVIS scan, the mice were culled and the tissues were collected for haematoxylin and eosin (H&E) staining.

3.12.2 Subcutaneous injection with hydrogel beads and measuring inflammatory response

To evaluate the *in vivo* biocompatibility of hydrogel beads, the inflammatory cytokine production following subcutaneous injection were evaluated. Chitosan-genipin hydrogel beads were prepared as detailed in Section 3.2.2. The beads were dispersed in PBS to achieve a density of 10 million particles per mL. Mice were subcutaneously injected with 200 µL of bead suspension using 25 G needle. The needle was inserted into the lower right quadrant of abdomen avoiding the abdominal midline and the hydrogel was injected. The mice were examined everyday (body weight, any signs of local skin lesion, and inflammation). At scheduled times, blood samples were taken, and the obtained plasma was screened for cytokine production by ELISA. The mice were culled after taking blood samples and the lymph nodes were retrieved to analyse cytokine gene expression by RT-PCR. The tissues around injection sites were also collected for H&E staining.

3.13 Statistical analysis

Data are expressed as mean ± standard deviation (SD). Two-way ANOVA with multiple comparisons and unpaired two-tailed Student's *t* tests were performed. Statistical significance is defined as * $P < 0.05$, ** $P < 0.01$, *** $P < 0.001$, and **** $P < 0.0001$. OriginPro was used to perform all data analysis.

Chapter 4 Hydrogels' formation and physico-chemical characteristics

Genipin crosslinked chitosan hydrogels, with and without PEG, synthesised in disc and bead shapes using the method detailed in Section 3.2, were characterised using FTIR, fluorescence spectroscopy, SEM, and DSC to evaluate the hydrogels' microstructure and the relation between their composition and the physico-chemical properties. The pH-responsive property was characterised by measuring changes in hydrogels' weight upon immersion in different pH buffer solutions. The rheological properties (gelation point, viscoelasticity, and mechanical stability) were measured as a function of genipin and PEG content. The release of two biomolecules (perindopril erbumine and 1-methyl D-tryptophan) from the crosslinked hydrogels was recorded. Some of the content in this Chapter have been previously published in 'PEG-interpenetrated genipin-crosslinked chitosan hydrogels: structure, pH-responsiveness, gelation kinetics, and rheology', Journal of Applied Polymer Science [31].

4.1 Formation of crosslinked hydrogels in disc and bead shapes

4.1.1 Formation of hydrogel discs

Disc-shaped chitosan-genipin hydrogels, with and without PEG, were synthesised in polyethylene vials using the method defined in Section 3.2.1 (Table 3.1 and Table 3.2). These disc-shaped hydrogels were used for FTIR, SEM, swelling measurement, DSC, and release study.

Hydrogel discs were formed with diameter of 13 mm and thickness of 8 mm. Hydrogel discs can be formed with different diameters using various vials available on the market. The visual appearance of the hydrogels was associated with gelation time (**Figure 4.1**).

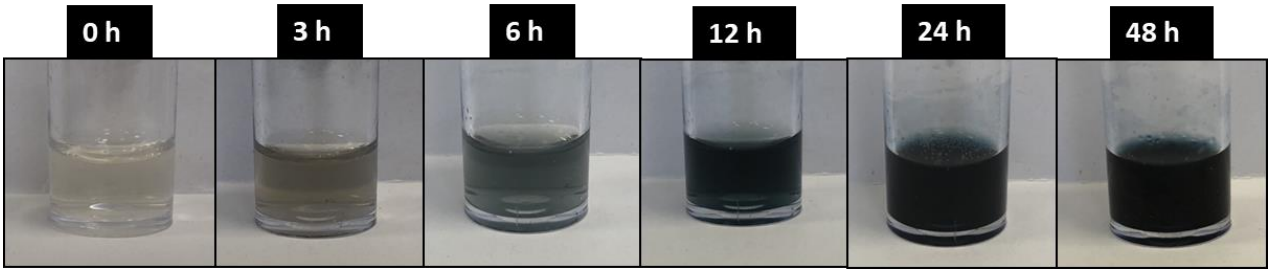

Figure 4.1 Changes in colour of a disc-shaped chitosan-genipin-PEG hydrogel (sample CP5G5, Table 3.1, prepared at 37^{o}C) over gelation time.

Before gelation, chitosan solution was initially viscous and slightly yellow while PEG and genipin solutions were initially clear and colourless. After mixing in vials, the mixture of chitosan, genipin, and PEG had a pale-yellow colour. As the gelation progressed, the hydrogel colour changed from

pale-yellow to green hue and finally dark blue. The blue colour is related to the oxygen radical-induced polymerisation of genipin that occurs once the heterocyclic genipin links with chitosan molecules, as discussed in Section 2.2.1 [109]. The reaction between chitosan and genipin is moderate, and the gradual deepening of hydrogel colour over time reflects an increase in crosslinking degree [113]. Changes in physical appearance of chitosan-genipin-PEG mixture were observed as a function of gelation time and temperature (**Table 4.1**). The speed and extent of crosslinking reaction were dependent on incubation temperature, as at 37^{o}C the dark blue gel was formed within 24 h, much faster than at 20^{o}C.

Table 4.1 Visually observed changes in physical appearance of chitosan-genipin-PEG reaction mixture (sample CP5G5, Table 3.1) as a function of gelation time and temperature.

Incubation temperature (^{o}C)	**Incubation time (h)**					
	0	3	6	12	24	48
37	Clear, light yellow	Clear, green-yellow	Clear, green-blue	Partly gelled, dark blue	Gelled, dark blue	Gelled, dark blue
20	Clear, light yellow	Clear, yellow	Clear, yellow	Clear, green-blue	Partly gelled, green-blue	Gelled, dark blue

4.1.2 Formation of hydrogel beads

Bead-shaped chitosan-genipin hydrogels, with and without PEG, were synthesised using emulsion crosslinking as detailed in Section 3.2.2. These bead-shaped hydrogels were used for SEM as well as for *in vitro* and *in vivo* biocompatibility studies. The hydrogels were formed in oil phase (mineral oil with the presence of surfactant, Span 80), where chitosan droplets were hardened by crosslinking with genipin. Span 80 was added to stabilise the emulsion while genipin was dissolved in ethanol to increase its solubility. During the crosslinking, the emulsion colour changed from colourless to milky blue and finally clear bluish fluid with dark blue particles dispersed. Stirring is important to ensure the formation of discrete particles with well-defined shapes. In the preliminary experiments, the aqueous chitosan solution could not be broken to form uniform droplets when the magnetic stirring speed was below 200 rpm. The stirring speed of above 200 rpm was deemed suitable to produce bead-shaped hydrogels. Meanwhile, when the stirring speed of above 900 rpm was applied, almost all particles were stuck at the wall of glassware during emulsification. Thus, stirring speeds of 250 - 500 - 750 rpm were chosen to evaluate the effect of stirring rate on the particles' morphology and size.

Several studies have confirmed that the rate of crosslinking reaction between chitosan and genipin can be increased by increasing gelation temperature due to the higher level of molecular mobility, compared with lower temperature [89, 240, 241]. The effect of gelation temperature on bead morphology was investigated by setting up temperature at 20 - 37 - 50^{o}C. As the crosslinking reaction occurred in water-in-oil emulsion follows a moving front evolving from the outside to the inside [140, 242], some time is required to assure the production of structurally stable particles. Moura et al. found that a period of less than 6 h produced unstable chitosan-genipin microparticles which were collapsed during washing and drying steps [243]. Since mild conditions were used (under 50^{o}C), the reaction was conducted for 24 h. After washing steps with hexane and ethanol to remove excess oil and unreacted/intermediate residuals, the hydrogel beads were dehydrated using ethanol and HMDS gradient. HMDS is a low-cost drying agent which does not require expensive machinery but manual handling, which is gentler on biological specimens [244].

The particle yield was calculated based on the weight of dried particles compared to the total amount of dry solids in the initial feed solution. The adopted fabrication process is deemed reliable as the particle yield was high, ranging from 50% to 65% depending on stirring rate (lower stirring rate yielded higher amount of particles). As opposed to hydrogel discs, hydrogel beads produce larger surface areas which ensure efficient contact with cells for sufficient responses. The versatility in methods of fabrication to produce various shapes expands the uses of chitosan hydrogels for various administrative routes, such as oral, implantation, and nasal delivery.

4.2 Chemical changes induced by chitosan-genipin crosslinking

Disc-shaped chitosan-genipin hydrogels, with and without PEG, were synthesised (as detailed in Section 3.2.1, Table 3.1) and freeze-dried (as detailed in Section 3.3). FTIR spectra were recorded (as detailed in Section 3.3) to investigate structural changes upon crosslinking between chitosan and genipin as well as interactions between polymeric segments within a sample (**Figure 4.2**). To provide a closer inspection of the recorded spectra, **Table 4.2** summarises characteristic bands observed in individual gel constituents (chitosan, genipin, and PEG) as well as in some hydrogel samples (CP0G5, CP5G5, and CP5G10; Table 3.1; formed at 37°C/24 h).

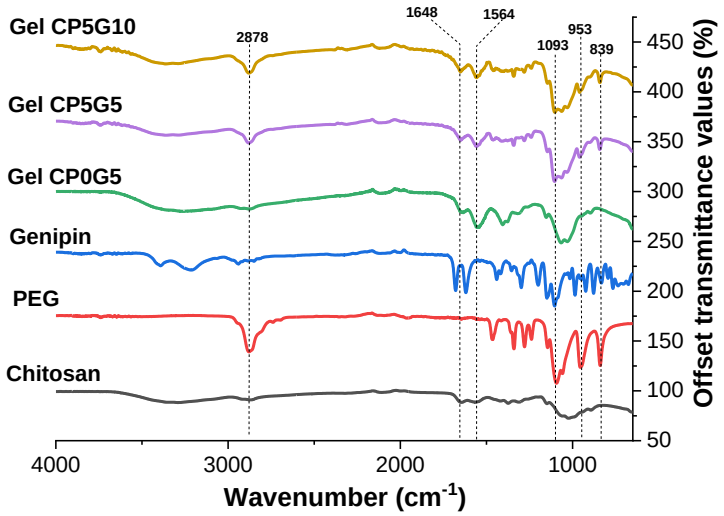

Figure 4.2 FTIR spectra of individual gel constituents (chitosan, genipin, and PEG) as well as disc-shaped chitosan-genipin hydrogels, with and without PEG (CP0G5, CP5G5, and CP5G10; Table 3.1; formed at 37°C/24 h).

Table 4.2 FTIR characteristic bands denoted in individual gel constituents (chitosan, genipin, and PEG) as well as in disc-shaped chitosan-genipin hydrogels, with and without PEG (CP0G5, CP5G5, and CP5G10; Table 3.1; formed at 37°C/24 h).

	Peaks (cm^{-1})					
Assignments	**Chitosan** [245, 246]	**PEG** [247]	**Genipin** [248]	**CP0G5**	**CP5G5**	**CP5G10**
–OH stretching	3351		3327-3390	3353	3362	3362
–C=O (amide)	1648			1641	1647	1649
–NH (amine II)	1564			1542	1555	1559
–OH bending (CH_2OH)	1418			1405	1401	1409
–C=O stretching (CH_2OH)	1372			1378	1370	1369
–CH bending (CH_2OH)	1312			1319	1315	1321
–CH stretching		2878	2939		2879	2878
–C–OH bending		1093			1063	1062
–C–C– chain vibration		953-839			959-841	958-841
–C=C– stretching			1678			
–C–C– stretching (cycloolefin)			1619			

The recorded spectra (**Figure 4.2**) show that characteristic peaks of both chitosan and PEG were observed in the hydrogel spectra, indicating their contributions in the resulting networks. The spectrum of uncrosslinked chitosan reveals characteristic peaks at 1648 cm^{-1} which was assigned to –C=O stretching of amide bond and 1564 cm^{-1} which was assigned to –NH bending of amine band II [246]. These two peaks were observed in the hydrogel spectra but were shifted to lower wavenumbers (**Table 4.2**). With regard to the spectrum of genipin, the peak at 1678 cm^{-1} represented –C=C– stretching and the peak at 1619 cm^{-1} was characteristic of –C–C– stretching of cycloolefin [248]. The spectrum of PEG shows a characteristic peak at 2878 cm^{-1} assigned to –CH stretching, which was unchanged in PEG-containing hydrogels. The peak at 1090 cm^{-1} in PEG's spectrum was assigned to –C–OH bending, which was shifted to a lower wavenumber (1062 - 1063 cm^{-1}) in PEG-containing hydrogels indicating a potential interaction between PEG and chitosan. Indeed, the attractive intermolecular hydrogen bond between –C–OH (PEG) and –OH (chitosan) was previously studied by viscometry with thermodynamic parameters [249]. These parameters were estimated from the experimental viscosity data with different PEG MWs in polyblends of chitosan and PEG. Based on these values, the molecular interaction in chitosan-PEG polyblends was demonstrated to be attractive.

Figure 4.2 also shows that there was a new broad peak at 1350 - 1450 cm^{-1} in the hydrogel spectra, indicating the appearance of heterocyclic amine ring-stretching. The reason for this is related to the crosslinking reaction between chitosan and genipin, which are discussed in Section 2.2.1 [15, 30, 88, 110]. Prior to the addition of genipin, the mixture of chitosan and PEG had a pH around 5. In such acidic condition, primary amino groups of chitosan drive a nucleophilic attack on the olefinic carbon atom (C-3) of genipin, resulting in the opening of the dihydropyran ring and formation of an aldehyde. The aldehyde group is subsequently attacked by secondary amino groups formed in the first step of the reaction leading to the formation of a heterocyclic compound of genipin linked to the glucosamine residue in chitosan [15, 122]. To demonstrate the chemical changes of chitosan during reacting with genipin, disc-shaped chitosan-genipin-PEG hydrogels (sample CP5G5, Table 3.1) were synthesised at different gelation times using method described in Section 3.2.1 and analysed by FTIR (**Figure 4.3**).

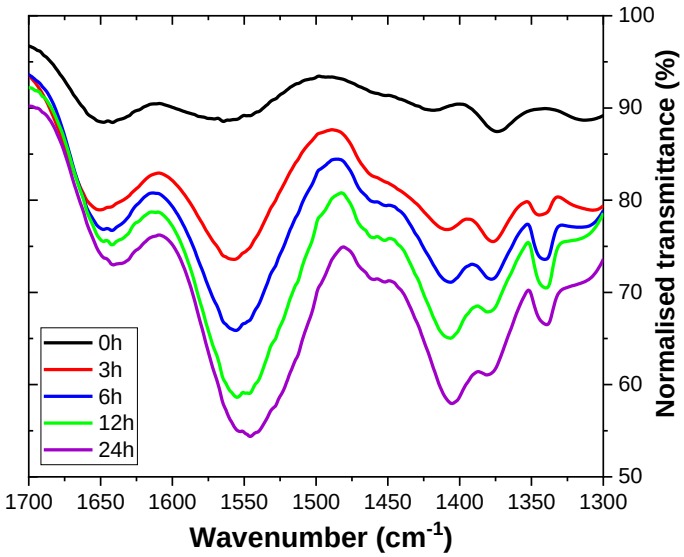

Figure 4.3. FTIR spectra of chitosan-genipin-PEG hydrogels (sample CP5G5, Table 3.1, formed at 37°C) recorded at different curing times.

From **Figure 4.3**, it is apparent that initially the intensity of peaks at 1648 cm^{-1} and 1564 cm^{-1} were about equal. As the gelation progressed, the intensity of amine band II at 1564 cm^{-1} continuously increased over time. Consistent with previous reports [116, 243, 250], this finding indicates the evolution of secondary amino groups as a result of the reaction between carboxylmethyl groups of genipin and primary amino groups of chitosan. FTIR analysis confirms the chemical structure of the synthesised hydrogels and suggests the potential interaction between chitosan and PEG.

4.3 Intrinsic fluorescence upon chitosan-genipin crosslinking

Disc-shaped chitosan-genipin hydrogels, with and without PEG, were synthesised in 24-well black plates with clear bottom (as detailed in Section 3.2.3, Table 3.3) to determine the excitation and emission wavelengths and monitor changes in fluorescence intensity of the hydrogels over gelation time using a monochromator-based fluorescence reader (as detailed in Section 3.4). From the 3D scanning, a detailed plot of excitation wavelength (λ_{EX}), emission wavelength (λ_{EX}), and relative fluorescent units (RFU) is presented (**Figure 4.4a**). Multipoint bottom reading was performed to enhance the signals' sensitivity and changes in RFU over gelation time were recorded (**Figure 4.4b**).

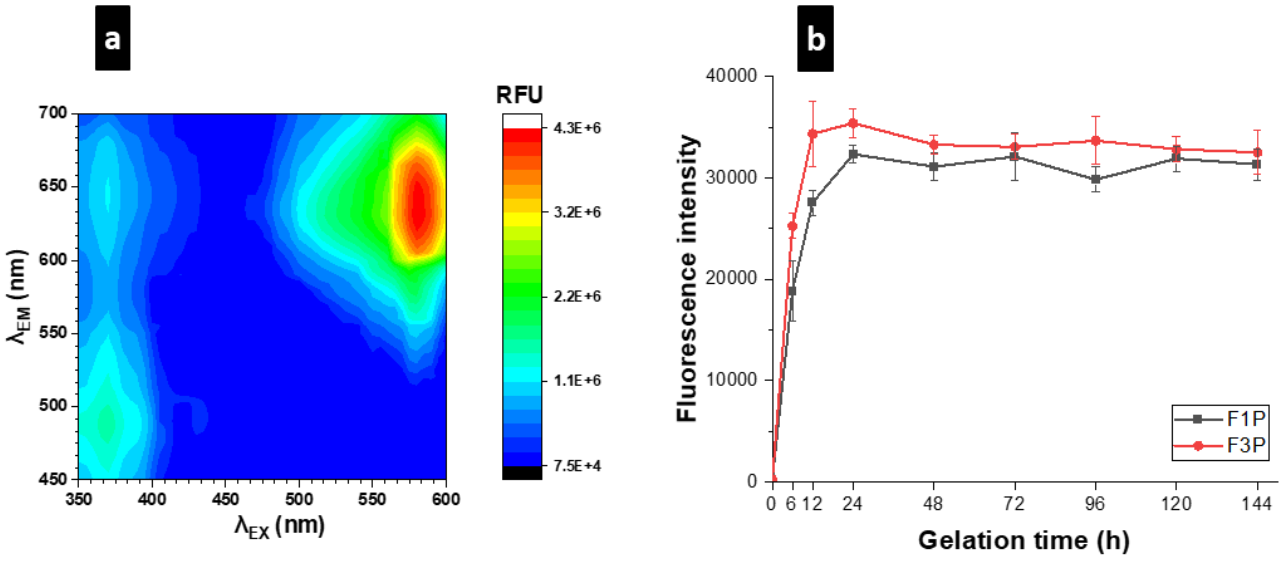

Figure 4.4 (a) Fluorescence contour map of chitosan-genipin-PEG hydrogels prepared in multi-well black plates (sample F1P, Table 3.3, formed at 37°C/24 h). (b) Evolution of fluorescence intensity of chitosan-genipin-PEG hydrogels (sample F1P and F3P, Table 3.3, formed at 37°C) during gelation process. Fluorescence was recorded at excitation/emission wavelengths of 580/630 nm. Data are representative of two independent experiments (n = 4/group). The connecting lines are given as a guide for the eye only and do not represent actual data.

It is evident that genipin-crosslinked networks are able to fluoresce, in result of highly π-π* conjugated derivatives formed by the crosslinking reaction, as shown in the postulated reaction mechanism (Section 2.2.1, Figure 2.4) [240]. Their intrinsic fluorescence is of interest as it can be used to follow the extent of crosslinking, visualise, and track the degradation/distribution in living bodies. To perform the experiment in a non-destructive way without compromising resolution, the hydrogels were prepared in clear-bottomed black plate to reduce the crosstalk and background noise. The 3D scans confirm the presence of a fluorescence peak at the excitation/emission wavelengths of 370/470 nm (**Figure 4.4a**), which is consistent with previous reports [104, 240]. However, **Figure 4.4a** also shows that the hydrogels exhibited a stronger red fluorescence at 580/630 nm, which were then used as optimal excitation/emission wavelengths for fluorescence characterisation.

Figure 4.4b shows the effect gelation time and genipin content have on the hydrogels' fluorescence intensity. There was a speedy increase in fluorescence during the first 12 h, which may reflect the spontaneous reaction of genipin with primary amino groups on chitosan chains. After peak at 24 h, the fluorescence slightly decreased. There are some possible explanations for this observation.

Chen et al. claimed that the small decrease in fluorescence after 24 h may present the collisional quenching during a diffusive encounter with amines and the complex formation by further polymerisation [240, 251]. Later, Matcham et al. also observed reduced fluorescence intensity after a peak value at 18 h which may be caused by interaction of the hydrogel with methanol, the main by-product formed by crosslinking reaction [104]. Based on the amount of genipin used (maximum 0.0063 mmol) in each 1 mL feed solution (containing chitosan, genipin, and PEG), 0.2025 mg of methanol could be theoretically produced, which is much lower than the reference dose for oral exposure to methanol (2 mg/kg/day) [104]. Additionally, the by-products and any remaining residuals can be washed out upon administration, retaining the suitability of these hydrogels for biomedical applications. It is evident that gelation temperature also significantly affects the hydrogels' fluorescence. Chen et al. demonstrated that the hydrogels polymerised at higher temperature (37^{o}C) fluoresced more strongly than those reacted at lower temperature (20^{o}C, 4^{o}C), possibly due to the accelerated molecular mobility at 37^{o}C [240]. These results correspond with the changes in physical appearance shown in Table 4.1.

Changes in fluorescence intensity as a function of genipin content are also presented in **Figure 4.4b**. The hydrogels with lowest amount of genipin (F1P) reached a lower fluorescence peak compare to those with highest genipin content (F3P), consistent with previous reports [104, 252]. As PEG itself is non-fluorescent, addition of PEG to form semi-IPN network did not alter the hydrogel fluorescence significantly. It should be noted that there are several variables which make it difficult to standardise fluorescent measurements such as the type of equipment, set-up parameters, and the detection method. As different fluorophores excite and emit at different wavelengths, it presents a challenge to compare fluorescent results from hydrogels made of different constituent chemicals. However, for hydrogel materials composed of the same constituent molecules, fluorescent imaging provides a non-destruction approach for real-time monitoring of material production, conformation changes, and degradation. In Chapter 5, the intrinsic fluorescence of hydrogels was exploited for tracking biodegradation *in vitro* (Section 5.3) and *in vivo* (Section 5.4). Another promising application of this technique is in drug delivery. The loaded drug containing functional groups may preferentially interact with chitosan, limit the target site with genipin, and quench the fluorescence. Thus, changes in fluorescence upon drug loading and release could inform the potential interaction between moieties and can be used a measurement for drug release.

Bead-shaped chitosan-genipin hydrogels, with and without PEG, were synthesised using emulsion crosslinking (as detailed in Section 3.2.2) and their fluorescence was visually observed under a fluorescence microscope (as detailed in Section 3.4).

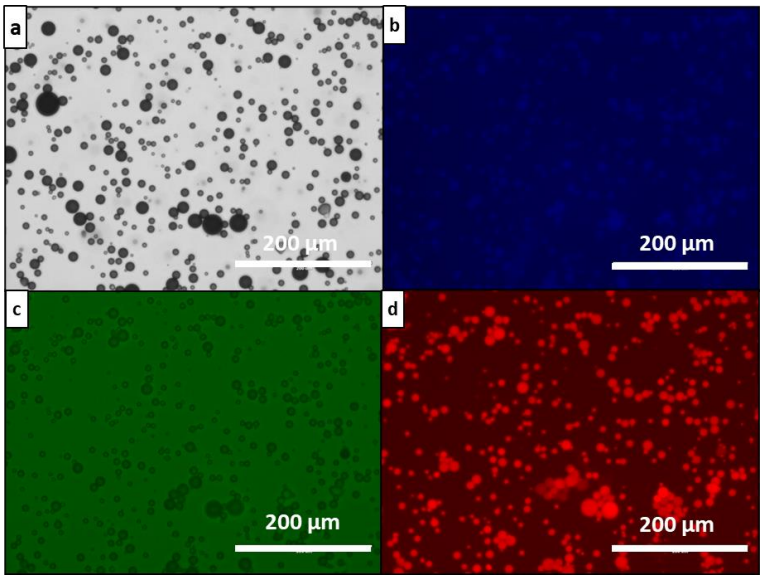

Figure 4.5 Bead-shaped chitosan-genipin hydrogels prepared at 37°C and stirring speed of 250 rpm under fluorescence microscope with (a) transparent filter; (b) DAPI filter; (c) GFP filter; (d) RFP filter.

As shown in **Figure 4.5**, the hydrogel beads showed brightest emitted light using RFP (red) filter, compared to DAPI (blue) and GFP (green) filters. Either prepared in disc shape or bead shape, the resulting hydrogels possessed intrinsic fluorescence. Therefore, there is no need for introduction of a fluorescent tag (such as fluorescein isothiocyanate (FITC), Cy 5.5, and Texas Red) which is commonly required for visualising non-fluorescent materials. The labelling approach using a fluorescent marker involves the covalent linking and basic blending of fluorescent marker and the polymers [253]. Upon fluorescence-labelling step, the fluorescent marker may react with some functional groups on polymeric backbones, and hence affect the mechanical integrity of the materials. In addition, the fluorescent marker may attach loosely at the intended sites and migrate into other sites, compromising intended results. The labelling efficiency and stability are also persistent issues. Such common problems are negligible within this system, which enables efficient visualisation with no prior fluorescence-labelling step required. Another major advantage of using genipin as a crosslinker is its high selectivity. It is evidence that primary amino group ($–NH_2$) is the only site targeted by genipin, while the nucleophilic –OH groups (-OH and –COOH) do not react with genipin [108, 254]. In a study, it was confirmed that no changes in physical appearance

were detected upon genipin-alginate reaction (alginate contains only –OH and –COOH without –NH_2 groups) and no bright images under fluorescent channels of CLSM acquired from genipin-alginate beads [240]. On the other hand, common fluorescent markers, such as FITC and Rhodamine B isothiocyanate, contain activated isothiocyanate groups reacting with both –NH_2 and –OH groups [253]. Thus, they are deemed not suitable for labelling to distinguish between chitosan and alginate simultaneously in a hybrid system. The high sensitivity towards chitosan (or any amine-containing compounds) with the potential to generate blue-coloured fluorescent products makes genipin a promising crosslinker/visualisation reagent.

4.4 Morphological characteristics of crosslinked hydrogels in disc and bead shapes

4.4.1 Disc-shaped hydrogels

SEM was chosen to visualise the network structure. Disc-shaped chitosan-genipin hydrogels, with and without PEG, were synthesised (as detailed in Section 3.2.1, Table 3.1) and freeze-dried (as detailed in Section 3.3). The images taken at different positions across the surface and cross-sections of freeze-dried disc-shaped chitosan-genipin-PEG hydrogels (sample CP5G5, Table 3.1) were chosen to demonstrate the outer and inner porous structures of the crosslinked hydrogels (**Figure 4.6**). To evaluate the effect of genipin and PEG content on sample porosity, the images from the horizontal sections of all freeze-dried disc-shaped hydrogels denoted in Table 3.1 were chosen for the ease of comparison (**Figure 4.7**).

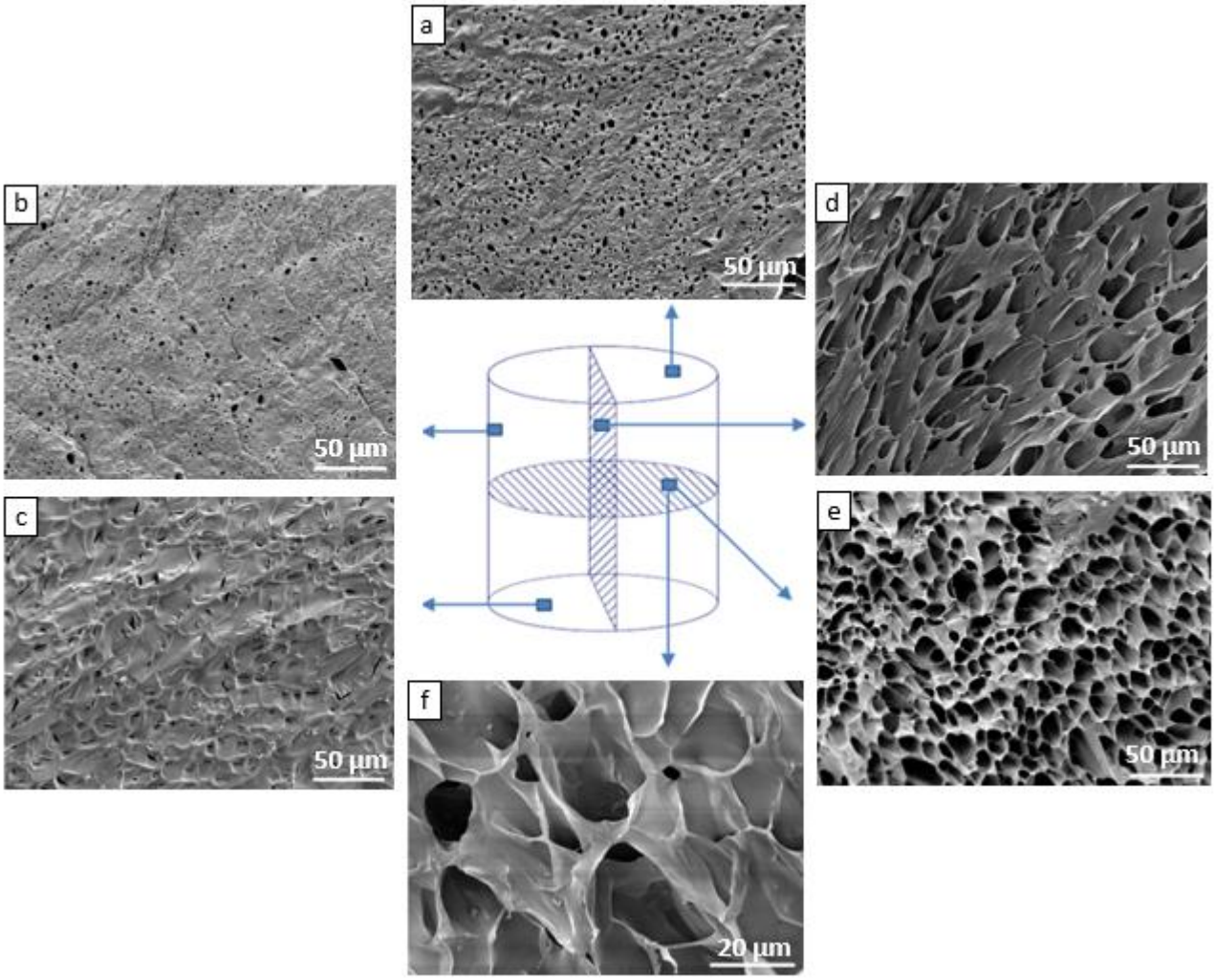

Figure 4.6. SEM images (with magnification of 1000x) taken across the surface area and cross-sections of disc-shaped chitosan-genipin-PEG hydrogels (sample CP5G5, Table 3.1, formed at 37^{o}C/24 h): (a) top surface; (b) curved surface; (c) bottom surface; (d) vertical section; (e) horizontal section; (f) horizontal section with higher magnification (2000x).

Looking at the outer surface only, it can be noted that the gels had a rough surface with more pores on the top (**Figure 4.6a**) than at the side (curved) surface (**Figure 4.6b**) and bottom surface (**Figure 4.6c**). While freeze-drying is the most suitable method to preserve the porous structure, compared to air drying or critical point drying, freezing stresses occur at the hydrogel surface resulting in shrinkage and collapse of the sample surface to some extent [255, 256]. This is the reason for the difference in porosity between surface and internal sections. The scans from horizontal and vertical cross-sections indicate the pore arrangement resembling long hollow tubes (**Figure 4.6d,e**) in which the pores were interconnected (**Figure 4.6f**). Having interconnected pores is important to

allow not only the encapsulation of bioactive materials but also the subsequent release in a desirable medium. The pore size, pore morphology, and interconnectivity are interrelated and influence the permeability of fluid through hydrogels [257, 258]. Regardless of variation in genipin and PEG content, representative electron micrographs of horizontal sections confirm the porous architecture of all crosslinked hydrogels studied (**Figure 4.7**). To evaluate the internal porosity quantitatively, ImageJ software was used to calculate the pore sizes and pore areas based on images from horizontal sections. The results are presented in **Table 4.3**.

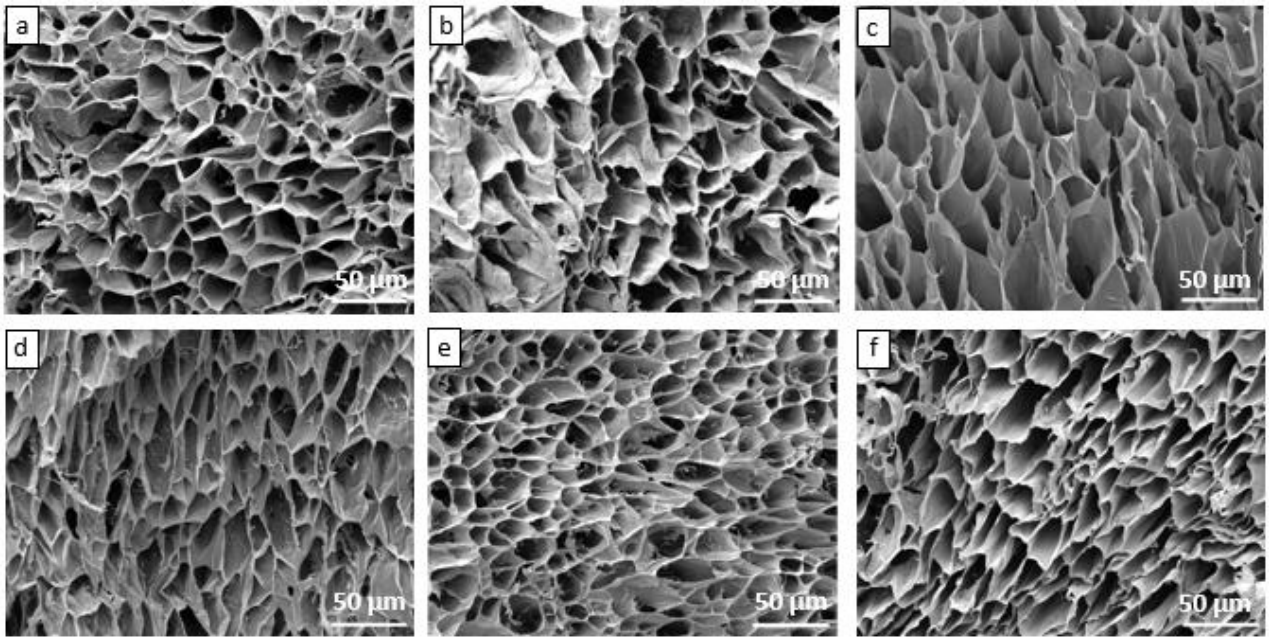

Figure 4.7. SEM images of horizontal sections of disc-shaped chitosan-genipin hydrogels, with and without PEG (Table 3.1, formed at 37ºC/24 h): (a) CP0G5; (b) CP5G5; (c) CP15G5; (d) CP0G10; (e) CP5G10; (f) CP15G10.

Table 4.3. Pore size distribution, average pore size, and porous area of horizontal sections of disc-shaped chitosan-genipin hydrogels, with and without PEG (Table 3.1, formed at 37ºC/24 h) analysed using ImageJ software.

Sample name	**Pore size distribution range (µm)**	**Average pore size (µm)**	**Porous area (%)**
CP0G5	19.89 - 55.89	38.16 ± 9.58	40.22 ± 4.53
CP0G10	12.73 - 57.41	33.65 ± 9.49	42.14 ± 8.65
CP5G5	12.97 - 34.81	24.63 ± 3.55	52.59 ± 5.89
CP5G10	11.48 - 26.30	18.14 ± 2.16	50.19 ± 3.24
CP15G5	15.65 - 36.29	25.04 ± 2.89	64.21 ± 2.45
CP15G10	13.70 - 37.62	21.71 ± 3.62	59.54 ± 1.96

From **Figure 4.7** and **Table 4.3**, it can be noted that in the absence of PEG, pore size distribution was broader than in PEG-containing hydrogels. Addition of PEG (1.2 mM) decreased average pore size significantly and increased porous area, compared to non-PEG-added hydrogels. A further increase in PEG content to 3.6 mM did not make significant changes in average pore size but further increased porous area (compared to gels with 1.2 mM PEG). It is also apparent that in samples containing constant concentrations of chitosan and PEG (CP5G5, CP5G10; as well as CP15G5, CP15G10), increasing genipin content (from 3.1 mM to 6.3 mM) reduced pore size distribution and average pore size (**Table 4.3**). Such a trend is expected as an increase in concentration of crosslinking agent should result in a higher number of linked chains and therefore a decrease in average pore size. Taking all samples studied into account, it can be noted that a direct correlation between pore size distribution and total porous area was not observed.

4.4.2 Bead-shaped hydrogels

Bead-shaped chitosan-genipin hydrogels were synthesised using emulsion crosslinking (as detailed in Section 3.2.2). To visualise the particles, light microscope was used (**Figure 4.8**). To strengthen the findings obtained by light microscope and quantify the particle size, SEM was performed on air-dried bead-shaped hydrogels (as detailed in Section 3.5), synthesised with different stirring rates (**Figure 4.9**) and gelation temperature (**Figure 4.10**).

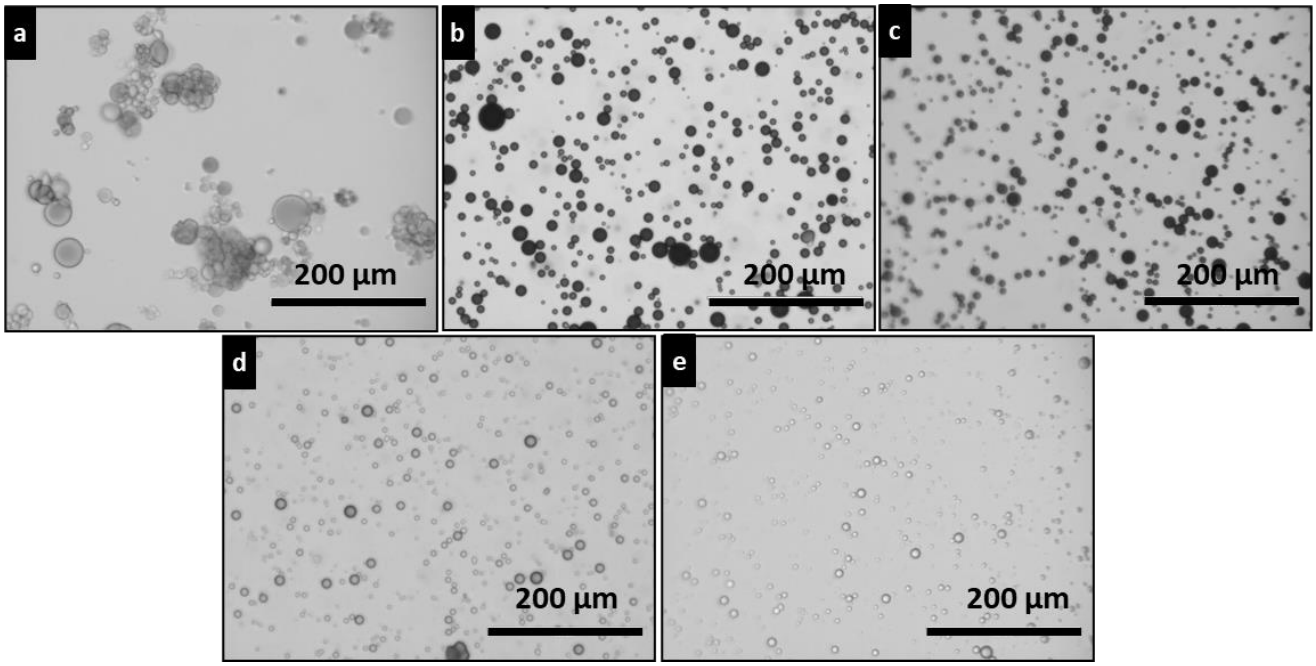

Figure 4.8 Light microscope images of bead-shaped chitosan-genipin hydrogels prepared at different incubation temperatures and stirring rates, and dispersed in ethanol: (a) 20^{o}C, 250 rpm; (b) 37^{o}C, 250 rpm; (c) 50^{o}C, 250 rpm; (d) 37^{o}C, 500 rpm; (e) 37^{o}C, 750 rpm.

As shown in **Figure 4.8**, under optical microscope, the hydrogel beads were discrete and spherical with heterogeneous size distribution, except the particles prepared at 20^{o}C and stirring speed of 250 rpm, which were not completely formed and appeared as large aggregates. Light microscope images also show that an increase in stirring speed from 250 rpm to 500 rpm or 750 rpm reduced the particle size. Under SEM, the hydrogel particles were globular, compact, and rough (**Figure 4.9**). The images also show no visible pores on the beads' surface. Air-dried by evaporation of HMDS is deemed suitable as most particles retained their physical integrity with minimum collapse. An incubation period of 24 h is appropriate as the hydrogels appeared physically stable and were completely formed (except the particles prepared at 20^{o}C, 250 rpm). Visual analysis by SEM also shows the effect of stirring rate (**Figure 4.9**) and incubation temperature (**Figure 4.10**) on the hydrogel beads' morphology.

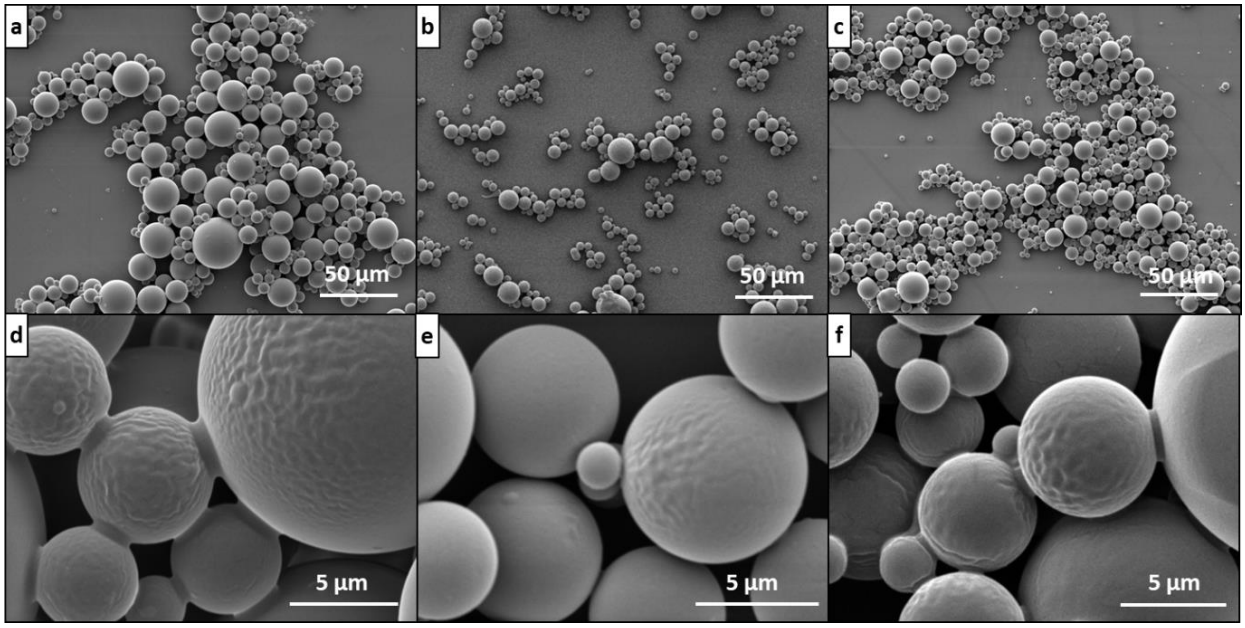

Figure 4.9 SEM images of bead-shaped chitosan-genipin hydrogels prepared at 37ºC with different stirring rates, scanned at different magnifications: (a, d) 250 rpm; (b, e) 500 rpm; (c, f) 750 rpm.

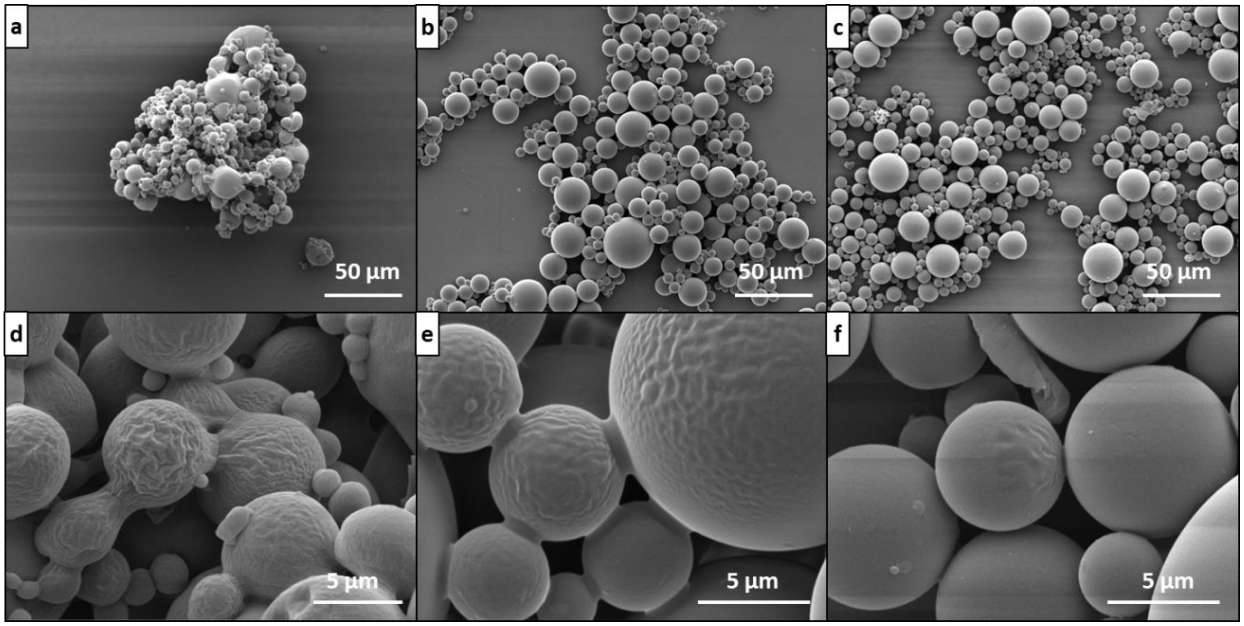

Figure 4.10 SEM images of bead-shaped chitosan-genipin hydrogels prepared at stirring rate of 250 rpm with different incubation temperatures, scanned at different magnifications: (a, d) 20ºC; (b, e) 37ºC; (c, f) 50ºC.

At a constant incubation temperature of 37ºC, a stirring speed of 250 rpm produced stable particles with well-defined round shape, rough surface, and no visible pores (**Figure 4.9a,d)**. Increasing stirring speed to 500 rpm or 750 rpm produced smaller spherical particles with less rough and non-

porous surface (**Figure 4.9b-f**). Such observation is explainable as stirring causes the dispersion of polymeric particles in organic phase and higher stirring speed induces higher shearing force and more homogeneous dispersion of the particles. Generally, the higher stirring speed applied, size of particles decreases with narrow particle size distribution (PSD) [243, 259].

At a constant stirring speed of 250 rpm, an incubation temperature of 20^{o}C produced macroscopically non-homogeneous multi shape structures (**Figure 4.10a**) with rough surface and no visible pores (**Figure 4.10d**). Increasing the temperature to 37^{o}C, the beads appeared spherical (**Figure 4.10b**) with fairly smooth surface (**Figure 4.10e**). At 50^{o}C, the particle solidification occurred at faster rate, as the reaction turned from milky white to bluish clear fluid within 8 h, much faster than the reaction occurred at 37^{o}C. The produced hydrogel beads at 50^{o}C were globular, compact, and smooth without visible pores (**Figure 4.10c,f**). In the light of this analysis, the incubation temperature of 37^{o}C (to resemble physiological condition) and stirring rate of 500 rpm were chosen to produce hydrogel beads for biological evaluation (presented in Chapter 5). A moderate stirring rate (500 rpm) was chosen to ensure the formation of small particles and increase the surface areas in contact with cells. A high stirring rate of 750 rpm caused more particles stuck at the wall of glassware and reduced the particle yield.

Several SEM images per sample were used to determine mean particle sizes instead of scattering methods (suspended in water/ethanol) because of the preferential swelling/shrinking and dissolution of the particles. ImageJ software was used to measure the particle diameters. Mean particle diameter and its distribution were calculated for each composition by counting a minimum of 100 particles per image. The results are shown in **Figure 4.11**.

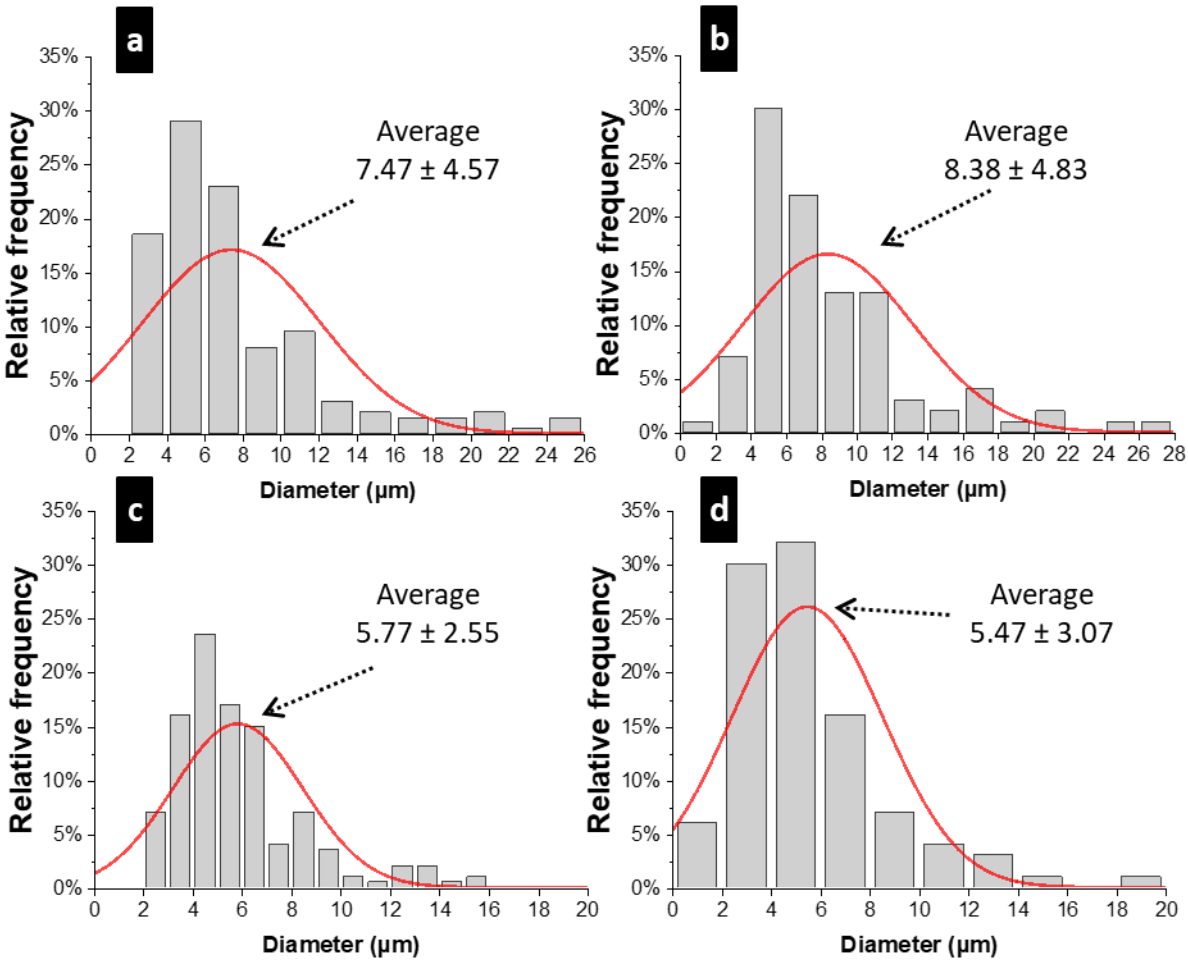

Figure 4.11 Histogram and particle size distribution of bead-shaped chitosan-genipin hydrogels prepared at different incubation temperatures and stirring rates: (a) 37°C, 250 rpm; (b) 50°C, 250 rpm; (c) 37°C, 500 rpm; (d) 37°C, 750 rpm.

The sizes of hydrogel beads, measured by ImageJ software based on SEM images, were all within micrometre range, from 1 µm to 30 µm. It also shows that stirring rate had more profound effect on particle size, than those of incubation temperature. An increase in stirring rate from 250 rpm to 500 rpm produced smaller particles with heterogeneous size distribution (**Figure 4.11a,c**). At 750 rpm, the particles appeared smaller with narrow PSD (**Figure 4.11d**). Changes in incubation temperature from 37°C to 50°C did not induce a distinct difference in particle size (high dispersity in size with average diameter of around 7 - 8 µm, **Figure 4.11a,b**). In addition to stirring speed, size of the particles is found to be dependent on the proportion of crosslinker used [216]. Generally, particle size increases as the polymer concentration or the crosslinker to polymer ratio increases [243, 260]. In term of drug delivery, control in particle size is crucial as particle size would affect

the rate and extent of drug release and subsequent pharmacokinetics. The production process is deemed reliable to achieve the intended end-point with specific size range, suitable for various routes of administration.

As discussed in Section 2.1.3, addition of linear polymers (such as PEG) into chitosan-genipin matrix to form semi-IPN hydrogels is favourable as it might enhance reproducibility, achieve consistency in physical properties, and further improve mechanical robustness. Bead-shaped chitosan-genipin hydrogels, with adding PEG, were synthesised using emulsion crosslinking (as detailed in Section 3.2.2). SEM images of PEG-added chitosan-genipin hydrogel beads (**Figure 4.12a,c**) show no profound differences in surface morphology compared to non-modified beads. Size analysis of PEG-added chitosan-genipin particles using ImageJ shows a similar size range as chitosan-genipin particles (average particle diameter: 8.03 ± 5.32 µm).

Surface modification by coating with PEG, so-called PEGylated particles, might help to avoid opsonisation and increase the hydrophilicity as well as circulation of particles upon administration [261]. Post-synthesis modification was carried out by placing the pre-formed chitosan-genipin particles in PEG solution (5% w/v) for 6 h. SEM images of PEG-coated particles show the initial absorption of polymer on the particles' surface within 6 h, indicating that longer incubation time (more than 6 h) is required for a complete coating layer (**Figure 4.12b,d**).

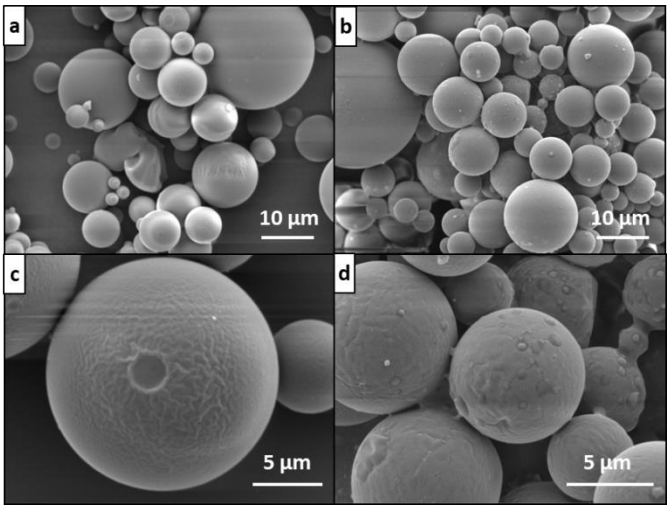

Figure 4.12 SEM images of bead-shaped chitosan-genipin hydrogels prepared at 37^{o}C and stirring rate of 250 rpm, and modified with PEG during or post synthesis, scanned at different magnifications: (a, c) PEG-added particles; (b, d) PEG-coated particles.

4.5 Swelling characteristics of crosslinked hydrogels in disc shape

Gravimetric swelling experiments were conducted to examine the pH responsiveness of disc-shaped chitosan-genipin hydrogels, with and without PEG. To examine the pH-responsiveness in different buffer solutions, disc-shaped chitosan-genipin-PEG hydrogels (sample CP5G5, Table 3.1) were synthesised (as detailed in Section 3.2.1) and placed in different buffer solutions to observe the variation in mass (**Figure 4.13**) (as detailed in Section 3.6.1). Two sets of disc-shaped chitosan-genipin hydrogels, with and without PEG (denoted in Table 3.1 and Table 3.2, Section 3.2.1) were used to assess the effect of genipin and PEG content on swelling behaviours (**Figure 4.14** and **Figure 4.15**).

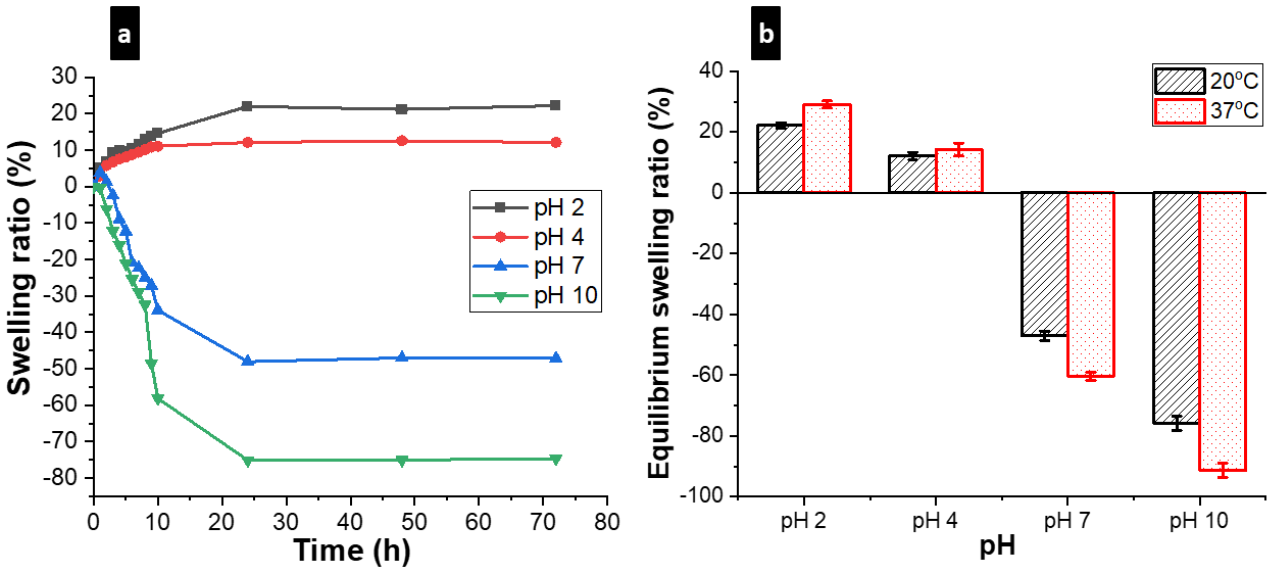

Figure 4.13 (a) The swelling ratio (%) over time and (b) equilibrium swelling ratio of disc-shaped chitosan-genipin-PEG hydrogels (sample CP5G5, Table 3.1, formed at 37°C/24 h), in different buffer solutions at 20°C. In figure (a), the connecting lines are given as a guide for the eye only and do not represent actual data. In figure (b), data are representative of two independent experiments (n = 6/group).

As seen in **Figure 4.13**, the differences in swelling in different pH buffer solutions were significant. The gels achieved the highest swelling degree in pH 2 buffer followed by pH 4 buffer and contracted significantly in pH 7 buffer and even more in pH 10 buffer. The observed trends are anticipated as chitosan hydrogels fall under the category of cationic hydrogels in which their functional groups are protonated below their dissociation constant (pKa) causing the hydrogels to swell. The swelling process is a complex phenomenon involving three successive steps, the

diffusion of solvent into the network, the chain relaxation within the hydrated gels, and the expansion of network [154]. When environmental pH is lower than the pKa of chitosan (6.5 to 6.7 depending on the degree of deacetylation), free amino groups of chitosan receive protons introduced by the uptake of solvent [262]. The protonated amino groups of chitosan induce electrostatic repulsion within the network and the gel begins to swell, eventually reaching equilibrium. It can be said that the higher level of free amino groups within the network, the greater is the electrostatic repulsion between polymeric chains, and the higher swelling rate. When environmental pH is above the pKa of chitosan, free amino groups of chitosan donate protons as solvent diffuses into the network. The deprotonated amino groups of chitosan reduce electrostatic repulsion within the network, leading to hydrogel contraction until equilibrium is reached. **Figure 4.13a** shows that the equilibrium swelling state of gel CP5G5 achieved after approximately 24 h (or less, as the previous sample was taken at approximately 10 h and equilibrium may have been reached between these two time points) of immersion in buffer solutions. **Figure 4.13b** shows that an increase in buffer temperature (from 20^{o}C to 37^{o}C) led to higher swelling ratio. It is possibility that higher temperature would induce faster segmental mobility and chain relaxation rate, resulting in higher swelling degree observed.

To investigate the effect of hydrogel composition on swelling, all disc-shaped hydrogels (Table 3.1, Section 3.2.1) were gravimetrically evaluated for swelling in pH 2 glycine buffer solutions at 20^{o}C until they reached the equilibrium state after approximately 24 h (**Figure 4.14**).

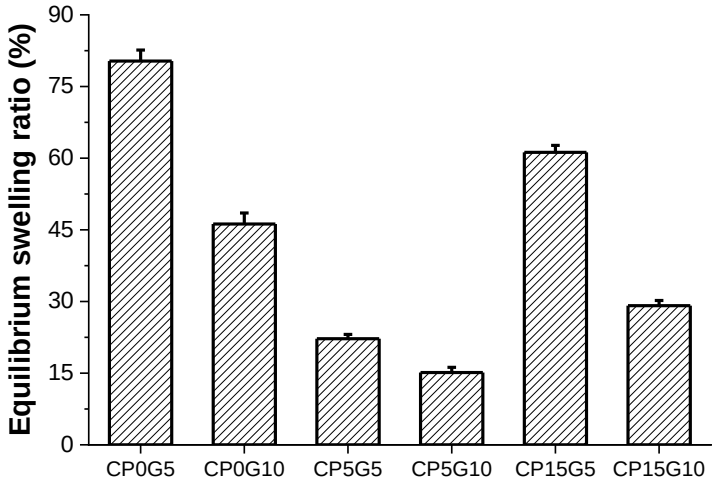

Figure 4.14 Equilibrium swelling ratio of disc-shaped chitosan-genipin hydrogels, with and without PEG (Table 3.1, formed at 37^{o}C/24 h), in pH 2 buffer solutions at 20^{o}C for 24 h. Data are representative of two independent experiments (n = 6/group).

In all cases, at a constant concentration of chitosan and PEG, increasing genipin content decreased the swelling ratio (**Figure 4.14**). A higher genipin content is associated with a more crosslinked structure and a lower level of free amino groups on chitosan chains, leading to a lower relaxation rate of polymeric segments in acidic conditions and hence a reduced swelling ratio. A lower swelling degree was also achieved by addition of PEG to form a semi-IPN network. Interestingly, adding less PEG (1.2 mM; in CP5G5 and CP5G10) resulted in a greater decrease in swelling ratio, than when more PEG was added (3.6 mM; in CP15G5 and CP15G10). To further investigate the effect of PEG addition on swelling, a series of disc-shaped chitosan-genipin hydrogels with varied PEG content (Table 3.2, Section 3.2.1) were gravimetrically monitored in pH 2 glycine buffer solutions at 20^{o}C until they reached the equilibrium state (approximately 24 h). The data are presented in **Figure 4.15**.

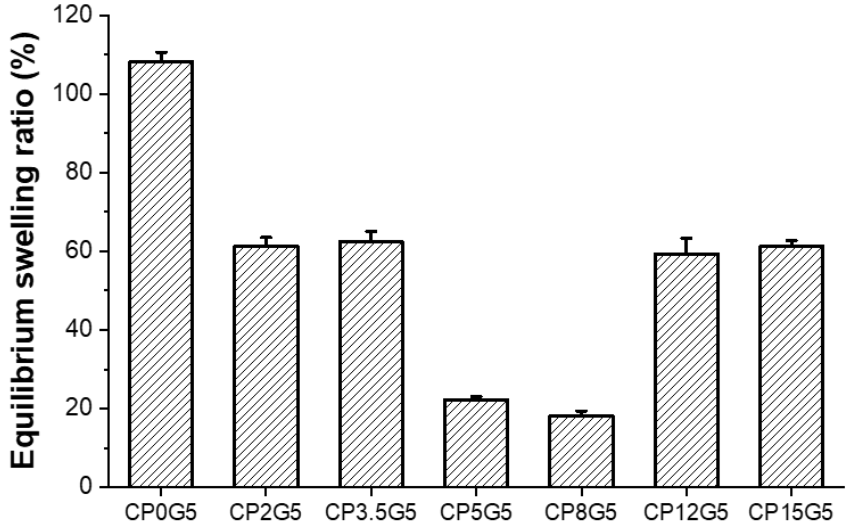

Figure 4.15 Equilibrium swelling ratio of disc-shaped chitosan-genipin hydrogels with varied PEG content (Table 3.2, formed at 37^{o}C/24 h), in pH 2 buffer solutions at 20^{o}C for 24 h. Data are representative of two independent experiments (n = 6/group).

It can be noted that for the range of samples studied, addition of PEG reduced the swelling ratio of hydrogels. At the same time, the recorded correlation between PEG content and swelling capability was non-linear. Addition of PEG in a lower concentration, up to 0.8 mM (CP2G5 and CP3.5G5), decreased swelling degree to around 60% (**Figure 4.15**). Further increasing PEG concentration up to 1.9 mM (CP5G5 and CP8G5), yielded further decrease in swelling degree to approximately 20%. Interestingly, further addition of PEG (2.9 mM and 3.6 mM, in CP12G5 and CP15G5 respectively) increased swelling ratio to approximately 60%. It can be postulated that the presence

of PEG in smaller quantities (up to 1.9 mM) contributes to filling the spaces within the hydrogel network, resulting in the formation of a more interpenetrating network, which limits the solvent diffusion into the gel and induces a lower swelling ratio. As noted from morphological studies (Section 4.4), the swelling capacity cannot be simply related to only the degree of porosity or the pore size, as the pore geometry and interconnectivity also affect the response kinetic of porous hydrogels [257]. PEG concentration of 2.9 - 3.6 mM may interact more strongly with chitosan and impair the crosslinking reaction between chitosan and genipin, resulting in a reduced crosslinking density and hence a looser network [249]. The inhibitory effect of additional polymer (such as cellulose nanocrystals [263] and hemicellulose [264]) on chitosan-crosslinked hydrogels was previously reported. Additionally, such a high amount of PEG may induce hydrophilicity and provide a super-absorbing nature for solvent uptake.

To further evaluate the effect of gelling conditions on swelling, disc-shaped chitosan-genipin-PEG hydrogels (sample CP2G5, Table 3.2) were synthesised at different gelation times and gelation temperatures and placed in pH 2 buffer solutions (as detailed in Section 3.6.1). The results presented in **Figure 4.16a** show that when temperature increased from 20^{o}C to 37^{o}C, the equilibrium swelling ratio decreased significantly due to higher crosslinking density within polymeric networks that may hinder the water absorption. Gelling process at higher temperature from 45^{o}C to 60^{o}C led to an increase in water absorption capacity. It has been reported that high temperature may damage hydrogel network through physical interactions (such as hydrogen bonding, Van der Waals, and electrostatic attraction) or the potential cleavage of glycosidic bonds in chitosan backbone [248].

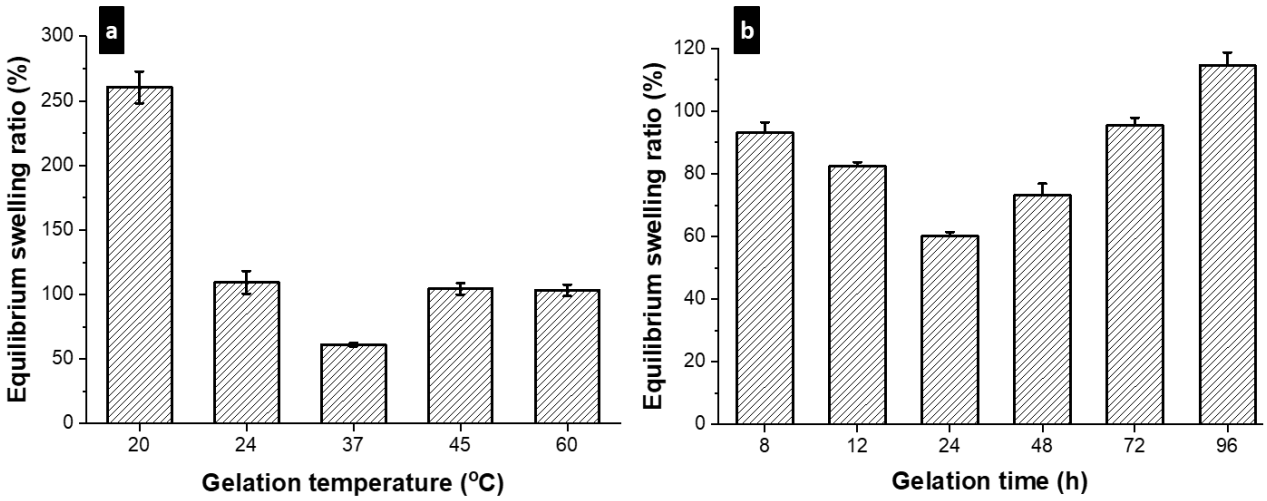

Figure 4.16 Equilibrium swelling ratio of disc-shaped chitosan-genipin-PEG hydrogels (sample CP2G5, Table 3.2) prepared at different (a) incubation temperatures and (b) gelation times, in pH 2 buffer solutions at 20°C for 24 h. Data are representative of two independent experiments (n = 6/group).

Figure 4.16b shows that when gelation time increased from 8 h to 24 h, there was a moderate decrease in swelling ratio. This is probably because the longer the gelation time (up to 24 h), the higher is the crosslinking density within gel network. The higher crosslinking density leads to smaller pores and denser network which can obstruct the water uptake, resulting in decreased swelling ratio. However, with further exposure to oven temperature (from 48 h to 96 h), there was a significant increase in the volume transition of these gels. The longer the exposure time, the more likely is that the damage of physical bonding occurred leading to the reduced network stability and lower swelling ratio. The effect of gelation time on swelling was also reported previously. In study of another semi-IPN hydrogels composed of chitosan/ poly vinylpyrrolidone crosslinked with genipin, they showed that as gelation time increased, the number and size of pores within bulk structure decreased significantly [248]. Understanding the impact of incubation temperature and gelation time on swelling is beneficial to tailor the hydrogels' microstructure and meet end-use applications.

As mentioned in Section 2.2.2, an autonomous 'all polymeric' system for optimal drug delivery can be achieved by coupling pH-responsive hydrogels with an oscillatory chemical reaction which produces profound oscillations in pH and works as an internal driving force to achieve a pulsed release of entrapped biomolecules. As a part of strategic development of pulsatile drug delivery devices pursued in Novakovic group, the feasibility of these chitosan-genipin-PEG hydrogels to be

coupled with PCPOC reaction is of interest. Served as a preliminary experiment, the swelling response was investigated under a manually pH-controlled oscillatory course. Disc-shaped chitosan-genipin-PEG hydrogels (sample CP2G5, Table 3.2) were synthesised (as detailed in Section 3.2.1) and placed in an alternate fashion between pH 2 and pH 4 or pH 7 buffers with a period of 15 min (as detailed in Section 3.6.2). As the PCPOC reaction exhibits oscillations between pH 2 and 5 with a period of oscillation that can be varied but in general remains in the region of 30 min [38], a period of 15 min is deemed appropriate as this is faster than what is required in a real oscillatory system. The results are presented in **Figure 4.17**.

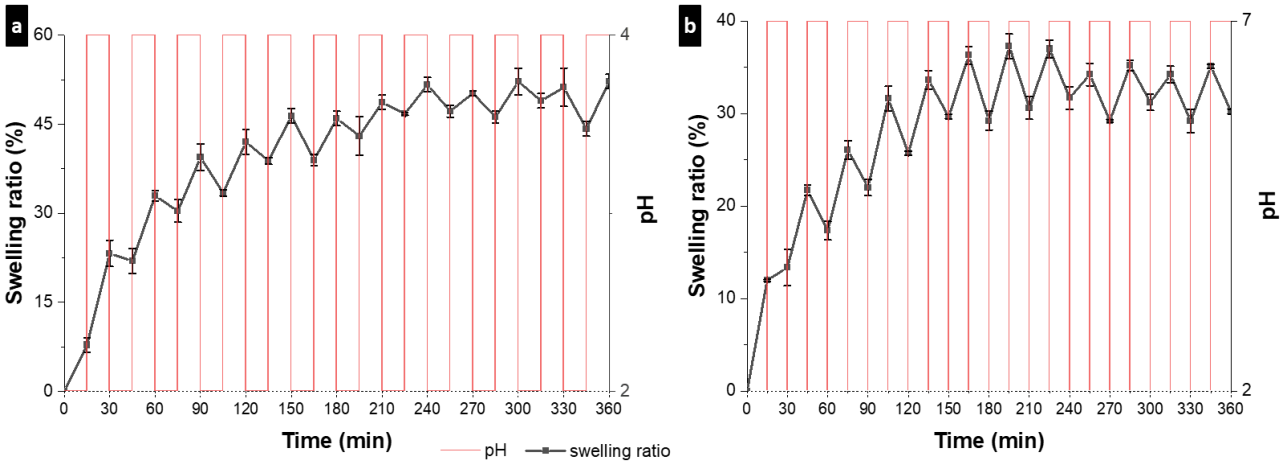

Figure 4.17 Oscillatory swelling of disc-shaped chitosan-genipin-PEG hydrogels (sample CP2G5, Table 3.2, formed at 37ºC/24 h), immersed in buffer solutions at 20ºC, in an alternate fashion: (a) pH 2 first then pH 4; (b) pH 2 first then pH 7. The connecting lines are given as a guide for the eye only and do not represent actual data. Data are representative of two independent experiments (n = 4/group).

As shown in **Figure 4.17a**, there was a slight oscillation where the gel was placed in a pH 2 buffer first then transferred to pH 4 buffer. Following initial swelling within first 30 min, oscillatory behaviour in swelling was observed with relatively small amplitude. The overall swelling ratio increased gradually until 4 h before reaching the equilibrium state, then oscillated around a set volume. Increasing the amplitude of pH oscillation (changing between pH 2 and 7) induced more profound swelling oscillations (**Figure 4.17b)**. After a steady increase in swelling ratio within the first 45 min, the gel started to exhibit oscillations in swelling as the oscillations in pH were manually induced. These findings suggest that to drive changes in swelling/deswelling promptly in a response to pH oscillations, it is necessary that the pH changes happen inside the hydrogels, in the proximity of functional groups. This is the concept studied in Novakovic group and currently

under development (as discussed in Section 2.2.2). Within this concept, an imine-functionalised palladium-bearing chitosan crosslinked with genipin and a polymer substrate (monoalkyne-terminated PEG) are combined in a gel matrix so that both substrate and catalyst are part of the hydrogel structure [39].

Despite showing oscillatory behaviours over small pH range, gravimetric measurements face some major problems, such as the fragmentation issue when transferring the samples between buffer solutions and weighing scales, and the fragile nature of hydrogels leading to extensive mass loss. Some other techniques could be employed to visualise the swelling behaviour in a non-invasive way, such as confocal laser scanning microscope.

4.6 Rheological characteristics of crosslinked hydrogels

4.6.1 Gelation point

Gelation point is an important parameter that needs to be considered in the development of crosslinked hydrogels. At the gel point, the viscoelastic properties change abruptly from a liquid-like state to a solid-like state, resulting in a sudden loss of flow [238, 265, 266]. Oscillatory time sweeps were performed to track the temporal evolution of dynamic shear moduli over time and determine the gelation point. Hydrogel samples were loaded onto a rheometer as a liquid (initial feed solution as defined in Section 3.2.1, Table 3.1) and dynamic shear moduli were monitored over gelation time (as detailed in Section 3.7.1). The results are presented in **Figure 4.18**.

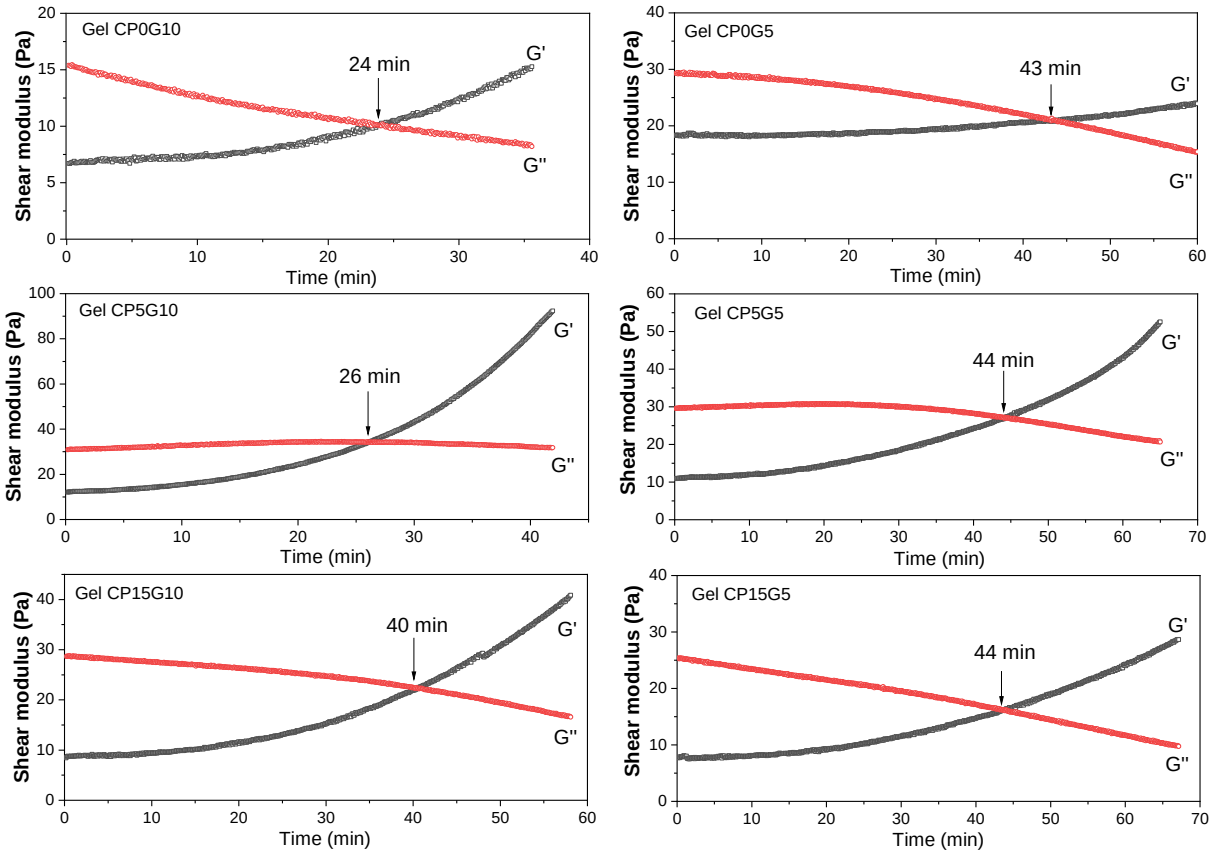

Figure 4.18 Dynamic of shear elastic modulus (G') and viscous modulus (G'') of chitosan-genipin hydrogels, with and without PEG (Table 3.1, formed at 37ºC) during crosslinking process, measured at a constant frequency of 10 Hz and a constant strain of 1%.

From **Figure 4.18**, it can be noted that elastic modulus (G') was initially much smaller than the viscous modulus (G''). This is expected as the sample was loaded in liquid state where the viscous property dominates and the small elastic contribution is a result of the stretching of polymeric chains under applied forces and potentially physical entanglements between the polymers [238, 267]. As the gelation progressed, the elastic modulus began to increase as the elastic property started to dominate. Consequently, there was a cross-over point at which G' intersects G''. The time required for this cross-over point to occur was taken as the gelation time. The G'' value decreased over time, however it never dropped to zero indicating the viscoelastic nature of the resulting hydrogels [238, 268].

The effect of gel composition on gelation kinetics is also revealed. As expected, an increase in genipin content led to a lower gelation time. In gels with 1.2 mM PEG (CP5G5, CP5G10), the gelation time decreased by 41% (from 44 min to 26 min) by increasing genipin concentration in hydrogel samples from 3.1 mM to 6.3 mM. In gels with 3.6 mM PEG (CP15G5, CP15G10), same

increase in genipin concentration did not show a significant effect on gelation time (dropped from 44 min to 40 min). In gels with 3.1 mM genipin (CP5G5, CP15G5), the gelation time was about 44 min regardless of the amount of PEG. In gels with 6.3 mM genipin (CP5G10, CP15G10), the gelation time decreased by 35% (from 40 min to 26 min) by decreasing PEG concentration from 3.6 mM to 1.2 mM. The results suggest that the gelation kinetics of chitosan-genipin hydrogels can be optimised effectively to meet various applications by changing the amount of crosslinker genipin and/or by the addition of a linear PEG polymer. The gelation time was also evaluated by the Winter-Chambon criterion for validation purposes. Obtained experimental data were in good agreement with the gelation times reported in **Figure 4.18**.

4.6.2 Viscoelastic properties

The rheological properties of a viscoelastic material are independent of strain up to a critical level. Beyond this point, the viscoelastic behaviour becomes non-linear and the storage modulus declines [237]. Therefore, a strain sweep would establish the extent of a material's linearity. Hydrogel samples were loaded onto a rheometer as a liquid (initial feed solution as defined in Section 3.2.1, Table 3.1) and allowed to cure for 6 h (as detailed in Section 3.7.2). Oscillatory strain sweeps were performed to determine the LVR and the results are presented in **Figure 4.19**.

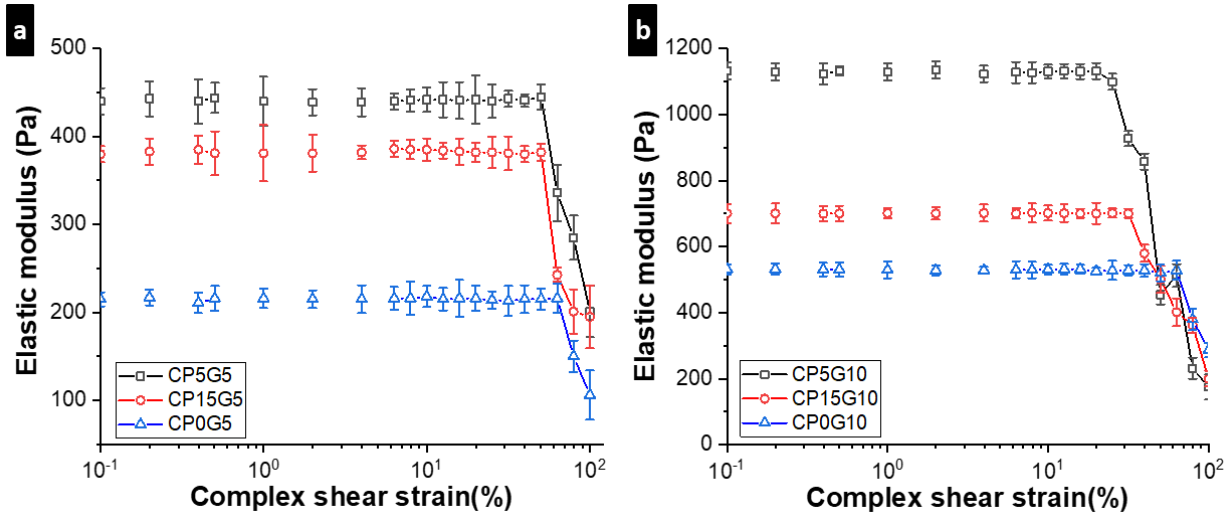

Figure 4.19 Determination of linear viscoelastic region of chitosan-genipin hydrogels, with and without PEG (Table 3.1, formed at 37°C/6 h). Figure (a) shows hydrogels with 3.1 mM genipin and figure (b) shows hydrogels with 6.3 mM genipin. The connecting lines are given as a guide for the eye only and do not represent actual data. Data are representative of two independent experiments (n = 4/group).

The data show that the elastic modulus (G') of these crosslinked hydrogels was strongly dependent on the amount of genipin and PEG in the networks. The measured G' was proportional to genipin concentration. In gels with 1.2 mM PEG, the elastic strength was around 1100 Pa and 445 Pa for those gels with 6.3 mM genipin and 3.1 mM genipin, respectively (**Figure 4.19**). The strong relationship between the measured G' and the crosslinking density has been extensively reported [181, 238, 266, 269-271]. An increase in crosslinking density leads to an expected increase in G', as G' reflects the elastic component of the deformation and hence the number of effective intermolecular cross-links formed in the hydrogel network [270]. The data show that the LVR was inversely proportional to genipin concentration. Gels with 3.1 mM genipin (CP5G5, CP15G5) had an extended LVR of up to 50% strain while gels with 6.3 mM genipin had a short LVR of up to 25% strain (CP5G10) or 30% strain (CP15G10). This is because with higher crosslinking density, the networks are stiffer in nature and their flexibility is reduced.

As seen in **Figure 4.19**, the addition of a linear polymer PEG (1.2 mM; in CP5G5 and CP5G10) into the chitosan-genipin network led to: (i) an expected increase in G' due to the formation of a compact network in which PEG may contribute to the rigidity by physical interaction with chitosan and filling up more spaces within the network; (ii) a shortened LVR due to the limited flexibility under applied shear stress. However, a higher amount of PEG (3.6 mM; in CP15G5 and CP15G10) may also interfere with the crosslinking reaction, reducing the number of effective cross-links and hence the storage modulus of the crosslinked hydrogels.

Figure 4.19 shows that an increase in PEG concentration from 1.2 mM to 3.6 mM led to a significant decrease in G' (36% for gels with 6.3 mM genipin and 15% for gels with 3.1 mM genipin). These results are in agreement with the findings from SEM scans and swelling experiments. With a higher amount of PEG (3.6 mM), the resulting hydrogels had a higher porosity (**Table 4.3**) and a higher swelling degree (**Figure 4.14**) resulting in a decreased strength modulus. The results suggest that addition of PEG to form a semi-IPN network is favourable in terms of increased mechanical strength and integrity of the resulting network, which can be beneficial for drug delivery applications. As all the formulations studied showed an LVR of at least up to 25% strain, a strain value of 1% was chosen for the subsequent oscillatory frequency sweep. While a small strain value is favourable, to avoid an effect on the crosslinking reaction, the strain value needs to be high enough to provide sufficiently high signals.

4.6.3 Mechanical stability

After the LVR profiles were established by strain sweeps, the rheological properties were further characterised using frequency sweeps at a strain within the LVR. Hydrogel samples were loaded onto a rheometer as a liquid (initial feed solution as defined in Section 3.2.1, Table 3.1) and allowed to cure for 6 h (as detailed in Section 3.7.3). Oscillatory frequency sweeps were performed to determine the structural stability and the results are presented in **Figure 4.20**.

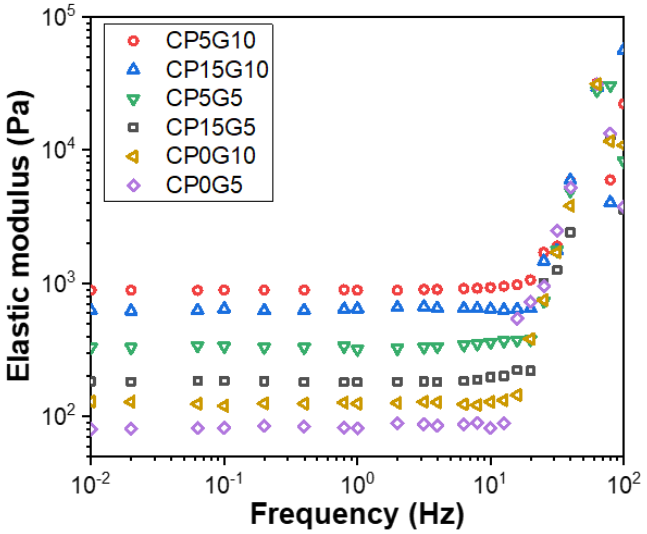

Figure 4.20 Evolution of elastic modulus of chitosan-genipin hydrogels, with and without PEG (Table 3.1, formed at 37 ^{o}C/6 h) as a function of applied frequency.

As shown in **Figure 4.20**, for gels with 6.3 mM genipin (CP5G10, CP15G10), G' exhibited a plateau up to 20 Hz, except for gels without PEG (CP0G10) which showed a plateau up to 12 Hz. For gels with 3.1 mM genipin (CP5G5, CP15G5), the G' frequency-independent range was from 0.01 Hz to 15 Hz, except for gels without PEG (CP0G5) which had a range up to 10 Hz. This is expected as high genipin content is correlated with the number of effective intermolecular crosslinks which is, in turn, linked with the measured G'. The higher the genipin content, the stiffer the networks formed, which resist higher forces better, resulting in structure breakdown at higher frequencies. The data also indicate the formation of a stable, crosslinked network and a 'gel-like' structure of the cured hydrogels. As discussed in the preceding section, addition of PEG led to a higher storage modulus (compared to non-PEG-added hydrogels). However, a higher amount of PEG (3.6 mM) was not correlated with a higher G' value (compared to gels with 1.2 mM PEG) as the increased amount of PEG may interfere with the crosslinking reaction. The rate of increase in elastic modulus versus applied frequency is plotted in **Figure 4.21**.

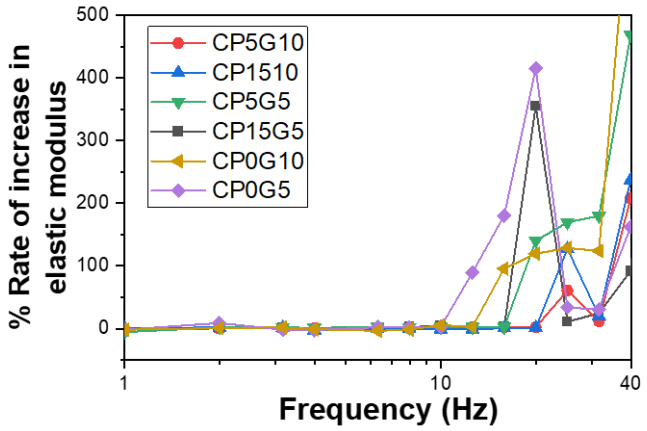

Figure 4.21 Rate of increase in elastic modulus of chitosan-genipin hydrogels, with and without PEG (Table 3.1, formed at 37°C/6 h) as a function of applied frequency. The connecting lines are given as a guide for the eye only and do not represent actual data.

At higher frequencies (beyond the frequency-independent range of G'), the storage modulus increased rapidly for all gels. The highest rate of increase was seen in gel CP15G5, while the lowest rate was observed in gel CP5G10 (**Figure 4.21**). This feature has been reported previously [181, 238, 270, 271]. The magnitude of the viscoelastic response of a polymeric network is attributed to two factors: the length of the flexible polymeric chains and the nature of the imposed mechanical motion [179, 238]. Longer chains have longer relaxation times, which is equivalent to lower frequencies of molecular motion. The length of polymeric chains between crosslinks is longer in the less crosslinked hydrogels (3.1 mM genipin) than the more crosslinked hydrogels (6.3 mM genipin). Therefore, the less crosslinked hydrogels will have comparatively longer relaxation times and lower frequencies of molecular motion than the more crosslinked hydrogels. When the applied frequency increases, long polymeric chains tend to stiffen up as they fail to rearrange themselves in the time scale of the imposed motion, resulting in a more 'solid-like' structure and hence a sharp increase of G'. **Figure 4.21** shows that the highest rate of the increment in G' was in gel CP15G5, as the stiffen-up response was enhanced by the addition of linear PEG chains. Short polymeric chains exhibit short relaxation times and high frequencies of molecule motion, so they require higher applied frequencies to elicit a similar response. This is the reason for the lowest rate of the increase in G' observed in gel CP5G10. Together these results provide valuable insights into the mechanical properties of the hydrogels. In the case of developing a hydrogel as an implantable device, it is important to ensure that cells of the targeted tissue interact favourably with the hydrogel. Different tissues feature different elasticities. For examples, the elasticity of brain tissue is 0.2 - 1 kPa, muscle is 8.5 - 15 kPa, cartilage is 20 - 25 kPa, and cortical bone is 100 - 200 MPa

[182, 272, 273]. The gel presented in this study is considered as a weak gel, as the equilibrium modulus was found to be around 1 kPa. Therefore, it could be a good candidate for central nervous system regeneration as its mechanical properties are similar to those of central nervous system tissue.

4.7 Thermal characteristics of crosslinked hydrogels in disc shape

DSC analysis was carried out to investigate the thermal properties of crosslinked hydrogels. Disc-shaped chitosan-genipin hydrogels, with and without PEG (CP0G5, CP5G5, and CP5G10; Table 3.1) were synthesised (as detailed in Section 3.2.1) and freeze-dried (as detailed in Section 3.3). DSC experiments were performed in both heating and cooling modes to evaluate the reversibility of thermal transition (as detailed in Section 3.8, Table 3.5). The results are presented in **Table 4.4** and **Figure 4.22**.

Table 4.4 Thermal properties of individual gel constituents (chitosan and PEG) and disc-shaped chitosan-genipin hydrogels, with and without PEG (CP0G5, CP5G5, and CP5G10; Table 3.1; formed at 37°C/24 h).

FIRST CYCLE															
Event	**PEG Melting**			**PEG Crystallization**			**Water evaporation**			**Chitosan degradation**			**PEG degradation**		
Peaks*	T_{onset} (°C)	T_m (°C)	ΔH (J/g)	T_{onset} (°C)	T_m (°C)	ΔH (J/g)	T_{onset} (°C)	T_m (°C)	ΔH (J/g)	T_{onset} (°C)	T_m (°C)	ΔH (J/g)	T_{onset} (°C)	T_m (°C)	ΔH (J/g)
Pure PEG	56.51 ± 0.53	61.34 ± 1.94	138.71 ± 5.7	39.31 ± 0.23	34.42 ± 0.92	126.86 ± 6.80									
Pure chitosan							53.44 ± 2.22	106.31 ± 0.32	301.32 ± 2.23						
CP0G5							57.34 ± 1.21	103.93 ± 0.85	342.44 ± 7.55						
CP5G5	47.22 ± 0.72	51.34 ± 0.55	16.11 ± 0.32	35.34 ± 2.22	30.33 ± 0.95	12.41 ± 1.22	61.60 ± 0.70	103.86 ± 1.77	204.06 ± 5.47						
CP5G10	46.71 ± 1.71	51.97 ± 0.30	22.54 ± 1.94	36.80 ± 1.12	30.53 ± 0.34	16.74 ± 2.35	63.98 ± 0.98	106.08 ± 1.55	180.58 ± 2.83						
SECOND CYCLE															
Pure PEG	56.12 ± 1.32	60.27 ± 2.51	142.80 ± 0.40										383.12 ± 2.43	402.12 ± 4.21	191.61 ± 9.21
Pure chitosan										282.81 ± 1.52	301.51 ± 2.23	179.71 ± 4.64			
CP0G5										260.33 ± 0.24	283.95 ± 0.53	203.93 ± 1.92			
CP5G5	57.91 ± 0.32	60.34 ± 1.25	14.70 ± 0.31							260.55 ± 1.76	281.40 ± 0.99	128.52 ± 3.59	381.45 ± 0.46	416.01 ± 0.82	70.21 ± 2.73
CP5G10	56.66 ± 1.24	60.26 ± 0.93	20.34 ± 1.22							259.61 ± 1.04	280.99 ± 1.16	145.45 ± 4.44	382.06 ± 0.95	417.94 ± 0.27	86.96 ± 5.30
THIRD CYCLE: no peaks detected															

* Peak integration: T_{onset} = the onset temperature of a transition event; T_m = the peak temperature of a transition event; ΔH = the enthalpy of a transition. The experiment was performed in triplicate.

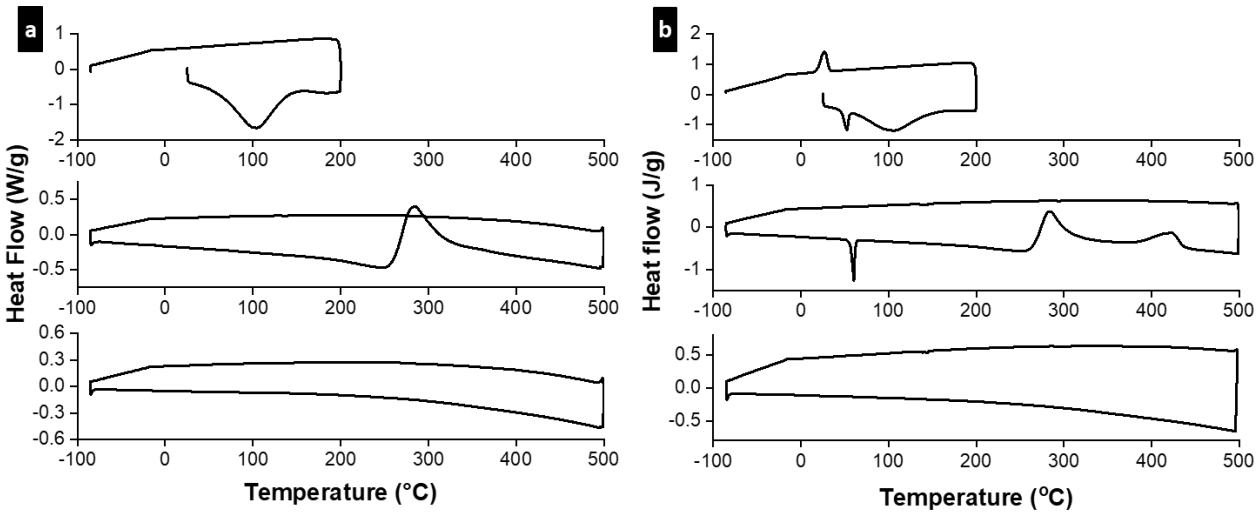

Figure 4.22 DSC curves of disc-shaped hydrogels (Table 3.1, formed at 37°C/24 h) containing: (a) chitosan-genipin (sample CP0G5); (b) chitosan-genipin-PEG (sample CP5G5). All samples are subjected to three heating and cooling cycles as detailed in Table 3.5 (top graphs = 1st cycle; middle graphs = 2nd cycle; bottom graphs = 3rd cycle).

Table 4.4 presents the transition events occurred within the samples under applied temperature programs. For pure chitosan, there was a broad endothermic peak at 106°C assigned to the loss of water during evaporation [274]. In the second heating cycle, the exothermic peak at 301°C was related to chitosan degradation [275]. Chitosan degradation starts with the decomposition of main chains by splitting glycosidic bonds and hence the deacetylation via N-acetyl linkage [21]. Generally, the depolymerisation of main chains should result in an endothermic peak as it requires more heat to split the bonds. However, the observed exothermic peak is associated with the interchain crosslinking formed between fragments of chitosan. Pawlak and Mucha (2002) confirmed the formation of crosslinking of chitosan macromolecules during its thermal degradation [245]. For pure PEG (MW 6000 g/mol), the first heating-cooling cycle had a melting transition at 61°C and subsequently a crystallization phase at 34°C (**Table 4.4**). In the second heating cycle, PEG had a melting phase at the same temperature compared to the first heating cycle. When temperature increased up to 380°C, there was an onset of an endothermic peak which is related to the decomposition of PEG by chain scission [274].

As expected, DSC curves from chitosan-genipin hydrogels without PEG did not show any melting peaks or crystallization peaks related to PEG (**Figure 4.22a**) while having similar transition peaks observed in pure chitosan. In chitosan-genipin-PEG hydrogels, the endothermic peak related to melting phase of PEG was observed in the first heating cycle with lower onset temperature at 46°C

and melting temperature at 51^{o}C (**Figure 4.22b**). In the second heating cycle, the melting peak of PEG was observed with the same temperature as those with pure PEG. The difference in melting temperature between the first two cycles was related to hydrogen bonding between hydroxyl groups of PEG and water molecules. In all hydrogel samples analysed, the endothermic peaks related to water evaporation were observed in the first heating cycle and disappeared in the second heating cycle, indicating that some bound water within gel network was not completely removed by freeze-drying.

When the crosslinked gels were heated up to 260^{o}C, there was an onset of an exothermic peak which reached the highest enthalpy value at 280^{o}C (**Figure 4.22**). This exothermic peak was related to chitosan degradation and for all the tested samples, the degradation temperatures related to chitosan chains were similar and shifted to lower values (from 300^{o}C in pure chitosan to 280^{o}C in crosslinked hydrogels). The enthalpy value of this transition was higher in chitosan-genipin hydrogels (203.93 ± 1.92 J/g) than those recorded in chitosan-genipin-PEG hydrogels (120 - 145 J/g) (**Table 4.4**). These observations indicate the effect of PEG on molecular motion within the crosslinked network, probably via the interaction with chitosan. When temperature increased up to 380^{o}C, there was an exothermic peak with the maximum value at 417^{o}C obtained only in PEG-added hydrogels (CP5G5 and CP5G10). Interestingly, the following cooling cycle did not show the crystallization peak of PEG and during the last run, there was no peak observed (**Figure 4.22b**). To confirm the thermal transition related to the last exothermic peak (at 417^{o}C) obtained in the second heating cycle, more DSC experiments were conducted using the thermal program detailed in Table 3.5 with minor modification (**Figure 4.23**).

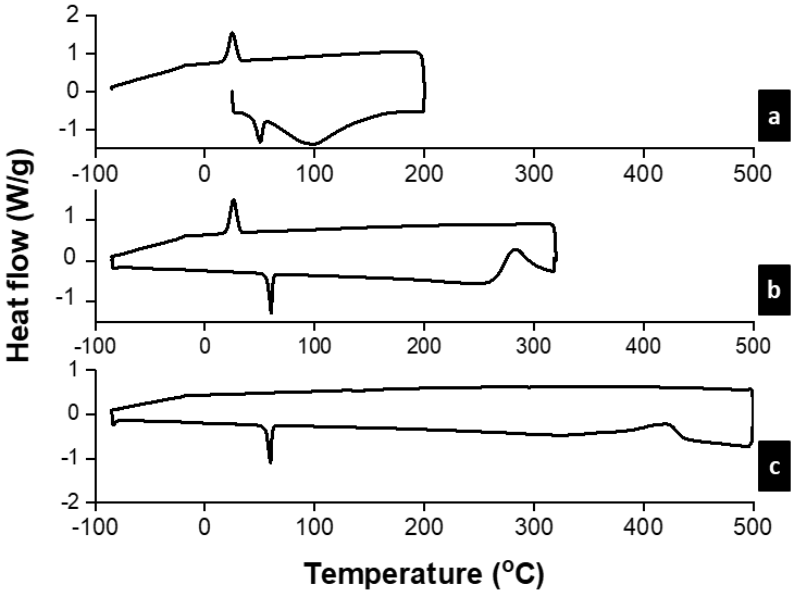

Figure 4.23 DSC curves of disc-shaped chitosan-genipin-PEG hydrogels (sample CP5G5, Table 3.1, formed at 37°C/24 h) subjected to three heating and cooling cycles as detailed in Table 3.5 with minor modification in the 2nd cycle: (a) 1st cycle; (b) 2nd cycle - ramp 10°C/min to 320°C, isothermal at 320°C for 5 min, ramp 20°C/min to -90°C; (c) 3rd cycle.

The first cycle had the similar phase transition as the thermal program was unchanged (**Figure 4.23a**). In the second heating cycle, instead of heating the gels from -90°C to 500°C, the samples were heated up to 320°C. As expected, after chitosan degradation peak appeared at around 280°C, there was an exothermic peak related to crystallization of PEG in the subsequent cooling run (**Figure 4.23b**). In the third cycle, the samples were heat up from -90°C to 500°C and then cooled down from 500°C to -90°C. The melting peak of PEG was observed again at similar temperature and the exothermic peak at around 417°C was observed. The subsequent cooling process did not obtain any peaks as predicted (**Figure 4.23c**). DSC experiments were also carried out with chitosan/PEG blend by mixing an appropriate amount of chitosan and PEG solutions, casting on a Petri dish and drying in an oven. The exothermic peak during the second heating cycle was also seen and shifted to 422°C. Taking all the finding into accounts, it is possibility that when the gels were heated up to 380°C, PEG began the decomposition by chain scissions and the resulting PEG fragments may form hydrogen bonding with chitosan fragments, appearing as an exothermic peak at around 417°C. DSC analysis confirms the formation of thermally stable chitosan-genipin hydrogels (up to 250°C). For drug delivery application, DSC analysis can be used to evaluate any interactions between loaded moieties and polymeric constituents which could induce major changes in their thermal profiles.

4.8 Release kinetics of loaded therapeutic agents from disc-shaped hydrogels

The physical and chemical properties of hydrogels and the chosen loading method will affect directly the mechanism by which the encapsulated drug is released from the polymeric network [34]. To evaluate the release kinetics of loaded therapeutic agents from hydrogels, two different biomolecules with different solubility in water, which are perindopril erbumine (PER) and 1-methyl D-tryptophan (D-1MT), were used as drug models. PER-loaded and D-1MT-loaded disc-shaped chitosan-genipin-PEG hydrogels (F1P, F2P, and F3P, Table 3.3) were synthesised by direct entrapment method (as detailed in Section 3.2.4). The hydrogels were placed in pH 2 buffer solution and the amount of drug released were quantified by HPLC (as detailed in Section 3.9). The results are presented in **Figure 4.24**.

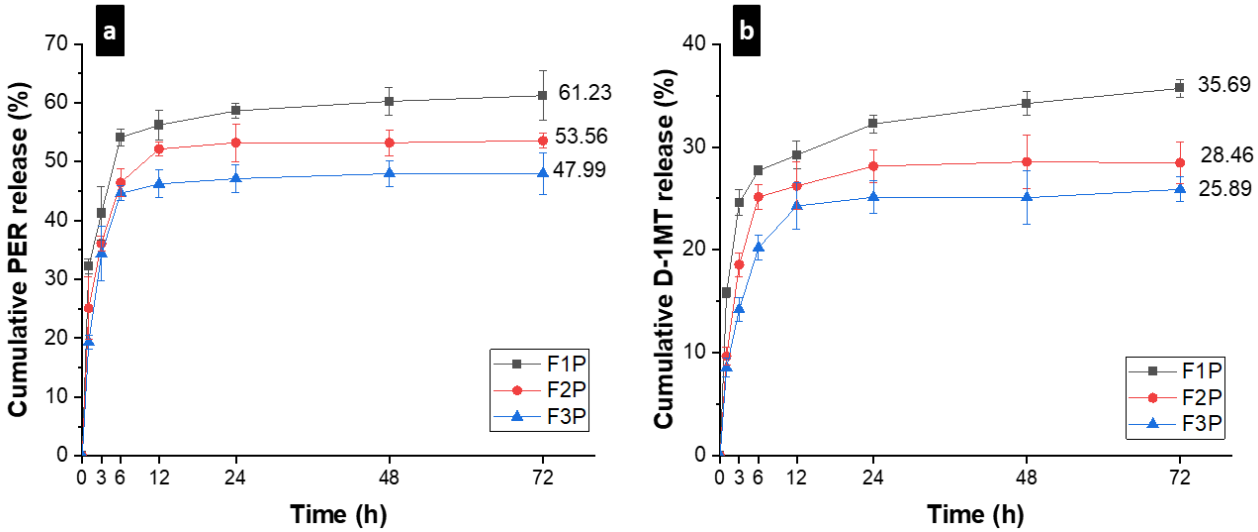

Figure 4.24 Cumulative amount of (a) PER and (b) D-1MT released from disc-shaped chitosan-genipin-PEG hydrogels (Table 3.3, formed at 37ºC/24 h) in pH 2 buffer solutions at 20ºC. The connecting lines are given as a guide for the eye only and do not represent actual data. Data are representative of two independent experiments (n = 6/group).

PER (MW 441.6 g/mol), freely soluble in water (solubility: 1.22 mg/mL), is the ethyl ester of a non-sulfhydryl angiotensin converting enzyme inhibitor with anti-hypertensive activity (a starting therapeutic dose of 2 mg is recommended) [276]. D-1MT (MW 218.3 g/mol), is the D-isomer of 1-MT which can inhibit the indoleamine 2,3-dioxygenase-related enzyme and is currently used in phase I clinical trials as an adjunct to conventional chemotherapy, causing regression of tumours and prolonging survival [277]. D-1MT is less soluble in water than PER (solubility: 1mg/mL with

gentle warming) [278]. Thus, PER and D-1MT, with different solubility, were used to evaluate the release kinetics of hydrogels.

As seen in **Figure 4.24**, the release profiles of PER and D-1MT could be described as a bi-phasic pattern with an initial burst effect (within 3 - 6 h) and a sustained release before reaching equilibrium state. As a swelling-controlled release system in which drug is dispersed within polymeric network, once in contact with acidic buffers, the hydrogels begin to swell. The relaxation of polymer chains allows the system to expand beyond its boundary leading to fast release of drug within the first hours. The concentration gradient between the hydrogel and surrounding solutions permits the diffusion of the loaded drug. When the swelling reaches an equilibrium state, the release rate becomes constant [158]. The drug release rate is dependent on the swelling rate of polymeric network [3]. The effect of crosslinking density on the release pattern is noticeable. As expected, at a constant concentration of chitosan and PEG, increasing genipin content produces higher crosslinking density, leading to a slower network relaxation rate in acidic buffers. After 72 h, the amount of PER or D-1MT released from gel F3P was lowest compare to those released from gels F1P and F2P (**Figure 4.24**). In acidic conditions, the total amount of PER released from a single hydrogel sample at equilibrium state was almost twice as much as that of D-1MT (53.56% of PER from gel F2P compared to 28.46% of D-1MT at 72 h of incubation). At a fixed time point and from same hydrogel samples, the dissolution of PER was faster than that of D-1MT due to its higher solubility in aqueous solution. As the drug concentrations in the acidic medium and in the gel matrix are equal, the driving force for drug diffusion achieves its balance leading to the end of release activity. The amount of medium withdrawn at a fixed time point also affects the release kinetics as shown in **Figure 4.25**.

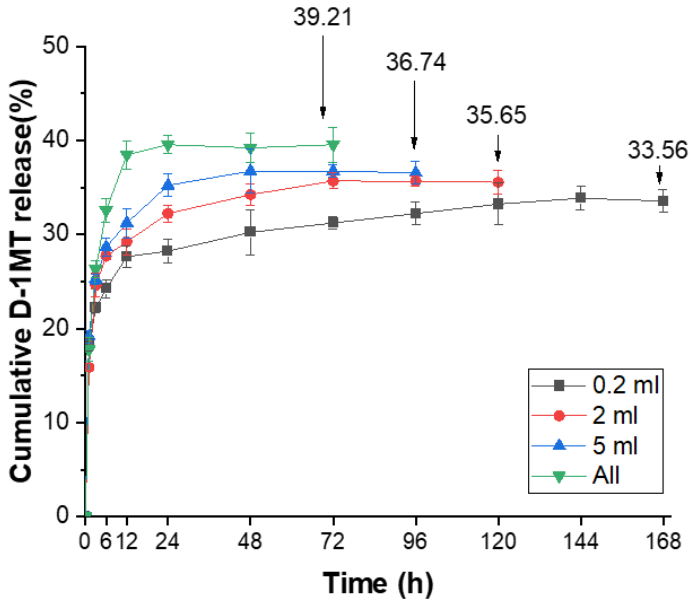

Figure 4.25 Cumulative amount of D-1MT released from disc-shaped chitosan-genipin-PEG hydrogels (sample F1P, Table 3.3, formed at 37°C/24 h) in pH 2 buffer solutions at 20°C, with different amount of media withdrawn at a certain time point. The connecting lines are given as a guide for the eye only and do not represent actual data. Data are representative of two independent experiments (n = 6/group).

It can be seen that when more medium was replaced, the faster the release rate was and the higher amount of loaded moieties diffused out of the gel matrix. When all the medium (20 mL) was taken out and replaced by adding fresh buffer, D-1MT achieved the highest released amount of around 40% after 12 h and sustained the release up to 72 h. When 5 mL of medium was replaced at each time point, the highest amount of released D-1MT (around 35%) achieved at 48 h of incubation. Thus, sustained driving forces are essential to induce sustained release from polymeric matrix. With respect to the future applications where hydrogel can be injected or implanted into the body, the amount of drug released from the matrix will be used by virtue of its physiological action leading to the sustained driving forces. As discussed in Section 2.3.3.2, several kinetic models can be used to describe the release profiles of drugs from polymeric network. By fitting the experimental data into various kinetic models (zero order, first order, Higuchi, and Kormeyer-Peppas), the drug-loaded disc-shaped hydrogels fitted well to the Kormeyer-Peppas model ($R^2 > 0.98$) with release component, $0.45 < n < 0.89$, indicating non-Fickian transport mechanism (**Figure 4.26**). This is expected as Korsmeyer-Peppas model takes into account the moving boundary phenomena using a dimensionless swelling interface number [279], unlike the empirical

power law, commonly used for diffusion-controlled release, which does not consider the expanding boundary conditions during the swelling process [158]. By using PER and D-1MT as drug models, the developed hydrogels are deemed sufficient to entrap and release the loaded moieties in a controlled manner.

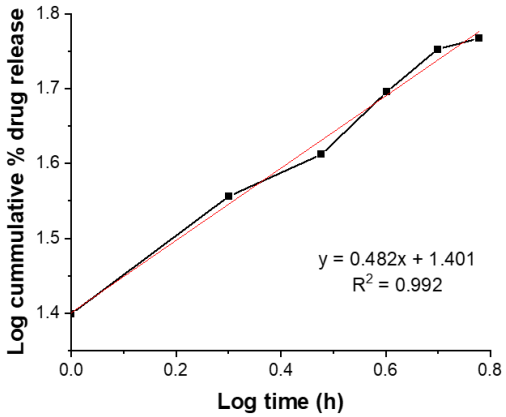

Figure 4.26 Kormeyer-Peppas model kinetic release of PER from disc-shaped chitosan-genipin-PEG hydrogels (sample F1P, Table 3.3, formed at 37^{o}C/24 h) in pH 2 buffer solutions at 20^{o}C.

4.9 Summary

For chitosan-based hydrogels studied, the hydrogel integrity was maintained by a chemically crosslinked network formed between primary amino groups of chitosan and genipin in acidic conditions. Based on literature, it is well-known that MW and DDA of chitosan are two most important intrinsic factors that affect its physical and chemical properties. Batch-to-batch variations also pose a challenge in consistently achieving hydrogels with reproducible properties. Therefore, throughout all experiments, only one batch of chitosan (medium MW, DDA of 82%) was used to ensure comparable results with our previous studies. Furthermore, low MW chitosan was found to be poor in term of mucosal adhesion and in controlling the cargo release while high MW chitosan exhibited a lower adhesion and a lower release rate of loaded drug than medium MW chitosan [280]. The use of genipin as a crosslinker was supported by its high selectivity, good biocompatibility, and intriguing bioactivity. Genipin is found to react only with primary amino groups and its cytotoxicity is found to be 10000 times lower than that of glutaraldehyde [89]. Previous studies have also reported the potential anti-inflammatory, anti-thrombotic, and anti-angiogenesis properties of genipin in mice models [281]. Therefore, aiming to reach clinical applications, a potential bio-safe crosslinker like genipin was chosen. At the same time, the use of a linear polymer entrenched within the crosslinked network might improve reproducibility in

synthesis and add extra levels of control in achieving tailor-made hydrogels to meet various end-use applications. The use of PEG was encouraged as it might provide a solid foundation to further develop these hydrogels as self-oscillating hydrogels. As discussed in Section 4.6, the idea behind the concept of self-oscillating hydrogels is to chemically couple pH-responsive hydrogels with an oscillatory reaction (that produces oscillations in pH) so that the pH changes can occur inside the smart gels (eliminating the need of external stimuli) and cause the gels to swell/collapse promptly and release the loaded moieties in pulses. Our research group led by Dr. Novakovic has intensively studied the oscillatory PCPOC reaction employing polymeric substrates (monoalkyne-terminated PEG) and smart hydrogels, aiming to develop an 'all-polymeric' self-oscillating system able to expand and collapse its volume fully autonomously in a predesigned rhythm for a predesigned duration. Such systems would lead to reduced side effects of the target drugs and offer truly personalised treatment regimes (especially for diseases with established oscillatory rhythms in their pathogenesis, e.g. arthritis, duodenal ulcers, or cardiovascular diseases). Additionally, aging population would significantly benefit from such reliable hands-free drug delivery technologies. Therefore, to bring them one step closer to applications, addition of PEG to the crosslinked network forming a semi-IPN network is studied.

Either prepared in disc shape or bead shape, the gels had dark blue colour which is related to the oxygen radical-induced polymerisation of genipin as well as the reaction with amino groups of chitosan [111, 240]. FTIR scans confirm gel formation as the differences between the non-crosslinked chitosan and the crosslinked gel network were related to the development of secondary amine and heterocyclic amine ring-stretching. Crosslinking with genipin also generated a fluorescent product, which had optimal excitation and emission wavelengths at 580 nm and 630 nm, respectively. The freeze-dried disc-shaped hydrogels had microporous structure with an average cross-sectional porosity ranging from approximately 40% to 64%, and the pore sizes ranging from 11 μm to 57 μm, depending on the amount of genipin and PEG. The hydrogels were also prepared in bead shape using emulsion crosslinking. As observed by light microscope and SEM, the obtained particles were discrete, spherical, and within micrometre range (from 1 μm to 30 μm). The size of hydrogel beads increased as incubation temperature and stirring rate decreased. Incorporation of PEG into hydrogel beads did not significantly affect the particles' morphology and size. Preliminary experiments to produce PEG-coated particles suggest that longer incubation time (more than 6 h) is required to achieve a complete coating layer.

Based on results presented in Chapter 4, **Figure 4.27** displays a bubble and colour map graph summarising key characteristics of the hydrogels as a function of genipin and PEG content. In this figure, the gelation time (Section 4.6.1) is given at x-axes and the equilibrium swelling (Section 4.5) at y-axes; the average pore size **(**Section 4.4.1) defines the bubble size; while the elastic modulus (Section 4.6.3) defines the bubble colour.

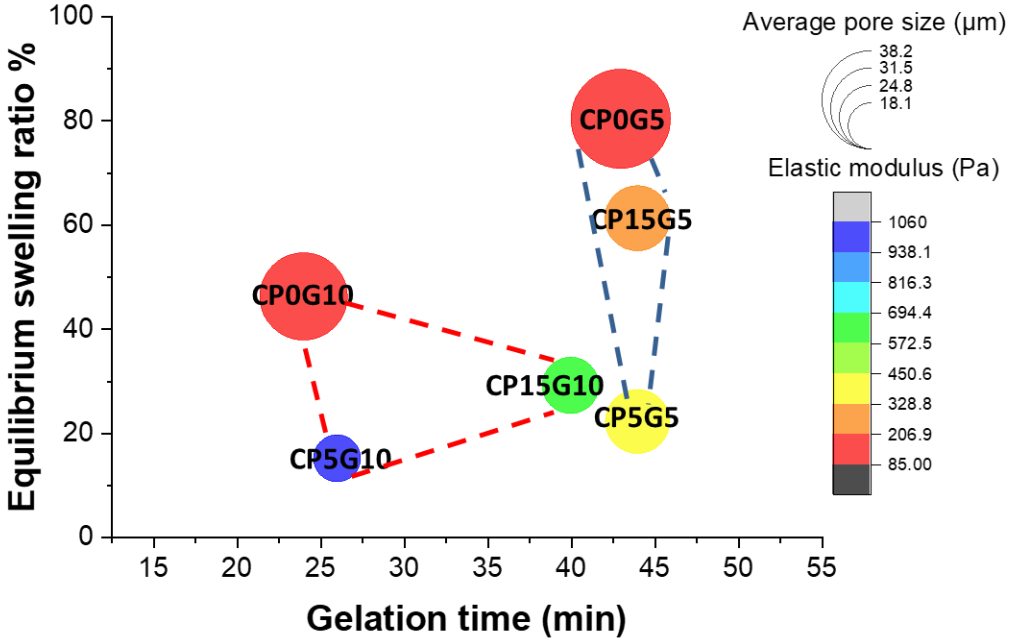

Figure 4.27. Equilibrium swelling, gelation time, average pore size, and elastic modulus of disc-shaped chitosan-genipin hydrogels, with and without PEG (Table 3.1, formed at 37ºC/24 h). Dashed lines are used to group samples with higher genipin content (red dashed lines) and lower genipin content (blue dashed line).

As seen in **Figure 4.27**, in disc-shaped chitosan-genipin hydrogels, addition of PEG can be used to alter properties of hydrogel material, tailor desirable swelling response, reduce average pore size, and reduce cost of the fabrication by reducing the amount of expensive crosslinking agent needed. The presence of PEG not only reduced average pore size, but also improved pore uniformity and yielded a significantly narrower pore distribution. This is an excellent feature that should aid reproducible synthesis and large-scale manufacturing of these materials. The resulting hydrogels are confirmed to be pH responsive, swelling in acidic and shrinking in basic environments, in line with chitosan pKa values. Manually induced pH oscillations triggered the oscillatory swelling response, highlighting their potential for coupling with a real oscillatory reaction to produce self-oscillating hydrogels. These results show that changes in conformation can

be efficiently controlled by either changing the crosslinking density or adding PEG polymer. Higher genipin concentration reduced the pore size and swelling degree while increasing elastic modulus (**Figure 4.27**). The addition of PEG up to 1.9 mM decreased swelling ratio, yielding the same effect as the increase in genipin content. Considering cost of genipin (£345 for 125 mg, Sigma-Aldrich) and scale-up production, replacing some genipin with PEG polymer is favourable. On-going improvements in the genipin extraction process show promising results, anticipated to reduce cost of commercial genipin and pave the way for the more cost-effective developments of genipin-based hydrogels. Interestingly, PEG concentration of above 2.9 mM increased swelling ratio and reduced elastic modulus, likely due to the inhibitory effect addition of PEG may have on chitosan-genipin crosslinking reaction and the hydrophilicity of PEG. Other factors (such as gelation time and temperature) also influenced the hydrogels' microstructure. For instance, long incubation time (from 48 h up to 96 h) or high oven temperature (from 45^{o}C to 60^{o}C) might damage the physical bonding within hydrogel network and reduce the network stability, resulting in high swelling ratios recorded.

Gelation point is an important parameter that needs to be considered in the development of crosslinked hydrogels. At the gel point, the viscoelastic properties change abruptly from a liquid-like state to a solid-like state resulting in a sudden loss of flow [238, 265, 266]. Understanding gelation kinetics opens the possibilities for more effective network design, particularly relevant to the envisioned *in vivo* applications. When aiming for *in vivo* applications, a slow gelation time may lead to hydrogel leakage from target sites and potentially the loss of loaded-biomolecules. On the other hand, a rapid gelation time could lead to a hydrogel-tissue mismatch as it may inhibit the hydrogel from conforming to the lesion geometry [182]. During hydrogel synthesis, oscillatory time sweeps were performed to determine the gelation time. The gelation time obtained by both crossover of G' and G'' and the Winter-Chambon criterion were in good agreement. Thermal properties were evaluated using freeze-dried disc-shaped hydrogels, indicating that the fabrication process produced thermally stable hydrogels (up to 250^{o}C). Two drug molecules (PER and D-1MT) with different solubility were chosen to evaluate the release kinetics from disc-shaped hydrogels and were loaded into hydrogels by direct entrapment. The results show the highest release rate within the first 3 - 6 h and a sustained release (up to 48 - 72 h) in which PER was released more and at faster rate compare to D-1MT due to its higher solubility. The swelling-controlled release kinetic of hydrogels followed the Korsmeyer-Peppas model with non-Fickian transport mechanism.

In summary, the Chapter 4 presents the physical and chemical characterisation and evaluation of chitosan-genipin hydrogels, with and without PEG, using a wide range of techniques. Their microstructure, smart nature of a pH-responsive system, and mechanical stability are found to depend on many factors, such as the amount of crosslinker, addition of linear polymer, and gelation conditions (incubation temperature, gelation time, and stirring rate). The evaluation presented in this work allows the production of tailor-made hydrogel structure with desirable physico-chemical properties. To reach clinical applications, a biomedical system should be non- or low-cytotoxic and enzymatically or hydrolytically degradable. Thus, in Chapter 5, the biological evaluation of hydrogels is discussed.

Chapter 5 Biocompatibility of crosslinked chitosan-based hydrogels

As discussed in Chapter 4, chitosan-genipin hydrogels interpenetrated by PEG displayed several promising properties as a potential controlled drug delivery platform but it is important to evaluate their biocompatibility. In this Chapter, biological activities of the crosslinked hydrogels *in vitro* and *in vivo* are discussed. The cytotoxicity of hydrogel films was investigated on mouse 3T3 fibroblast cells as a function of genipin content and PEG addition. The inflammatory responses to uncrosslinked chitosan films and crosslinked chitosan-genipin hydrogel films/beads were evaluated using DC 2.4, RAW 264.7, and BMDM cells. Biodegradation of hydrogels was monitored non-invasively using their intrinsic fluorescence *in vitro* and *in vivo*. Biocompatibility was evaluated by injecting mice with two types of hydrogels, which were macrogels prepared directly in syringes and hydrogel beads suspended in PBS. Some of the content in this Chapter have been previously published in 'Genipin-crosslinked chitosan hydrogels: preliminary evaluation of the *in vitro* biocompatibility and biodegradation', Journal of Applied Polymer Science.

5.1 Cytotoxicity of hydrogel films towards 3T3 fibroblast cells

The chitosan-genipin hydrogel films, with and without PEG (Table 3.3) were prepared in multi-well plates (as detailed in Section 3.2.3). To evaluate the cytotoxicity of hydrogel films, 3T3 fibroblasts were cultured on hydrogel surfaces (as detailed in Section 3.10.2). Changes in cell morphology were assessed microscopically, using light microscope (**Figure 5.1a)** and SEM (**Figure 5.1b**) while cell viability was assessed using an ATP-based assay (**Figure 5.1c**).

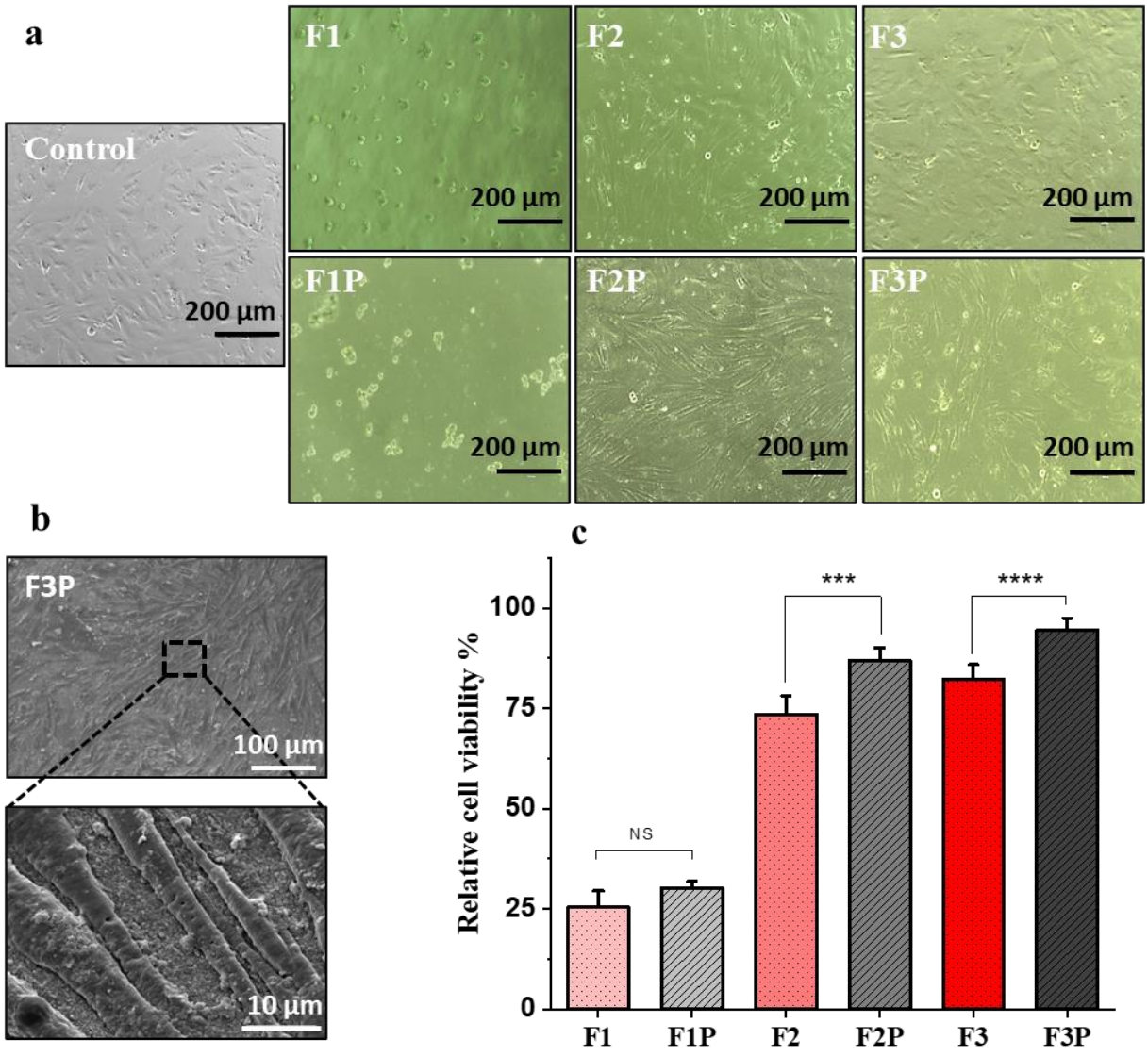

Figure 5.1 Cytotoxicity evaluation using 3T3 fibroblasts cultured on chitosan-genipin hydrogel films (F1, F2, and F3; Table 3.3) and chitosan-genipin-PEG hydrogel films (F1P, F2P, and F3P; Table 3.3) for 48 h at 37ºC. (a) Light microscope images of control cells and gel-exposed cells. (b) SEM image of fibroblasts cultured on sample F3P and its magnified section. (c) Cell viability measured by CellTiter-Glo® 2.0 assay. Data in the experimental groups are percentages relative to the control group (cells seeded in wells containing fresh culture medium only). Data are representative of two independent experiments (n = 6/group). Statistical significance was determined by two-tailed unpaired Student's *t* test; ***, $P < 0.001$; ****, $P < 0.0001$; NS, not significant.

As shown in **Figure 5.1**, chitosan hydrogels crosslinked by genipin presented a wide range of cytotoxicity to fibroblasts, with a strong correlation between genipin concentration and cellular

adhesion/viability, supporting previous reports [193, 195, 282]. Microscopic images show that the cells maintained normal morphology on hydrogels with higher genipin content. Fibroblasts cultured on gels with 1.7 mM genipin (F1 and F1P) remained round or oval (**Figure 5.1a**), revealing a weak contact with the surface and low viability (around 25 - 30%, **Figure 5.1c**). Fibroblasts cultured on gels with 3.1 mM (F2 and F2P) or 4.4 mM genipin (F3 and F3P) formed elongated or spindle-like shapes, showing good spreading morphology and higher viability (around 73 - 95%). SEM images of fibroblasts cultured on gel F3P show confluent growth of cells on the gel surface where the cells attached, flattened, and spread with assembly of filopodia (**Figure 5.1b**). Section 4.6 shows that higher genipin content increased crosslinking density and mechanical stiffness of the hydrogels, consistent with previous studies [31, 116, 181, 194]. The observation of better fibroblast compatibility of these higher stiffness gels is similar to those reported previously, which described key roles of matrix stiffness in cellular behaviours. For example, microporous cellulose scaffolds with Young's modulus above 1.6 MPa promoted osteoprogenitor cell growth [283]. Bovine chondrocytes showed a rapid attachment time of 2.7 h on crosslinked alginate gels with 147 kPa (measured by stress-relaxation testing) compared to 17.5 h on 16 kPa gels [284]. Stiffer surfaces may offer more adhesion anchors for cells to attach and form more focal complexes, which promote cell proliferation and prevent apoptosis of anchorage-dependent fibroblasts [285-289].

As shown in **Figure 5.1c**, in gels with 1.7 mM genipin (F1 and F1P), addition of PEG (1.3 mM) improved cell viability (although not statistically significant, $P > 0.05$). In gels with 3.1 mM genipin (F2 and F2P) and 4.4 mM genipin (F3 and F3P), addition of PEG (up to 1.2 mM) enhanced cell viability significantly (**Figure 5.1c**). Section 4.6 shows that adding PEG (1.2 mM) increased the elastic modulus and rigidity of the network, which may contribute to the enhanced cytocompatibility of PEG-added hydrogels. Another key factor that affects cellular responses is surface hydrophilicity. Cells show favourable adhesion to moderate hydrophilic surfaces compared to hydrophobic or extremely hydrophilic surfaces [290-293]. The increased hydrophilicity of hydrogel surfaces by addition of PEG may promote cell adhesion and growth.

5.2 Inflammatory property of chitosan-genipin hydrogels

To test if chitosan-genipin hydrogels induce inflammatory cytokines, the inflammatory responses to both uncrosslinked chitosan and crosslinked chitosan hydrogels were investigated, using several *in vitro* cultured murine cell lines (DC 2.4 and RAW 264.7) and primary mouse cells (BMDM). The uncrosslinked chitosan films were prepared as detailed in Section 3.2.3. The chitosan-genipin

hydrogel films with highest genipin content (gel F3, Table 3.3) were selected to study further and synthesised as detailed in Section 3.2.3. The chitosan-genipin hydrogel beads were prepared at 37^{o}C with a stirring speed of 500 rpm, following the procedure described in Section 3.2.2.

5.2.1 Inflammatory response by DC 2.4 dendritic cells

As dendritic cells act as a critical bridge between innate and adaptive immunity [294], a well-characterised dendritic cell line, DC 2.4, was used to investigate the inflammatory response to these chitosan-based materials. The experiments were carried out as detailed in Section 3.10 and the results are presented in **Figure 5.2**.

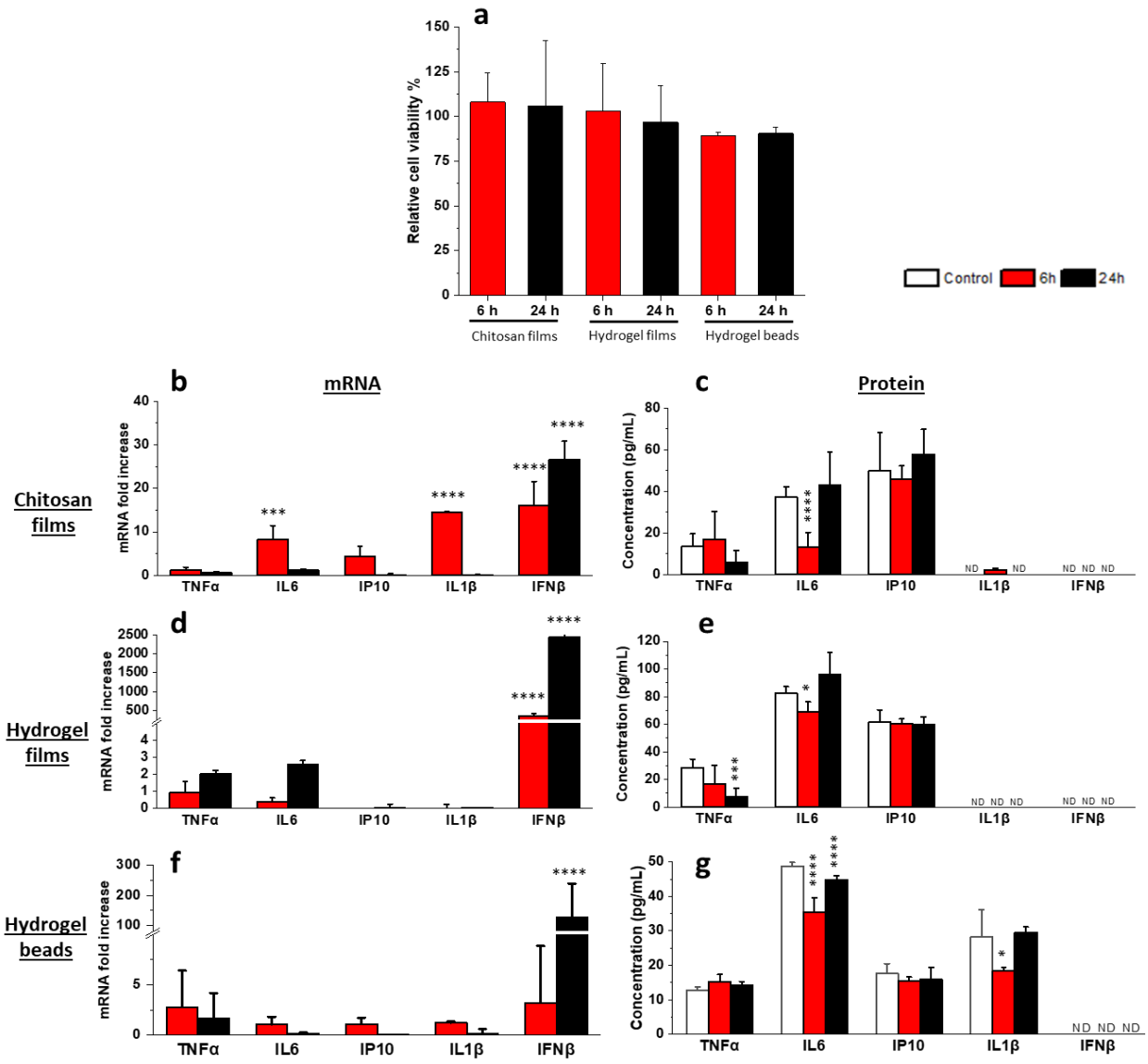

Figure 5.2 Inflammatory cytokine production by DC 2.4 cells exposed to uncrosslinked chitosan films and crosslinked hydrogel films/beads. Assays were carried out at 6 h and 24 h of incubation.

(a) DC 2.4 cell viability measured by CellTiter-Glo® 2.0 assay. Data in the experimental groups are percentages relative to the control group (cells seeded in wells containing fresh culture medium only). Cytokine gene transcription (b, d, f) and protein expression (c, e, g) by DC 2.4 cells were assessed using RT-PCR and ELISA respectively, after exposure to chitosan films (b, c), hydrogel films (d, e), or hydrogel beads (f, g). Fold increases in cytokine gene transcription are relative to the control group measured at the same time point. Data are representative of two independent experiments (n = 6/group). Statistical significance was determined by two-tailed unpaired Student's *t* test; *, $P < 0.05$; **, $P < 0.01$; ***, $P < 0.001$; ****, $P < 0.0001$; ND, not detected.

As shown in **Figure 5.2a**, the percentages of viability of chitosan film-exposed DC 2.4 were 108% (at 6 h) and 106% (at 24 h), with no significant difference compared to the control group. The percentages of viability of hydrogel film-exposed DC 2.4 were 103% (at 6 h) and 97% (at 24 h), with no significant difference compared to the control group. The percentages of viability of hydrogel bead-exposed DC 2.4 were 90% (at 6 h) and 91% (at 24 h), with no significant difference compared to the control group. Thus, compared to uncrosslinked chitosan films, the crosslinked hydrogel network with genipin is deemed minimally cytotoxic towards DC 2.4, although not statistically significant ($P > 0.05$).

To evaluate the inflammatory properties of the crosslinked hydrogels, several inflammatory cytokines (TNF-α, IL-6, IP-10, IL-1β, and IFN-β) were chosen to study the inflammatory response to chitosan-based materials. In **chitosan film**-exposed DC 2.4, increased IL-6 (8-fold) and IL-1β (14-fold) mRNA expression were observed at 6 h (**Figure 5.2b)** while IL-6 level (13 pg/mL) was surprisingly 2-fold lower than control cells and IL-1β level (2 pg/mL) was comparable to control cells (**Figure 5.2c**). mRNA transcription and protein expression of TNF-α and IP-10 in chitosan film-exposed cells were comparable to control cells at the same time point. Interestingly, IFN-β gene transcription was increased significantly (16-fold at 6 h and 27-fold at 24 h) but no IFN-β protein was detected in supernatants measured by ELISA (even though ELISA worked well for IFN-β standard with detection limit of 5 pg/mL). This suggests that post-transcriptional control processes prevent translation of IFN-β mRNA to produce protein or protein secretion. Further studies will be necessary to examine this possibility but lack of IFN-β protein expression in response to chitosan-based materials is consistent with hypo-inflammatory properties, as IFN-β is a pivotal cytokine that elaborates innate and adaptive immunity.

In **hydrogel film**-exposed DC 2.4, increased TNF-α (2-fold) and IL-6 (3-fold) mRNA expression were observed at 24 h (although not statistically significant, $P > 0.05$, **Figure 5.2d**) while TNF-α level (7 pg/mL) was 4-fold lower than control cells and IL-6 level (96 pg/mL) was comparable to control cells (**Figure 5.2e**). mRNA transcription and protein expression of IP-10 in hydrogel film-exposed cells were comparable to control cells at the same time point. IL-1β mRNA expression was not elevated and no IL-1β protein was detected. IFN-β gene transcription was increased significantly (356-fold at 6 h and 2435-fold at 24 h) but no IFN-β protein was detected, similar to outcomes in chitosan film-exposed DC 2.4.

In **hydrogel bead**-exposed DC 2.4, increased TNF-α (3-fold) mRNA expression was observed at 6 h (although not statistically significant, $P > 0.05$, **Figure 5.2f**) while TNF-α level was comparable to control cells (**Figure 5.2g**). At 6 h, mRNA transcription of IL-6 and IL-1β were not elevated while concentrations of IL-6 (35 pg/mL) and IL-1β (18 pg/mL) were significantly lower than control cells. mRNA transcription and protein expression of IP-10 in hydrogel bead-exposed cells were comparable to control cells at each time point. IFN-β gene transcription was increased significantly (126-fold at 24 h) but still no IFN-β protein was detected, as observed for responses to chitosan films and hydrogel films.

These findings support the conclusion that uncrosslinked chitosan films and crosslinked hydrogels are hypo-inflammatory towards DC 2.4, as no increased levels of inflammatory cytokines including TNF-α, IL-6, IP-10, IL-1β, and IFN-β were detected despite increasing in gene transcriptional activity for IL6, IL-1β, and IFN-β. Conducting bioassays to measure IFN-β activity would address if ELISA read-outs are valid and if translational control blocks production or secretion of IFN-β protein.

5.2.2 Inflammatory response by RAW 264.7 macrophage cells

As macrophages mediate innate immunity by phagocytosing bacteria and secreting pro-inflammatory and anti-microbial mediators [295, 296], a well-characterised macrophage cell line, RAW 264.7, was used to study the inflammatory response to hydrogels. The experiments were carried out as detailed in Section 3.10 and the results are presented in **Figure 5.3**.

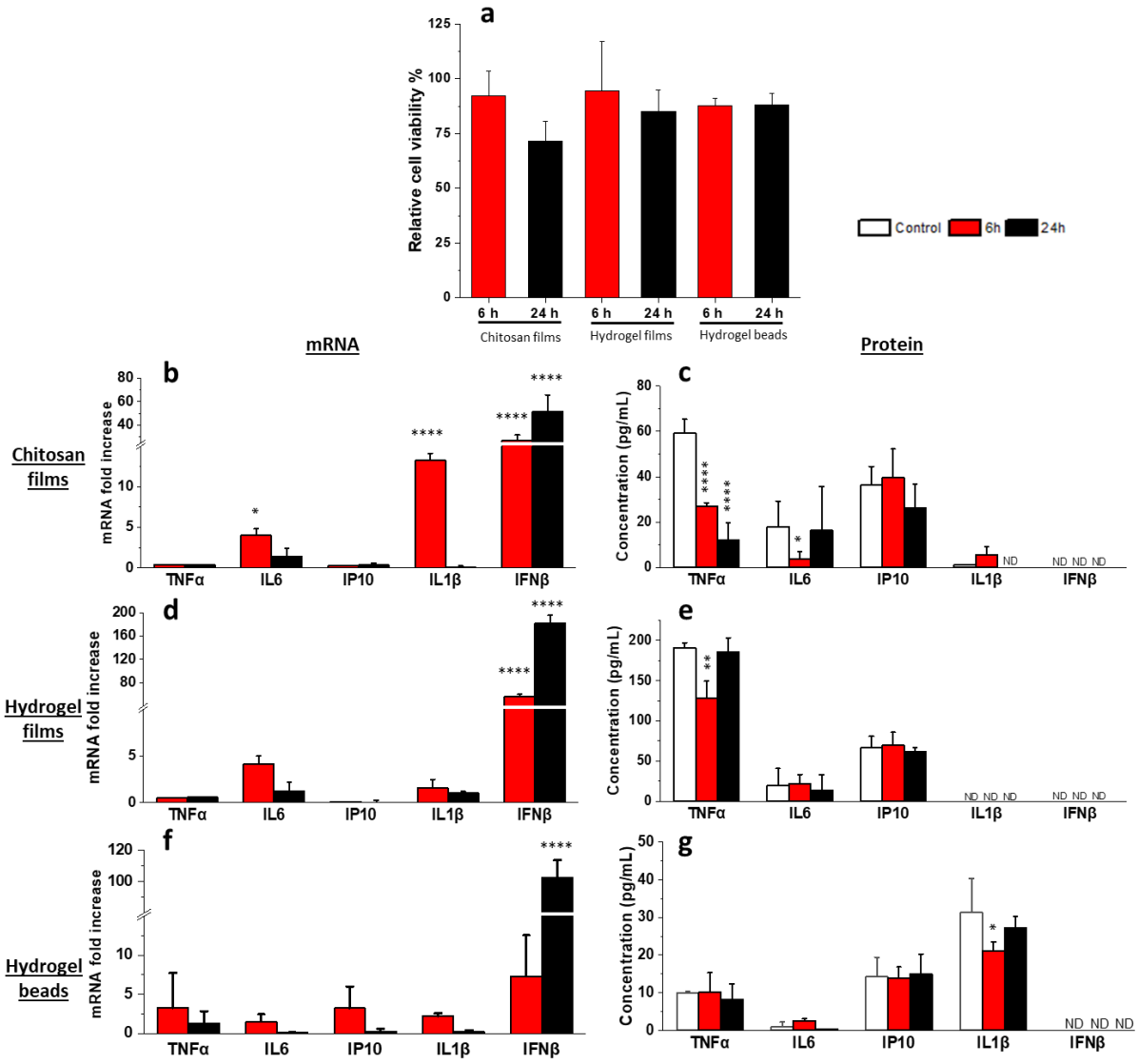

Figure 5.3 Inflammatory cytokine production by RAW 264.7 cells exposed to uncrosslinked chitosan films and crosslinked hydrogel films/beads. Assays were carried out at 6 h and 24 h of incubation. (a) RAW 264.7 cell viability measured by CellTiter-Glo® 2.0 assay. Data in the experimental groups are percentages relative to the control group (cells seeded in wells containing fresh culture medium only). Cytokine gene transcription (b, d, f) and protein expression (c, e, g) by RAW 264.7 cells were assessed using RT-PCR and ELISA respectively, after exposure to chitosan films (b, c), hydrogel films (d, e), or hydrogel beads (f, g). Fold increases in cytokine gene transcription are relative to the control group measured at the same time point. Data are representative of two independent experiments (n = 6/group). Statistical significance was determined by two-tailed unpaired Student's *t* test; *, $P < 0.05$; **, $P < 0.01$; ***, $P < 0.001$; ****, $P < 0.0001$; ND, not detected.

As shown in **Figure 5.3a**, the percentages of viability of chitosan film-exposed RAW 264.7 were 92% (at 6 h) and 75% (at 24 h), with no significant difference compared to the control group. The percentages of viability of hydrogel film-exposed RAW 264.7 were 94% (at 6 h) and 85% (at 24 h), with no significant difference compared to the control group. The percentages of viability of hydrogel bead-exposed RAW 264.7 were 87% (at 6 h) and 88% (at 24 h), with no significant difference compared to the control group. Thus, compared to uncrosslinked chitosan films, the crosslinked hydrogel network with genipin is deemed minimally cytotoxic towards RAW 264.7 although not statistically significant ($P > 0.05$).

Similar to the experiment with DC 2.4, several inflammatory cytokines (TNF-α, IL-6, IP10, IL-1β, and IFN-β) were chosen to study the inflammatory response to chitosan-based materials. In **chitosan film**-exposed RAW 264.7, increased IL-6 (4-fold) and IL-1β (13-fold) mRNA expression were observed at 6 h (**Figure 5.3b**) while IL-6 level (3 pg/mL) was surprisingly 5-fold lower than control cells and IL-1β level (5 pg/mL) was comparable to control cells (**Figure 5.3c**). TNF-α mRNA transcription was not elevated and TNF-α levels in chitosan film-exposed cells were significantly lower than control cells at the same time point. mRNA transcription and protein expression of IP-10 in chitosan film-exposed cells were comparable to control cells at the same time point. IFN-β gene transcription was increased significantly (27-fold at 6 h and 51-fold at 24 h) but no IFN-β protein was detected, similar to outcomes in chitosan film-exposed DC 2.4.

In **hydrogel film**-exposed RAW 264.7, increased IL-6 (4-fold) mRNA expression was observed at 6 h (although not statistically significant, $P > 0.05$, **Figure 5.3d**) while IL-6 level (22 pg/mL) was comparable to control cells (**Figure 5.3e**). TNF-α mRNA transcription was not elevated and TNF-α levels in chitosan film-exposed cells were significantly lower (at 6 h) or comparable (at 24 h) to control cells. mRNA transcription and protein expression of IP-10 in hydrogel film-exposed cells were comparable to control cells at the same time point. IL-1β mRNA expression was not elevated and no IL-1β protein was detected. IFN-β gene transcription was increased significantly (56-fold at 6 h and 181-fold at 24 h) but no IFN-β protein was detected, similar to outcomes in hydrogel film-exposed DC 2.4.

In **hydrogel bead**-exposed RAW 264.7, mRNA transcription and protein expression of TNF-α, IL-6, and IP10 were comparable to control cells at the same time point. At 6 h, increased IL-1β (2-fold) mRNA expression was observed (although not statistically significant, $P > 0.05$, **Figure 5.3f**) while IL-1β level (21 pg/mL) was comparable to control cells (**Figure 5.3g**). IFN-β gene

transcription was increased significantly (102-fold at 24 h) but no IFN-β protein was detected, as observed in RAW 264.7 exposed to chitosan films and hydrogel films.

Consistent with outcomes in DC 2.4 experiments, these findings support the conclusion that uncrosslinked chitosan films and crosslinked hydrogels are hypo-inflammatory towards RAW 264.7, as no increased levels of inflammatory cytokines including TNF-α, IL-6, IP-10, IL-1β, and IFN-β were detected despite increasing in gene transcriptional activity for IL6, IL-1β, and IFN-β.

5.2.3 Inflammatory response by primary mouse macrophages

As primary macrophages reflect physiological functions (such as phagocytic activity, cytokine production, and regulation of the oxidative burst) better than macrophage cell lines, inflammatory responses to hydrogels were investigated using mouse bone marrow-derived macrophages (BMDM). BMDM cells were generated by culturing bone marrow with the M-CSF (as described in Section 3.10.1) and were seeded on uncrosslinked chitosan films and crosslinked hydrogel films/beads (as described in Section 3.10). Cytokine analysis was carried out at 6 h of incubation. The results are presented in **Figure 5.4**.

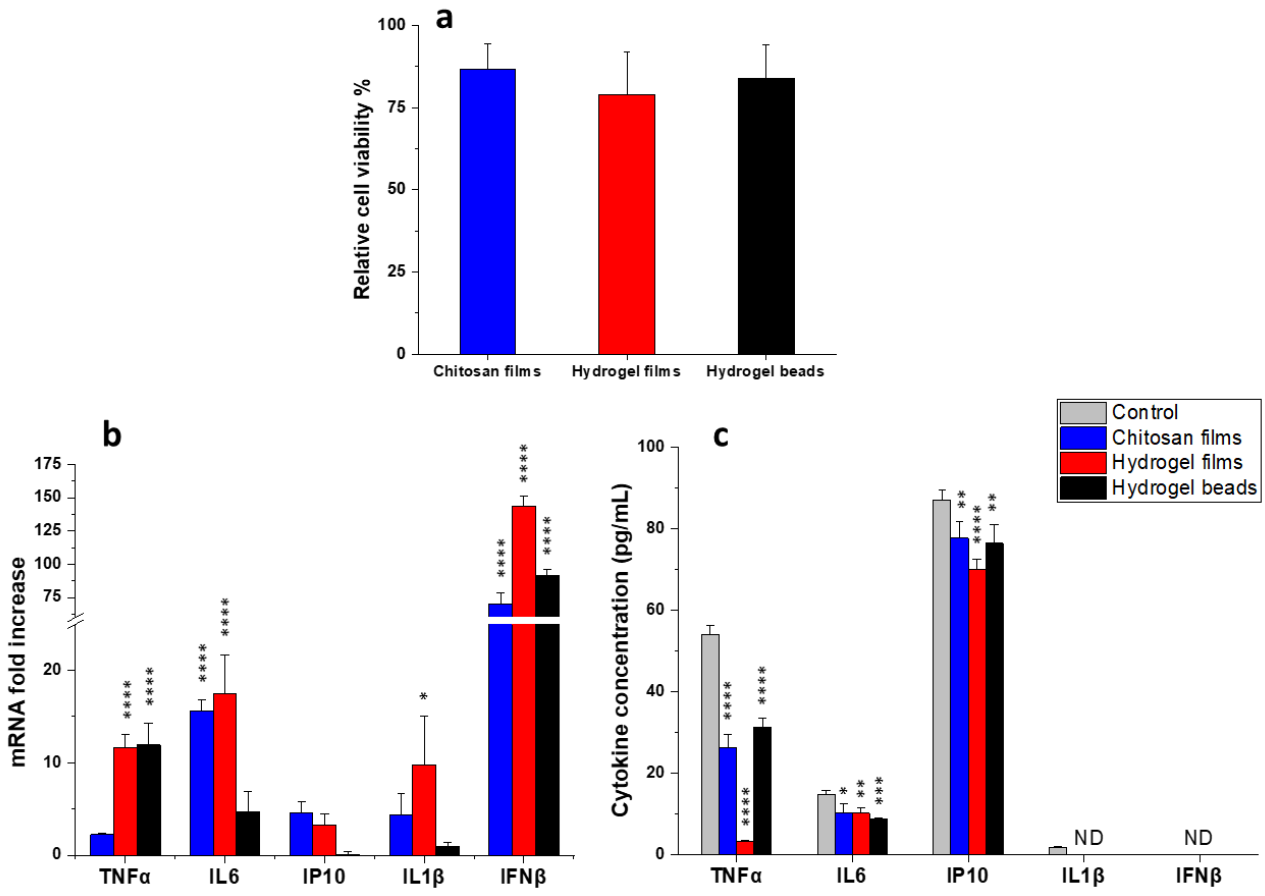

Figure 5.4 Inflammatory cytokine production by BMDM cells exposed to uncrosslinked chitosan films and crosslinked hydrogel films/beads. Assays were carried out at 6 h of incubation. (a) BMDM cell viability measured by CellTiter-Glo® 2.0 assay. Data in the experimental groups are percentages relative to the control group (cells seeded in wells containing fresh culture medium only). Cytokine gene transcription (b) and protein expression (c) by BMDM cells were assessed using RT-PCR and ELISA, respectively. Fold increases in cytokine gene transcription are relative to the control group measured at the same time point. Data are representative of two independent experiments (n = 6/group). Statistical significance was determined by two-tailed unpaired Student's *t* test; *, $P < 0.05$; **, $P < 0.01$; ***, $P < 0.001$; ****, $P < 0.0001$; ND, not detected.

As shown in **Figure 5.4a**, at 6 h incubation, the percentages of viability of BMDM exposed to chitosan films, hydrogel films, and hydrogel beads were 86%, 79%, and 84%, respectively, suggesting that uncrosslinked chitosan films and crosslinked hydrogel films/beads have minimal cytotoxic towards BMDM (although not statistically significant, $P > 0.05$).

Similar to the experiments with DC 2.4 and RAW 264.7, several inflammatory cytokines (TNF-α, IL-6, IP10, IL-1β, and IFN-β) were chosen to study the inflammatory response to chitosan-based materials. In **chitosan film**-exposed BMDM, increased IL-6 (16-fold) mRNA expression was observed while IL-6 level (10 pg/mL) was significantly lower than control cells (**Figure 5.4b**), consistent with outcomes in DC 2.4 and RAW 264.7 exposed to chitosan film. In **hydrogel film**-exposed cells, increased TNF-α (12-fold), IL-6 (17-fold), and IL-1β (10-fold) mRNA expression were observed. In **hydrogel bead**-exposed cells, increased TNF-α (12-fold) mRNA expression was observed. Despite increasing in gene transcriptional activity found in some cases, concentrations of TNF-α, IL-6, and IP-10 protein released by treated cells were significantly lower than control cells and no IL-1β protein was detected (**Figure 5.4c**).

IFN-β gene transcription was increased significantly. IFN-β gene transcriptions in BMDM exposed to chitosan films, hydrogel films, and hydrogel beads were 70-fold, 143-fold, and 92-fold increase compared to control cells, respectively. However, no IFN-β protein was detected in supernatants measured by ELISA, consistent with what observed in DC 2.4 and RAW 264.7. Taking these findings into accounts, the inflammatory responses by several *in vitro* cultured cells and primary macrophages to hydrogels confirm the hydrogels' hypo-inflammatory property.

5.3 *In vitro* degradation upon exposure to lysozyme

To assess the enzymatic degradation of hydrogels, chitosan-genipin hydrogels, with and without PEG were prepared in 24-well clear-bottomed black plates (as detailed in Section 3.2.3). As the gels had optimal excitation and emission wavelengths at 580 and 630 nm respectively (Section 4.3), changes in the fluorescence of hydrogels during incubation with lysozyme were recorded at these wavelengths (as detailed in Section 3.11). The results are presented in **Figure 5.5**.

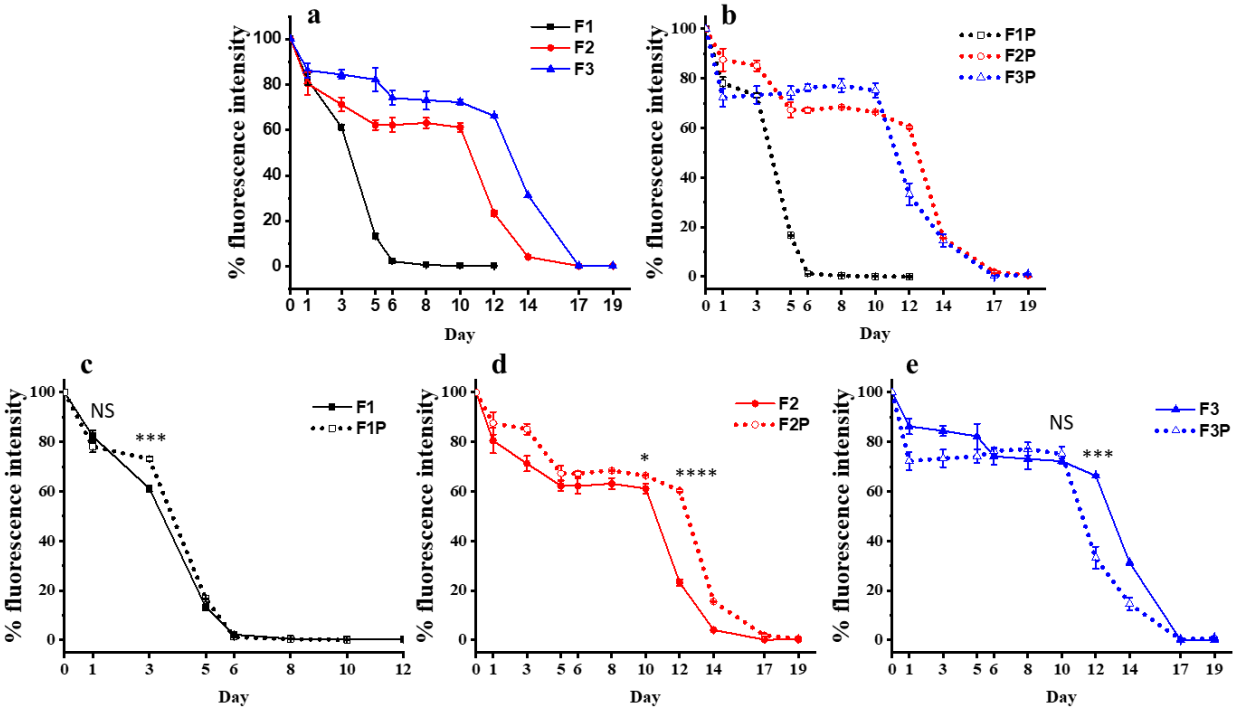

Figure 5.5 Changes in fluorescence intensity of chitosan-genipin hydrogels, with and without PEG (Table 3.3, formed at 37°C/24 h), upon exposure to lysozyme, recorded at excitation/emission wavelengths of 580/630 nm. Fluorescence of hydrogels grouped by presence of PEG: (a) chitosan-genipin hydrogels and (b) chitosan-genipin-PEG hydrogels. Fluorescence of hydrogels grouped by genipin content: gels with (c) 1.7 mM genipin, (d) 3.1 mM genipin, and (e) 4.4 mM genipin. The connecting lines are given as a guide for the eye only and do not represent actual data. Data are representative of two independent experiments (n = 4 at each data point). Statistical significance was determined by two-way ANOVA with multiple comparisons; *, $P < 0.05$; **, $P < 0.01$; ***, $P < 0.001$; ****, $P < 0.0001$; NS, not significant.

Previous studies have commonly monitored changes in hydrogel mass to evaluate the degradation [297-299]. However, gravimetric measurement is a highly invasive procedure with several intermediate steps (such as transferring gels between enzyme solution and balance, removing excess solvent, and gel fragmentation during the handling) which could affect the results. Thus, the hydrogels' intrinsic fluorescence was exploited to track the enzymatic degradation efficiently and non-invasively. As shown in **Figure 5.5**, enzymatic degradation of all hydrogels studied was apparent after 3 days, as fluorescence intensity decreased from 100% to 70 - 80% in this period. The hydrogels incubated in PBS solution displayed no degradation as the recorded fluorescence intensity remained unchanged over time. The results show that the rate and extent of hydrogel

degradation were dependent on the degree of crosslinking as well as the presence of PEG. Gels with 1.7 mM genipin (F1 and F1P) showed a significant decrease in fluorescence during the first 5 days, while gels with 3.1 mM genipin (F2 and F2P) or 4.4 mM genipin (F3 and F3P) had a slight decrease during the first 5 days and remained considerably stable until day 10 before their fluorescence intensity started to decrease, reaching zero at around day 17 (**Figure 5.5a,b**). The highest rates of fluorescence loss in gels F1, F2, and F3 were 24%, 19%, and 18% per day, respectively; and in gels F1P, F2P, and F3P were 28%, 22%, and 21% per day, respectively. Collectively, these findings indicate that chitosan-genipin hydrogels are sensitive to lysozyme-mediated degradation and preserve the biodegradable properties of uncrosslinked chitosan. Increasing genipin content (from 1.7 mM to 4.4 mM) delayed degradation significantly, potentially due to the higher crosslinked network suppressing the mobility of polymer chains. Moreover, chitosan chains bridged by genipin form a cyclic crosslinking structure with increased stereohindrance for the penetration of lysozyme due to the bulky heterocyclic-structure of genipin [193]. These observations are consistent with previous reports [8, 193, 194, 252], indicating that genipin concentration is a suitable variable to modulate the rate of hydrogel degradation.

Figure 5.5 also shows the effect addition of PEG has on degradation in relation to genipin content. In gels with 1.7 mM genipin, addition of PEG (1.3 mM) showed little effect on degradation as gels F1 and F1P had similar degradation patterns (**Figure 5.5c**). In gels with 3.1 mM genipin, addition of PEG (1.2 mM) slightly retarded degradation as gels F2 and F2P started to degrade at day 10 and day 12, respectively (**Figure 5.5d**). This is possibly due to PEG filling up the spaces within the gel network and binding to the hydroxyl groups on chitosan chains via hydrogen bonding, resulting in a denser structure suppressing the mobility of polymer chains. In gels with 4.4 mM genipin, addition of PEG (1.1 mM) did not further delay degradation as gels F3 and F3P started to degrade at day 12 and day 10, respectively (**Figure 5.5e**). In this case, PEG may interact with chitosan more effectively, reducing the number of effective crosslinks between chitosan and genipin [31], and confining the ability of genipin to suppress degradation. Once the hydrogels start to degrade, the increased hydrophilicity induced by PEG addition appears to accelerate degradation, resulting in a faster degradation rate observed in PEG-added hydrogels compared to non-PEG-added hydrogels, regardless of genipin content. Thus, addition of PEG delays hydrogel degradation to some extent in relation to genipin content, which showed most distinct impact on degradation of hydrogels employing moderate genipin concentration (F2 and F2P), compared to the counterparts with lowest (F1 and F1P) or highest (F3 and F3P) genipin content. This suggests existence of an optimal range

of PEG concentration beyond which PEG addition may lead to a reduced number of effective crosslinking between chitosan and genipin. These findings support the results presented in Chapter 4, which reveal the link between PEG content (2.9 mM and above) and the sudden changes in hydrogels' swelling capacity, gelation kinetics, and mechanical strengths [31]. The present work suggests an innovative and yet simple approach to deploy the intrinsic fluorescence of the crosslinked hydrogels for tracking the biodegradation *in vitro* and *in vivo*.

5.4 *In vivo* degradation upon subcutaneous injection in mice with macrogels

The intrinsic fluorescence of hydrogels was exploited to monitor biodegradation *in vivo*. Chitosan-genipin-PEG hydrogels were prepared directly in syringes (as detailed in Section 3.2.5) and immediately injected subcutaneously into 3 mice (as detailed in Section 3.12.1). *In Vivo* Imaging System (IVIS) was deployed to scan and measure fluorescence intensity of hydrogel depots following subcutaneous injection. The results are presented in **Figure 5.6**.

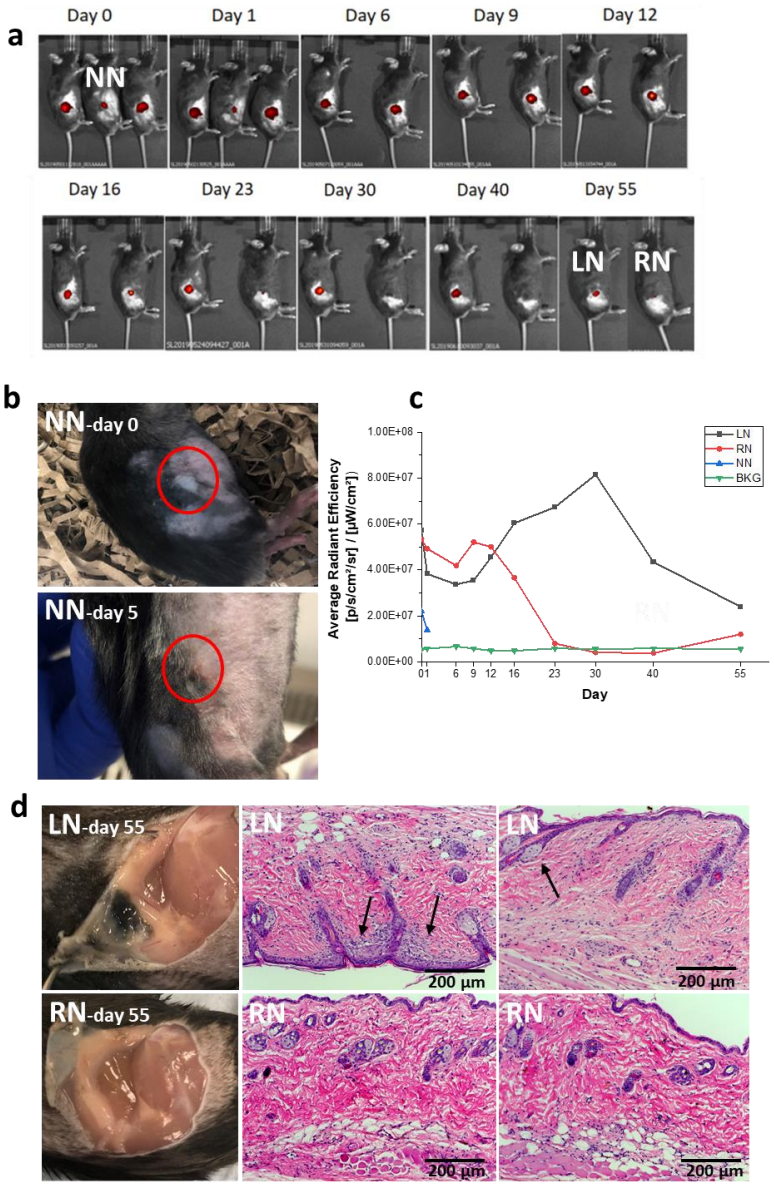

Figure 5.6 *In vivo* biodegradation of chitosan-genipin-PEG hydrogels following subcutaneous injection. Mice are identified by notching their ears: left ear-notched mouse (LN), right ear-notched mouse (RN) and no notched mouse (NN). (a) Fluorescence imaging of mice at indicated time point using IVIS. (b) Local skin reaction of NN mouse occurred within 5 days post-injection. (c) Changes in fluorescence intensity of hydrogel depot over time measured by IVIS. The connecting lines are given as a guide for the eye only and do not represent actual data. (d) Retrieved tissues at injection sites at day 55 and their H&E staining images from LN and RN mice. Black arrows indicate the thickened dermis layer and damaged hair follicles in LN mouse.

The results show that the intrinsic fluorescence of hydrogels was detectable using IVIS. Hydrogels emitted bright red light at excitation wavelength of 605 nm and emission wavelength of 660 nm

with minimal interference from the auto-fluorescence nature of living tissues (**Figure 5.6a**). The intrinsic fluorescence of hydrogels allows real time and non-invasive tracking of degradation *in vivo* without sacrificing mice or injection of a fluorescent marker. General assessment of mouse health status was carried out to detect any adverse systemic effects, including piloerection, decreased activity, abnormal posture, and weight loss. No piloerection, reduced activity, and abnormal posture were evident. Body weight measurements reveal no significant changes upon injection and during the study duration. The injected hydrogels appeared as a round or irregular shaped protrusion at injection sites, which became smaller over time. Visual observation at injection sites reveals the appearance of ulceration. LN and RN mice had a mild transient reaction, as skin at injection sites appeared red and swollen, while NN mouse had a severe skin reaction with the appearance of necrotic skin (black scab) within 5 days post-injection (**Figure 5.6b**). As NN mouse continued to self-traumatise, it was culled humanely at day 6. Skin ulceration reflects an acute inflammatory response against polymeric compounds, but the extent of ulceration varied in severity amongst individual mice. LN and RN mice remained normally active and prolonged gel persistence (up to day 23 or day 55) was observed without signs of self-trauma, indicating that acute inflammatory responses were minimal, non-invasive, and transient. It is worth noting that the hydrogels were prepared directly in syringes without further washing steps prior to injection (as opposed to hydrogel films or beads, which were washed intensely prior to testing *in vitro*). Thus, undesirable skin reactions may indicate irritation effects in tissues caused by unreacted crosslinkers, intermediate compounds or by-products of crosslinking reaction. Hence, post-processing steps, such as washing and inactivation, prior to injection/implantation may be necessary to reduce inflammatory responses *in vivo.*

IVIS images reveal that LN mouse had weak fluorescent signal up to day 55 while signal from RN mouse reduced gradually from day 12 post-injection (**Figure 5.6a**). The initial fluorescence intensity of hydrogel depot in NN mouse (measured right after injection) was one third than those in LN and RN mice, which might be a dosing error (as the gel was highly viscous and it is hard to precisely control volume of injection) or might reflect nuanced differences of hydrogel deposition in skin. Despite similar fluorescence intensity recorded right after injection (day 0 in **Figure 5.6c**) in LN and RN mice, their fluorescence intensity developed in different ways in the next few days. In the RN mouse, hydrogel fluorescence was reduced slightly at day 6, but then increased to peak at day 9 before gradually reducing and becoming negligible at day 23 post-injection. In the LN mouse, hydrogel fluorescence was also reduced slightly at day 6, but then increased gradually to

peak at day 30 before reducing and reaching its minimal value at day 55. The increase in hydrogels' fluorescence from day 6 may be an indication of continuous crosslinking reaction going on after the injection.

To conduct histological assessments, LN and NN mice were culled humanely at day 55 and the gel samples were retrieved with unaffected surrounding tissues. Samples were processed and stained with H&E to evaluate cellular infiltration throughout the gels. As seen in **Figure 5.6d**, tissue retrieved from the LN mouse contained a small piece of hydrogel which was not degraded after 55 days, while the hydrogel depot had disappeared completely in RN mouse. The difference in degradation rates in the two mice may depend on the position where hydrogels were deposited, as the hydrogel may have been deposited intradermally in LN mouse, while the hydrogel may have been deposited subcutaneously in RN mouse. At day 55, sustained chronic inflammation was identified by immune cell infiltrates in the tissue surrounding injection site in the LN mouse. Some areas of the dermal layer appeared thickened with visible signs of protein and hair follicle damage (as indicated by black arrows in **Figure 5.6d**). The cause of tissue damage is unclear but may be associated with the position where the hydrogel was deposited in the LN mouse. Upon tissue processing for H&E staining in the LN mouse, remaining gel was not visible. H&E staining images of retrieved tissues in RN mouse reveal minimal infiltrating cells, normal dermis layer, and healthy hair follicles. These findings are consistent with the conclusion that following subcutaneous injection, hydrogels are degraded enzymatically into small fragments, which are gradually eliminated from subcutaneous regions via the systemic blood or lymphatic circulatory systems, indicating that chitosan-genipin-PEG hydrogels, as well as their degradation products, may be biocompatible *in vivo*. Further *in vivo* experiments will be required using more mice and additional read-outs (such as inflammatory cytokine production in tissues) at experimental endpoints to generate robust conclusions regarding hydrogel biocompatibility.

5.5 *In vivo* biocompatibility upon subcutaneous injection with hydrogel beads

To assess the biocompatibility of hydrogel beads, chitosan-genipin particles were prepared at 37^{o}C and stirring speed of 500 rpm (as described in Section 3.2.2). The beads were dispersed in PBS and subcutaneously injected in 6 mice (as detailed in Section 3.12.2). The results are presented in **Figure 5.7**.

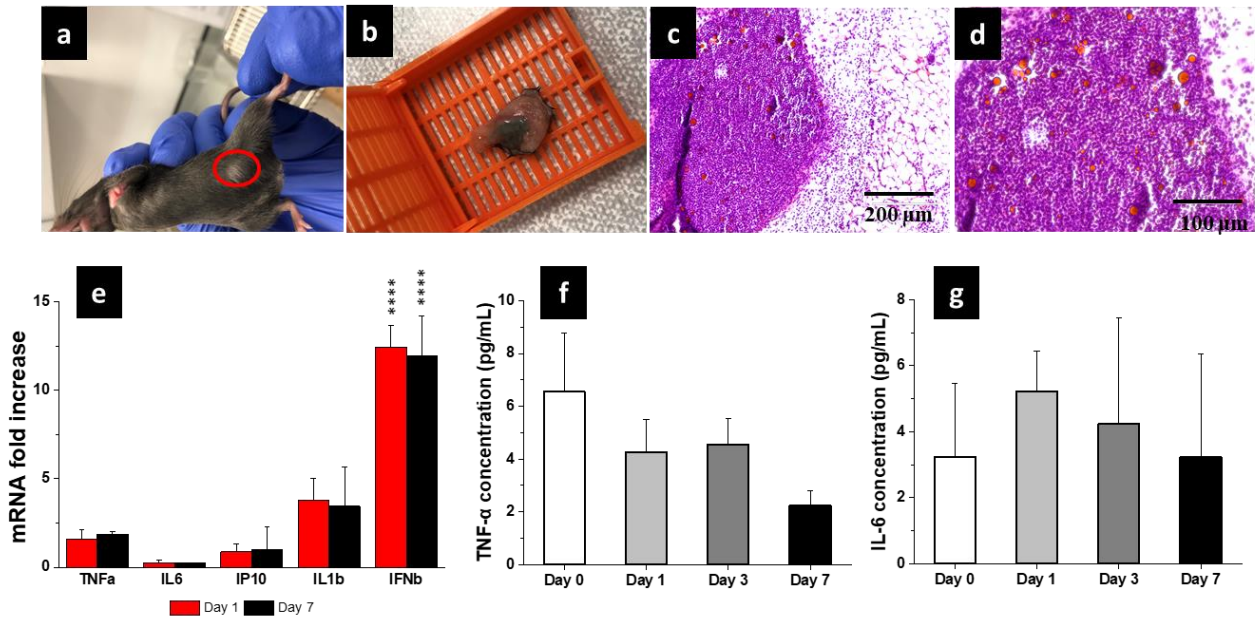

Figure 5.7 *In vivo* biocompatibility of chitosan-genipin hydrogel beads following subcutaneous injection. (a) Injection site (red cycle) of a treated mouse observed at day 7 post-injection showing no sign of local skin reaction. (b) Retrieved tissues at injection site of a treated mouse showing the remaining gels at day 1 post-injection. (c) H&E staining image of the retrieved tissues and (d) its magnified section. (e) Cytokine gene transcription (measured by RT-PCR) in lymph nodes collected at indicated time points. Fold increases in cytokine gene expression are relative to the control group measured at the same time point. (f) TNF-α and (g) IL-6 concentrations (measured by ELISA) in plasma samples collected at indicated time points. Data are expressed as mean ± SD; n = 3 at each data point. Statistical significance was determined by two-tailed unpaired Student's *t* test; ****, $P < 0.0001$.

For all treated mice, no local skin reaction at injected sites was evident (**Figure 5.7a**), as opposed to the skin inflammation found in macrogel-injected mice. At day 1, three mice were culled humanely after collecting blood samples. In two mice, no obvious sign of hydrogel accumulation under the skin was found, suggesting hydrogels might be completely degraded or widely distributed around the adjacent area, while in the other mouse, a small piece of visible subcutaneous lump was found and retrieved (**Figure 5.7b**). Further histological analysis shows the presence of hydrogel remains (as red dots in **Figure 5.7c,d)** and immune cell infiltrates, suggesting an acute inflammation induced. At day 3, blood samples were collected in three remaining mice and at day 7, mice were culled humanely after collecting additional blood samples. No signs of skin reaction

were observed at 7 days post-injection and the retrieved tissues from those three mice contained no hydrogel pieces.

The retrieved local draining lymph nodes from the control and treated mice were processed to measure cytokine gene expression by RT-PCR (TNF-α, IL-6, IP-10, IL-1β, and IFN-β). mRNA expression of TNF-α, IL-6, IP-10, and IL-1β in treated mice were comparable to control mice at the same time point. Increased IFN-β (13-fold at day 1 and 12-fold at day 7) mRNA expression was observed in treated mice (**Figure 5.7e**), consistent with the *in vitro* results. Cytokine levels in plasma were evaluated by ELISA, showing that no IFN-β in plasma was detected and the hydrogel beads did not increase the production of TNF-α and IL-6 within 7 days post-injection (**Figure 5.7f,g**). Though further *in vivo* experiments are required to draw significant conclusions, these initial findings suggest that hydrogel beads are more biocompatible than macrogels following subcutaneous injection. One reason may be that hydrogel beads were washed thoroughly with hexane and ethanol upon emulsion crosslinking and did not contain unreacted moieties that may provoke inflammatory responses *in vivo*.

5.6 Summary

For clinical application, a biomedical polymer must be minimally cytotoxic and biodegradable enzymatically or hydrolytically. The biocompatibility profiles of individual components of chitosan-genipin-PEG hydrogels do not guarantee that resulting hydrogels will be biocompatible. Cytotoxic effects may arise from the crosslinking process or unanticipated impact of different constituent concentrations on the biocompatibility of the resulting hydrogels. Despite the well-established links between hydrogel composition and physico-chemical properties detailed in Chapter 4, the biological functions of chitosan-genipin hydrogels are poorly understood, even less so with the presence of PEG. Currently, evaluation of the biocompatibility and biodegradation of chitosan-genipin hydrogels is very limited. Knowledge about the *in vivo* behaviour of genipin crosslinked hydrogels is frequently extrapolated from the intrinsic biocompatibility of individual constituents [203]. Furthermore, it is important to track the degradation of hydrogels *in vivo,* as it is highly relevant to the release kinetics of cargo therapeutic agents. Thus, in this Chapter, biological activities of the crosslinked hydrogels *in vitro* and *in vivo* were evaluated.

The cytotoxicity of crosslinked hydrogel films was investigated using 3T3 fibroblast cells. SEM images and ATP assays show that 3T3 cells maintained good spreading morphology (with elongated or spindle-like shape) and high viability (73 - 95%) on hydrogels with higher genipin

content (3.1 - 4.4 mM), while they remained round/oval and had low viability on hydrogels with lower genipin content (1.7 mM). Section 4.6 shows that higher genipin content increased mechanical stiffness of hydrogels, suggesting that sufficient stiffness is a prerequisite for polymeric matrices to provide effective cell attachment. Addition of PEG is deemed favourable for cell adhesion and growth because PEG may increase the elastic modulus and rigidity of the network, as well as the hydrophilicity of hydrogel surfaces. Even though further *in vivo* studies are needed, these initial results provide guidance to support hydrogel design for the specific application of drug delivery and controlled release. For instance, these results suggest that for implantation, a stiffer gel with higher genipin content and good mechanical robustness is more biocompatible and more suitable for *in vivo* application.

As dendritic cells and macrophages play critical roles for the induction of protective immune responses against pathogens [300], the inflammatory responses of DC 2.4 dendritic cells, RAW 264.7 macrophages cells, and primary macrophages (BMDM) to both uncrosslinked chitosan and crosslinked chitosan-genipin hydrogels were investigated. The results show that uncrosslinked chitosan films had minimal cytotoxic effects on DC 2.4 (cell viability: 105 - 108%), RAW 264.7 (cell viability: 75 - 92%), and BMDM (cell viability: 80 - 95%). The cells exposed to hydrogel films and beads also had good viability (85 - 103%), suggesting that chitosan-genipin crosslinked networks had minimal cytotoxic effects on inflammatory cells. Inflammatory cytokine gene transcription (TNF-α, IL-6, IP-10, IL-1β, and IFN-β) measured by RT-PCR suggests that mRNA expression of some cytokines was induced in all examined immune cell types, nevertheless no increased levels of cytokine protein were found, indicating that the hypo-inflammatory properties of the chitosan-based materials are not due to inhibiting of inflammatory gene transcription, rather through regulating more complex biological mechanisms such as protein translation or secretion pathways. This may be more reflected in the case of IFN-β. Consistently observed in all three cell types (DC 2.4, RAW 264.7, and BMDM), IFN-β gene transcription was increased significantly (up to 2435-fold in DC 2.4), supporting previous studies which reported the induction of type 1 interferon via cGAS-STING pathway of chitosan [26, 225]. However, no IFN-β protein was ever detected in all conditions (even though ELISA worked well for IFN-β standard with detection limit of 5 pg/mL).

Biodegradable polymeric materials are of considerable interest as they can be broken down and eliminated from tissues after they have served specific functions without the need of surgical removal [301]. The biodegradation properties of crosslinked chitosan hydrogels remain unclear, as

crosslinking with genipin might yield physically stable hydrogels, which either persist or are sensitive to enzymatic degradation. The *in vitro* biodegradation of hydrogels was investigated non-invasively using their intrinsic fluorescence upon crosslinking reaction. As discussed in Section 4.3, crosslinking with genipin yielded a fluorescent product which emitted strong red light upon excitation. Enzymatic degradation is a significant source of chitosan depolymerisation, in which chitosan is degraded by lysozyme and bacterial enzymes present in the colon [302-304]. Thus, lysozyme was the enzyme chosen for this study. The active site of lysozyme consists of six subsites that bind to D-glucosamine units of chitosan and form enzyme-material complex [305]. The cleavage of glycosidic linkage occurs when the alternate sites of lysozyme interact with acetamide side chains of N-acetyl glucosamine units of chitosan. Simultaneously with chitosan chain scission, cleavage and/or destruction of its functional groups (amino, carbonyl, and hydroxyl) occur [21]. In this study, the degradation process showed a biphasic pattern, which involved a gradual decrease in fluorescence within the first few days, followed by a sudden loss in fluorescence until the hydrogels were completely broken down. The first phase of the degradation process exhibited moderate fluorescent loss, possibly due to the initial diffusion of lysozyme from surrounding solution to the gel matrix and the gradual recognition of acetamide side chain of N-acetyl glucosamine units to activate its hydrolysis activity. Once cleavage of glycosidic linkage occurred, the degradation products, including low MW chitosan, chitooligomer, and N-acetyl glucosamine D-residues, may be subsequently released and dissolved into the surrounding media [22]. As lysozyme solution was refreshed after each fluorescence reading and the hydrogel networks were loosened over time, the hydrolysis activity was accelerated, leading to an abrupt decrease in fluorescence intensity, which coincides with the sudden mass loss observed visually.

In this study, the results show that crosslinking with genipin yielded an enzymatically degradable product and a prolonged degradation with a slow degradation rate was achieved by increasing genipin content, resulting in a highly crosslinked network that suppresses the mobility of polymer chains. Addition of PEG delayed the degradation to a certain extent associated with genipin content, indicating that the degradation of CS-Gen-PEG hydrogels can be effectively controlled by modulating their composition. The non-destructive nature of the method is particularly relevant to real-time monitoring of material formation, conformation change or degradation in living bodies.

The intrinsic fluorescence of hydrogels was also exploited to track their fate non-invasively following subcutaneous injection into mice. As preliminary experiments, a group of 3 mice were injected with 200 µL of chitosan-genipin-PEG hydrogels subcutaneously. Local skin reaction at

injected sites was observed but varied in severity amongst individual mice. One mouse (NN) was self-traumatised with severe necrosis (appearance of black scab) and was culled humanely at day 6, while two other mice (LN and RN) had transient reactions and remained normally active up to day 55. IVIS imaging reveals that the hydrogel fluorescence in both mice developed in different ways during the study, despite similar initial fluorescence at day 0. In the LN mouse, the hydrogel was partly degraded and persisted at the injection site until day 55, while in the RN mouse, the hydrogel was degraded and eliminated by day 55. H&E staining images of tissues surrounding injection sites reveal immune cell infiltrates, reflecting a chronic inflammation in the LN mouse, but not in the RN mouse. These findings suggest that hydrogel degradation rates may depend on where they are deposited in skin tissues. In the LN mouse, the hydrogel may have been deposited intradermally, while in the RN mouse, the hydrogel may have been deposited subcutaneously. Intradermal injection may lead to prolonged gel persistence (up to 8 weeks) and chronic inflammation, while subcutaneous injection may lead to faster degradation (up to 4 weeks). Due to the limited number of mice treated in this preliminary experiment, significant conclusions cannot be drawn. However, supported by literature which has reported good biocompatibility of genipin-related hydrogels *in vivo* [113, 209, 213, 306], these findings suggest that chitosan-genipin-PEG hydrogels may have acceptable biocompatibility *in vivo*, and may have the ability to serve as long-lasting drug delivery depots.

As the local skin reaction observed in the macrogel-injected mice may come from unreacted crosslinker and by-products of crosslinking reaction that remained within the newly-formed macrogels, subcutaneous injection of the hydrogel beads was carried out. No local skin reaction was observed in any treated-mice up to 7 days post-injection. The hydrogels were partly degraded at day 1 (a gel depot remained in one mouse) and fully degraded at day 7. H&E stanning images of the gel-containing tissues show immune cell infiltrates, indicating on-going inflammation reaction. The plasma concentrations of TNF-α and IL-6 protein in mice injected with hydrogel beads were comparable to control mice within 7 days post-injection and remained within normal range. Despite no IFN-β detected in plasma samples, the injection of hydrogel beads induced IFN-β mRNA expression significantly (12-fold). Even though more *in vivo* studies are required to understand the biodegradation of hydrogel beads, these results suggest a good biocompatibility of hydrogel beads *in vivo*, and post-processing steps to remove the unreacted moieties and by-products is necessary to reduce inflammatory responses to hydrogel polymers.

Chapter 6 Conclusion and future directions

6.1 Conclusions

Owing to the ability to sense surrounding environments and release entrapped molecules in a controlled manner, stimuli-responsive hydrogels have great potential as chronotherapeutic carriers. Furthermore, the hydrophilicity and the swelling ability in biological conditions endow hydrogels with excellent biocompatibility, resembling extracellular matrix with a soft and rubbery consistency. Among biomaterials utilised for hydrogel fabrication, chitosan is of increasing interest for development of pH-responsive hydrogels due to its low toxicity, good biocompatibility, biodegradability, rich source, low cost, and wide variety of derivatives. Even though there has been an upsurge in publications related to chitosan-based hydrogels, their transition to clinical applications is still at its early stage and requires experimental. As long chitosan chains need to be crosslinked to form a stable hydrogel, there is an imperative need to utilise a biocompatible crosslinker to bridge chitosan chains. Owing to the high variability in chitosan structure as a natural-derived polymer, it is necessary to enhance reproducibility and consistency of the developed hydrogels, as well as improve mechanical robustness and reduce burst release effect. Therefore, in this project, genipin, a low toxic and biocompatible crosslinker, was employed to crosslink chitosan chains and PEG was added to form semi-IPN hydrogels to enhance the level of control in hydrogel's microarchitecture.

The main aim of this study was to develop and evaluate injectable and degradable pH-responsive chitosan hydrogels crosslinked by genipin and interpenetrated by PEG for drug delivery applications. The project firstly focused on the hydrogels' fabrication process to produce hydrogels in a range of shapes (disc, bead, and film) for different measurements. To be able to tailor the hydrogels' properties according to end-use applications, the physical and chemical properties were evaluated as a function of their composition (genipin and PEG content) and gelation conditions. To target these pH-responsive hydrogels for controlled drug delivery, the release kinetics of two therapeutic agents were characterised. To bring them one step closer to clinical trials, *in vitro* and *in vivo* biocompatibility of the resulting hydrogels was assessed. The study offers following findings.

1) Versatile approach in hydrogels' fabrication. The crosslinked hydrogels, composed of chitosan, genipin, and PEG (combined as aqueous solution), were synthesised under mild conditions (37^{o}C, 24 h) and in a range of shapes (disc, bead, and film) to facilitate different

measurements. The dark blue colour and intrinsic fluorescence upon chitosan-genipin reaction were observed in all hydrogels studies. The bead-shaped hydrogels (diameters ranging from 1 μm to 30 μm), prepared by emulsion crosslinking, were discrete, compact, and rough without visible pores on the beads' surface. The disc-shaped hydrogels (13 mm in diameter and 8 mm in height), prepared in polyethylene vials, had microporous structure with diameters ranging from 11 μm to 57 μm and average cross-sectional porous areas of 40% to 64%. By means of gravimetric measurements, it is confirmed that the hydrogels were pH-responsive, which could swell in acidic conditions (pH 2 and pH 4 buffers) and shrink in neutral/basic conditions (pH 7 and pH 10 buffers). The hydrogels also exhibited oscillations in swelling (with relatively small amplitude) under manually induced pH oscillations (changing buffers between pH 2 and pH 4/pH 7).

2) Remarkable effect of gelation conditions on hydrogels' microstructure. Either prepared in disc shape or bead shape, gelation conditions (incubation time/temperature and stirring speed) affected the hydrogels' microarchitecture significantly. In disc-shaped hydrogels, increasing incubation temperature (from 20^{o}C to 37^{o}C) reduced the swelling ratio while further increasing temperature up to 45 - 60^{o}C led to higher swelling ratio. Increasing incubation time (from 8 h to 24 h) produced hydrogels with lower swelling capacity while long incubation time up of 48 - 96 h increased the swelling degree. In bead-shaped hydrogels, increasing incubation temperature (from 20^{o}C to 37^{o}C) produced smaller particles while there was no distinct difference in sizes of particles prepared at 37^{o}C and 50^{o}C. Increasing stirring speed (from 250 rpm to 500 - 750 rpm) produced smaller particles and narrower size distribution.

3) Profound effect of genipin and PEG content on hydrogels' physico-chemical properties. In disc-shaped hydrogels, changes in hydrogels' conformation can be efficiently controlled by either changing genipin content or adding PEG. In hydrogels with 1.2 mM PEG, increasing genipin content (from 3.1 mM to 6.3 mM) reduced average pore size (from 24 μm to 18 μm), swelling ratio (from 22% to 15%), and gelation time by 41% (from 44 min to 26 min) while increasing elastic modulus (from 445 Pa to 1100 Pa). In hydrogels with 3.6 mM PEG, increasing genipin content (from 3.1 mM to 6.3 mM) yielded similar effect (average pore size reduced from 25 μm to 21 μm; swelling ratio reduced from 60% to 30%; and elastic modulus increased from 380 Pa to 700 Pa), while showing negligible effect on gelation time (dropping from 44 min to 40 min).

Compared to chitosan-genipin hydrogels only, addition of PEG (1.2 mM) to form semi-IPN hydrogels decreased average pore size and increased porosity and elastic modulus. Further

increasing PEG content (3.6 mM) did not make significant change in average pore size but further increased porous area and decreased elastic modulus. Addition of PEG up to 0.8 mM decreased swelling degree to 60% and further increasing PEG content to 1.9 mM reduced swelling degree to 20%. Interestingly, a higher PEG content from 2.9 mM to 3.6 mM increased swelling degree to 60%, suggesting existence of an optimal range of PEG concentration beyond which PEG addition may lead to a reduced number of effective crosslinking between chitosan and genipin. In gels with 3.1 mM genipin, the gelation time was around 44 min regardless of the amount of PEG added while in gels with 6.3 mM genipin, increasing PEG content from 1.2 mM to 3.6 mM led to longer gelation time (from 26 min to 40 min). Collectively, genipin and PEG content can be used to tailor desirable physico-chemical properties of the resulting hydrogels. Considering cost of genipin (£345 for 125 mg, Sigma-Aldrich), scale-up production, and the fact that addition of PEG (up to a critical concentration) yielded same effect as increasing genipin content, cost of fabrication can be optimised by replacing some genipin with PEG polymer.

4) **Controlled drug delivery with non-Fickian transport mechanism**. Two therapeutic agents (PER and D-1MT) with different solubility were chosen to evaluate the release kinetics from crosslinked hydrogels. The results show that the amount of PER or D-1MT released from gels with highest genipin content (4.4 mM) was lowest compared to those released from gels with 3.1 mM or 1.7 mM genipin. As PER is more soluble in water than D-1MT, the amount of PER released from a single composition at equilibrium state was almost twice as much as that of D-1MT. The swelling-controlled release kinetics fitted well to Kormeyer-Peppas models, with release component, $0.45 < n < 0.89$, indicating non-Fickian transport mechanism.

5) Hypo-inflammatory properties. 3T3 fibroblasts cultured on hydrogel films showed different cellular behaviours as a function of genipin content. The cells retained normal adhesive properties and high viability (73 - 95%) on gels with 3.1 mM and 4.4 mM genipin but not on gels with 1.7 mM genipin, suggesting a strong correlation between hydrogels' stiffness and cell attachment/growth. Addition of PEG (up to 1.3 mM) enhanced the viability of 3T3 cells cultured on hydrogel surfaces. Three different types of chitosan were used towards inflammatory cells (DC 2.4, RAW 264.7, and BMDM), including uncrosslinked chitosan films and crosslinked hydrogels in bead and film shapes. The cells exposed to hydrogel films and beads had good viability (> 85%), suggesting that chitosan-genipin crosslinked network had minimal cytotoxic effects on inflammatory cells. Despite increasing in gene transcriptional activity in some treated cells, no increased levels of five inflammatory cytokines (TNF-α, IL-6, IP10, IL-1β, and IFN-β) were

detected, suggesting the hypo-inflammatory properties of chitosan-genipin hydrogels. The induction of IFN-β gene transcription was consistently observed in all treated immune cell types, but no IFN-β protein was detected, suggesting that the hypo-inflammatory properties are regulated through more complex biological mechanisms (such as protein translation or secretion pathway), rather than inhibiting of inflammatory gene transcription.

6) Efficient approach to track biodegradation *in vitro* and *in vivo* using hydrogels' fluorescence. Owing to the intrinsic fluorescence upon chitosan-genipin crosslinking, the biodegradation of crosslinked hydrogels was monitored *in vitro* and *in vivo* by tracking their fluorescence. Enzymatic degradation under lysozyme activity shows that increasing genipin content (from 1.7 mM to 3.1 - 4.4 mM) prolonged the degradation with a slower degradation rate while adding PEG (up to 1.3 mM) also delayed the degradation to some extent. *In vivo* biodegradation upon subcutaneous injection of chitosan-genipin-PEG macrogels was tracking using IVIS. Even though there was a severe skin reaction appeared in one treated mouse, the acute inflammation is deemed bearable and associated with the position where the hydrogel is deposited, suggesting the need of post-processing steps to remove the unreacted/intermediate residuals or by-products of chitosan-genipin reaction. Fluorescence intensity recorded by IVIS suggests that the degradation may depend on where the hydrogel is deposited, as prolonged gel persistence (up to 8 weeks) occurred when the hydrogel was deposited intradermally. *In vivo* biocompatibility upon subcutaneous injection of chitosan-genipin hydrogel beads was also evaluated. Even though there were immune cell infiltrates seen in H&E images of tissues surrounding injection sites, no local skin ulceration was observed up to 7 days post-injection and the plasma levels of TNF-α and IL-6 were not increased, suggesting good biocompatibility of hydrogels beads following subcutaneous injection. Consistent with *in vitro* inflammatory response, the hydrogel beads induced IFN-β gene transcription significantly, but no IFN-β protein was detected.

Owing to many exceptional properties, including low toxicity, good biocompatibility, biodegradability, good mucoadhesion, and the ability to be functionalised into different derivatives according to the designated applications, chitosan is a strong candidate for biomedical applications. Compared to other natural polymers such as collagen, hyaluronic acid, and gelatin, chitosan hydrogels offer higher versatility in system design. Chitosan can be 1) physically combined with other compounds to form temperature-responsive hydrogels; 2) chemically crosslinked to enhance mechanical robustness and form pH-responsive hydrogels; 3) combined with different reagents to form multi-responsive hydrogels; 4) modified into more hydrophobic derivatives (e.g.

carboxylmethyl chitosan) to carry hydrophobic drugs; 5) formed in a variety of dimensions and forms. Despite these numerous striking features, only a limited number of chitosan hydrogels are currently used in clinical applications. One main drawback to polymers sourced from natural tissues is the concern over immunogenicity and batch-to-batch variation, which pose challenges in achieving consistent results and good correlation between accurate chemical structure and their effective biological responses. Owing to the poor mechanical resistance, chitosan is not ideally suited for applications which involve high mechanical stresses or load-bearing. Chemical crosslinking to enhance the mechanical robustness may impair the biocompatibility of the resulting hydrogels. For this reason, naturally derived crosslinkers, such as genipin, tannic acid, or plant-derived polyphenols (gallic acid and ferulic acid), have gained increasing interest. In this project, genipin was chosen as a crosslinker and the feasibility of PEG addition in modifying hydrogels' structure was investigated. With insights into the hydrogels' microstructure and smart behaviours as a pH-responsive system, the developed hydrogels show potential in various biomedical applications. The hydrogel microparticles can carry therapeutic agents (drugs, RNA, cells, etc.) by direct entrapment and surface attachment. The microgels then can be administered by either incorporating with microneedle arrays (e.g. pain-free vaccine delivery for COVID-19 by carrying mRNA spike protein) or by direct injection (e.g. intra-tumoral injection for cancer immunotherapy). The hydrogel particles can also be produced in nano-size, suitable for encapsulation of insoluble drugs and nasal route delivery as chitosan is known to have mucoadhesion property, which allows the delivery system to be retained better in the mucosal epithelial tissues. The hydrogel particles can be embedded in hydrogel scaffold (in film/disc shape) for implantation. Such systems are promising, as the scaffold and the particles are both based on chitosan backbone, reducing the complexity in chemical composition and increasing the biocompatibility of these composite systems. As chitosan can be developed into temperature-sensitive hydrogels, *in situ* forming hydrogels based on chitosan are highly potent, offering a multi-layer delivery of therapeutic agents (e.g. dual-delivery of chemotherapy drugs, where the first soluble drug is dissolved in hydrogel solution and the second insoluble drug is loaded in the form of particles which are dispersed in the solution). Despite those challenges mentioned above, chitosan hydrogels stand as a highly promising biomaterial and deserve combined efforts in synthesis, characterisation, and modelling to take them from the discovery to applications.

6.2 Future directions

This project has provided a deeper insight into the physical-chemical properties of the resulting pH-responsive chitosan-based hydrogels as well as their *in vitro* and *in vivo* biocompatibility. However, the transition from bench to market is still very challenging. Considerably, these present findings suggest the following directions for future research.

1) Exploring release profiles of loaded drug from hydrogel beads. This would be immediate experiments which could not be carried out because of the laboratory closure during COVID-19 pandemic. The *in vitro* and *in vivo* release of loaded drug from hydrogel beads would give valuable information on how the release kinetic is regulated and how the pH-sensitivity affects *in vivo* performance.

2) Gaining deeper understanding into the mechanism of biodegradation and translational control. As the present study shows that degradation rates varied amongst treated mice, further *in vivo* experiments with more mice and additional read-outs at experimental endpoints are required to understand the mechanism of degradation. As the present study provides strong evidence for the induction of IFN-β gene transcription both *in vitro* and *in vivo* while no IFN-β protein was detected, it would be beneficial to carry out bioassays to measure IFN-β activity and investigate translational control.

3) Developing self-oscillating hydrogels based on chitosan-genipin crosslinked. The present study provides deeper insight into how PEG addition affected the hydrogels' microstructure and how to tailor the hydrogels' properties efficiently to meet anticipated applications. As the chitosan-genipin-PEG hydrogels exhibited oscillations in swelling under manually induced pH oscillations, it is now of prime interest to develop the hydrogels further towards an autonomous rhythmic system where all the components (substrate, catalyst, and smart hydrogel) are combined within a single macromolecule.

4) Expanding the range of drug amenable for hydrogel-based delivery. Owing to the hydrophilic nature, the delivery of hydrophobic drug from hydrogels remains a challenge. Owing to the versatility in chemical modifications, chitosan can be functionalised into different derivatives (such as N-acylation chitosan) to present more hydrophobic domains. As the present study provides evidence to support the addition of PEG, future research could explore the use of other linear polymers (such as poloxamer F407 and polylactic acid) to be able to carry hydrophobic molecules. Incorporating particulate systems (such as microsphere, liposome, and micelles) into hydrogel

matrices to form composite hydrogels is a promising approach to prolong drug delivery and achieve a bi-phasic release pattern.

3) Validating different fabrication techniques to produce hydrogel micro/nanoparticles. Even though emulsion crosslinking is a simple method suitable for laboratory research and formulation development, scale-up production with controllable parameters remains challenging. As many techniques are available to produce hydrogel beads (such as microfluidics, lithography, and spraying), it is important to validate the efficiency of these techniques to produce particles with desirable size/shapes and uniformity. The effect of hydrogels' composition (such as genipin content) on the particles' microstructure needs further investigation.

References

[1] M.C. Koetting, J.T. Peters, S.D. Steichen, and N.A. Peppas, *Stimulus-responsive hydrogels: Theory, modern advances, and applications.* Materials Science and Engineering: R: Reports, 2015. **93**: p. 1-49.

[2] D. Das and S. Pal, *Modified biopolymer-dextrin based crosslinked hydrogels: application in controlled drug delivery.* RSC Adv., 2015. **5**(32): p. 25014-25050.

[3] P. Gupta, K. Vermani, and S. Garg, *Hydrogels: from controlled release to pH-responsive drug delivery.* Drug Discovery Today, 2002. **7**(10): p. 569-579.

[4] J. Fu, F. Yang, and Z. Guo, *The chitosan hydrogels: from structure to function.* New Journal of Chemistry, 2018. **42**(21): p. 17162-17180.

[5] F. Khan, R.S. Tare, R.O. Oreffo, and M. Bradley, *Versatile biocompatible polymer hydrogels: scaffolds for cell growth.* Angew Chem Int Ed Engl, 2009. **48**(5): p. 978-82.

[6] M.C.G. Pellá, M.K. Lima-Tenório, E.T. Tenório-Neto, M.R. Guilherme, E.C. Muniz, and A.F. Rubira, *Chitosan-based hydrogels: From preparation to biomedical applications.* Carbohydrate Polymers, 2018. **196**: p. 233-245.

[7] J. Li and D.J. Mooney, *Designing hydrogels for controlled drug delivery.* Nature reviews. Materials, 2016. **1**(12): p. 16071.

[8] F.L. Mi, Y.C. Tan, H.F. Liang, and H.W. Sung, *In vivo biocompatibility and degradability of a novel injectable-chitosan-based implant.* Biomaterials, 2002. **23**: p. 181-191.

[9] F. Sami El-banna, M.E. Mahfouz, S. Leporatti, M. El-Kemary, and N. A. N. Hanafy, *Chitosan as a Natural Copolymer with Unique Properties for the Development of Hydrogels.* Applied Sciences, 2019. **9**(11): p. 2193.

[10] F. Croisier and C. Jérôme, *Chitosan-based biomaterials for tissue engineering.* European Polymer Journal, 2013. **49**(4): p. 780-792.

[11] G. Crini, *Historical review on chitin and chitosan biopolymers.* Environmental Chemistry Letters, 2019. **17**(4): p. 1623-1643.

[12] L. Liu, Q. Gao, X. Lu, and H. Zhou, *In situ forming hydrogels based on chitosan for drug delivery and tissue regeneration.* Asian Journal of Pharmaceutical Sciences, 2016. **11**(6): p. 673-683.

[13] S.C. Chen, Y.C. Wu, F.L. Mi, Y.H. Lin, L.C. Yu, and H.W. Sung, *A novel pH-sensitive hydrogel composed of N,O-carboxymethyl chitosan and alginate cross-linked by genipin for protein drug delivery.* Journal of Controlled Release, 2004. **96**(2): p. 285-300.

[14] L.C. Keong and A.S. Halim, *In vitro models in biocompatibility assessment for biomedical-grade chitosan derivatives in wound management.* Int. J. Mol. Sci, 2009. **10**: p. 1300-1313.

[15] R.A.A. Muzzarelli, *Genipin-crosslinked chitosan hydrogels as biomedical and pharmaceutical aids.* Carbohydrate Polymers, 2009. **77**: p. 1-9.

[16] S. Sahu, S. Maiti, T. Maiti, S. Ghosh, and P. Pramanik, *Hydrophobically modified carboxymethyl chitosan nanoparticles targeted delivery of paclitaxel.* Journal of drug targeting, 2010. **19**: p. 104-13.

[17] B. Bellich, I. D'Agostino, S. Semeraro, A. Gamini, and A. Cesàro, *"The Good, the Bad and the Ugly" of Chitosans.* Marine Drugs, 2016. **14**(5): p. 99.

[18] H. Mittal, S.S. Ray, B.S. Kaith, J.K. Bhatia, Sukriti, J. Sharma, and S.M. Alhassan, *Recent progress in the structural modification of chitosan for applications in diversified biomedical fields.* European Polymer Journal, 2018. **109**: p. 402-434.

[19] T. Kean and M. Thanou, *Biodegradation, biodistribution and toxicity of chitosan.* Advanced Drug Delivery Reviews, 2010. **62**(1): p. 3-11.
[20] S.B. Rao and C.P. Sharma, *Use of chitosan as a biomaterial: Studies on its safety and hemostatic potential.* Journal of Biomedical Materials Research, 1997. **34**(1): p. 21-28.
[21] E. Szymanska and K. Winnicka, *Stability of chitosan-a challenge for pharmaceutical and biomedical applications.* Mar Drugs, 2015. **13**(4): p. 1819-46.
[22] D. Ren, H. Yi, W. Wang, and X. Ma, *The enzymatic degradation and swelling properties of chitosan matrices with different degrees of N-acetylation.* Carbohydrate Research, 2005. **340**(15): p. 2403-2410.
[23] X. Hu, Y. Zhang, H. Zhou, and H. Wan, *PEGylated chitosan microspheres as mucoadhesive drug-delivery carriers for puerarin.* Journal of Applied Polymer Science, 2015. **132**(40): p. 42623.
[24] M.A. Mohammed, J.T.M. Syeda, K.M. Wasan, and E.K. Wasan, *An Overview of Chitosan Nanoparticles and Its Application in Non-Parenteral Drug Delivery.* Pharmaceutics, 2017. **9**(4): p. 53.
[25] X. Jin, S.B. Zhang, S.M. Li, K. Liang, and Z.Y. Jia, *Influence of chitosan nanoparticles as the absorption enhancers on salvianolic acid B In vitro and In vivo evaluation.* Pharmacognosy Magazine, 2016. **12**(45): p. 57-63.
[26] D. Fong and C.D. Hoemann, *Chitosan immunomodulatory properties: perspectives on the impact of structural properties and dosage.* Future Sci OA, 2018. **4**(1): p. FSO225.
[27] M.A. Islam, J. Firdous, Y.J. Choi, C.H. Yun, and C.S. Cho, *Design and application of chitosan microspheres as oral and nasal vaccine carriers: an updated review.* Int J Nanomedicine, 2012. **7**: p. 6077-93.
[28] D.A. Zaharoff, C.J. Rogers, K.W. Hance, J. Schlom, and J.W. Greiner, *Chitosan solution enhances both humoral and cell-mediated immune responses to subcutaneous vaccination.* Vaccine, 2007. **25**(11): p. 2085-2094.
[29] J. Berger, M. Reist, J.M. Mayer, O. Felt, N.A. Peppas, and R. Gurny, *Structure and interactions in covalently and ionically crosslinked chitosan hydrogels for biomedical applications.* European Journal of Pharmaceutics and Biopharmaceutics 2004. **57**: p. 19-34.
[30] V.G. Tacias-Pascacio, E. García-Parra, G. Vela-Gutiérrez, J.J. Virgen-Ortiz, Á. Berenguer-Murcia, A.R. Alcántara, and R. Fernandez-Lafuente, *Genipin as An Emergent Tool in the Design of Biocatalysts: Mechanism of Reaction and Applications.* Catalysts, 2019. **9**(12): p. 1035.
[31] N.T.N. Vo, L. Huang, H. Lemos, A. Mellor, and K. Novakovic, *Poly(ethylene glycol)-interpenetrated genipin-crosslinked chitosan hydrogels: Structure, pH responsiveness, gelation kinetics, and rheology.* Journal of Applied Polymer Science, 2020. **137**(41): p. 49259.
[32] K.J. Pekarek, J.S. Jacob, and E. Mathiowltz, *Double-Walled Microspheres for Drug Delivery.* MRS Proceedings, 1993. **331**: p. 97.
[33] S.K. Mallapragada, N.A. Peppas, and P. Colombo, *Crystal dissolution-controlled release systems. II. Metronidazole release from semicrystalline poly(vinyl alcohol) systems.* Journal of Biomedical Materials Research, 1997. **36**(1): p. 125-130.
[34] N. Bhattarai, J. Gunn, and M. Zhang, *Chitosan-based hydrogels for controlled, localized drug delivery.* Adv Drug Deliv Rev, 2010. **62**(1): p. 83-99.
[35] S.N. Li, B. Li, L.X. Gong, Z.R. Yu, Y. Feng, D. Jia, Y. Zhou, and L.C. Tang, *Enhanced mechanical properties of polyacrylamide/chitosan hydrogels by tuning the molecular structure of hyperbranched polysiloxane.* Materials & Design, 2019. **162**: p. 162-170.

[36] F. Ahmadi, Z. Oveisi, S.M. Samani, and Z. Amoozgar, *Chitosan based hydrogels: characteristics and pharmaceutical applications.* Research in pharmaceutical sciences, 2015. **10**(1): p. 1-16.
[37] A. Vashist, A. Kaushik, K. Alexis, R. Dev Jayant, V. Sagar, A. Vashist, and M. Nair, *Bioresponsive Injectable Hydrogels for On-demand Drug Release and Tissue Engineering.* Current pharmaceutical design, 2017. **23**(24): p. 3595-3602.
[38] A. Isakova and K. Novakovic, *Oscillatory chemical reactions in the quest for rhythmic motion of smart materials.* European Polymer Journal, 2017. **95**: p. 430-439.
[39] A. Isakova and K. Novakovic, *Pulsatile release from a flat self-oscillating chitosan macrogel.* Journal of Materials Chemistry B, 2018. **6**(30): p. 5003-5010.
[40] K.L. Spiller and G. Vunjak-Novakovic, *Clinical translation of controlled protein delivery systems for tissue engineering.* Drug Deliv Transl Res, 2015. **5**(2): p. 101-15.
[41] Z. Cui, Y. Xiang, J. Si, M. Yang, Q. Zhang, and T. Zhang, *Ionic interactions between sulfuric acid and chitosan membranes.* Carbohydrate Polymers, 2008. **73**(1): p. 111-116.
[42] X.Z. Shu, K.J. Zhu, and W. Song, *Novel pH-sensitive citrate cross-linked chitosan film for drug controlled release.* International Journal of Pharmaceutics, 2001. **212**(1): p. 19-28.
[43] E.C. Shen, C. Wang, E. Fu, C.Y. Chiang, T.T. Chen, and S. Nieh, *Tetracycline release from tripolyphosphate-chitosan cross-linked sponge: a preliminary in vitro study.* J Periodontal Res, 2008. **43**(6): p. 642-8.
[44] X.Z. Shu and K.J. Zhu, *The influence of multivalent phosphate structure on the properties of ionically cross-linked chitosan films for controlled drug release.* Eur J Pharm Biopharm, 2002. **54**(2): p. 235-43.
[45] S. Hua, H. Yang, W. Wang, and A. Wang, *Controlled release of ofloxacin from chitosan–montmorillonite hydrogel.* Applied Clay Science, 2010. **50**(1): p. 112-117.
[46] M.C. Cardia, A.R. Carta, P. Caboni, A.M. Maccioni, S. Erbì, L. Boi, M.C. Meloni, F. Lai, and C. Sinico, *Trimethyl Chitosan Hydrogel Nanoparticles for Progesterone Delivery in Neurodegenerative Disorders.* Pharmaceutics, 2019. **11**(12): p. 657.
[47] N.K. Alruwaili, A. Zafar, S.S. Imam, K.S. Alharbi, N.H. Alotaibi, S. Alshehri, N.A. Alhakamy, A.I. Alzarea, M. Afzal, and M. Elmowafy, *Stimulus Responsive Ocular Gentamycin-Ferrying Chitosan Nanoparticles Hydrogel: Formulation Optimization, Ocular Safety and Antibacterial Assessment.* International Journal of Nanomedicine, 2020. **15**: p. 4717.
[48] M. Yadollahi, S. Farhoudian, and H. Namazi, *One-pot synthesis of antibacterial chitosan/silver bio-nanocomposite hydrogel beads as drug delivery systems.* Int J Biol Macromol, 2015. **79**: p. 37-43.
[49] M. Yadollahi, S. Farhoudian, S. Barkhordari, I. Gholamali, H. Farhadnejad, and H. Motasadizadeh, *Facile synthesis of chitosan/ZnO bio-nanocomposite hydrogel beads as drug delivery systems.* Int J Biol Macromol, 2016. **82**: p. 273-8.
[50] F. Wahid, H.S. Wang, Y.-S. Lu, C. Zhong, and L.Q. Chu, *Preparation, characterization and antibacterial applications of carboxymethyl chitosan/CuO nanocomposite hydrogels.* International journal of biological macromolecules, 2017. **101**: p. 690-695.
[51] S. Lankalapalli and V.R.M. Kolapalli, *Polyelectrolyte Complexes: A Review of their Applicability in Drug Delivery Technology.* Indian journal of pharmaceutical sciences, 2009. **71**(5): p. 481-487.
[52] D. Wu, L. Zhu, Y. Li, X. Zhang, S. Xu, G. Yang, and T. Delair, *Chitosan-based Colloidal Polyelectrolyte Complexes for Drug Delivery: A Review.* Carbohydrate Polymers, 2020. **238**: p. 116126.

[53] V.S. Meka, M.K. Sing, M.R. Pichika, S.R. Nali, V.R. Kolapalli, and P. Kesharwani, *A comprehensive review on polyelectrolyte complexes.* Drug discovery today, 2017. **22**(11): p. 1697-1706.
[54] Y. Hu, T. Yang, and X. Hu, *Novel polysaccharides-based nanoparticle carriers prepared by polyelectrolyte complexation for protein drug delivery.* Polymer Bulletin, 2012. **68**(4): p. 1183-1199.
[55] M.A. Krayukhina, N.A. Samoilova, and I.A. Yamskov, *Polyelectrolyte complexes of chitosan: formation, properties and applications.* Russian Chemical Reviews, 2008. **77**(9): p. 799-813.
[56] A.P. Constantinou and T.K. Georgiou, *Tuning the gelation of thermoresponsive gels.* European Polymer Journal, 2016. **78**: p. 366-375.
[57] S. Saravanan, S. Vimalraj, P. Thanikaivelan, S. Banudevi, and G. Manivasagam, *A review on injectable chitosan/beta glycerophosphate hydrogels for bone tissue regeneration.* International Journal of Biological Macromolecules, 2019. **121**: p. 38-54.
[58] H.Y. Zhou, L.J. Jiang, P.P. Cao, J.B. Li, and X.G. Chen, *Glycerophosphate-based chitosan thermosensitive hydrogels and their biomedical applications.* Carbohydrate Polymers, 2015. **117**: p. 524-536.
[59] J.P. Chen and T.H. Cheng, *Thermo-responsive chitosan-graft-poly(N-isopropylacrylamide) injectable hydrogel for cultivation of chondrocytes and meniscus cells.* Macromol Biosci, 2006. **6**(12): p. 1026-39.
[60] N. Bhattarai, H.R. Ramay, J. Gunn, F.A. Matsen, and M. Zhang, *PEG-grafted chitosan as an injectable thermosensitive hydrogel for sustained protein release.* J Control Release, 2005. **103**(3): p. 609-24.
[61] A. Ahsan, M.A. Farooq, and A. Parveen, *Thermosensitive Chitosan-Based Injectable Hydrogel as an Efficient Anticancer Drug Carrier.* ACS Omega, 2020. **5**(32): p. 20450-20460.
[62] L. Aulisa, H. Dong, and J.D. Hartgerink, *Self-Assembly of Multidomain Peptides: Sequence Variation Allows Control over Cross-Linking and Viscoelasticity.* Biomacromolecules, 2009. **10**(9): p. 2694-2698.
[63] M. Guvendiren, H.D. Lu, and J.A. Burdick, *Shear-thinning hydrogels for biomedical applications.* Soft Matter, 2012. **8**(2): p. 260-272.
[64] S. Uman, A. Dhand, and J.A. Burdick, *Recent advances in shear-thinning and self-healing hydrogels for biomedical applications.* Journal of Applied Polymer Science, 2020. **137**(25): p. 48668.
[65] D.J. Overstreet, D. Dutta, S.E. Stabenfeldt, and B.L. Vernon, *Injectable hydrogels.* Journal of Polymer Science Part B: Polymer Physics, 2012. **50**(13): p. 881-903.
[66] L. Haines-Butterick, K. Rajagopal, M. Branco, D. Salick, R. Rughani, M. Pilarz, M.S. Lamm, D.J. Pochan, and J.P. Schneider, *Controlling hydrogelation kinetics by peptide design for three-dimensional encapsulation and injectable delivery of cells.* Proceedings of the National Academy of Sciences, 2007. **104**(19): p. 7791-7796.
[67] Z.-X. Zhang, S.S. Liow, K. Xue, X. Zhang, Z. Li, and X.J. Loh, *Autonomous Chitosan-Based Self-Healing Hydrogel Formed through Noncovalent Interactions.* ACS Applied Polymer Materials, 2019. **1**(7): p. 1769-1777.
[68] J. Qu, X. Zhao, Y. Liang, T. Zhang, P.X. Ma, and B. Guo, *Antibacterial adhesive injectable hydrogels with rapid self-healing, extensibility and compressibility as wound dressing for joints skin wound healing.* Biomaterials, 2018. **183**: p. 185-199.

[69] J. Huang, Y. Deng, J. Ren, G. Chen, G. Wang, F. Wang, and X. Wu, *Novel in situ forming hydrogel based on xanthan and chitosan re-gelifying in liquids for local drug delivery.* Carbohydrate Polymers, 2018. **186**: p. 54-63.
[70] T.K. Giri, A. Thakur, A. Alexander, Ajazuddin, H. Badwaik, and D.K. Tripathi, *Modified chitosan hydrogels as drug delivery and tissue engineering systems: present status and applications.* Acta Pharmaceutica Sinica B, 2012. **2**(5): p. 439-449.
[71] S.J. Buwalda, T. Vermonden, and W.E. Hennink, *Hydrogels for Therapeutic Delivery: Current Developments and Future Directions.* Biomacromolecules, 2017. **18**(2): p. 316-330.
[72] K. Varaprasad, G.M. Raghavendra, T. Jayaramudu, M.M. Yallapu, and R. Sadiku, *A mini review on hydrogels classification and recent developments in miscellaneous applications.* Materials Science and Engineering: C, 2017. **79**: p. 958-971.
[73] A. Webster, M.D. Halling, and D.M. Grant, *Metal complexation of chitosan and its glutaraldehyde cross-linked derivative.* Carbohydr Res, 2007. **342**(9): p. 1189-201.
[74] A. Singh, S.S. Narvi, P.K. Dutta, and N.D. Pandey, *External stimuli response on a novel chitosan hydrogel crosslinked with formaldehyde.* Bulletin of Materials Science, 2006. **29**(3): p. 233-238.
[75] M.-M. Iftime, S. Morariu, and L. Marin, *Salicyl-imine-chitosan hydrogels: Supramolecular architecturing as a crosslinking method toward multifunctional hydrogels.* Carbohydrate Polymers, 2017. **165**: p. 39-50.
[76] L. Baldino, S. Concilio, S. Cardea, I. De Marco, and E. Reverchon, *Complete glutaraldehyde elimination during chitosan hydrogel drying by SC-CO2 processing.* The Journal of Supercritical Fluids, 2015. **103**: p. 70-76.
[77] D. Sakloetsakun, J.M. Hombach, and A. Bernkop-Schnürch, *In situ gelling properties of chitosan-thioglycolic acid conjugate in the presence of oxidizing agents.* Biomaterials, 2009. **30**(31): p. 6151-7.
[78] F. Li, W.G. Liu, and K.D. Yao, *Preparation of oxidized glucose-crosslinked N-alkylated chitosan membrane and in vitro studies of pH-sensitive drug delivery behaviour.* Biomaterials, 2002. **23**(2): p. 343-7.
[79] L. Weng, X. Chen, and W. Chen, *Rheological characterization of in situ crosslinkable hydrogels formulated from oxidized dextran and N-carboxyethyl chitosan.* Biomacromolecules, 2007. **8**(4): p. 1109-15.
[80] X. Li, Y. Weng, X. Kong, B. Zhang, M. Li, K. Diao, Z. Zhang, X. Wang, and H. Chen, *A covalently crosslinked polysaccharide hydrogel for potential applications in drug delivery and tissue engineering.* J Mater Sci Mater Med, 2012. **23**(12): p. 2857-65.
[81] L. Li, N. Wang, X. Jin, R. Deng, S. Nie, L. Sun, Q. Wu, Y. Wei, and C. Gong, *Biodegradable and injectable in situ cross-linking chitosan-hyaluronic acid based hydrogels for postoperative adhesion prevention.* Biomaterials, 2014. **35**(12): p. 3903-17.
[82] M. Rinaudo, *New way to crosslink chitosan in aqueous solution.* European Polymer Journal, 2010. **46**(7): p. 1537-1544.
[83] Y. Zhang, L. Tao, S. Li, and Y. Wei, *Synthesis of multiresponsive and dynamic chitosan-based hydrogels for controlled release of bioactive molecules.* Biomacromolecules, 2011. **12**(8): p. 2894-901.
[84] K. Hye-Rim, K. Ho-Joong, and J. Jin, *Antioxidant Activity of Hydrogel Lens Applied with Gallic Acid.* The Korean Journal of Vision Science, 2020. **22**(2): p. 135-145.
[85] C.T. Tsao, M.H. Hsiao, M.Y. Zhang, S.L. Levengood, and M. Zhang, *Chitosan-PEG hydrogel with sol-gel transition triggerable by multiple external stimuli.* Macromol Rapid Commun, 2015. **36**(3): p. 332-8.

[86] J. Araki, Y. Yamanaka, and K. Ohkawa, *Chitin-chitosan nanocomposite gels: reinforcement of chitosan hydrogels with rod-like chitin nanowhiskers.* Polymer Journal, 2012. **44**(7): p. 713-717.
[87] K. Zhang, S. Yan, G. Li, L. Cui, and J. Yin, *In-situ birth of MSCs multicellular spheroids in poly(L-glutamic acid)/chitosan scaffold for hyaline-like cartilage regeneration.* Biomaterials, 2015. **71**: p. 24-34.
[88] J. Jin, M. Song, and D.J. Hourston, *Novel chitosan-based films cross-linked by genipin with improved physical properties.* Biomacromolecules, 2004. **5**(1): p. 162-168.
[89] H. Sung, R. Huang, L. Huang, and C. Tsai, *In vitro evaluation of cytotoxicity of a naturally occuring cross-linking reagent for biological tissue fixation* J Biomater Sci Polym Ed., 1999. **10**(1): p. 63-78.
[90] S. Bratskaya, Y. Privar, D. Nesterov, E. Modin, M. Kodess, A. Slobodyuk, D. Marinin, and A. Pestov, *Chitosan Gels and Cryogels Cross-Linked with Diglycidyl Ethers of Ethylene Glycol and Polyethylene Glycol in Acidic Media.* Biomacromolecules, 2019. **20**(4): p. 1635-1643.
[91] T. Jóźwiak and U. Filipkowska, *Sorption kinetics and isotherm studies of a Reactive Black 5 dye on chitosan hydrogel beads modified with various ionic and covalent cross-linking agents.* Journal of Environmental Chemical Engineering, 2020. **8**(2): p. 103564.
[92] A. Subramanian and H.Y. Lin, *Crosslinked chitosan: its physical properties and the effects of matrix stiffness on chondrocyte cell morphology and proliferation.* J Biomed Mater Res A, 2005. **75**(3): p. 742-53.
[93] S.L. Vega, M.Y. Kwon, and J.A. Burdick, *Recent advances in hydrogels for cartilage tissue engineering.* European Cells and Materials, 2017. **33**: p. 59-75.
[94] N. Das, *Preparation methods and properties of hydrogel: A review.* Int J Pharm Pharm Sci, 2013. **5**(3): p. 112-117.
[95] E.S. Dragan, *Design and applications of interpenetrating polymer network hydrogels. A review.* Chemical Engineering Journal, 2014. **243**: p. 572-590.
[96] N. Zoratto and P. Matricardi, *Semi-IPN- and IPN-Based Hydrogels.* Adv Exp Med Biol, 2018. **1059**: p. 155-188.
[97] Y. Wang, X. Zhang, D. Qiu, Y. Li, L. Yao, and J. Duan, *Ultrasonic assisted microwave synthesis of poly (Chitosan-co-gelatin)/polyvinyl pyrrolidone IPN hydrogel.* Ultrasonics Sonochemistry, 2018. **40**: p. 714-719.
[98] J. Liu, W. Wang, and A. Wang, *Synthesis, characterization, and swelling behaviors of chitosan-g-poly(acrylic acid)/poly(vinyl alcohol) semi-IPN superabsorbent hydrogels.* Polymers for Advanced Technologies, 2011. **22**(5): p. 627-634.
[99] B. Kang, T.P. Vales, B.K. Cho, J.K. Kim, and H.J. Kim, *Development of Gallic Acid-Modified Hydrogels Using Interpenetrating Chitosan Network and Evaluation of Their Antioxidant Activity.* Molecules, 2017. **22**(11): p. 1976.
[100] H. Suo, D. Zhang, J. Yin, J. Qian, Z.L. Wu, and J. Fu, *Interpenetrating polymer network hydrogels composed of chitosan and photocrosslinkable gelatin with enhanced mechanical properties for tissue engineering.* Materials Science and Engineering: C, 2018. **92**: p. 612-620.
[101] R.S. Tiğli and M. Gümüşderelioğlu, *Evaluation of alginate-chitosan semi IPNs as cartilage scaffolds.* J Mater Sci Mater Med, 2009. **20**(3): p. 699-709.
[102] A.A. Al-Kahtani and B.S. Sherigara, *Controlled release of theophylline through semi-interpenetrating network microspheres of chitosan-(dextran-g-acrylamide).* J Mater Sci Mater Med, 2009. **20**(7): p. 1437-45.

[103] T.R. Hoare and D.S. Kohane, *Hydrogels in drug delivery: Progress and challenges.* Polymer, 2008. **49**(8): p. 1993-2007.
[104] S. Matcham and K. Novakovic, *Fluorescene imaging of genipin crosslinked chitosan - poly (vinyl pyrrolidone) hydrogels.* Polymers 2016. **8**(11): p. 385.
[105] M. Balamurugan, S. Rajesh, and E. Manogaran, *'Genipin' – The Natural Water Soluble Cross-linking Agent and Its Importance in the Modified Drug Delivery Systems: An Overview.* Current Drug Delivery, 2014. **11**(1): p. 139-145.
[106] R.A.A. Muzzarelli, M. El Mehtedi, C. Bottegoni, A. Aquili, and A. Gigante, *Genipin-Crosslinked Chitosan Gels and Scaffolds for Tissue Engineering and Regeneration of Cartilage and Bone.* Marine Drugs, 2015. **13**(12): p. 7314-7338.
[107] N.L. Delgadillo-Armendariz, N.A. Rangel-Vazquez, E.A. Marquez-Brazon, and B. Rojas-De Gascue, *Interactions of chitosan/genipin hydrogels during drug delivery: a QSPR approach.* Química Nova, 2014. **37**: p. 1503-1509.
[108] R. Touyama, Y. Takeda, K. Inoue, I. Kawamura, M. Yatsuzuka, T. Ikumoto, T. Shingu, T. Yokoi, and H. Inouye, *Studies on the Blue Pigments Produced from Genipin and Methylamine. I. Structures of the Brownish-Red Pigments, Intermediates Leading to the Blue Pigments.* Chemical & Pharmaceutical Bulletin, 1994. **42**(3): p. 668-673.
[109] H. Chen, W. Ouyang, B. Lawuyi, C. Martoni, and S. Prakash, *Reaction of chitosan with genipin and its fluorogenic attributes for potential microcapsule membrane characterization.* Journal of biomedical materials research, 2005. **75A**(4): p. 917-927.
[110] F.L. Mi, S.S. Shyu, and C.K. Peng, *Characterization of ring‐opening polymerization of genipin and pH‐dependent cross‐linking reactions between chitosan and genipin.* Journal of Polymer Science Part A: Polymer Chemistry, 2005. **43**(10): p. 1985-2000.
[111] M.F. Butler, Y.F. Ng, and P.D.A. Pudney, *Mechanism and kinetics of the crosslinking reaction between biopolymers containing primary amine groups and genipin.* Journal of polymer science., 2003. **41**(24): p. 3941-3953.
[112] J.E. Park, J.Y. Lee, H.G. Kim, T.R. Hahn, and Y.S. Paik, *Isolation and Characterization of Water-Soluble Intermediates of Blue Pigments Transformed from Geniposide of Gardenia jasminoides.* Journal of Agricultural and Food Chemistry, 2002. **50**(22): p. 6511-6514.
[113] A.M. Heimbuck, T.R. Priddy-Arrington, M.L. Padgett, C.B. Llamas, H.H. Barnett, B.A. Bunnell, and M.E. Caldorera-Moore, *Development of Responsive Chitosan–Genipin Hydrogels for the Treatment of Wounds.* ACS Applied Bio Materials, 2019. **2**(7): p. 2879-2888.
[114] W. Zhang, G. Ren, H. Xu, J. Zhang, H. Liu, S. Mu, X. Cai, and T. Wu, *Genipin cross-linked chitosan hydrogel for the controlled release of tetracycline with controlled release property, lower cytotoxicity, and long-term bioactivity.* Journal of Polymer Research, 2016. **23**(8): p. 156.
[115] S. Maiz-Fernández, O. Guaresti, L. Pérez-Álvarez, L. Ruiz-Rubio, N. Gabilondo, J.L. Vilas-Vilela, and S. Lanceros-Mendez, *β-Glycerol phosphate/genipin chitosan hydrogels: A comparative study of their properties and diclofenac delivery.* Carbohydrate Polymers, 2020. **248**: p. 116811.
[116] M. Ubaid and G. Murtaza, *Fabrication and characterization of genipin cross-linked chitosan/gelatin hydrogel for pH-sensitive, oral delivery of metformin with an application of response surface methodology.* International Journal of Biological Macromolecules, 2018. **114**: p. 1174-1185.

[117] Y. Song, N. Nagai, S. Saijo, H. Kaji, M. Nishizawa, and T. Abe, *In situ formation of injectable chitosan-gelatin hydrogels through double crosslinking for sustained intraocular drug delivery.* Materials Science and Engineering: C, 2018. **88**: p. 1-12.
[118] S.S. Silva, A. Motta, M.T. Rodrigues, A.F. Pinheiro, M.E. Gomes, J.F. Mano, R.L. Reis, and C. Migliaresi, *Novel genipin-cross-linked chitosan/silk fibroin sponges for cartilage engineering strategies.* Biomacromolecules, 2008. **9**(10): p. 2764-74.
[119] J.E. Arikibe, R. Lata, K. Kuboyama, T. Ougizawa, and D. Rohindra, *pH-Responsive Studies of Bacterial Cellulose /Chitosan Hydrogels Crosslinked with Genipin: Swelling and Drug Release Behaviour.* ChemistrySelect, 2019. **4**(34): p. 9915-9926.
[120] R. Shah, P. Stodulka, K. Skopalova, and P. Saha, *Dual Crosslinked Collagen/Chitosan Film for Potential Biomedical Applications.* Polymers, 2019. **11**(12): p. 2094.
[121] D. Aycan, N.A. Yayla, and Y.A. Aydin, *Chitosan polyvinyl alcohol blend films for ibuprofen encapsulation: Fabrication, characterization and kinetics.* Polymer Degradation and Stability, 2020. **181**: p. 109346.
[122] C.J. Nwosu, G.A. Hurst, and K. Novakovic, *Genipin Cross-Linked Chitosan-Polyvinylpyrrolidone Hydrogels: Influence of Composition and Postsynthesis Treatment on pH Responsive Behaviour.* Advances in Materials Science and Engineering, 2015. **2015**: p. 1-10.
[123] A.A.d.N. Pomari, T.L.d.A. Montanheiro, C.P. de Siqueira, R.S. Silva, D.B. Tada, and A.P. Lemes, *Chitosan Hydrogels Crosslinked by Genipin and Reinforced with Cellulose Nanocrystals: Production and Characterization.* Journal of Composites Science, 2019. **3**(3): p. 84.
[124] L. Gao, H. Gan, Z. Meng, R. Gu, Z. Wu, X. Zhu, W. Sun, J. Li, Y. Zheng, T. Sun, and G. Dou, *Evaluation of genipin-crosslinked chitosan hydrogels as a potential carrier for silver sulfadiazine nanocrystals.* Colloids and Surfaces B: Biointerfaces, 2016. **148**: p. 343-353.
[125] L. Ding, X. Shan, X. Zhao, H. Zha, X. Chen, J. Wang, C. Cai, X. Wang, G. Li, J. Hao, and G. Yu, *Spongy bilayer dressing composed of chitosan–Ag nanoparticles and chitosan–Bletilla striata polysaccharide for wound healing applications.* Carbohydrate Polymers, 2017. **157**: p. 1538-1547.
[126] T.Y. Liu, S.Y. Chen, Y.L. Lin, and D.M. Liu, *Synthesis and Characterization of Amphiphatic Carboxymethyl-hexanoyl Chitosan Hydrogel: Water-Retention Ability and Drug Encapsulation.* Langmuir, 2006. **22**(23): p. 9740-9745.
[127] Y. Yu, R. Feng, J. Li, Y. Wang, Y. Song, G. Tan, D. Liu, W. Liu, X. Yang, H. Pan, and S. Li, *A hybrid genipin-crosslinked dual-sensitive hydrogel/nanostructured lipid carrier ocular drug delivery platform.* Asian Journal of Pharmaceutical Sciences, 2019. **14**(4): p. 423-434.
[128] P.D. Topham, J.R. Howse, C.J. Crook, S.P. Armes, R.A.L. Jones, and A.J. Ryan, *Antagonistic Triblock Polymer Gels Powered by pH Oscillations.* Macromolecules, 2007. **40**(13): p. 4393-4395.
[129] R. Yoshida, T. Takahashi, T. Yamaguchi, and H. Ichijo, *Self-oscillating gel.* Journal of the American Chemical Society, 1996. **118**(21): p. 5134-5135.
[130] J. Horváth, *Peristaltic waves in a responsive gel sustained by a halogen-free non-oscillatory chemical reaction.* Polymer, 2015. **79**: p. 243-254.
[131] K. Novakovic, C. Grosjean, S.K. Scott, A. Whiting, M.J. Willis, and A.R. Wright, *Achieving pH and Qr oscillations in a palladium-catalysed phenylacetylene oxidative carbonylation reaction using an automated reactor system.* Chemical Physics Letters, 2007. **435**(1): p. 142-147.

[132] K. Novakovic, A. Mukherjee, M. Willis, A. Wright, and S. Scott, *The influence of reaction temperature on the oscillatory behaviour in the palladium-catalysed phenylacetylene oxidative carbonylation reaction.* Physical Chemistry Chemical Physics, 2009. **11**(40): p. 9044-9049.
[133] J. Parker and K. Novakovic, *Influence of Water and the Reactant Addition Sequence on Palladium(II) Iodide-Catalyzed Phenylacetylene Carbonylation.* Industrial & Engineering Chemistry Research, 2013. **52**(7): p. 2520-2527.
[134] L. Donlon, J. Parker, and K. Novakovic, *Oscillatory carbonylation of phenylacetylene in the absence of externally supplied oxidant.* Reaction Kinetics, Mechanisms and Catalysis, 2014. **112**(1): p. 1-13.
[135] L. Donlon and K. Novakovic, *Oscillatory carbonylation using alkyne-functionalised poly(ethylene glycol).* Chem Commun (Camb), 2014. **50**(98): p. 15506-8.
[136] A. Mitra and B. Dey, *Chitosan microspheres in novel drug delivery systems.* Indian journal of pharmaceutical sciences, 2011. **73**(4): p. 355-366.
[137] J.M. Gallo and E.E. Hassan, *Receptor-Mediated Magnetic Carriers: Basis for Targeting.* Pharmaceutical Research, 1988. **5**(5): p. 300-304.
[138] F.L. Mi, H.W. Sung, and S.S. Shyu, *Release of indomethacin from a novel chitosan microsphere prepared by a naturally occurring crosslinker: Examination of crosslinking and polycation–anionic drug interaction.* Journal of Applied Polymer Science, 2001. **81**(7): p. 1700-1711.
[139] J. Kawadkar and M.K. Chauhan, *Intra-articular delivery of genipin cross-linked chitosan microspheres of flurbiprofen: Preparation, characterization, in vitro and in vivo studies.* European Journal of Pharmaceutics and Biopharmaceutics, 2012. **81**(3): p. 563-572.
[140] J. Karnchanajindanun, M. Srisa-ard, and Y. Baimark, *Genipin-cross-linked chitosan microspheres prepared by a water-in-oil emulsion solvent diffusion method for protein delivery.* Carbohydrate Polymers, 2011. **85**(3): p. 674-680.
[141] R. Harris, E. Lecumberri, and A. Heras, *Chitosan-genipin microspheres for the controlled release of drugs: clarithromycin, tramadol and heparin.* Marine drugs, 2010. **8**(6): p. 1750-1762.
[142] G.J.S. Lacerda, B.L. Piantino, E.V. Gonzaga, V.d.M.L. Naves, L.N. Pedreiro, M.P.D. Gremião, G.R. Pereira, and F.C. Carvalho, *Evaluation of polyelectrolyte and emulsion covalent crosslink of chitosan for producing mesalasine loaded submicron particles.* Brazilian Journal of Pharmaceutical Sciences, 2019. **55**: p. e17847.
[143] M.C. Gaspar, J.J.S. Sousa, A.A.C.C. Pais, O. Cardoso, D. Murtinho, M.E.S. Serra, F. Tewes, and J.-C. Olivier, *Optimization of levofloxacin-loaded crosslinked chitosan microspheres for inhaled aerosol therapy.* European Journal of Pharmaceutics and Biopharmaceutics, 2015. **96**: p. 65-75.
[144] W. Yang, J. Zhang, N. He, and Z. Li, *Investigation of Sonic Hedgehog Loading Chitosan/Sodium Tripolyphosphate Microspheres with Genipin as Cross-Linker.* Journal of Bionanoscience, 2015. **9**(5): p. 341-345.
[145] F.O.S. Abreu, M.M. Forte, T. Kist, and L. Honaiser, *Effect of the preparation method on the drug loading of alginate-chitosan microspheres.* Express Polymer Letters, 2010. **4**(8): p. 456-464.
[146] C. Del Gaudio, V. Crognale, G. Serino, P. Galloni, A. Audenino, D. Ribatti, and U. Morbiducci, *Natural polymeric microspheres for modulated drug delivery.* Materials Science and Engineering: C, 2017. **75**: p. 408-417.

[147] P. Singh, B. Medronho, T.d. Santos, I. Nunes-Correia, P. Granja, M.G. Miguel, and B. Lindman, *On the viability, cytotoxicity and stability of probiotic bacteria entrapped in cellulose-based particles.* Food Hydrocolloids, 2018. **82**: p. 457-465.
[148] H. Feng, L. Zhang, and C. Zhu, *Genipin crosslinked ethyl cellulose–chitosan complex microspheres for anti-tuberculosis delivery.* Colloids and Surfaces B: Biointerfaces, 2013. **103**: p. 530-537.
[149] S. Zeng, M. Ye, J. Qiu, W. Fang, M. Rong, Z. Guo, and W. Gao, *Preparation and characterization of genipin-cross-linked silk fibroin/chitosan sustained-release microspheres.* Drug design, development and therapy, 2015. **9**: p. 2501-2514.
[150] K. Kamiński, K. Zazakowny, K. Szczubiałka, and M. Nowakowska, *pH-sensitive genipin-cross-linked chitosan microspheres for heparin removal.* Biomacromolecules, 2008. **9**(11): p. 3127-32.
[151] Y. Zhang, Y. Yang, and T. Guo, *Genipin-crosslinked hydrophobical chitosan microspheres and their interactions with bovine serum albumin.* Carbohydrate Polymers, 2011. **83**(4): p. 2016-2021.
[152] A. Luzardo-Álvarez, Á. Antelo-Queijo, V.H. Soto, and J. Blanco-Méndez, *Preparation and characterization of β-cyclodextrin-linked chitosan microparticles.* Journal of Applied Polymer Science, 2012. **123**(6): p. 3595-3604.
[153] F. Ganji, S. Vasheghani-Farahani, and E. Vasheghani-Farahani, *Theoretical description of hydrogel swelling: A review.* Iranian Polymer Journal (English Edition), 2010. **19**(5): p. 375-398.
[154] H. Li, *Multi-Effect-Coupling pH-Stimulus (MECpH) Model for pH-Sensitive Hydrogel*, in *Smart Hydrogel Modelling*, H. Li, Editor. 2009, Springer Berlin Heidelberg: Berlin, Heidelberg. p. 57-114.
[155] H. Almeida, M.H. Amaral, and P. Lobao, *Temperature and pH stimuli-responsive polymers and their applications in controlled and self-regulated drug delivery.* Journal of Applied Pharmaceutical Science, 2012. **02**: p. 01-10.
[156] N.A. Peppas, Y. Huang, M. Torres-Lugo, J.H. Ward, and J. Zhang, *Physicochemical Foundations and Structural Design of Hydrogels in Medicine and Biology.* Annual Review of Biomedical Engineering, 2000. **2**(1): p. 9-29.
[157] R. Bashir, J.Z. Hilt, O. Elibol, A. Gupta, and N.A. Peppas, *Micromechanical cantilever as an ultrasensitive pH microsensor.* Applied Physics Letters, 2002. **81**(16): p. 3091-3093.
[158] C.C. Lin and A.T. Metters, *Hydrogels in controlled release formulations: Network design and mathematical modeling.* Advanced Drug Delivery Reviews, 2006. **58**(12-13): p. 1379-1408.
[159] M. Kalagasidis Krušić, M. Ilić, and J. Filipović, *Swelling behaviour and paracetamol release from poly(N-isopropylacrylamide-itaconic acid) hydrogels.* Polymer Bulletin, 2009. **63**(2): p. 197-211.
[160] U. Brunk, V.P. Collins, and E. Arro, *The fixation, dehydration, drying and coating of cultured cells for SEM.* Journal of Microscopy, 1981. **123**(2): p. 121-131.
[161] A.K. Pathan, J. Bond, and R.E. Gaskin, *Sample preparation for SEM of plant surfaces.* Materials today, 2009. **12**: p. 32-43.
[162] A. Mayeen, L.K. Shaji, A.K. Nair, and N. Kalarikkal, *Chapter 12 - Morphological Characterization of Nanomaterials*, in *Characterization of Nanomaterials*, S. Mohan Bhagyaraj, O.S. Oluwafemi, N. Kalarikkal, and S. Thomas, Editors. 2018, Woodhead Publishing. p. 335-364.

[163] M. Hanthamrongwit, M.H. Grant, and R. Wilkinson, *Confocal laser scanning microscopy (CLSM) for the study of collagen sponge microstructure.* Journal of Biomedical Materials Research, 1994. **28**(2): p. 213-216.
[164] M.A. Ilie, C. Caruntu, M. Lupu, D. Lixandru, M. Tampa, S.-R. Georgescu, A. Bastian, C. Constantin, M. Neagu, S.A. Zurac, and D. Boda, *Current and future applications of confocal laser scanning microscopy imaging in skin oncology (Review).* Oncol Lett, 2019. **17**(5): p. 4102-4111.
[165] M. Farré and D. Barceló, *Chapter 1 - Introduction to the Analysis and Risk of Nanomaterials in Environmental and Food Samples*, in *Comprehensive Analytical Chemistry*, M. Farré and D. Barceló, Editors. 2012, Elsevier. p. 1-32.
[166] S.W. Kim, Y.H. Bae, and T. Okano, *Hydrogels: Swelling, Drug Loading, and Release.* Pharmaceutical Research, 1992. **9**(3): p. 283-290.
[167] J.K. Tessmar and A.M. Göpferich, *Matrices and scaffolds for protein delivery in tissue engineering.* Advanced Drug Delivery Reviews, 2007. **59**(4): p. 274-291.
[168] X. Huang and C.S. Brazel, *On the importance and mechanisms of burst release in matrix-controlled drug delivery systems.* J Control Release, 2001. **73**(2-3): p. 121-36.
[169] M.P. Lutolf and J.A. Hubbell, *Synthetic biomaterials as instructive extracellular microenvironments for morphogenesis in tissue engineering.* Nature Biotechnology, 2005. **23**(1): p. 47-55.
[170] B. Sarmento and J.d. Neves, *Approaches of functional modification of cross-linking of chitosan*, in *Chitosan-based system for Biopharmaceuticals: Delivery, targeting and Polymer therapeutics*, A. Anitha, N.S. Rejinold, J.D. Bumgardner, S.V. Nair, and R. Jayakumar, Editors. 2012.
[171] G.-B. Jiang, D. Quan, K. Liao, and H. Wang, *Preparation of polymeric micelles based on chitosan bearing a small amount of highly hydrophobic groups.* Carbohydrate Polymers, 2006. **66**(4): p. 514-520.
[172] M. Prabaharan and J.F. Mano, *Chitosan-Based Particles as Controlled Drug Delivery Systems.* Drug Delivery, 2004. **12**(1): p. 41-57.
[173] K. Pal, A.K. Banthia, and D.K. Majumdar, *Polymeric hydrogels: Characterization and biomedical applications.* Designed Monomers and Polymers, 2009. **12**(3): p. 197-220.
[174] M.P. Paarakh, P.A. Jose, C. Setty, and G. Christoper, *Release kinetics–concepts and applications.* Int. J. Pharm. Res. Tech, 2018. **8**(1): p. 12-20.
[175] S. Dash, P.N. Murthy, L. Nath, and P. Chowdhury, *Kinetic modeling on drug release from controlled drug delivery systems.* Acta Pol Pharm, 2010. **67**(3): p. 217-223.
[176] T. Higuchi, *Mechanism of sustained‐action medication. Theoretical analysis of rate of release of solid drugs dispersed in solid matrices.* Journal of Pharmaceutical Sciences, 1963. **52**(12): p. 1145-1149.
[177] R.W. Korsmeyer and N.A. Peppas, *Effect of the morphology of hydrophilic polymeric matrices on the diffusion and release of water soluble drugs.* Journal of Membrane Science, 1981. **9**(3): p. 211-227.
[178] K. Mayumi, A. Marcellan, G. Ducouret, C. Creton, and T. Narita, *Stress–Strain Relationship of Highly Stretchable Dual Cross-Link Gels: Separability of Strain and Time Effect.* ACS Macro Letters, 2013. **2**(12): p. 1065-1068.
[179] K.S. Anseth, C.N. Bowman, and L. Brannon-Peppas, *Mechanical properties of hydrogels and their experimental determination.* Biomaterials, 1996. **17**(17): p. 1647-1657.
[180] M.L. Oyen, *Mechanical characterisation of hydrogel materials.* International Materials Reviews, 2014. **59**(1): p. 44-59.

[181] M.J. Moura, M.M. Figueiredo, and M.H. Gil, *Rheological Study of Genipin Cross-Linked Chitosan Hydrogels.* Biomacromolecules, 2007. **8**(12): p. 3823-3829.
[182] J.M. Zuidema, C.J. Rivet, R.J. Gilbert, and F.A. Morrison, *A protocol for rheological characterization of hydrogels for tissue engineering strategies.* Journal of biomedical materials research., 2014. **102**(5): p. 1063-1073.
[183] B. Choi, X.J. Loh, A. Tan, C.K. Loh, E. Ye, M.K. Joo, and B. Jeong, *Introduction to In Situ Forming Hydrogels for Biomedical Applications*, in *In-Situ Gelling Polymers: For Biomedical Applications*, X.J. Loh, Editor. 2015, Springer Singapore: Singapore. p. 5-35.
[184] D.R. Picout and S.B. Ross-Murphy, *Rheology of biopolymer solutions and gels.* TheScientificWorldJournal, 2003. **3**: p. 105-121.
[185] P. Matricardi, M. Dentini, and V. Crescenzi, *Rheological gel-point determination for a polysaccharide system undergoing chemical cross-linking.* Macromolecules, 1993. **26**(16): p. 4386-4387.
[186] L. Mertz, *What Is Biocompatibility?: A New Definition Based on the Latest Technology.* IEEE Pulse, 2013. **4**(4): p. 14-15.
[187] G.K. Srivastava, M.L. Alonso-Alonso, I. Fernandez-Bueno, M.T. Garcia-Gutierrez, F. Rull, J. Medina, R.M. Coco, and J.C. Pastor, *Comparison between direct contact and extract exposure methods for PFO cytotoxicity evaluation.* Scientific Reports, 2018. **8**(1): p. 1425.
[188] O. Ostling and K.J. Johanson, *Microelectrophoretic study of radiation-induced DNA damages in individual mammalian cells.* Biochem Biophys Res Commun, 1984. **123**(1): p. 291-8.
[189] B.N. Ames, F.D. Lee, and W.E. Durston, *An improved bacterial test system for the detection and classification of mutagens and carcinogens.* Proceedings of the National Academy of Sciences of the United States of America, 1973. **70**(3): p. 782-786.
[190] K. Muramatsu, M. Nakajima, M. Kikuchi, S. Shimada, K. Sasaki, S. Masuda, and Y. Yoshihara, *In vitro cytocompatibility assessment of beta-tricalcium phosphate/carboxymethyl-chitin composite.* J Biomed Mater Res A, 2004. **71**(4): p. 635-43.
[191] T. Debnath, S. Ghosh, U.S. Potlapuvu, L. Kona, S.R. Kamaraju, S. Sarkar, S. Gaddam, and L.K. Chelluri, *Proliferation and Differentiation Potential of Human Adipose-Derived Stem Cells Grown on Chitosan Hydrogel.* PLOS ONE, 2015. **10**(3): p. e0120803.
[192] C.K. Yao, J.D. Liao, C.W. Chung, W.I. Sung, and N.J. Chang, *Porous chitosan scaffold cross-linked by chemical and natural procedure applied to investigate cell regeneration.* Applied Surface Science, 2012. **262**: p. 218-221.
[193] F.L. Mi, Y.C. Tan, H.C. Liang, R.N. Huang, and H.W. Sung, *In vitro evaluation of a chitosan membrane cross-linked with genipin.* J Biomater Sci Polym Ed, 2001. **12**(8): p. 835-850.
[194] S. Dimida, A. Barca, N. Cancelli, V. De Benedictis, M. Raucci, and C. Demitri, *Effects of genipin concentration on cross-linked chitosan scaffolds for bone tissue engineering: Structural characterization and evidence of biocompatibility features.* International Journal of Polymer Science, 2017. **2017**: p. 8410750.
[195] J.Y. Lai, Y.T. Li, and T.P. Wang, *In vitro response of retinal pigment epithelial cells exposed to chitosan materials prepared with different cross-linkers.* International journal of molecular sciences, 2010. **11**(12): p. 5256-5272.
[196] F.L. Mi, H.W. Sung, and S.S. Shyu, *Drug release from chitosan–alginate complex beads reinforced by a naturally occurring cross-linking agent.* Carbohydrate Polymers, 2002. **48**(1): p. 61-72.

[197] K. Chung, M. Birch, and K. Novakovic, *Genipin-crosslinked Chitosan Hydrogels as Scaffolds for Mammalian Cell Growt.* International Journal of Advances in Science Engineering and Technology, 2018. **6**: p. 37.
[198] L.P. Yan, Y.J. Wang, L. Ren, G. Wu, S.G. Caridade, J.B. Fan, L.Y. Wang, P.H. Ji, J.M. Oliveira, J.T. Oliveira, J.F. Mano, and R.L. Reis, *Genipin-cross-linked collagen/chitosan biomimetic scaffolds for articular cartilage tissue engineering applications.* Journal of Biomedical Materials Research Part A, 2010. **95A**(2): p. 465-475.
[199] J.R. Swearengen, *Choosing the right animal model for infectious disease research.* Animal models and experimental medicine, 2018. **1**(2): p. 100-108.
[200] K.H. Sun, Z. Liu, C. Liu, T. Yu, T. Shang, C. Huang, M. Zhou, C. Liu, F. Ran, Y. Li, Y. Shi, and L. Pan, *Evaluation of in vitro and in vivo biocompatibility of a myo-inositol hexakisphosphate gelated polyaniline hydrogel in a rat model.* Scientific Reports, 2016. **6**(1): p. 23931.
[201] A.M. Olaru, L. Marin, S. Morariu, G. Pricope, M. Pinteala, and L. Tartau-Mititelu, *Biocompatible chitosan based hydrogels for potential application in local tumour therapy.* Carbohydrate Polymers, 2018. **179**: p. 59-70.
[202] A. Jafari, S. Hassanajili, N. Azarpira, M. Bagher Karimi, and B. Geramizadeh, *Development of thermal-crosslinkable chitosan/maleic terminated polyethylene glycol hydrogels for full thickness wound healing: In vitro and in vivo evaluation.* European Polymer Journal, 2019. **118**: p. 113-127.
[203] M.J. Moura, J. Brochado, M.H. Gil, and M.M. Figueiredo, *In situ forming chitosan hydrogels: Preliminary evaluation of the in vivo inflammatory response.* Materials Science and Engineering: C, 2017. **75**: p. 279-285.
[204] F. Su, Y. Wang, X. Liu, X. Shen, X. Zhang, Q. Xing, L. Wang, and Y. Chen, *Biocompatibility and in vivo degradation of chitosan based hydrogels as potential drug carrier.* Journal of Biomaterials Science, Polymer Edition, 2018. **29**(13): p. 1515-1528.
[205] C.D.F. Moreira, S.M. Carvalho, R.M. Florentino, A. França, B.S. Okano, C.M.F. Rezende, H.S. Mansur, and M.M. Pereira, *Injectable chitosan/gelatin/bioactive glass nanocomposite hydrogels for potential bone regeneration: In vitro and in vivo analyses.* International Journal of Biological Macromolecules, 2019. **132**: p. 811-821.
[206] P.V. Turner, T. Brabb, C. Pekow, and M.A. Vasbinder, *Administration of substances to laboratory animals: routes of administration and factors to consider.* Journal of the American Association for Laboratory Animal Science : JAALAS, 2011. **50**(5): p. 600-613.
[207] J.Y. Lai, *Biocompatibility of genipin and glutaraldehyde cross-linked chitosan materials in the anterior chamber of the eye.* International journal of molecular sciences, 2012. **13**(9): p. 10970-10985.
[208] M. Ubaid and G. Murtaza, *Fabrication and characterization of genipin cross-linked chitosan/gelatin hydrogel for pH-sensitive, oral delivery of metformin with an application of response surface methodology.* Int J Biol Macromol, 2018. **114**: p. 1174-1185.
[209] G. Jalani, D.H. Rosenzweig, G. Makhoul, S. Abdalla, R. Cecere, F. Vetrone, L. Haglund, and M. Cerruti, *Tough, In-Situ Thermogelling, Injectable Hydrogels for Biomedical Applications.* Macromolecular Bioscience, 2015. **15**(4): p. 473-480.
[210] J. Xu, S. Strandman, J.X.X. Zhu, J. Barralet, and M. Cerruti, *Genipin-crosslinked catechol-chitosan mucoadhesive hydrogels for buccal drug delivery.* Biomaterials, 2015. **37**: p. 395-404.

[211] F. Mwale, M. Iordanova, C.N. Demers, T. Steffen, P. Roughley, and J. Antoniou, *Biological evaluation of chitosan salts cross-linked to genipin as a cell scaffold for disk tissue engineering.* Tissue Eng, 2005. **11**(1-2): p. 130-40.
[212] L.Q. Yang, Y.Q. Lan, H. Guo, L.Z. Cheng, J.Z. Fan, X. Cai, L.M. Zhang, R.F. Chen, and H.S. Zhou, *Ophthalmic drug-loaded N,O-carboxymethyl chitosan hydrogels: synthesis, in vitro and in vivo evaluation.* Acta pharmacologica Sinica, 2010. **31**(12): p. 1625-1634.
[213] Y. Yu, S. Xu, S. Yu, J. Li, G. Tan, S. Li, and W. Pan, *A Hybrid Genipin-Cross-Linked Hydrogel/Nanostructured Lipid Carrier for Ocular Drug Delivery: Cellular, ex Vivo, and in Vivo Evaluation.* ACS Biomaterials Science & Engineering, 2020. **6**(3): p. 1543-1552.
[214] N. Artzi, N. Oliva, C. Puron, S. Shitreet, S. Artzi, A. bon Ramos, A. Groothuis, G. Sahagian, and E.R. Edelman, *In vivo and in vitro tracking of erosion in biodegradable materials using non-invasive fluorescence imaging.* Nature Materials, 2011. **10**(9): p. 890-890.
[215] J. Liu, Y. Zhang, T. Yang, Y. Ge, S. Zhang, Z. Chen, and N. Gu, *Synthesis, characterization, and application of composite alginate microspheres with magnetic and fluorescent functionalities.* Journal of Applied Polymer Science, 2009. **113**(6): p. 4042-4051.
[216] L. Wang, B. Li, F. Xu, Y. Li, Z. Xu, D. Wei, Y. Feng, Y. Wang, D. Jia, and Y. Zhou, *Visual in vivo degradation of injectable hydrogel by real-time and non-invasive tracking using carbon nanodots as fluorescent indicator.* Biomaterials, 2017. **145**: p. 192-206.
[217] C. Cunha-Reis, A.J. El Haj, X. Yang, and Y. Yang, *Fluorescent labeling of chitosan for use in non-invasive monitoring of degradation in tissue engineering.* J Tissue Eng Regen Med, 2013. **7**(1): p. 39-50.
[218] F.L. Mi, H.W. Sung, S.S. Shyu, C.C. Su, and C.K. Peng, *Synthesis and characterization of biodegradable TPP/genipin co-crosslinked chitosan gel beads.* Polymer, 2003. **44**(21): p. 6521-6530.
[219] A. Gilarska, J. Lewandowska-Łańcucka, W. Horak, and M. Nowakowska, *Collagen/chitosan/hyaluronic acid – based injectable hydrogels for tissue engineering applications – design, physicochemical and biological characterization.* Colloids and Surfaces B: Biointerfaces, 2018. **170**: p. 152-162.
[220] Y. Li, S. Sun, P. Gao, M. Zhang, C. Fan, Q. Lu, C. Li, C. Chen, B. Lin, and Y. Jiang, *A tough chitosan-alginate porous hydrogel prepared by simple foaming method.* Journal of Solid State Chemistry, 2021. **294**: p. 121797.
[221] S. Sapru, A.K. Ghosh, and S.C. Kundu, *Non-immunogenic, porous and antibacterial chitosan and Antheraea mylitta silk sericin hydrogels as potential dermal substitute.* Carbohydrate Polymers, 2017. **167**: p. 196-209.
[222] C.D. Hoemann and D. Fong, *3 - Immunological responses to chitosan for biomedical applications*, in *Chitosan Based Biomaterials Volume 1*, J.A. Jennings and J.D. Bumgardner, Editors. 2017, Woodhead Publishing. p. 45-79.
[223] X. Li, M. Min, N. Du, Y. Gu, T. Hode, M. Naylor, D. Chen, R.E. Nordquist, and W.R. Chen, *Chitin, chitosan, and glycated chitosan regulate immune responses: the novel adjuvants for cancer vaccine.* Clinical & developmental immunology, 2013. **2013**: p. 387023-387023.
[224] P.G. Seferian and M.L. Martinez, *Immune stimulating activity of two new chitosan containing adjuvant formulations.* Vaccine, 2000. **19**(6): p. 661-668.
[225] E.C. Carroll, L. Jin, A. Mori, N. Munoz-Wolf, E. Oleszycka, H.B.T. Moran, S. Mansouri, C.P. McEntee, E. Lambe, E.M. Agger, P. Andersen, C. Cunningham, P. Hertzog, K.A. Fitzgerald, A.G. Bowie, and E.C. Lavelle, *The Vaccine Adjuvant Chitosan Promotes*

Cellular Immunity via DNA Sensor cGAS-STING-Dependent Induction of Type I Interferons. Immunity, 2016. **44**(3): p. 597-608.
[226] C.L. Bueter, C.K. Lee, J.P. Wang, G.R. Ostroff, C.A. Specht, and S.M. Levitz, *Spectrum and mechanisms of inflammasome activation by chitosan.* J Immunol, 2014. **192**(12): p. 5943-51.
[227] I.M. Van der Lubben, F.A.C. Van Opdorp, M.R. Hengeveld, J.J.M. Onderwater, H.K. Koerten, J.C. Verhoef, G. Borchard, and H.E. Junginger, *Transport of Chitosan Microparticles for Mucosal Vaccine Delivery in a Human Intestinal M-cell Model.* Journal of Drug Targeting, 2002. **10**(6): p. 449-456.
[228] E. Onuigbo, J. Iseghohimhen, K. Chah, M. Gyang, and A. Attama, *Chitosan/alginate microparticles for the oral delivery of fowl typhoid vaccine: Innate and acquired immunity.* Vaccine, 2018. **36**(33): p. 4973-4978.
[229] H.L. Jiang, M.L. Kang, J.S. Quan, S.G. Kang, T. Akaike, H.S. Yoo, and C.S. Cho, *The potential of mannosylated chitosan microspheres to target macrophage mannose receptors in an adjuvant-delivery system for intranasal immunization.* Biomaterials, 2008. **29**(12): p. 1931-9.
[230] M.A. Westerink, S.L. Smithson, N. Srivastava, J. Blonder, C. Coeshott, and G.J. Rosenthal, *ProJuvant (Pluronic F127/chitosan) enhances the immune response to intranasally administered tetanus toxoid.* Vaccine, 2001. **20**(5-6): p. 711-23.
[231] M. Mehrabi, N.M. Dounighi, S.M. Rezayat Sorkhabadi, D. Doroud, A. Amani, M. Khoobi, S. Ajdary, and Y. Pilehvar-Soltanahmadi, *Development and physicochemical, toxicity and immunogenicity assessments of recombinant hepatitis B surface antigen (rHBsAg) entrapped in chitosan and mannosylated chitosan nanoparticles: as a novel vaccine delivery system and adjuvant.* Artificial Cells, Nanomedicine, and Biotechnology, 2018. **46**: p. 230-240.
[232] K. Roy, H.Q. Mao, S.K. Huang, and K.W. Leong, *Oral gene delivery with chitosan--DNA nanoparticles generates immunologic protection in a murine model of peanut allergy.* Nat Med, 1999. **5**(4): p. 387-91.
[233] N. Marasini, A.K. Giddam, Z.G. Khalil, W.M. Hussein, R.J. Capon, M.R. Batzloff, M.F. Good, I. Toth, and M. Skwarczynski, *Double adjuvanting strategy for peptide-based vaccines: trimethyl chitosan nanoparticles for lipopeptide delivery.* Nanomedicine (Lond), 2016. **11**(24): p. 3223-3235.
[234] H.S. Mansur, C.M. Sadahira, A.N. Souza, and A.A.P. Mansur, *FTIR spectroscopy characterization of poly (vinyl alcohol) hydrogel with different hydrolysis degree and chemically crosslinked with glutaraldehyde.* Materials Science and Engineering: C, 2008. **28**(4): p. 539-548.
[235] J.I. Goldstein, D.E. Newbury, J.R. Michael, N.W.M. Ritchie, J.H.J. Scott, and D.C. Joy, *Scanning electron microscopy and X-ray microanalysis*. 2017: Springer.
[236] C. Yan and D.J. Pochan, *Rheological properties of peptide-based hydrogels for biomedical and other applications.* Chemical Society reviews, 2010. **39**(9): p. 3528-3540.
[237] S. Nesrinne and A. Djamel, *Synthesis, characterization and rheological behavior of pH sensitive poly(acrylamide-co-acrylic acid) hydrogels.* Arabian Journal of Chemistry, 2017. **10**(4): p. 539-547.
[238] K. Ghosh, X.Z. Shu, R. Mou, J. Lombardi, G.D. Prestwich, M.H. Rafailovich, and R.A.F. Clark, *Rheological Characterization of in Situ Cross-Linkable Hyaluronan Hydrogels.* Biomacromolecules, 2005. **6**(5): p. 2857-2865.

[239] V. Trouplin, N. Boucherit, L. Gorvel, F. Conti, G. Mottola, and E. Ghigo, *Bone marrow-derived macrophage production.* Journal of visualized experiments 2013. **13**(81): p. e50966.
[240] H. Chen, W. Ouyang, B. Lawuyi, C. Martoni, and S. Prakash, *Reaction of chitosan with genipin and its fluorogenic attributes for potential microcapsule membrane characterization.* J Biomed Mater Res A, 2005. **75**(4): p. 917-927.
[241] J. Kawadkar and M.K. Chauhan, *Intra-articular delivery of genipin cross-linked chitosan microspheres of flurbiprofen: preparation, characterization, in vitro and in vivo studies.* Eur J Pharm Biopharm, 2012. **81**(3): p. 563-72.
[242] M. Arteche Pujana, L. Pérez-Álvarez, L.C. Cesteros Iturbe, and I. Katime, *Biodegradable chitosan nanogels crosslinked with genipin.* Carbohydrate Polymers, 2013. **94**(2): p. 836-842.
[243] M.J. Moura, S.P. Martins, and B.P.M. Duarte, *Production of chitosan microparticles cross-linked with genipin – Identification of factors influencing size and shape properties.* Biochemical Engineering Journal, 2015. **104**: p. 82-90.
[244] N.H. Hazrin-Chong and M. Manefield, *An alternative SEM drying method using hexamethyldisilazane (HMDS) for microbial cell attachment studies on sub-bituminous coal.* Journal of Microbiological Methods, 2012. **90**(2): p. 96-99.
[245] M. Mucha and A. Pawlak, *Complex study on chitosan degradability.* Polymery, 2002. **47**(7/8): p. 509-516.
[246] K. Nawrotek, Z. Modrzejewska, D. Paluch, R. Zarzycki, and A. Rusak, *Cytotoxicity of Chitosan Based Thermo-Sensitive Hydrogels Intended for Nervous Tissue Engineering.* Progress on Chemistry and Application of Chitin and Its Derivatives, 2015. **20**: p. 222-235.
[247] K. Shameli, M.B. Ahmad, S.D. Jazayeri, S. Sedaghat, P. Shabanzadeh, H. Jahangrian, M. Mahdavi, and Y. Abdollahi, *Synthesis and characterization of polyethylene glycol mediated silver nanoparticles by the green method.* Int. J. Mol. Sci, 2012. **13**(6): p. 6639-6650.
[248] G.A. Hurst, *The studies of genipin-crosslinked chitosan-poly (vinylpyrrolidone) hydrogels as smart pH responsive materials*, in *School of Chemical Engineering and Advanced Materials*. 2016, Newcastle University: Newcastle upon Tyne.
[249] W.H. Jiang and S.J. Han, *Study of interaction between poly ethyleneglycol and chitosan by viscosity method.* Journal of Polymer Science, 1998. **36**: p. 1275-1281.
[250] K. Aliakbari, A. Ghasemi, M. Mohtashami, and S.S. Sheijani, *Chitosan-genipin nanohydrogel as a vehicle for sustained delivery of alpha-1 antitrypsin.* Research in Pharmaceutical sciences, 2015. **10**(6): p. 523-524.
[251] *Quenching of Fluorescence*, in *Principles of Fluorescence Spectroscopy*, J.R. Lakowicz, Editor. 2006, Springer US: Boston, MA. p. 277-330.
[252] L. Bi, Z. Cao, Y. Hu, Y. Song, L. Yu, B. Yang, J. Mu, Z. Huang, and Y. Han, *Effects of different cross-linking conditions on the properties of genipin-cross-linked chitosan/collagen scaffolds for cartilage tissue engineering.* J Mater Sci Mater Med, 2011. **22**(1): p. 51-62.
[253] A. Lamprecht, U.F. Schäfer, and C.M. Lehr, *Characterization of microcapsules by confocal laser scanning microscopy: structure, capsule wall composition and encapsulation rate.* European Journal of Pharmaceutics and Biopharmaceutics, 2000. **49**(1): p. 1-9.

[254] C. Djerassi, J.D. Gray, and F.A. Kincl, *Naturally Occurring Oxygen Heterocyclics. IX.1 Isolation and Characterization of Genipin2.* The Journal of Organic Chemistry, 1960. **25**(12): p. 2174-2177.
[255] G.A. Hurst and K. Novakovic, *A facile in situ morphological characterization of smart genipin-crosslinked chitosan–poly(vinyl pyrrolidone) hydrogels.* Journal of Materials Research, 2013. **28**(17): p. 2401-2408.
[256] R.C. Simoni, G.F. Lemes, S. Fialho, O.H. Goncalves, A.M. Gozzo, V. Chiaradia, C. Sayer, M.A. Shirai, and F.V. Leimann, *Effect of drying method on mechanical, thermal and water absorption properties of enzymatically crosslinked gelatin hydrogels.* An Acad Bras Cienc, 2017. **89**: p. 745-755.
[257] Z. Xu, J. Li, H. Zhou, X. Jiang, C. yang, F. Wang, Y. Pan, N. Li, X. Li, L. Shi, and X. Shi, *Morphological and swelling behavior of cellulose nanofiber (CNF)/poly (vinyl alcohol) (PVA) hydrogels: poly (ethylene glycol) (PEG) as porogent.* RSC Adv., 2016. **6**: p. 43626-43633.
[258] E.A. Sander and E.A. Nauman, *Permeability of musculoskeletal tissues and scaffolding materials: experimental results and theoretical predictions.* Crit Rev Biomed Eng, 2003. **31**(1-2): p. 1-26.
[259] M.A. Aravand and M.A. Semsarzadeh, *Particle Formation by Emulsion Inversion Method: Effect of the Stirring Speed on Inversion and Formation of Spherical Particles.* Macromolecular Symposia, 2008. **274**(1): p. 141-147.
[260] K. Ofokansi, F. Kenechukwu, A. Isah, and E. Okigbo, *Formulation and evaluation of glutaraldehyde-crosslinked chitosan microparticles for the delivery of ibuprofen.* Tropical Journal of Pharmaceutical Research, 2013. **12**(1): p. 19-25.
[261] Y. Mi, C.T.T. Hagan, B.G. Vincent, and A.Z. Wang, *Emerging Nano-/Microapproaches for Cancer Immunotherapy.* Adv Sci (Weinh), 2019. **6**(6): p. 1801847.
[262] M. Dash, F. Chiellini, R.M. Ottenbrite, and E. Chiellini, *Chitosan—A versatile semi-synthetic polymer in biomedical applications.* Progress in Polymer Science, 2011. **36**(8): p. 981-1014.
[263] U.G.T.M. Sampath, Y.C. Ching, C.H. Chuah, R. Singh, and P.C. Lin, *Preparation and characterization of nanocellulose reinforced semi-interpenetrating polymer network of chitosan hydrogel.* Cellulose, 2017. **24**(5): p. 2215-2228.
[264] A.M. Karaaslan, M.A. Tshabalala, and G. Buschle-Diller, *Wood hemicellulose/chitosan-based semi-interpenetrating network hydrogels: mechanical, swelling and controlled drug release properties.* BioResources, 2010. **5**(2): p. 1036-1054.
[265] F. Chambon and H.H. Winter, *Linear Viscoelasticity at the Gel Point of a Crosslinking PDMS with Imbalanced Stoichiometry.* Journal of rheology online, 1987. **31**(8): p. 683-697.
[266] S. Supper, N. Anton, J. Boisclair, N. Seidel, M. Riemenschnitter, C. Curdy, and T. Vandamme, *Chitosan/glucose 1-phosphate as new stable in situ forming depot system for controlled drug delivery.* Eur J Pharm Biopharm, 2014. **88**(2): p. 361-73.
[267] A.M. Grillet, N.B. Wyatt, and L.M. Gloe, *Polymer Gel Rheology and Adhesion,* in *Rheology*, J.D. Vicente, Editor. 2012, IntechOpen. p. 59-80.
[268] X. Zheng Shu, Y. Liu, F.S. Palumbo, Y. Luo, and G.D. Prestwich, *In situ crosslinkable hyaluronan hydrogels for tissue engineering.* Biomaterials, 2004. **25**(7): p. 1339-1348.
[269] S. Kim, S.K. Nishimoto, J.D. Bumgardner, W.O. Haggard, M.W. Gaber, and Y. Yang, *A chitosan/beta-glycerophosphate thermo-sensitive gel for the delivery of ellagic acid for the treatment of brain cancer.* Biomaterials, 2010. **31**(14): p. 4157-66.

[270] J. Li and Z. Xu, *Physical Characterization of a Chitosan‐Based Hydrogel Delivery System.* JOurnal of Pharmaceutical Sciences, 2002. **91**(7): p. 1669-1677.
[271] L. Vervoort, I. Vinckier, P. Moldenaers, G. Van Den Mooter, P. Augustijns, and R. Kinget, *Inulin hydrogels as carriers for colonic drug targeting. Rheological characterization of the hydrogel formation and the hydrogel network.* Journal of Pharmaceutical Sciences, 1999. **88**(2): p. 209-214.
[272] A. Buxboim, I.L. Ivanovska, and D.E. Discher, *Matrix elasticity, cytoskeletal forces and physics of the nucleus: how deeply do cells 'feel' outside and in?* J Cell Sci, 2010. **123**: p. 297-308.
[273] D. Vukajlovic, J. Parker, O. Bretcanu, and K. Novakovic, *Chitosan based polymer/bioglass composites for tissue engineering applications.* Materials Science and Engineering C, 2019. **96**: p. 955-967.
[274] C.G.T. Neto, J.A. Giacometti, A.E. Job, F.C. Ferreira, J.L.C. Fonseca, and M.R. Pereira, *Thermal Analysis of Chitosan Based Networks.* Carbohydrate Polymers, 2005. **62**(2): p. 97-103.
[275] T. Wanjun, W. Cunxin, and C. Donghua, *Kinetic studies on the pyrolysis of chitin and chitosan.* Polymer Degradation and Stability, 2005. **87**(3): p. 389-394.
[276] V. Buda, M. Andor, A. Ledeti, I. Ledeti, G. Vlase, T. Vlase, C. Cristescu, M. Voicu, L. Suciu, and M.C. Tomescu, *Comparative Solid-State Stability of Perindopril Active Substance vs. Pharmaceutical Formulation.* International journal of molecular sciences, 2017. **18**(1): p. 164.
[277] C.A. Opitz, U.M. Litzenburger, U. Opitz, F. Sahm, K. Ochs, C. Lutz, W. Wick, and M. Platten, *The indoleamine-2,3-dioxygenase (IDO) inhibitor 1-methyl-D-tryptophan upregulates IDO1 in human cancer cells.* PloS one, 2011. **6**(5): p. e19823-e19823.
[278] C.J. Austin and L.M. Rendina, *Targeting key dioxygenases in tryptophan–kynurenine metabolism for immunomodulation and cancer chemotherapy.* Drug Discovery Today 2015. **20**(5): p. 609-617.
[279] R.W. Korsmeyer, S.R. Lustig, and N.A. Peppas, *Solute and penetrant diffusion in swellable polymers. I. Mathematical modeling.* Journal of Polymer Science Part B: Polymer Physics, 1986. **24**(2): p. 395-408.
[280] Y. Sun, F. Cui, K. Shi, J. Wang, M. Niu, and R. Ma, *The effect of chitosan molecular weight on the characteristics of spray-dried methotrexate-loaded chitosan microspheres for nasal administration.* Drug Dev Ind Pharm, 2009. **35**(3): p. 379-86.
[281] J.E. Brauch, *15 - Underutilized Fruits and Vegetables as Potential Novel Pigment Sources*, in *Handbook on Natural Pigments in Food and Beverages*, R. Carle and R.M. Schweiggert, Editors. 2016, Woodhead Publishing. p. 305-335.
[282] F.L. Mi, C.T. Huang, H.F. Liang, M.C. Chen, Y.L. Chiu, C.H. Chen, and H.W. Sung, *Physicochemical, antimicrobial, and cytotoxic characteristics of a chitosan film cross-linked by a naturally occurring cross-linking agent, aglycone geniposidic acid.* J Agric Food Chem, 2006. **54**(9): p. 3290-3296.
[283] M. Zaborowska, A. Bodin, H. Bäckdahl, J. Popp, A. Goldstein, and P. Gatenholm, *Microporous bacterial cellulose as a potential scaffold for bone regeneration.* Acta Biomaterialia, 2010. **6**(7): p. 2540-2547.
[284] N.G. Genes, J.A. Rowley, D.J. Mooney, and L.J. Bonassar, *Effect of substrate mechanics on chondrocyte adhesion to modified alginate surfaces.* Archives of Biochemistry and Biophysics, 2004. **422**(2): p. 161-167.
[285] S. Rhee, *Fibroblasts in three dimensional matrices: cell migration and matrix remodeling.* Experimental & Molecular Medicine, 2009. **41**(12): p. 858-865.

[286] J. Solon, I. Levental, K. Sengupta, P.C. Georges, and P.A. Janmey, *Fibroblast adaptation and stiffness matching to soft elastic substrates.* Biophysical journal, 2007. **93**(12): p. 4453-4461.
[287] K. Wilhelmsen, S.H.M. Litjens, and A. Sonnenberg, *Multiple functions of the integrin alpha6beta4 in epidermal homeostasis and tumorigenesis.* Molecular and cellular biology, 2006. **26**(8): p. 2877-2886.
[288] D.J. Tschumperlin, *Fibroblasts and the ground they walk on.* Physiology 2013. **28**(6): p. 380-390.
[289] F. Liu, J.D. Mih, B.S. Shea, A.T. Kho, A.S. Sharif, A.M. Tager, and D.J. Tschumperlin, *Feedback amplification of fibrosis through matrix stiffening and COX-2 suppression.* The Journal of cell biology, 2010. **190**(4): p. 693-706.
[290] M. Grolik, K. Szczubiałka, B. Wowra, D. Dobrowolski, B. Orzechowska-Wylęgała, E. Wylęgała, and M. Nowakowska, *Hydrogel membranes based on genipin-cross-linked chitosan blends for corneal epithelium tissue engineering.* Journal of Materials Science: Materials in Medicine, 2012. **23**(8): p. 1991-2000.
[291] K. Ren, T. Crouzier, C. Roy, and C. Picart, *Polyelectrolyte Multilayer Films of Controlled Stiffness Modulate Myoblast Cell Differentiation.* Advanced Functional Materials, 2008. **18**(9): p. 1378-1389.
[292] A.L. Hillberg, C.A. Holmes, and M. Tabrizian, *Effect of genipin cross-linking on the cellular adhesion properties of layer-by-layer assembled polyelectrolyte films.* Biomaterials, 2009. **30**(27): p. 4463-4470.
[293] B.S. Liu and T.B. Huang, *Nanocomposites of genipin-crosslinked chitosan/silver nanoparticles--structural reinforcement and antimicrobial properties.* Macromol Biosci, 2008. **8**(10): p. 932-941.
[294] E. Martin-Gayo and X.G. Yu, *Role of Dendritic Cells in Natural Immune Control of HIV-1 Infection.* Frontiers in Immunology, 2019. **10**(1306).
[295] B. Taciak, M. Białasek, A. Braniewska, Z. Sas, P. Sawicka, Ł. Kiraga, T. Rygiel, and M. Król, *Evaluation of phenotypic and functional stability of RAW 264.7 cell line through serial passages.* PLoS One, 2018. **13**(6): p. e0198943.
[296] D. Hirayama, T. Iida, and H. Nakase, *The Phagocytic Function of Macrophage-Enforcing Innate Immunity and Tissue Homeostasis.* International journal of molecular sciences, 2017. **19**(1): p. 92.
[297] H. Tan, H. Li, J.P. Rubin, and K.G. Marra, *Controlled gelation and degradation rates of injectable hyaluronic acid-based hydrogels through a double crosslinking strategy.* J Tissue Eng Regen Med, 2011. **5**(10): p. 790-797.
[298] A.R. Costa-Pinto, A.M. Martins, M.J. Castelhano-Carlos, V.M. Correlo, P.C. Sol, A. Longatto-Filho, M. Battacharya, R.L. Reis, and N.M. Neves, *In vitro degradation and in vivo biocompatibility of chitosan–poly(butylene succinate) fiber mesh scaffolds.* Journal of Bioactive and Compatible Polymers, 2014. **29**(2): p. 137-151.
[299] Y. Hong, H. Song, Y. Gong, Z. Mao, C. Gao, and J. Shen, *Covalently crosslinked chitosan hydrogel: Properties of in vitro degradation and chondrocyte encapsulation.* Acta Biomaterialia, 2007. **3**(1): p. 23-31.
[300] N. Germic, Z. Frangez, S. Yousefi, and H.-U. Simon, *Regulation of the innate immune system by autophagy: monocytes, macrophages, dendritic cells and antigen presentation.* Cell Death & Differentiation, 2019. **26**(4): p. 715-727.
[301] B.D. Ulery, L.S. Nair, and C.T. Laurencin, *Biomedical Applications of Biodegradable Polymers.* Journal of polymer science. Part B, Polymer physics, 2011. **49**(12): p. 832-864.

[302] A. Altinisik and K. Yurdakoc, *Synthesis, characterization, and enzymatic degradation of chitosan/PEG hydrogel films.* Journal of Applied Polymer Science, 2011. **122**(3): p. 1556-1563.
[303] A. Lončarević, M. Ivanković, and A. Rogina, *Lysozyme-induced degradation of chitosan: the characterisation of degraded chitosan scaffolds.* Journal of Tissue Repair and Regeneration, 2017. **1**(1): p. 12.
[304] A. Matica, G. Menghiu, and V. Ostafe, *Biodegradability of chitosan based products.* New Frontiers in Chemistry, 2017. **26**(1): p. 75-86.
[305] S.H. Pangburn, P.V. Trescony, and J. Heller, *Lysozyme degradation of partially deacetylated chitin, its films and hydrogels.* Biomaterials, 1982. **3**(2): p. 105-8.
[306] A.J. Bavariya, P. Andrew Norowski, Jr., K. Mark Anderson, P.C. Adatrow, F. Garcia-Godoy, S.H. Stein, and J.D. Bumgardner, *Evaluation of biocompatibility and degradation of chitosan nanofiber membrane crosslinked with genipin.* J Biomed Mater Res B Appl Biomater, 2014. **102**(5): p. 1084-92.